ISSN 1019-5149 - E ISSN 2651-5032 - NLM ID 9423821

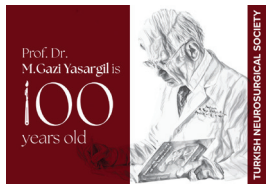

Turkish Neurosurgery

Official Journal of the Turkish Neurosurgical Society

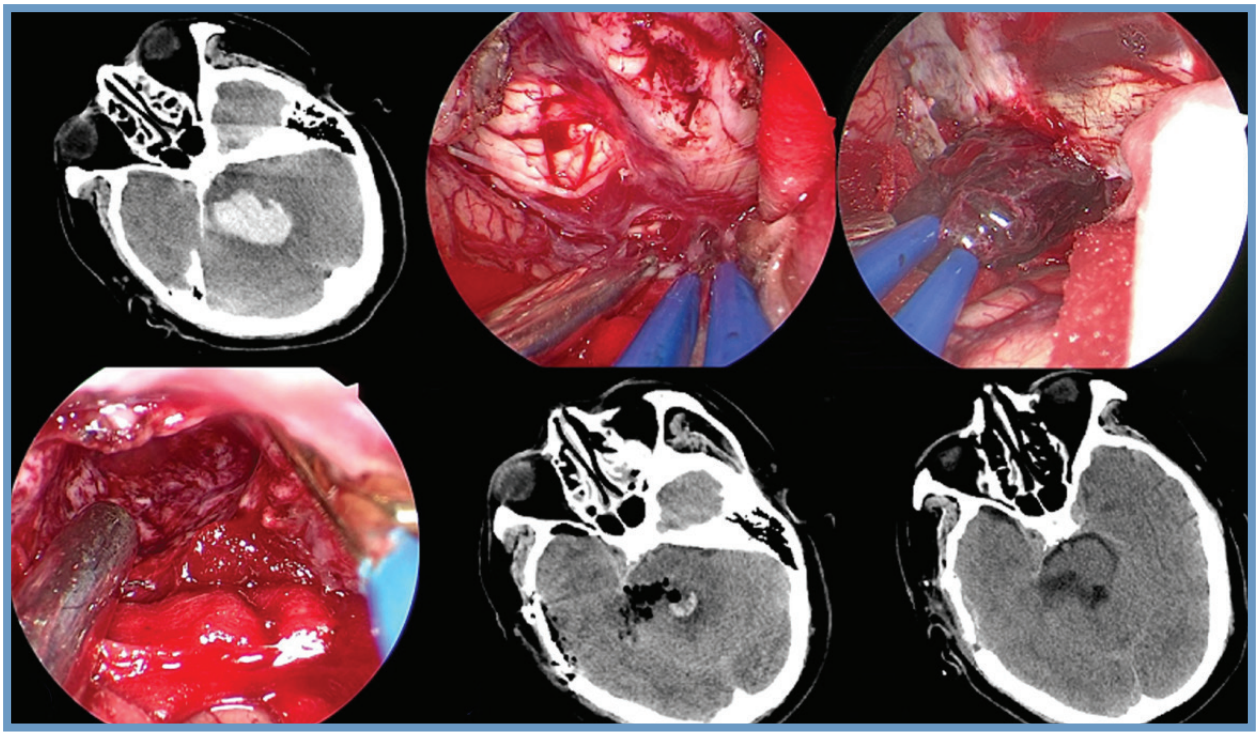

Volume 35 • Number 4 • July 2025

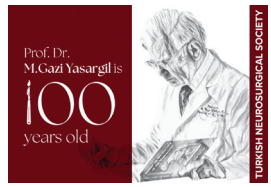

Turkish Neurosurgery

Official Journal of the Turkish Neurosurgical Society

ISSN: 1019-5149,
E-ISSN: 2651-5032
NLM ID: 9423821

TURKISH NEUROSURGICAL SOCIETY

Volume: 35 Number: 4 Year: 2025

www.turkishneurosurgery.org.tr

Turkish Neurosurgery has been accepted for indexing in: SCIENCE CITATION INDEX EXPANDED, INDEX MEDICUS, MEDLINE, PubMed, EBSCO, Scopus, TR Index, Islamic World Science Citation Center (ISC)

Impact Factor* : 0.8
5yr-Impact Factor*: 0.8
Journal Citation Indicator*TM: 0.34

*ISI Web of Knowledge℠, Journal Citation Reports®, 2024 JCR Science Edition

Turkish
Neurosurgery

Volume: 35 Number: 4 Year: 2025

Official Journal of the Turkish Neurosurgical Society

Turkish Neurosurgery is published six times per year (bimonthly) by the Turkish Neurosurgical Society
(January, March, May, July, September, and November)

Owned and controlled by the Turkish Neurosurgical Society

Copyright owner on behalf of the Turkish Neurosurgical Society:
Hüseyin Hayri KERTMEN

Publishing Manager:
İlker SOLMAZ

Key title: Turkish Neurosurgery
Abbreviated key title: Turk Neurosurg
www.turkishneurosurgery.org.tr

ISSN: 1019-5149, **E-ISSN:** 2651-5032
NLM ID: 9423821

Turkish Neurosurgery is an open access and totally free journal.
All electronic materials can be found on internet without any charge. Please visit: http://www.turkishneurosurgery.org.tr/
2025 Subscription Rates for Printed Materials:
Within Türkiye 4000 TL (shipping costs not included); Outside Türkiye 100 € (shipping costs not included)
For further information and questions; please contact: bulus@bulustasarim.com.tr

Page layout and publishing services
BULUŞ DESIGN AND PRINTING SERVICES COMPANY
Bahriye Üçok Caddesi 9/1 Beşevler, 06500 Ankara, Türkiye
Phone: +90 312 222 44 06 Fax: +90 312 222 44 07
E-mail: bulus@bulustasarim.com.tr

Advertisement: editor@turkishneurosurgery.org.tr

Publishing Date: 18.07.2025

Cover picture: Yin, p. 556

Turkish Neurosurgical Society
Taşkent Caddesi 13/4 06500 Bahçelievler, Ankara/TÜRKİYE
Phone: +90 312 212 64 08 Fax : +90 312 215 46 26
E-mail: info@turknorosirurji.org.tr
www.turknorosirurji.org.tr www.turkishneurosurgery.org.tr

Yayın Türü: Yaygın süreli yayın
Yayın Sahibi: Türk Nöroşirürji Derneği adına Hüseyin Hayri KERTMEN
Sorumlu Yazı İşleri Müdürü: İlker SOLMAZ

5187 Sayılı Basın Yasasının 7. maddesi uyarınca dergi künyesinin Türkçesi belirtilmiştir.

Review of the articles in the journal to make sure they conform to publishing standards, typesetting, getting the journal ready for publication and finally the publishing process has been the responsibility of Buluş Design and Printing Services Company.

The paper used to print this journal conforms to ISO 9706: 1994 standard (Requirements for Permanence).
The National Library of Medicine suggests that biomedical publications be printed on acid-free paper (alkaline paper).

22
PAP

ENVIRONMENTAL INFORMATION

The company that manufactures the paper used in this journal has an ISO 14001 environmental management certificate. The company obtains all wood fiber in a sustainable manner. The forests and plantations of the company are certified. The water used in production is purified and used after recovery.

Heavy metals or film are not used for the publication of this journal. The fluids used for developing the aluminum printing templates are purified. The templates are recycled. The inks used for printing do not contain toxic heavy metals.

This journal can be recycled. Please dispose of it in recycling containers.

INSTRUCTION TO THE AUTHORS

Journal Description

Turkish Neurosurgery is a peer-reviewed, multidisciplinary, open access journal directed at an audience of neurosurgery physicians and scientists. The official language of the journal is *English*. The journal publishes original articles in the form of clinical and basic research. *Turkish Neurosurgery* will only publish studies that have institutional review board (IRB) approval and have strictly observed an acceptable follow-up period. With the exception of reference presentation, *Turkish Neurosurgery* requires that all manuscripts be prepared in accordance with the *Uniform Requirements for Manuscripts Submitted to Biomedical Journals*.

Turkish Neurosurgery periodically publishes the following papers: Research (Original Investigation, Clinical and Experimental Studies), Review Article, Case Report, Letter to Editor, Technical Note and Turkish Neuro-Excursion.

Our mission is providing a scientific forum relevant to neurosurgeons and health care providers.

Open Access Policy

As the Turkish Neurosurgery Journal, we believe science is a common denominator of the humanity which should be publicly available and free. Since its establishment in 1989, all our effort and workforce were based on volunteers and their efforts.

Definition of Open Access Publication[1]

An Open Access Publication [A] is one that meets the following two conditions:

1. The author(s) and copyright holder(s) grant(s) to all users a free, irrevocable, worldwide, perpetual right of access to, and a license to copy, use, distribute, transmit and display the work publicly and to make and distribute derivative works, in any digital medium for any responsible purpose, subject to proper attribution of authorship [B], as well as the right to make small numbers of printed copies for their personal use.
2. Complete version of the work and all supplemental materials, including a copy of the permission as stated above, in a suitable standard electronic format is deposited immediately upon initial publication in at least one online repository that is supported by an academic institution, scholarly society, government agency, or other well-established organization that seeks to enable open access, unrestricted distribution, interoperability, and long-term archiving (for the biomedical sciences, PubMed Central is such a repository).

Notes:

A. Open access is a property of individual works, not necessarily journals or publishers.

B. Community standards, rather than copyright law, will continue to provide the mechanism for enforcement of proper attribution and responsible use of the published work, as they do now.

[1] https://dash.harvard.edu/bitstream/handle/1/4725199/Suber_bethesda.htm#note1

Digital Archiving

Bulus Tasarim and the "Turkish Neurosurgery" journal provide for long-term digital preservation through Portico.

Portico is a leading digital preservation service worldwide. The content is preserved as an archival version and is not publically accessible via Portico, but is provided when required under specific conditions, such as discontinuation of the collection or catastrophic failure of the website.

Manuscript Submission

Authors are to submit their manuscripts through the web based tracking system at http://www.turkishneurosurgery.org.tr. The site contains instructions and advice on how to submit manuscripts, guidance on the creation / scanning and saving of electronic art and supporting documentation. **ORCID** identifier (ID) is required for **ALL** authors during the submission process. **ORCID ID** can be obtained free of charge at http://orcid.org. **E-mail address of all authors** should also be provided during the submission process. In addition to allowing authors to submit manuscripts on the web, the site allows authors to follow the progression of their manuscript through the peer review process. Authors who submit their manuscripts through the web-based tracking system are asked **not** to send hard copies of the manuscript to the editorial office. Please address all inquiries regarding manuscripts not yet accepted or published to the Journal's editorial office. The editorial office will acknowledge receipt of your manuscript and will send you a manuscript number for reference.

Before submission please ensure that:

One author has been designated as the correspondent with full contact details including e-mail address, postal address

and phone number. In any case of editorial board could not contact with the corresponding author, Turkish Neurosurgery journal have the right to decide what is appropriate.

Submission Checklist;

1) Your title page is in .doc or .docx format, includes title of your manuscript, author names, affiliations and ORCID numbers; name and full contact information of corresponding author, running title, keywords, and authorship contribution statements-the latter can be found on the Copyright transfer and authorship contribution statement Form. Please be sure that authorship contribution statements are presented in the form as well as in the title page. Of note, authors should indicate conflicts of interest relating to their research-if any.

   The Journal is not responsible for published misspelled names due to author error and the title page **must be uploaded as a separate file**. Running Head in the title page should be no more than three to five words from the title, and should NOT include the authors' names.

2) Your main document is in .doc or .docx format includes **structured abstract, key words, abbreviation list, structured main text, disclosure and conflicts of interest, references and figure legends** sections in this order. Structured main text should be organized as **Introduction, Material and Methods, Results, Discussion, and Conclusion.** Do not add any information about institution names. Also do not add figures and tables in the main document. **Be sure your main document is written in Calibri or Times New Roman, line gap set to double spaced and justified on both sides.** Journal's official language is English. Refer to drugs and therapeutic agents by their accepted generic or chemical names, and do not abbreviate them. Use code numbers only when a generic name is not yet available. In that case, supply the chemical name and a figure giving the chemical structure of the drug. Capitalize the trade names of drugs and place them in parentheses after the generic names. To comply with trademark law, include the name and location (city and country) of the manufacturer of any drug, supply, or equipment mentioned in the manuscript. Use the metric system to express the units of measure and degrees Celsius to express temperatures, and SI units rather than conventional units. Define abbreviations at first mention in text and in each table and figure. If a brand name is cited, supply the manufacturer's name and address (city and state/country).

3) All your figures are in **TIFF** format. Color figures should have a resolution of at least **300 dpi**, black and white figures should have a resolution of at least **600 dpi**. Turkish Neurosurgery does not demand any color figure fee.

4) All your video files are in .mpeg and .mp4 format, not longer than 10 minutes, and not bigger than 40 MB. Video files should include an embedded audio narration and subtitles in English.

5) All your tables are in .doc or .docx format, created using the table creating and editing feature of the word processing software. Do not use Excel or comparable software. Upload a single text file which includes **ALL the tables in separate pages.** Cite tables consecutively in the text, and number them in that order. Key each on a separate sheet, include the table title, appropriate column heads, and explanatory legends (including definitions of any **abbreviations** used). Do not embed tables within the main text.

If your manuscript does not meet these requirements, manuscript **WILL BE RETURNED** to the corresponding author for technical revision before undergoing peer review.

Submission Steps

1. Upload signed copyright form by the corresponding author which is available at http://neurosurgery.dergisi.org/submit/Copyright_transfer_form.pdf. Choose your manuscript type and click continue.
2. Add names of institutions of all authors. If one or more author has affiliation with more institutions, specify it in the title page. Then click continue.
3. Write last name and first name of all authors. Add their institution numbers, e-mails and ORCID numbers. Standard page appears with spaces enough for 8 author names. If your paper has more authors, please fill all the first 8 authors names and affiliations then click add author. Without filling all required fields, you cannot add more authors. Do not use abbreviations in the author names. Then click continue.
4. Write the title of the manuscript. If the title contains special characters use the left below table. You can copy-paste the title from your title page. Then click continue.
5. Write the abstract of your manuscript to the field**.** Abstracts should be structured including Aim, Material and Methods, Results and Conclusion. **Abstracts should not exceed 300 words. There is no need of Turkish abstract.** Then click continue.
6. Write the keywords separated by commas. Please use keywords from https://meshb.nlm.nih.gov/search. Then click continue.
7. Click the appropriate answer stating if your manuscript has not been published and / or is not being considered for publication elsewhere or your manuscript was presented in the congress indicated below and was published in abstract form in the proceedings of the congress. Then write your cover letter to the editor to the field. Then click continue.
8. Upload your manuscript files. Be sure your files are main document (manuscript), figure(s), video(s), title page, and table(s). For every file, write the description of your file and click upload button. The names of the files you have submitted should not resemble the names or institutions of the authors. Be sure all your text files are in .doc or .docx format. When you are sure you uploaded all your files click continue.

9. When you complete all the submission process click approve for all the files you want to submit and click **Submit your Manuscript** button.

Revised Submission

Author's comments to the reviewers are required for revised submissions. Authors must address all the reviewer's concerns/suggestions and whether the change was made or not. Authors must also highlight the changes made within the text. Do not track the additions or deletions to the manuscript. If the authors do not want to revise the manuscript within a period of **two months**, the manuscript will be declined.

Ethics, patient anonymity and informed consent:

This journal adheres to the ethical standards described by the Committee on Publication Ethics (https://publicationethics.org/) and the International Committee of Medical Journal Editors (https://www.icmje.org/). Authors are expected to adhere to these standards.

It is the author's responsibility to ensure that a patient's anonymity is carefully protected and to verify that any experimental investigation with human subjects reported in the manuscript was performed with informed consent and followed all the guidelines for experimental studies with human subjects required by the institution(s) with which all the authors are affiliated. Authors should mask patients' eyes, private parts and remove patients' names from all figures. Editorial board of the Turkish Neurosurgery have the right to demand ethical committee forms or informed consent forms **at any stage of the submission and publication.** All animal experiments should comply with the ARRIVE guidelines https://www.nc3rs.org.uk/arrive-guidelines. Also, Editorial board of the Turkish Neurosurgery have the right to withdraw any paper, even it is accepted, if there is any ethical issue.

Authorship should be limited to those who have made a significant contribution to the conception, design, execution, or interpretation of the reported study. The authors should ensure that they have written entirely original works, and if the authors have used the work and/or words of others, that this has been appropriately cited or quoted. Editorial board of the Turkish Neurosurgery have the right to withdraw any paper if there is any plagiarism. All submissions must include disclosure of all relationships that could be viewed as presenting a potential conflict of interest. All authors must disclose any financial and personal relationships with other people or organizations that could inappropriately influence (bias) their work. Examples of potential competing interests include employment, consultancies, stock ownership, honoraria, paid expert testimony, patent applications/registrations, and grants or other funding. Authors must disclose any interests in the disclosure and conflicts of interest section of the main document.

Authorship Change

Authors are expected to consider carefully the list and order of authors before submitting their manuscript and provide the definitive list of authors at the time of the original submission. Any addition, deletion or rearrangement of author names in the authorship list after submitting the paper is **inappropriate and prohibited**. Authors should **withdraw** their paper if there is a need for authorship change.

Types of Manuscripts

Turkish Neuro-Excursion: The editor will invite experts for these special types of papers which may cover a broad spectrum in various fields of medicine, science, art, history, law as well as any important theme on actuality other than core neurosurgery. The number of words, figures, tables and references are not restricted.

Research (Original Investigation, Clinical and Experimental Studies): The main text should not exceed 4500 words **excluding the** references, tables, and figure legends for original articles, including randomized controlled trials, observational (cohort, case-control or cross-sectional) studies, diagnostic accuracy studies, nonrandomized behavioral and public health intervention trials, experimental animal trials and any other retrospective or prospective clinical or experimental studies. The number of figures, tables, videos and references are not restricted. The specifications for figures and video files are given.

Review Article: All review articles should be systematic reviews and meta-analyses. A systematic review protocol describes the rationale, hypothesis, and planned methods of the review. It should be prepared before a review is started and used as a guide to carry out the review. Turkish Neurosurgery no more accept papers as "Case Report and Review of the Literature". All systematic reviews and meta-analyses SHOULD COMPLY with **PRISMA** guidelines http://www.prisma-statement.org/. Systematic reviews and meta analyses SHOULD INCLUDE a **CONSORT** Flow Diagram http://www.consort-statement.org/consort-statement/flow-diagram. Any systematic review and meta-analysis without a CONSORT Flow Diagram will be rejected.

Case Report: Turkish Neurosurgery values **demonstrative and unique case reports** with **high quality figures**. A case report should be so clear and easy to understand that the reader could replicate the case in his/her daily practice. Word count must not exceed 1500 (excluding references, tables, and figure legends). Case reports cannot have more than 15 references, and 6 figures or tables. Turkish Neurosurgery **does not accept** papers as **"Case Report and Review of the Literature"** anymore.

Technical Note: Turkish Neurosurgery values **demonstrative technical notes** with **high quality figures**. Technical notes reinforced with high-quality anatomical studies are welcome. A technical note should be so clear and easy to understand that the reader could replicate the technique in the operating room or on cadaveric specimen. The number of words must not exceed 2000, and there should not be more than 20 references. The number of figures and tables are not restricted.

Letter to the Editor: Letters should refer to the title and authors of a recent Turkish Neurosurgery article. The letter should be no longer than 300 words with no more than 3 references. Unpublished data should not be used Letters to

the Editor are sent to the article authors for response. The Editor-in-Chief makes the final decision on whether letters to the editor and the responses are published.

References

The authors are responsible for the accuracy of the references. Key the references (double-spaced) at the end of the manuscript. Cite references in the text in alphabetical order within parentheses. Do not link the references to the text. Cite unpublished data, such as papers submitted but not yet accepted for publication or personal communications, in parentheses in the text (please be sure that such have a DOI number to be presented). **Do not use "et al." in the references.** List all the authors of the reference. Refer to the List of Journals Indexed in Index Medicus for abbreviations of journal names, or access the list at "http://www.nlm.nih.gov/tsd/serials/lji.html. The DOI numbers are mandatory in accordance with the library indexes; please be sure to present the DOI numbers for each reference at the end of its sentence. The reference styles for Zotero and EndNote are available on the journal's home page.

Sample references are given below:

A. Journal article

Umeoka K, Mizunari T, Murai Y, Kobayashi S, Morita A: Occlusion of the ascending pharyngeal artery during carotid artery surgery: Importance and technique. Turk Neurosurg 24: 546-548, 2014. https://doi.org/10.5137/1019-5149.JTN.9527-13.0

B. Book chapter

Martin A: Literacies for the digital age. In: Martin A, Madigan D (eds), Digital literacies for learning. Facet, 2006:3-25. DOI: https://doi.org/10.29085/9781856049870.003

C. Entire book

Smith T, Williams BM, Streefkerk R: The citation manual for students: A quick guide (2nd ed). Wiley, 2020. https://doi.org/10.1000/182

D. Example of thesis

Kanpolat Y: Experimental percutaneous access to the trigeminal ganglion and the histopathological evaluation of radiofrequency thermic lesion (Unpublished dissertation), Ankara: Ankara University, 1978:1- 52

E. Software

Epi Info [computer program]. Version 6. Atlanta: Centers for Disease Control and Prevention, 1994

F. Online journals

Friedman SA. Preeclampsia: A review of the role of prostaglandins. Obstet Gynecol [serial online]. January 1988;71:22-37. Available from: BRS Information Technologies, McLean, VA. Accessed December 15, 1990

G. Database

CANCERNET-PDQ [database online]. Bethesda, MD: National Cancer Institute, 1996. Updated March 29, 1996

H. World Wide Web

Gostin LO. Drug use and HIV/AIDS [JAMA HIV/AIDS web site]. June 1, 1996. Available at: http://www.ama-assn.org/ special/hiv/ethics. Accessed June 26, 1997

ChatGPT USE in MANUSCRIPTS*

- Please use ChatGPT only if allowed by your institution, research lab, and the journal (in any question).
- Please acknowledge and cite ChatGPT within your manuscript/published paper wherever you are using it.
- Please do not fabricate or plagiarize data.
- ChatGPT can be used only for summarizing texts, improving English writeups, and brainstorming ideas, and not for creating fabricated research raw data.
- The Editorial Board have the right to request revisions or withdraw any paper if there is any misuse of ChatGPT.

*Biswas, SS. ChatGPT-for-Research-and-Publication-A-Step-by-Step Guide (https://meridian.allenpress.com/jppt/article/28/6/576/496601/ChatGPT-for-Research-and-Publication-A-Step-by)(https://doi.org/10.5863/1551-6776-28.6.576)

PEER REVIEW PROCESS

This journal uses double-blind review, which means that both the reviewer and author identities are concealed from the reviewers, and vice versa, throughout the review process.

1. Manuscript Submission

The corresponding or submitting author submits the paper to the journal through http://turkishneurosurgery.org.tr/.

2. Assessment of the Paper for Journal Requirements

The editorial office checks the paper's composition and arrangement against the journal's Author Guidelines - Instruction to the Authors (http://turkishneurosurgery.org.tr/static.php?id=7) - to make sure it includes the required sections and stylizations.

3. Evaluation by the Editor-in-Chief (EIC)

The EIC checks the paper's scientifical appropriateness for the journal, its originality and actuality. If not, the paper may be rejected without being reviewed any further.

4. EIC Assigns a Section Editor (SE)

Section Editors handle the peer review process. All manuscripts that reach this step will go through a double-blind peer-review process. In order to ensure an unbiased evaluation process, each submission will be reviewed by at least two external, independent peer reviewers who are experts in the field.

5. Invitation to Reviewers

The SE sends invitations to individuals he or she believes would be appropriate reviewers. As responses are received, further invitations are issued, if necessary, until the required number of acceptances is obtained.

6. Response to Invitations

Potential reviewers consider the invitation against their own expertise, conflicts of interest and availability. They then accept or decline.

7. Review is Conducted

The reviewer sets time aside to read the paper several times. The first read is used to form an initial impression of the work. If major problems are found at this stage, the reviewer may feel comfortable rejecting the paper without further work. Otherwise they will read the paper several more times, taking notes so as to build a detailed point-by-point review. The review is then submitted to the journal, with a recommendation to accept or reject it – or else with a request for revision (either major or minor) before it is reconsidered.

8. Journal Evaluates the Reviews

The SE considers all the returned reviews before making an overall decision. If the reviews differ widely, the editor may invite an additional reviewer so as to get an extra opinion before making a decision.

9. The Decision is Communicated

The EIC is the final authority in the decision-making process for all submissions. He or She sends a decision e-mail to the author including any relevant reviewer comments.

AFTER ACCEPTANCE

Online Proof Correction

Corresponding authors will receive an e-mail including final PDF version of their manuscript. Authors are obligated to proofreading their manuscript in 72 hours.

Turkish Neurosurgery workflow processes to get your article published quickly and accurately. Please use this proof only for checking the typesetting, editing, completeness and correctness of the text, tables and figures. Significant changes to the article as accepted for publication will only be considered at this stage with permission from the Editor. It is important to ensure that all corrections are sent back to us in one communication. Please check carefully before replying, as inclusion of any subsequent corrections cannot be guaranteed. Proofreading is solely your responsibility. **Authorship change is not accepted during proofreading and is prohibited.**

Rapid Publication Option

In accordance with the Turkish Neurosurgical Society's Board Decision on August 5, 2023, "Turkish Neurosurgery" journal is starting to publish articles with a rapid publication option (RPO). This type of publication choice will have no effect on the peer review process or acceptance of the submission since it will be requested by the authors after acceptance of the article.

What is RPO?: The RPO ensures the accepted article will be immediately prepared in electronic format (e-pdf), and it will be printed in one of the upcoming issues of the journal. This service has a publication fee that needs to be met by the authors, their institutions, or the research funders for each article that is published in a timely manner. The decision for RPO will be made by the authors, and they will only be charged upon their requests and if their paper is accepted. As there is a limited space for such option in each publishable issue, this process will be granted on a first-come, first-served basis, and the Turkish Neurosurgical Society is responsible for organizing the demands and informing the Editorial Board as well as the Publisher.

Why RPO?: There is a waiting list, and the number of articles per issue is constant and limited. It generally takes 6–14 months for a research paper to be published in a printed journal. This service allows immediate publication of the article in both electronic and printed formats. Of note, the printed article will be published in one of the upcoming issues of the journal.

Please be sure to use the RPO service and contact the society, even if you are in early need of an e-pdf manuscript.

Benefits of RPO: Here, it's important to make sure that articles are published as soon as possible, are subject to the proper quality controls, and are extensively read. By using RPO, the authors are able to publish their ideas faster, receive credit for the idea and the manuscript, get ready to strengthen their enrollment for future applications and grants, and last but not least, have increased visibility in a quick-paced setting.[1]

[1] https://www.editage.com/insights/publish-faster-progress-faster-the-basics-of-rapid-publication

RPO Price and Communication Details: The RPO charge for the journal is EUR 1000/article, including taxes.

This service is carried out by Turkish Neurosurgical Society. Please contact with: Turkish Neurosurgical Society, Taskent Caddesi 13/4 06500 Bahcelievler, Ankara/TÜRKİYE

E-mail: info@turknorosirurji.org.tr

Reprints

Reprint requests should be faxed or e-mailed with the corrected proofs by the corresponding author, if needed. Reprints are normally shipped 6 to 8 weeks after publication of the issue in which the item appears. Contact with the Publisher: Bulus Tasarim, Bahriye Üçok Caddesi 9/1, Beşevler, Ankara, TÜRKİYE.

E-mail: bulus@bulustasarim.com.tr

The price for 2 sets of hardcopy journal:

Within Türkiye 1500 TL (shipping costs not included);
Outside Türkiye 40 € (shipping costs not included)

**Depend on shipping cost. Please contact Bulus Tasarim.*

Manuscript Checklist (before submission. For author reference only)

1. ORCID identifier (ID) is required for all authors during the submission process. ORCID ID can be obtained free of charge at http://orcid.org ☐
2. E-mail address of all authors should be provided during the submission process. ☐
3. Title page
   - Title (brief, definite, didactic) ☐
   - Corresponding author designated, and full mailing address included on title page ☐
   - E-mail address of corresponding author included on title page ☐
   - Running head ☐
   - Approval of Institutional Review Board (Decision No/Date) and/or signed patient consent forms ☐
   - Permission to reproduce copyrighted material ☐
   - Acknowledgements listed for grants, technical support, and corporate support on title page ☐
4. Structured abstract with key words (300 words) ☐
5. Manuscript text with page numbers [Microsoft Word (.doc)] (without author names and affiliations) ☐
6. Figure legends ☐
7. Tables (Word, Wordperfect) ☐
8. Figures (TIFF) ☐
9. Videos (avi, mpeg, mp4) with narration and/or subtitles ☐
10. References double-spaced and cited in alphabetical order ☐

CONTENTS

Turkish Neurosurgery

Volume: 35 Number: 4 Year: 2025

REVIEW

ORIGINAL INVESTIGATIONS

■ Cerebrovascular-Endovascular

TECHNICAL NOTE

■ Cerebrovascular-Endovascular

ORIGINAL INVESTIGATIONS

Turk Neurosurg 35(4):527-536, 2025
DOI: 10.5137/1019-5149.JTN.46950-24.4

Review

Received: 27.05.2024
Accepted: 28.11.2024
Published Online: 25.06.2025

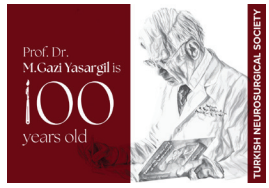

Chronic Subdural Hematoma and Tranexamic Acid: A Systematic Review

Beatriz Rodrigues MESSIAS[1], João Paulo Macedo BORGES[1], Andre Felix GENTIL[2]

[1]Albert Einstein Instituto Israelita de Ensino e Pesquisa, São Paulo – São Paulo (SP), Brazil
[2]Albert Einstein Hospital, Department of Neurosurgery, São Paulo - São Paulo (SP), Brazil

Corresponding author: Beatriz Rodrigues MESSIAS ✉ biamessias7@gmail.com

ABSTRACT

AIM: To systematically evaluate the existing literature regarding adjuvant or primary treatment of chronic subdural hematoma (cSDH) with tranexamic acid (TXA).

MATERIAL and METHODS: This systematic review followed the parameters set by the Preferred Reporting Items for Systematic Reviews and Meta-Analyses (PRISMA). A search in the available literature was conducted up to February 2024 in five databases using the keywords “chronic subdural hematoma” and “tranexamic acid.” Randomized clinical trials, prospective or retrospective cohorts, systematic reviews, and case series (> five patients) relevant to the analysis were included.

RESULTS: In total, 10 studies were included, encompassing a total of 912 patients diagnosed with cSDH who underwent treatment with TXA. Seven studies evaluated the use of TXA as an adjunctive to surgical treatment, and three articles investigated the effect of TXA as primary therapy.

CONCLUSION: TXA can be considered a safe and effective option in adjunct to surgical management. Further studies are needed to establish its role as primary treatment.

KEYWORDS: Tranexamic acid, Chronic subdural hematoma, Systematic review

ABBREVIATIONS: AT: Antithrombotics, **CI:** Confidence Interval, **cSDH:** Chronic Subdural Hematoma, **CSF:** Cerebrospinal Fluid, **CT:** Computed Tomography, **GCS:** Glasgow Coma Scale, **KKS:** Kallikrein-Kinin System, **MRI:** Magnetic Resonance Imaging, **NOS:** Newcastle-Ottawa Scale, **PRISMA:** Preferred Reporting Items for Systematic Reviews and Meta-Analyses, **OR:** Odds Ratio, **RR:** Relative Risk, **SEPS:** Subdural Evacuation Port System, **TBI:** Traumatic Brain Injury, **t-PA:** Tissue Plasminogen Activator, **TRACS:** Tranexamic Acid in Chronic Subdural Hematomas, **TORCH:** Tranexamic Acid to Prevent Operation in Chronic Subdural Hematoma, **TXA:** Tranexamic Acid: **VEGF:** Vascular Endothelial Growth Factor

INTRODUCTION

Chronic subdural hematoma (cSDH) is an encapsulated collection of blood in various stages of coagulation, accumulating at the dural border cell layer. Symptoms vary and are typically insidious, including headache, gait instability, mental confusion, fluctuating hemiparesis, and seizures (11,30,32). However, patients can remain asymptomatic, and cSDH may only be detected as an incidental finding on imaging.

The sometimes-subclinical course of the disease may contribute to the imprecise reported incidence, estimated at 1.72 to 20.6 cases per 100.000 population per year (46). As it predominantly affects the elderly population, there is an expectation of a significant increase in surgical approaches for cSDH, following the trend of increasing life expectancy and the use of antiplatelet and anticoagulant medications (17,32). It is estimated that by 2030, approximately 60.000 cases of cSDH will occur annually in the United States alone (2).

Beatriz Rodrigues MESSIAS : 0000-0002-8910-293X
João Paulo Macedo BORGES : 0009-0001-8789-9586
Andre Felix GENTIL : 0000-0002-5228-2033

Despite its significant prevalence, there is currently no consensus on treatment, adjunct therapy, or pre- and post-surgical care. Surgical management is considered the gold standard for symptomatic cSDH treatment (34). Among various indications, large hematomas (> 10 mm) or midline shifts (> 5 mm) on computed tomography (CT) scans, combined with the presence of symptoms, are often cited (20). Although the surgical procedure is considered safe with a low mortality rate (approximately 2%) (3), recurrence is estimated at 10 to 20% (17). Considering a primarily elderly population with multiple comorbidities, less invasive therapeutic proposals assume significance, especially in asymptomatic or oligosymptomatic patients.

Current research suggests that the constitution of cSDH is more complex than theorized by Virchow in 1857 (14), who attributed hematoma formation to traumatic injury and subsequent rupture of tributary veins of the dural venous sinuses. The pathophysiology of cSDH involves the coexistence of various predisposing factors, such as sustained inflammation, angiogenesis, and fibrinolysis (11). The cascade of inflammatory and fibrinogenic processes leads to the formation of internal, thin, avascular membranes and external, highly vascularized membranes, forming a thick capsule (6). This capsule, in turn, promotes the processes that generated it through the production of substances such as tissue plasminogen activator (t-PA) and vascular endothelial growth factor (VEGF) (11).

Hyperfibrinolysis plays a prominent role in the liquefaction and expansion of the hematoma between the internal membrane and the capsule. At the biomolecular level, the degradation of fibrin clots primarily occurs through the activity of plasmin, converted from plasminogen by tPA (4).

Given this panorama, tranexamic acid (TXA) may be an alternative to reduce the volume of surgical procedures. It is an antifibrinolytic agent that competitively inhibits plasmin activation and interrupts the fibrinolysis process (27). Its use has been shown to be safe for patients with intracranial bleeding post-traumatic brain injury (TBI), reducing the risk of TBI-related death when treatment is initiated within 3 hours after moderate traumas (8).

Although treatment with TXA holds promise, evidence regarding its use in cSDH cases remains insufficient. Larger-scale clinical trials such as "Tranexamic Acid in Chronic Subdural Hematomas" – TRACS (Canada) (19) and "Tranexamic Acid to Prevent Operation in Chronic Subdural Hematoma" – TORCH (Netherlands) (18) are underway, with publication expected within the next 3 years.

MATERIAL and METHODS

This study consists of a systematic review of international medical literature using the PRISMA (Preferred Reporting Items for Systematic Reviews and Meta-Analyses) guidelines published in 2020 (28).

The following databases were selected for consultation: Embase, Lilacs, PubMed/MEDLINE, Scopus, and Web of Science. Searches were conducted on March 18, 2023, and again on February 14, 2024, by two independent researchers (B.R.M. and J.P.M.B.), with no initial restrictions on language and/or publication date. A manual search of the references of selected papers and systematic reviews published on the same topic was also conducted to identify additional studies. To add information on ongoing clinical trials, the Cochrane Library and ClinicalTrials.gov databases were consulted in February 2024.

The search terms used to identify studies regarding the use of TXA for cSDH were "chronic subdural hematoma" and "tranexamic acid" [MeSH], combined with Boolean operators ("AND" and "OR"). Eligible articles included those in which participants were adults (age ≥ 18 years) with a confirmed diagnosis of cSDH, regardless of severity, for which TXA was used as either the primary or adjunctive therapy to surgical treatment in any dosage or administration scheme.

Letters to the editor, comments, editorials, narrative or literature reviews, and case reports were excluded. Ongoing clinical trials with unknown status or no updates in the last year were also excluded. Trials with expired end dates and no published results were searched by title on PubMed/MEDLINE and Google to ensure no related publication was unreported in the databases (Cochrane Library and ClinicalTrials.gov).

Initially, two authors (B.R.M and J.P.M.B.) independently assessed all retrieved articles for eligibility based on title and abstract. For studies not fully available, the author whose email was listed in the publication was contacted to assess the availability of the full text. Duplicates and articles accessible only partially were then removed. Finally, the full text of eligible studies was examined for inclusion. Any doubts or discrepancies were discussed and resolved with the project supervisor (A.F.G).

Data from the selected references for this systematic review were extracted in a structured manner: article characteristics, including lead investigator, year of publication, study design, and country of origin; demographic and clinical data of patients, such as mean age, male-to-female ratio, and sample size; description of administered treatment (TXA dose and duration, surgical necessity, placebo control); and evaluated outcomes.

Bias risk was independently assessed by two authors (B.R.M and J.P.M.B.) for each included study, using three tools depending on the evaluated article's methodology: Newcastle Ottawa Scale (NOS) (43) for non-randomized clinical trials and prospective or retrospective cohorts; ROB 2 Risk of Bias Tool for randomized clinical trials (36); and AMSTAR 2 (33) for systematic reviews.

Articles whose bias was analyzed using the NOS tool had their evidence quality classified as "good," "fair," or "poor," based on the criteria adopted by Mascolo et al. (25). It was considered "good" if NOS had 3 or 4 stars for the "selection" domain, 1 or 2 stars for the "comparability" domain, and 2 or 3 stars for the "outcome" domain; "fair" if 2 stars in "selection," 1 or 2 stars in "comparability," and 2 or 3 stars in "outcome"; and "poor" if 0 or 1 star in "selection," or 0 stars in "comparability," or 0 or 1 star in "outcome."

Randomized clinical trials were evaluated for evidence quality using the ROB 2 Risk of Bias tool, based on the following domains: bias risk in the randomization process, deviations from the intended intervention, incomplete/missing data, bias risk in outcome assessment, and bias risk in result reporting. Each domain was subsequently classified as having a low risk of bias, some concerns, or a high risk of bias. The results were then presented in a figure constructed using the robvis (Risk-of-Bias VISualization) instrument (26).

AMSTAR 2 includes 16 items to assess the reliability of results in systematic reviews. In this study, based on Shea et al.'s recommendations (33), the analyzed studies were classified with a confidence grade: 1) high if no or one non-critical flaw was detected, 2) moderate if more than one non-critical flaw, 3) low if one critical flaw, and 4) critically low if more than one critical flaw.

RESULTS

Systematic Search

From the initial systematic search, 365 articles were retrieved from seven databases. Duplicates (n=161) and ongoing clinical trials without available results (n=8) were excluded. The remaining 196 publications were evaluated based on title and abstract, resulting in 36 references selected for full-text analysis. Eight studies whose full text was not retrieved were excluded. Of the remaining 28 articles, 18 were excluded for not meeting the inclusion criteria of this research, namely: five case reports with a sample size of fewer than five patients, six narrative reviews, six systematic reviews and/or meta-analyses that included multiple drug therapies for cSDH, and one systematic review with methodological flaws. Finally, 10 articles were included in this article, including one non-randomized clinical trial, four retrospective analyses, three randomized clinical trials, one prospective study, and one systematic review. All included articles were published between 2013 and 2023. Figure 1 below summarizes the

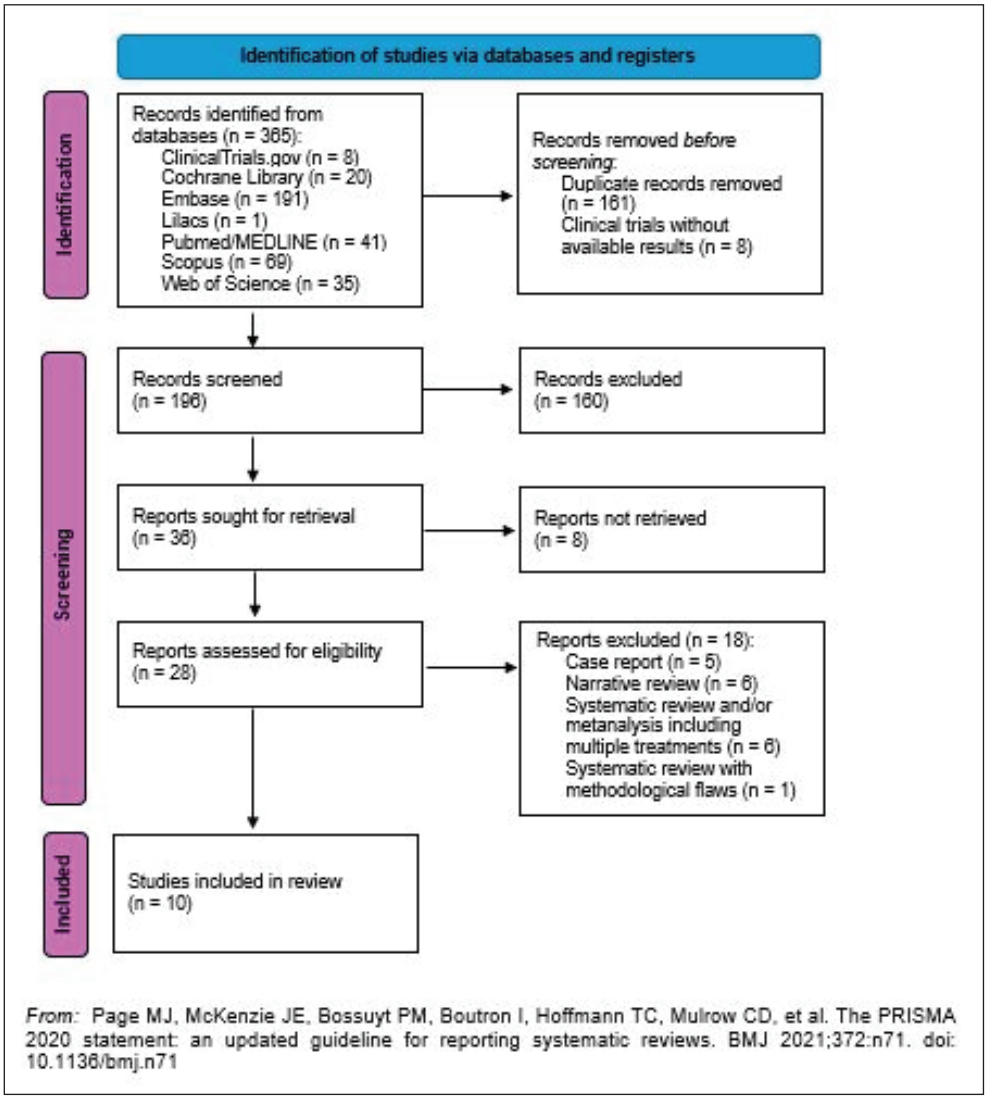

Figure 1: PRISMA flowchart.

study selection process using the flowchart proposed by the PRISMA guidelines (28).

Characteristics of the Included Studies

This systematic review included 912 patients diagnosed with cSDH who underwent treatment with TXA. Seven studies investigated the effect of TXA as an adjuvant therapy to surgical procedures, and one article investigated it as the primary treatment; two cohorts evaluated the use of TXA predominantly as a single intervention. The average age of participants in all studies was over 55 years, predominantly above 70 years in most cases. The follow-up time ranged from 28 days to 10 months. The results are summarized in Table I below.

Table I: Study Characteristics Included in the Systematic Review

Study	Design	Country	Standard treatment (sample size)	Male (%)	Mean age (years ± standard deviation)	TXA dosage	Treatment duration
Albalkhi et al., (1)	Systematic review and meta-analysis	Saudi Arabia	TXA (n=654) *versus* control (n=749)	440 (65.3%) *versus* 493 (65.8%)	75 [71-78.9] *versus* 74.9 [72.4-77.5]‡	Unreported	Unreported
De Paula et al., (9)	Randomized clinical trial	Brazil	TXA (n=24) *versus* control (n=26)◊	15 (62.5%) *versus* 16 (61.5%)	75.8 ± 11.8 *versus* 72.6 ± 11.9	750 mg/day	90 days
Kageyama et al., (22)	Retrospective cohort	Japan	TXA (n=21)	12 (57%)	78.7 ± 10.5	750 mg/day	28-137 days
Kutty et al., (23)	Prospective cohort	India	TXA (n=27)	15 (55.6%)	64.9 ± 11.8	750 mg/day	27-120 days
Lodewijkx et al., (24)	Non-randomized clinical trial	Netherlands	TXA (n=7)	7 (100%)	78.1 ± 4.7	1-2 g/day	5-56 days
Puente Tinoco et al., (29)	Retrospective cohort	Venezuela	TXA (n=11) *versus* Jackson-Pratt drain (n=11)◊	11 (100%) *versus* 10 (90.9%)	32-87 years¥	2 g/day	4 days
Tanweer et al., (38)	Retrospective cohort	United States	TXA (n=14)※	12 (86%)	56.4 ± 16.3	650 mg/day	180 days¶
Wan et al., (41)	Randomized clinical trial	Singapore	Control (n=49) *versus* TXA (n=41)*	36 (73.5%) *versus* 24 (58.5%)	69.6 ± 13.7 *versus* 72 ± 11.8	1000 mg/day	21 days
Yamada and Natori, (44)	Randomized clinical trial	Japan	Control (n=82) *versus* TXA (n=72) *versus* Goreisan (n=78)†	57 (62.5%) *versus* 43 (59.7%) *versus* 50 (64.1%)	78.8 ± 10.8 *versus* 78.2 ± 9.8 *versus* 79.2 ± 8.7	750 mg/day	90 days
Yang et al., (45)	Retrospective cohort	South Korea	TXA (n=41) *versus* non-TXA (n=114) *versus* AT (n=85)#	33 (80.4%) *versus* 87 (76.3%) *versus* 65 (76.4%)	72 (65-83) *versus* 71.5 (60-79) *versus* 77 (68-82)¨	750 mg/day	14-141 days

*‡ Mean [95% confidence interval]. ◊ All patients underwent drainage of the cSDH through burr-hole trepanation. ¥ Minimum-maximum age. ※ After evacuation of the cSDH at the bedside using a twist-drill and placement of a SEPS drain. ¶ Or until resolution of the cSDH on the follow-up CT scan. * The standard neurosurgical procedure consisted of evacuation of the cSDH through burr-hole trepanation or mini-craniotomy, with or without drainage. † All patients underwent burr-hole drainage and were randomly allocated into the three described groups (surgery, surgery + TXA, and surgery + Goreisan). The sample size described refers to the quantity of chronic subdural hematomas assessed. # All patients underwent single burr-hole drainage with subdural drain insertion. The antithrombotics (AT) group consisted of patients with a history of cerebrovascular or cardiovascular disease, on antiplatelet or anticoagulant therapy. Results are expressed as median (interquartile range).*

Regarding the Need for Surgical Procedure

Lodewijk et al. investigated the effect of off-label first-line treatment with TXA in seven patients diagnosed with cSDH (24). Treatment discontinuation was guided by the resolution of neurological symptoms, combined with a significant reduction or complete disappearance of the hematoma on follow-up CT scans. The primary outcome assessed was the surgical need for cSDH evacuation within the first 12 weeks of TXA treatment. Of the seven patients, five (71.2%) experienced complete resolution of neurological symptoms. One patient required burr-hole trepanation 5 days after initiating treatment due to worsening clinical condition.

Regarding Recurrence Prevention

In 2019, Yamada and Natori published a randomized clinical trial involving 193 patients (232 cSDHs) to assess the effect of TXA on recurrence prevention (44). Following burr-hole trepanation for hematoma drainage, patients were randomly assigned to three groups: surgery alone, TXA, and Goreisan—a Japanese traditional medicine composed of five herbal ingredients. The instituted treatment lasted for a total of 3 months post-surgery, after which the difference in recurrence rates (including reoperation) among the groups was evaluated. Regarding the primary outcome, the authors determined that there was no statistically significant difference in recurrence rates.

Wan et al. obtained similar results in their randomized clinical trial published in 2020 (41). Ninety symptomatic cSDH patients were recruited and randomly allocated to receive standard neurosurgical treatment—burr-hole evacuation or mini-craniotomy—or adjuvant TXA with surgical intervention. The primary outcome assessed was the reduction in symptomatic cSDH recurrence post-surgery, necessitating reoperation within 6 months. There were five recurrences (10.2%) in the first group and two (4.8%) in the second group, with no statistically significant difference in the recurrence rate (odds ratio [OR] 0.51, p=0.4).

In a more recent study from 2022, Yang et al. retrospectively analyzed 240 symptomatic patients undergoing cSDH evacuation with single burr-hole trepanation and subdural drain insertion to determine the efficacy of TXA as an adjuvant in recurrence prevention and hematoma resolution (45). The study population was divided into the following groups: TXA, non-TXA (observation), and antithrombotics (AT), the latter encompassing patients with a history of cardiac or cerebrovascular disease on antiplatelet or anticoagulant therapy. The primary outcome evaluated was cSDH recurrence, defined as hematoma reappearance requiring neurosurgical intervention.

The authors identified 16 recurrence cases (6.7%): one in the TXA group, eight in the non-TXA group, and seven in the AT group. Although the recurrence rate was lower in patients treated with TXA (2.4%), there was no statistically significant difference due to the small number of events. The authors concluded that TXA could be a viable therapeutic option for reducing recurrence in selected patients.

Conversely, de Paula et al. presented a different suggestion in their randomized controlled clinical trial, published in 2023 (9). Fifty unilateral or bilateral cSDH patients undergoing surgical burr-hole trepanation were randomized to receive postoperative TXA or not. The recurrence rate was determined based on symptom recurrence or the need for new surgical intervention.

Clinical and radiological recurrence occurred in two out of 24 patients in the TXA group (8.3%) and in one out of 26 cases in the control group (3.8%), with no statistically significant difference (p=0.5). Consequently, the authors suggested that TXA should not be used as a therapeutic measure to prevent CSDH recurrence.

Albalkhi et al. evaluated the role of TXA as an adjuvant treatment in preventing cSDH recurrence in a systematic review with meta-analysis (1). Six studies (four randomized clinical trials and two cohorts) were included, comprising 1,403 cSDH-diagnosed patients who underwent surgical intervention. Of these, 654 patients received adjuvant TXA therapy, while 749 received standard surgical treatment (control). The recurrence rate was estimated at 5.8% in the TXA group and 13.6% in the control group. The overall relative risk (RR) revealed a significant reduction in recurrence in the TXA group compared to controls (RR 0.41 [95% CI 0.29-0.59]). Based on these findings, Albalkhi et al. (1) suggested that adjuvant TXA may reduce cSDH recurrence in elderly patients who have undergone surgical procedures.

Regarding Volumetric Changes in cSDH

In their case series, Lodewijk et al. (24) demonstrated the volumetric reduction of cSDH in all patients during follow-up, with a median of 15 weeks. The total volume, initially 83 ml, decreased by 72% to a residual of 33 ml.

Kageyama et al. analyzed 21 patients diagnosed with cSDH by CT or magnetic resonance imaging (MRI) (22). Regardless of the choice of surgical approach or symptomatology, all participants received 750 mg of TXA per day until complete resolution or sufficient reduction of the hematoma, based on imaging evolution. TXA was used as the main treatment in 18 patients (86%) and as an adjuvant to surgery in three (14%). The median volume of cSDH showed a reduction from 58.5 ml initially to 3.7 ml after therapy. There were no records of recurrence or progression of hematomas.

As a secondary outcome, Yamada and Natori's clinical trial also recorded the residual volume of cSDH 1, 2, and 3 months after treatment (44). At baseline, there was no difference in preoperative hematoma volume. At all follow-up periods, the measured volume was significantly lower in the TXA group compared to patients treated only surgically or with adjuvant Goreisan.

Kutty et al., in turn, recruited 27 patients diagnosed with cSDH for TXA treatment, which was maintained until hematoma resolution (23). Twenty cases consisted of primary cSDH, and seven of these were recurrent cSDH after surgical treatment (trepanation with twist-drill). The mean thickness of cSDH was determined as 14.31 mm. The mean volume of the hematoma

initially measured 147.05 ml in the group primarily treated with TXA and 152.14 ml in the recurrent group. The authors considered that there was satisfactory resolution of cSDH in subsequent control CT scans.

Tanweer et al. evaluated the effect of TXA on the treatment of residual subdural hematoma after a surgical procedure (39). They retrospectively analyzed 14 patients undergoing drainage of moderate to large cSDH with twist-drill, followed by placement of a subdural evacuation port system (SEPS) drain. After SEPS removal, they opted for daily administration of 650 mg of TXA on an outpatient basis for 6 months or until cSDH resolution on CT follow-up.

In the study published in 2016, the mean initial volume was 145.96 ml, with a midline shift of 9.44 mm. After surgical evacuation, the cSDH volume decreased by 40.74% ($p<0.0001$) to a mean of 80 ml, and the midline shift reduced to 4.44 ml ($p=0.0046$). At the last follow-up, the mean cSDH volume was recorded as 7.41 ml, representing an additional reduction of 91.3% after TXA treatment was instituted ($p<0.0001$). The percentage volumetric reduction was significantly higher after TXA compared to SEPS (91.3% versus 40.74%).

Although they did not prove the effect of TXA in preventing recurrence, Wan et al. demonstrated that the "surgery + TXA" group showed greater volumetric reduction of cSDH between postoperative and 6-week follow-up compared to the "surgery" group (41). However, this effect did not persist at 12 and 24 weeks of follow-up, and the maximum hematoma volume did not show a statistically significant difference between the two study arms.

Similarly, Yang et al. analyzed as a secondary outcome the resolution of cSDH, defined as complete reabsorption (thickness < 5 mm) or near-total reabsorption (hematoma stability), associated with recovery of neurological deficits (45). Clinical and radiological resolution of cSDH was achieved in 85.8% of patients, with no disparities between groups. However, the median time to resolution was significantly faster ($p<0.001$) in the TXA group (51 days) than in the non-TXA group (109 days) and AT group (88 days). In multivariate analysis, the administration of TXA adjuvant to surgical treatment was considered a positive factor for the reabsorption of residual bleeding.

Regarding Symptomatology

In the case series by Kageyama et al., all participants showed significant improvement in symptoms (22). In Tanweer et al.'s analysis, all 14 patients, except one with pre-existing dementia, showed symptomatic improvement in the follow-up, with the majority (71%) experiencing complete resolution (39).

With regard to clinical presentation, Puente Tinoco et al. evaluated 22 patients undergoing cSDH drainage, with half of them undergoing placement of a Jackson–Pratt external drainage system postoperatively (Group A), and the other half receiving TXA postoperatively (Group B) (29). Upon admission, the most reported symptom was hemiparesis (68.2% of cases). In both groups, most patients showed immediate improvement and normalization of the Glasgow Coma Scale (GCS) at 15 – 63.6% in Group A and 54.5% in Group B. Regarding hospitalization time, the authors identified an average stay of 8 days in Group A, versus 6 days in Group B, determining that the adjuvant use of TXA significantly reduced the number of hospitalization days compared to the use of the Jackson–Pratt drain ($p=0.004$).

Regarding the Incidence of Adverse Events

In Wan et al.'s analysis, there were four reported cases of serious adverse events in the "surgery + TXA" group, of which one—asymptomatic thalamic infarction—could potentially be related to the treatment, although the patient had a history of multiple small strokes on MRI (41). Kutty et al. did not record mortality, complications, or hematoma enlargement due to TXA treatment (23). Yang et al., in their 2022 article, also did not identify adverse effects related to the use of TXA (45).

As a secondary outcome, de Paula et al. assessed potential clinical and/or surgical complications related to TXA use (9). Two cases of postoperative complications were reported (pulmonary embolism, potentially associated with treatment, and surgical wound infection), both in the TXA group. There was no statistically significant difference between the groups regarding the incidence of adverse events ($p=0.5$).

In their 2023 meta-analysis, Albalkhi et al. identified only two studies that reported thrombosis occurrence (1). No statistically significant association was demonstrated between TXA treatment and the risk of thrombosis (RR 0.88 [95% CI 0.64-1.19]).

Bias Risk

Among the articles assessed by the NOS tool (43), the quality of evidence was classified as "good" in four cohorts (22,29,39,45). The analysis of one non-randomized clinical trial (25), and one prospective study were categorized as "fair" (24). Albalkhi et al.'s meta-analysis (1), which had a high level of confidence, did not present any critical flaws in the assessment by the AMSTAR 2 tool (33). Regarding the randomized clinical trials, the risk of bias established through ROB 2 (36) was low for the studies by Yamada et al. (44), and Wan et al. (41), and showed "some concerns" regarding the article published by de Paula et al. (9). The results of this analysis are compiled in Figure 2.

DISCUSSION

Currently, it is understood that the formation of cSDH is initiated by the rupture of the dural border, possibly due to a mild traumatic event (15). Consequently, there is extravasation of cerebrospinal fluid (CSF) and blood into the subdural space, initiating a cascade of inflammatory, angiogenic, and fibrinolytic processes. Local inflammation in response to bleeding is suggested by the elevation of pro-inflammatory cytokines, such as IL-6 and IL-8, in the CSF compared to serum levels (37). These inflammatory mediators, in turn, contribute to the development of cSDH through two central processes: increased vascular permeability and release of t-PA, resulting in plasmin formation.

Plasmin, in turn, leads to the activation of the kallikrein–kinin system (KKS), from which bradykinin is derived, responsible

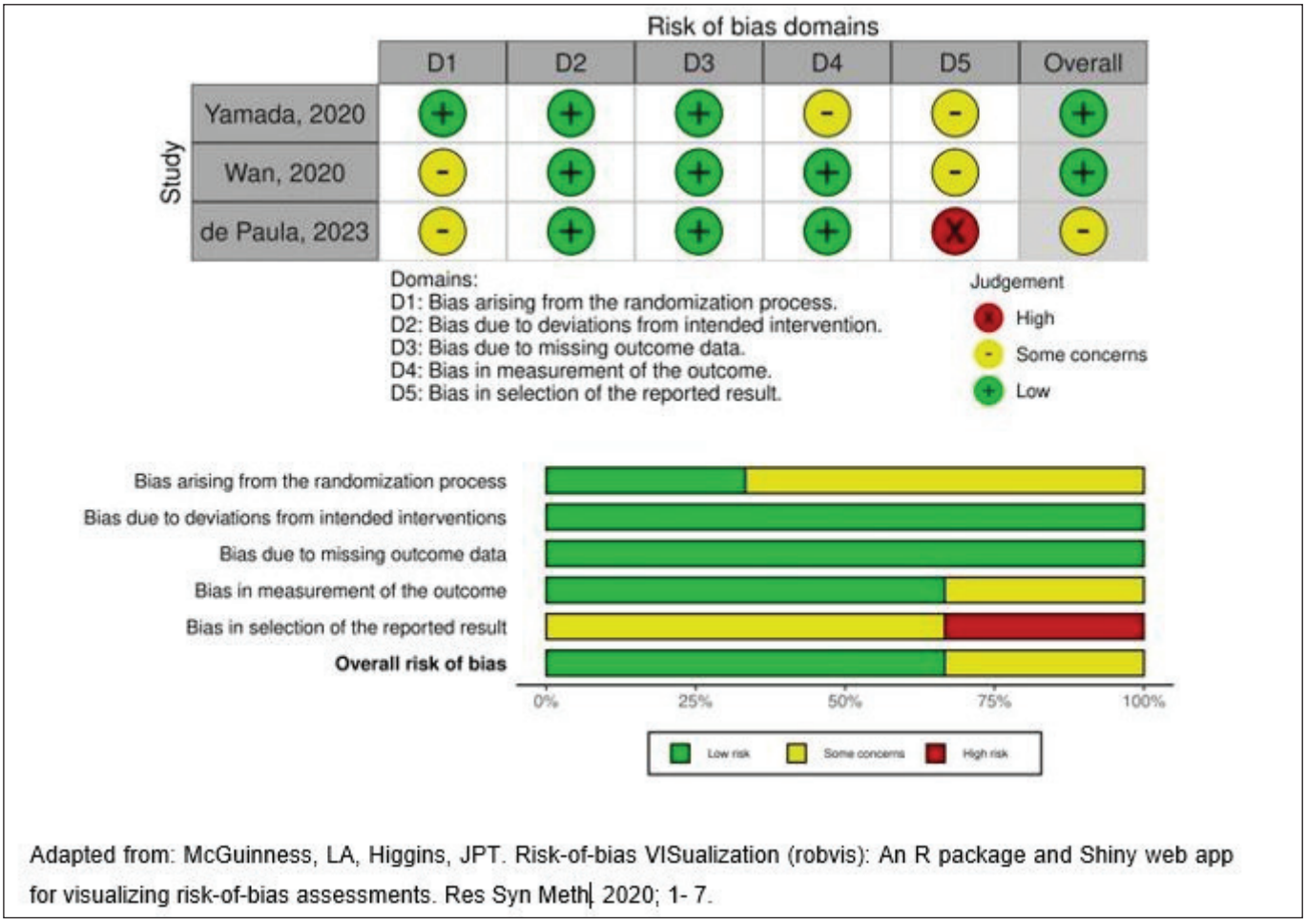

Figure 2: Risk of bias.

for increasing vascular permeability (12). Fujisawa et al. experimentally determined an elevation in bradykinin concentration in cSDH (13), suggesting a reciprocal stimulation between the KKS and coagulation and fibrinolysis pathways. The result involves angiogenesis, plasma exudation, and hyperfibrinolysis, critical events for hematoma progression.

Advancements in understanding the pathophysiology of cSDH have been accompanied by changes in the therapeutic paradigm. However, surgical evacuation of the hematoma remains the first-line treatment until now (21). Surgical treatment is generally accepted in patients with neurological symptoms and considerable radiological findings; conversely, asymptomatic cases without obvious mass effect are often clinically monitored (35). Amidst these two scenarios with more easily perceivable approaches, there are several controversies: when to indicate surgical management? What is the best surgical method? Is pharmacological treatment possible?

Although surgical intervention is considered effective, with a high cure rate (generally above 70%), the procedure's mortality is not negligible (approximately 2 to 4%) (42). Recurrence is also a relevant factor to be evaluated. Santarius et al. estimated recurrence at 9.3% in patients with postoperative drainage and 24% in cases where drainage placement was omitted (31). In their analysis of more than 60,000 patients, Toi et al. estimated the recurrence rate at 13.1% (40). Functional outcomes were considered poor in 28.4% (modified Rankin Scale 3-6), especially in elderly patients. Approximately 30% of patients experienced some degree of morbidity, requiring assistance after discharge. These outcomes raised questions about the previously perceived "benign" prognosis of cSDH.

The heterogeneity of surgical approaches, coupled with the inherent risk of recurrence and complications, prompted the search for new therapies, initially focusing on oligosymptomatic patients or those with prohibitive surgical risk. In this context, the option of TXA emerged, a synthetic antifibrinolytic that competitively blocks plasminogen activation into plasmin. Additionally, it has an indirect anti-inflammatory action through the KKS (27). It has wide clinical applicability, with evidence of reducing intraoperative bleeding and postpartum hemorrhage (16). Another alternative that has been studied to reduce the risk of recurrence of cSDH is middle meningeal artery embolization (EMMA). The meta-analysis published by Dian et al. included a total of four studies (n=888 patients) and, despite limited data, concluded that the relative risk of recurrence with EMMA was significantly lower compared to

surgical drainage (RR 0.17, [CI 95% 0.05-0.67]), making it a promising option to consider (10).

The biological rationale for using TXA in cases of cSDH is based on the hypothesis that its antifibrinolytic action would inhibit the ongoing hyperfibrinolysis and increased vascular permeability processes, thereby allowing gradual hematoma absorption (22).

Regarding the prevention of postoperative recurrence of cSDH with adjuvant use of TXA, the results of this systematic review are contradictory. Some of the included studies (9,41,44,45) did not show a reduction in recurrence with the use of TXA; however, a recent meta-analysis demonstrates the effectiveness of the antifibrinolytic in reducing recurrence in elderly patients (1).

Recently, Ridwan et al. investigated predictive factors for cSDH recurrence (30). The authors concluded that the residual hematoma volume in the postoperative period, as well as the composition and morphology of cSDH, are the most relevant predictors of recurrence and cure. In this systematic review, several studies demonstrated the effect of adjuvant TXA in reducing the residual volume of cSDH, which may indirectly contribute to preventing recurrence (22-24,29). The network meta-analysis by Yu et al. reinforces this hypothesis: TXA showed definitive efficacy in reducing recurrence (OR = 0.26, [95% CI 0.07-0.41]) (47).

With regard to the safety profile, TXA exhibits mostly mild side effects, such as headache, abdominal pain, nausea, and diarrhea (4). In a recent meta-analysis, the use of TXA reduced all-cause mortality in non-surgical patients without increasing the risk of arterial or venous thrombotic complications (7). Taeuber et al. (38), in a meta-analysis of 216 studies, concluded that intravenous TXA, regardless of the dose, is not associated with an increased risk of thromboembolic events and is safe for neurological patients.

Limitations

While the results of this systematic review are optimistic regarding the role of TXA as primary or adjuvant therapy in the surgical management of cSDH, some limitations need to be addressed. Firstly, many of the studies included in the analysis had a limited sample size and retrospective design. Among the clinical trials, there is a notable risk of bias due to the possibility of unblinding. Additionally, the follow-up period was less than 12 months in the examined studies, limiting the assessment of outcomes, particularly recurrence and late adverse effects of the medication. Furthermore, a meta-analysis was not performed due to the heterogeneity of the articles considered in this review.

It is suggested that multicenter randomized clinical trials with a larger number of participants and meta-analyses be conducted to obtain a higher level of confidence regarding the use of TXA in the treatment of cSDH. Given the limitation of currently available evidence, two larger-scale clinical trials are underway. The TRACS study is a phase IIB, multicenter, double-blind, randomized, placebo-controlled study with an expected completion date of June 2025 (19). Its aim is to determine if TXA can increase the rate of cSDH resolution, obviating the need for surgical intervention. The study intends to evaluate, in addition to clinical parameters, the impact of treatment on cognitive function, functional autonomy, and quality of life. Another phase III study, called TORCH (18), with an expected completion date in 2024, seeks to analyze the efficacy of the antifibrinolytic as a primary treatment in cSDH.

CONCLUSION

In summary, this systematic review suggests that TXA can be considered a safe and effective therapeutic adjunct in the surgical management of cSDH. Evidence regarding the use of the antifibrinolytic as primary, non-operative treatment is still limited. It is suggested to continue with further studies involving larger sample sizes to establish its role in neurosurgical practice conclusively.

Declarations

Funding: The authors have no personal, financial, or institutional interest in any of the materials or devices portrayed in this article. I, Beatriz Rodrigues Messias, certify that this manuscript is a unique submission and is not being considered for publication, in part or in full, with any other source in any medium. This publication is accepted by all authors. There is no financial support.

Availability of data and materials: The datasets generated and/or analyzed during the current study are available from the corresponding author by reasonable request.

Disclosure: The authors declare no competing interests.

AUTHORSHIP CONTRIBUTION

Study conception and design: AFG, BRM, JPMB
Data collection: BRM, JPMB
Analysis and interpretation of results: AFG, BRM, JPMB
Draft manuscript preparation: BRM
Critical revision of the article: AFG, BRM, JPMB
Other (study supervision, fundings, materials, etc...): AFG
All authors (BRM, JPMB, AFG) reviewed the results and approved the final version of the manuscript.

REFERENCES

1. Albalkhi I, Alaswad M, Saleh T, Senjab A, Helal B, Khan JA: Adjuvant tranexamic acid for reducing postoperative recurrence of chronic subdural hematoma in the elderly: A systematic review and meta-analysis. World Neurosurg182:e829-e836, 2024. https://doi.org/10.1016/j.wneu.2023.12.054.
2. Balser D, Farooq S, Mehmood T, Reyes M, Samadani U: Actual and projected incidence rates for chronic subdural hematomas in United States Veterans Administration and civilian populations. J Neurosurg 123:1209-1215, 2015. https://doi.org/10.3171/2014.9.JNS141550.
3. Brennan PM, Kolias AG, Joannides AJ, Shapey J, Marcus HJ, Gregson BA, Grover PJ, Hutchinson PJ, Coulter IC; British Neurosurgical Trainee Research Collaborative. The management and outcome for patients with chronic subdural hematoma: A prospective, multicenter, observational cohort study in the United Kingdom. J Neurosurg 127:732-739, 2017. https://doi.org/10.3171/2016.8.JNS16134.

4. Chapin JC, Hajjar KA: Fibrinolysis and the control of blood coagulation. Blood Rev 29:17-24, 2015. https://doi.org/10.1016/j.blre.2014.09.003.
5. Chauncey JM, Wieters JS: Tranexamic acid. In: StatPearls [website]. Treasure Island (FL): StatPearls Publishing. Available at: https://www.ncbi.nlm.nih.gov/books/NBK532909/. Accessed March 27, 2024.
6. Chen JW, Xu JC, Malkasian D, Perez-Rosendahl MA, Tran DK: The mini-craniotomy for cSDH revisited: New perspectives. Front Neurol 12:660885, 2021. https://doi.org/10.3389/fneur.2021.660885.
7. Chornenki NLJ, Um KJ, Mendoza PA, Samienezhad A, Swarup V, Chai-Adisaksopha C, Siegal DM: Risk of venous and arterial thrombosis in non-surgical patients receiving systemic tranexamic acid: A systematic review and meta-analysis. Thromb Res 79:81-86, 2019. https://doi.org/10.1016/j.thromres.2019.05.003.
8. CRASH-3 trial collaborators: Effects of tranexamic acid on death, disability, vascular occlusive events and other morbidities in patients with acute traumatic brain injury (CRASH-3): A randomised, placebo-controlled trial. Lancet 394:1713-1723, 2019. Erratum in: Lancet 394:1712, 2019.
9. de Paula MVCT, Ribeiro BDC, Melo MM, de Freitas PVV, Pahl FH, de Oliveira MF, Rotta JM: Effect of postoperative tranexamic acid on recurrence rate and complications in chronic subdural hematomas patients: Preliminary results of a randomized controlled clinical trial. Neurosurg Rev 46:90, 2023. https://doi.org/10.1007/s10143-023-01991-9.
10. Dian J, Linton J, Shankar JJ: Risk of recurrence of subdural hematoma after EMMA vs surgical drainage - Systematic review and meta-analysis. Interv Neuroradiol 27:577-583, 2021. https://doi.org/10.1177/1591019921990962.
11. Edlmann E, Giorgi-Coll S, Whitfield PC, Carpenter KLH, Hutchinson PJ: Pathophysiology of chronic subdural haematoma: Inflammation, angiogenesis and implications for pharmacotherapy. J Neuroinflammation 14:108, 2017. https://doi.org/10.1186/s12974-017-0881-y.
12. Ewald GA, Eisenberg PR: Plasmin-mediated activation of contact system in response to pharmacological thrombolysis. Circulation 91:28-36, 1995. https://doi.org/10.1161/01.cir.91.1.28.
13. Fujisawa H, Ito H, Kashiwagi S, Nomura S, Toyosawa M: Kallikrein-kinin system in chronic subdural haematomas: Its roles in vascular permeability and regulation of fibrinolysis and coagulation. J Neurol Neurosurg Psychiatry 59:388-394, 1995. https://doi.org/10.1136/jnnp.59.4.388.
14. Grant FC: Chronic subdural haematoma. Ann Surg 86:485-493, 1927. https://doi.org/10.1097/00000658-192710000-00003.
15. Holl DC, Volovici V, Dirven CMF, Peul WC, van Kooten F, Jellema K, van der Gaag NA, Miah IP, Kho KH, den Hertog HM, Lingsma HF, Dammers R; Dutch Chronic Subdural Hematoma Research Group (DSHR): Pathophysiology and nonsurgical treatment of chronic subdural hematoma: From Past to present to future. World Neurosurg 116:402-411.e2, 2018. https://doi.org/10.1016/j.wneu.2018.05.037.
16. Hunt BJ: The current place of tranexamic acid in the management of bleeding. Anaesthesia 70 Suppl 1:50-53, e18, 2015. https://doi.org/10.1111/anae.12910.
17. Hutchinson PJ, Edlmann E, Bulters D, Zolnourian A, Holton P, Suttner N, Agyemang K, Thomson S, Anderson IA, Al-Tamimi YZ, Henderson D, Whitfield PC, Gherle M, Brennan PM, Allison A, Thelin EP, Tarantino S, Pantaleo B, Caldwell K, Davis-Wilkie C, Mee H, Warburton EA, Barton G, Chari A, Marcus HJ, King AT, Belli A, Myint PK, Wilkinson I, Santarius T, Turner C, Bond S, Kolias AG; British Neurosurgical Trainee Research Collaborative; Dex-CSDH Trial Collaborators: Trial of dexamethasone for chronic subdural hematoma. N Engl J Med 383:2616-2627, 2020. https://doi.org/10.1056/NEJMoa2020473.
18. Immenga S, Lodewijkx R, Roos YBWEM, Middeldorp S, Majoie CBLM, Willems HC, Vandertop WP, Verbaan D: Tranexamic acid to prevent operation in chronic subdural haematoma (TORCH): Study protocol for a randomised placebo-controlled clinical trial. Trials 23:56, 2022. https://doi.org/10.1186/s13063-021-05907-0.
19. Iorio-Morin C, Blanchard J, Richer M, Mathieu D: Tranexamic acid in chronic subdural hematomas (TRACS): Study protocol for a randomized controlled trial. Trials 17:235, 2016. https://doi.org/10.1186/s13063-016-1358-5.
20. Kim HC, Ko JH, Yoo DS, Lee SK: Spontaneous resolution of chronic subdural hematoma: Close observation as a treatment strategy. J Korean Neurosurg Soc 59:628-636, 2016. https://doi.org/10.3340/jkns.2016.59.6.628.
21. Kolias AG, Chari A, Santarius T, Hutchinson PJ: Chronic subdural haematoma: Modern management and emerging therapies. Nat Rev Neurol 10:570-578, 2014. https://doi.org/10.1038/nrneurol.2014.163.
22. Kageyama H, Toyooka T, Tsuzuki N, Oka K: Nonsurgical treatment of chronic subdural hematoma with tranexamic acid. J Neurosurg 119:332-337, 2013. https://doi.org/10.3171/2013.3.JNS122162.
23. Kutty RK, Leela SK, Sreemathyamma SB, Sivanandapanicker JL, Asher P, Peethambaran A, Prabhakar RB: The outcome of medical management of chronic subdural hematoma with tranexamic acid - a prospective observational study. J Stroke Cerebrovasc Dis 29:105273, 2020. dhttps://doi.org/10.1016/j.jstrokecerebrovasdis.2020.105273.
24. Lodewijkx R, Immenga S, van den Berg R, Post R, Westerink LG, Nabuurs RJA, Can A, Vandertop WP, Verbaan D: Tranexamic acid for chronic subdural hematoma. Br J Neurosurg 35:564-569, 2021. https://doi.org/10.1080/02688697.2021.1918328.
25. Mascolo A, Scavone C, Scisciola L, Chiodini P, Capuano A, Paolisso G: SGLT-2 inhibitors reduce the risk of cerebrovascular/cardiovascular outcomes and mortality: A systematic review and meta-analysis of retrospective cohort studies. Pharmacol Res 172:105836, 2021. https://doi.org/10.1016/j.phrs.2021.105836.
26. McGuinness LA, Higgins JPT: Risk-of-bias VISualization (robvis): An R package and Shiny web app for visualizing risk-of-bias assessments. Res Synth Methods 12:55-61, 2021. https://doi.org/10.1002/jrsm.1411.

27. Ng W, Jerath A, Wąsowicz M: Tranexamic acid: A clinical review. Anaesthesiol Intensive Ther 47:339-350, 2015. https://doi.org/10.5603/AIT.a2015.0011.
28. Page MJ, McKenzie JE, Bossuyt PM, Boutron I, Hoffmann TC, Mulrow CD, Shamseer L, Tetzlaff JM, Akl EA, Brennan SE, Chou R, Glanville J, Grimshaw JM, Hróbjartsson A, Lalu MM, Li T, Loder EW, Mayo-Wilson E, McDonald S, McGuinness LA, Stewart LA, Thomas J, Tricco AC, Welch VA, Whiting P, Moher D: The PRISMA 2020 statement: An updated guideline for reporting systematic reviews. BMJ 372:n71, 2021. https://doi.org/10.1136/bmj.n71.
29. Puente Tinoco MR, Reyes Graterol EO, García Oduber SM: Recuperación de pacientes en postoperatorio de drenaje de hematoma subdural crónico asociado al uso de ácido tranexámico. Rev Chil Neurocirugía 42:45-51, 2016. Available at: https://www.neurocirugiachile.org/pdfrevista/v42_n1_2016/puente_p45_v42n1_2016.pdf. Accessed February 17, 2024. https://doi.org/10.36593/rev.chil.neurocir.v42i1.93
30. Ridwan S, Bohrer AM, Grote A, Simon M: Surgical treatment of chronic subdural hematoma: Predicting recurrence and cure. World Neurosurg 128:e1010-e1023, 2019. https://doi.org/10.1016/j.wneu.2019.05.063.
31. Santarius T, Kirkpatrick PJ, Ganesan D, Chia HL, Jalloh I, Smielewski P, Richards HK, Marcus H, Parker RA, Price SJ, Kirollos RW, Pickard JD, Hutchinson PJ: Use of drains versus no drains after burr-hole evacuation of chronic subdural haematoma: A randomised controlled trial. Lancet 374:1067-1073, 2009. https://doi.org/10.1016/S0140-6736(09)61115-6.
32. Santarius T, Kirkpatrick PJ, Kolias AG, Hutchinson PJ: Working toward rational and evidence-based treatment of chronic subdural hematoma. Clin Neurosurg 57:112-122, 2010.
33. Shea BJ, Reeves BC, Wells G, Thuku M, Hamel C, Moran J, Moher D, Tugwell P, Welch V, Kristjansson E, Henry DA: AMSTAR 2: A critical appraisal tool for systematic reviews that include randomised or non-randomised studies of healthcare interventions, or both. BMJ 358:j4008, 2017. https://doi.org/10.1136/bmj.j4008.
34. Soleman J, Nocera F, Mariani L: The conservative and pharmacological management of chronic subdural haematoma. Swiss Med Wkly 147:w14398, 2017. https://doi.org/10.57187/smw.2017.14398.
35. Solou M, Ydreos I, Gavra M, Papadopoulos EK, Banos S, Boviatsis EJ, Savvanis G, Stavrinou LC: Controversies in the surgical treatment of chronic subdural hematoma: A systematic scoping review. Diagnostics 12:2060, 2022. https://doi.org/10.3390/diagnostics12092060.
36. Sterne JAC, Savović J, Page MJ, Elbers RG, Blencowe NS, Boutron I, Cates CJ, Cheng HY, Corbett MS, Eldridge SM, Emberson JR, Hernán MA, Hopewell S, Hróbjartsson A, Junqueira DR, Jüni P, Kirkham JJ, Lasserson T, Li T, McAleenan A, Reeves BC, Shepperd S, Shrier I, Stewart LA, Tilling K, White IR, Whiting PF, Higgins JPT: RoB 2: A revised tool for assessing risk of bias in randomised trials. BMJ 366:l4898, 2019. https://doi.org/10.1136/bmj.l4898.
37. Suzuki M, Endo S, Inada K, Kudo A, Kitakami A, Kuroda K, Ogawa A: Inflammatory cytokines locally elevated in chronic subdural haematoma. Acta Neurochir 140:51-55, 1998. https://doi.org/10.1007/s007010050057.
38. Taeuber I, Weibel S, Herrmann E, Neef V, Schlesinger T, Kranke P, Messroghli L, Zacharowski K, Choorapoikayil S, Meybohm P: Association of intravenous tranexamic acid with thromboembolic events and mortality: A systematic review, meta-analysis, and meta-regression. JAMA Surg 156:e210884, 2021. https://doi.org/10.1001/jamasurg.2021.0884.
39. Tanweer O, Frisoli FA, Bravate C, Harrison G, Pacione D, Kondziolka D, Huang PP: Tranexamic acid for treatment of residual subdural hematoma after bedside twist-drill evacuation. World Neurosurg 91:29-33, 2016. https://doi.org/10.1016/j.wneu.2016.03.062.
40. Toi H, Kinoshita K, Hirai S, Takai H, Hara K, Matsushita N, Matsubara S, Otani M, Muramatsu K, Matsuda S, Fushimi K, Uno M: Present epidemiology of chronic subdural hematoma in Japan: Analysis of 63,358 cases recorded in a national administrative database. J Neurosurg 128:222-228, 2018. https://doi.org/10.3171/2016.9.JNS16623.
41. Wan KR, Qiu L, Saffari SE, Khong WXL, Ong JCL, See AA, Ng WH, King NKK: An open label randomized trial to assess the efficacy of tranexamic acid in reducing post-operative recurrence of chronic subdural haemorrhage. J Clin Neurosci 82:147-154, 2020. https://doi.org/10.1016/j.jocn.2020.10.053.
42. Weigel R, Schmiedek P, Krauss JK: Outcome of contemporary surgery for chronic subdural haematoma: Evidence based review. J Neurol Neurosurg Psychiatry 74:937-943, 2003. https://doi.org/10.1136/jnnp.74.7.937.
43. Wells GA, Shea B, O'Connel D, Peterson J, Welch V, Losos M, Tugwell P: The Newcastle-Ottawa scale (NOS) for assessing the quality of nonrandomised studies in meta-analyses. Available at: http://www ohri ca/programs/clinical_epidemiology/oxford. Accessed March 10, 2024.
44. Yamada T, Natori Y: Prospective study on the efficacy of orally administered tranexamic acid and goreisan for the prevention of recurrence after chronic subdural hematoma burr hole surgery. World Neurosurg 134:e549-e553, 2020. https://doi.org/10.1016/j.wneu.2019.10.134.
45. Yang K, Kim KH, Lee HJ, Jeong EO, Kwon HJ, Kim SH: Role of adjunctive tranexamic acid in facilitating resolution of chronic subdural hematoma after surgery. J Korean Neurosurg Soc 66:446-455, 2023. https://doi.org/10.3340/jkns.2022.0200.
46. Yang W, Huang J: Chronic subdural hematoma: Epidemiology and natural history. Neurosurg Clin N Am 28:205-210, 2017. https://doi.org/10.1016/j.nec.2016.11.002.
47. Yu W, Chen W, Jiang Y, Ma M, Zhang W, Zhang X, Cheng Y: Effectiveness comparisons of drug therapy on chronic subdural hematoma recurrence: A bayesian network meta-analysis and systematic review. Front Pharmacol 13:845386, 2022. https://doi.org/10.3389/fphar.2022.845386.

Turk Neurosurg 35(4):537-545, 2025
DOI: 10.5137/1019-5149.JTN.48420-25.2

Original Investigation

Cerebrovascular-Endovascular

Received: 14.01.2025
Accepted: 08.04.2025
Published Online: 25.06.2025

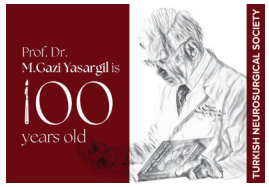

The Initial Experience of Turkish Neurosurgical Stroke Centers: A National Study

Serkan CIVLAN[1], Caghan TONGE[2], Emrah KESKIN[3], Cagri ELBIR[2], Goktug ULKU[2], Mehmet Selim GEL[4], Batuhan BAKIRARAR[5], Iskender Samet DALTABAN[6], Mert NAZIK[7], Ramazan FESLI[8], Eylem TEKE[9], Nazar CILTEMEK[1], Mustafa ARICI[1], Nevzat Dogukan ERBEK[1], Mehmet Erdal COSKUN[1], Mehmet Erhan TURKOGLU[10], Fatih YAKAR[1]

[1]Pamukkale University, School of Medicine, Department of Neurosurgery, Denizli, Türkiye
[2]Etlik City Hospital, Department of Neurosurgery, Ankara, Türkiye
[3]Zonguldak Bulent Ecevit University, Department of Neurosurgery, Zonguldak, Türkiye
[4]Kanuni Training and Research Hospital, Department of Neurosurgery, Trabzon, Türkiye
[5]Ado Group, Process Management Coordinator, Antalya, Türkiye
[6]A Life Health Group Hospital, Department of Neurosurgery, Ankara, Türkiye
[7]Balikesir Atatürk State Hospital, Department of Neurosurgery, Balikesir, Türkiye
[8]VM Medical Park Mersin Hospital, Department of Neurosurgery, Mersin, Türkiye
[9]Pamukkale University, School of Medicine, Department of Neurology, Denizli, Türkiye
[10]TOBB ETU School of Medicine Hospital, Department of Neurosurgery, Ankara, Türkiye

Corresponding author: Serkan CIVLAN ✉ serkancivlan@hotmail.com

ABSTRACT

AIM: To evaluate the clinical and radiological outcomes of newly established Turkish neurosurgical stroke centers , and to assess their competency in managing acute ischemic stroke from June 2023 to June 2024.

MATERIAL and METHODS: We retrospectively analyzed data from 69 patients (mean age = 69.06 ± 13.48 years) from three stroke centers in Türkiye by reviewing hospital records and patient interviews, focusing on demographic variables, comorbidities, treatment methodologies, outcomes (using the Modified Rankin Scale (mRS)), stroke severity (using the National Institutes of Health Stroke Scale [NIHSS]), Alberta Stroke Program Early CT (ASPECT) scores, reperfusion status (using the modified Thrombolysis in Cerebral Ischemia (mTICI) score), complications, blood glucose levels, and creatinine levels.

RESULTS: Of 392 acute ischemic stroke patients, 280 (71.4%) had no identifiable occlusion, 43 (11%) were out of the MT time window, and 69 (17.6%) underwent MT, with 57 (14.5%) having LVO and 12 (3%) MVO. Final reperfusion (mTICI ≥2b) was achieved in 78.3% of MT patients, and 29% achieved favorable outcomes (mRS ≤2) at three months. Younger age, lower baseline NIHSS, and higher ASPECT scores correlated with better outcomes, while elevated blood glucose (>127.50 mg/dL) and creatinine (>0.80 mg/dL) were linked to worse mRS scores. Complications occurred in 21.7%, including symptomatic intracranial hemorrhage in six patients.

CONCLUSION: While Turkish neurosurgical stroke centers have made significant strides in managing acute ischemic stroke, challenges remain in optimizing patient outcomes. This initial experience underscores the need for further research, continued training, and educational standardization for neurosurgeons in endovascular techniques to improve patient care.

KEYWORDS: Acute ischemic stroke, Mechanical thrombectomy, Stroke center, Neurosurgeon

Serkan CIVLAN : 0000-0001-8915-8186
Caghan TONGE : 0000-0002-9921-1750
Emrah KESKIN : 0000-0001-5326-741X
Cagri ELBIR : 0000-0002-8747-2187
Goktug ULKU : 0000-0003-1430-2977
Mehmet Selim GEL : 0000-0002-3678-5538
Batuhan BAKIRARAR : 0000-0002-5662-8193
I. Samet DALTABAN : 0000-0002-5786-2272
Mert NAZİK : 0000-0001-5086-2301
Ramazan FESLI : 0000-0003-2373-0164
Eylem TEKE : 0009-0002-1398-5753
Nazar CILTEMEK : 0009-0000-1900-8166
Mustafa ARICI : 0000-0003-2947-2880
Nevzat Dogukan ERBEK : 0009-0001-1995-5611
Mehmet Erdal COSKUN : 0000-0002-2816-0722
Mehmet Erhan TURKOGLU : 0000-0001-7044-617X
Fatih YAKAR : 0000-0001-7414-3766

ABBREVIATIONS: Mrs: Modified rankin scale, **NIHSS:** National institutes of health stroke scale, **LVO:** Large vessel occlusion, **MVO:** Medium vessel occlusion, **ASPECT:** Alberta stroke program early CT, **Mtici:** Modified thrombolysis in cerebral ıschemia, **ESO:** European stroke organization, **AHA:** American heart association, **ASA:** American stroke association, **MT:** Mechanical thrombectomy, **TA:** Thromboaspiration, **CT:** Computed tomography, **MRI:** Magnetic resonance imaging, **ICH:** Intracranial hemorrhage, **DWI:** Diffusion-weighted imaging, **IV-Tpa:** Intravenous tissue plasminogen activator, **SBP:** Systolic blood pressure, **WBC:** White blood cell, **DC:** Decompressive hemicraniectomy, **Sich:** Symptomatic ICH, **IQR:** Interquartile range, **ROC:** Receiver operating characteristic, **ICA-T:** Internal carotid artery terminus, **MCA:** Middle cerebral artery, **BA:** Basilar artery, **SAH:** Subarachnoid hemorrhage, **EVD:** External ventricular drainage, **AUC:** Area under the curve

INTRODUCTION

Stroke is the second leading cause of death and a major reason for disability across the globe. The burden of stroke has been consistently increasing, particularly in low- and middle-income countries (13). Since 2015, multiple pivotal randomized controlled trials have been published that revolutionized the management of acute ischemic stroke (5,6,14,15). The current guidelines for the management of acute stroke given by the European Stroke Organization (ESO) (32), and the American Heart Association (AHA)/American Stroke Association (ASA) recommend thrombolysis, mechanical thrombectomy (MT), and thromboaspiration (TA) as the primary treatment methods (16). Among these, MT is a recent and well-researched technique, which, in conjunction with intravenous thrombolysis, is considered the gold standard for the management of ischemic strokes of the anterior cerebral vessels within the first 6 hours (24).

Earlier, endovascular treatments in Türkiye were administered exclusively by radiologists; however, over the past 20 years, neurosurgeons have also been receiving training in endovascular techniques, particularly in countries like Japan and South Korea. Eventually, these neurosurgeons started practicing endovascular procedures and established hybrid neurosurgery clinics in Türkiye, leading to significant advancements in stroke interventions. In 2019, the Turkish Ministry of Health issued the Stroke Centers Directive authorizing specialists in radiology, neurology, neurosurgery, and cardiology to perform interventional procedures for stroke treatment, along with establishing the required case volumes for practitioners. This national-level study evaluated the clinical and radiological outcomes of the newly established neurosurgical stroke centers in Türkiye over one year to determine their competency levels.

MATERIAL and METHODS

Ethics approval was obtained from Pamukkale University Non-Interventional Clinical Research Ethics Committee, with the approval number 14 and date 06.08.2024.

Study Design and Sample Selection Criteria

In Turkish stroke centers, patients arriving at the emergency department are initially evaluated by emergency medicine specialists. Following this, a consultation with the neurology clinic is promptly initiated. Occlusions of the internal carotid artery terminus (ICA-T), M1 branch of the middle cerebral artery (MCA), and basilar artery (BA) are classified as large vessel occlusions (LVO), while occlusions of the M2 and M3 branches of the MCA, as well as the anterior and posterior cerebral arteries, are considered medium vessel occlusions (MVO) (26). If the neurology team determines an indication for mechanical thrombectomy after clinical and radiological assessment (e.g., identifying LVO or MVO), the patient is referred to a specialist from radiology, neurology, neurosurgery, or cardiology for the procedure, depending on the center's expertise and resources.

In this study, we retrospectively reviewed patient data from three stroke centers in Türkiye obtained through hospital systems and telephone interviews from June 2023 to June 2024. Ethical approval was obtained from the relevant ethics committee prior to conducting the study. Patients aged ≥18 years who were treated at these stroke centers were assessed for demographic variables, comorbidities, treatment methodologies, and outcomes measured by the Modified Rankin Scale (mRS). Patients were considered eligible for MT if they had a large vessel occlusion (determined by computed tomography (CT) or magnetic resonance imaging (MRI) angiography) and a National Institutes of Health Stroke Scale (NIHSS) score of ≥6 upon admission; intracranial hemorrhage (ICH) was ruled out via a non-contrast CT scan. Additionally, patients were included if they presented within the first 6 h and the infarct involved less than one-third of the territory as shown on a diffusion-weighted (DWI) MRI. With symptom onset of ≥6 hours, the presence of a DWI-Fluid-Attenuated Inversion Recovery mismatch was used as the criteria to undergo MT. Patients with posterior circulation strokes were not excluded. For those arriving within the first 4.5 h, intravenous tissue plasminogen activator (tPA) (IV-tPA) was administered in the Neurology Department (16).

Data for the following variables were extracted for all patients – age, gender, comorbidities, presence of myocardial infarction at the time of stroke, use of premorbid oral anticoagulants, current smoking status, time from the last "known well" status to hospital arrival, door-to-puncture time, systolic blood pressure (SBP), blood glucose levels, white blood cell (WBC) count, creatinine levels, pre-stroke mRS scores, baseline NIHSS scores, Alberta Stroke Program Early CT (ASPECT) scores, use of tPA, occlusion site, treatment types, manufacturer details of the thrombectomy device, complications including hemorrhage and reperfusion, need for decompressive hemicraniectomy (DC), the modified Thrombolysis in Cerebral Ischemia (mTICI) score, and mRS scores three months after the procedure.

All angiographic evaluations were conducted using the mTICI scale – mTICI grades ≤2a indicate unsuccessful recanalization, whereas grades 2b and 3 indicate successful recanalization (7). A non-contrast CT or MRI was routinely performed within 24 hours of the treatment or immediately after the procedure if the patient exhibited symptoms. Symptomatic ICH (sICH) was defined as an intracranial bleed that resulted in clinical deterioration, indicated by an increase of 4 points on the NIHSS (2). In the third month, patients with an mRS score of 0–2 were considered to have a favorable outcome, while those with an mRS score of 3–6 were classified as having a poor outcome (11).

We evaluated 392 acute ischemic stroke patients. Of these, 280 (71.4%) had no identifiable intracranial vascular occlusion, 43 (11%) were deemed out of the thrombectomy time window due to hyperintensity on MRI FLAIR sequences at presentation, and 69 (17.6%) met the inclusion criteria for MT. Within this cohort, LVO were identified in 57 patients (14.5%), and MVO in 12 patients (3%).

Endovascular Procedures

All procedures were performed under local anesthesia, with vital signs being continuously monitored through anesthesia monitoring for all patients. Arterial punctures could be performed using the transfemoral, transradial (18), or direct carotid (35) approaches; in our study, only the transfemoral approach was used. Initially, a diagnostic cerebral angiogram was conducted to determine the site of the intracranial clot. A 6-French long introducer sheath (Heety: Barty Medical, Hangzhou City, Zhejiang Province, China, or Infinity: Stryker, Ireland) was advanced into the most distal segment of the internal carotid artery. For thrombectomy procedures, when TA was planned, a distal aspiration catheter, such as SOFIA (MicroVention-Terumo, Tustin, CA, USA), Catalyst (Stryker, Ireland), Neurocatch (Taha Biomedical, Turkey), Glutton (Plusmedica, Düsseldorf, Germany), or Cylon (Zylon Tonbridge, Zhejiang Province, China) was used. In addition, a microcatheter (Excelsior XT-27, Stryker, Natick, MA), guidewire (Synchro; Stryker, Fremont, CA), and stent retriever (Aperio Hybrid: Acandis, Pforzheim, Germany, Trevo: Stryker Neurovascular, Fremont, CA, or Solitaire: ev3/Covidien, Irvine, CA) were used. Intra- or extracranial arterial stenoses were treated with balloon angioplasty (Micro Therapeutics, Irvine, CA, USA) and carotid stenting (Protégé; Medtronic, USA).

Statistical Analysis

All analyses were performed using SPSS (version 11.5). Descriptive statistics were presented as mean ± standard deviation and median (interquartile range, IQR) for continuous variables, while frequencies (percentages) were used for categorical variables. Between-group comparisons for continuous variables were performed using Student's t-test or the Mann-Whitney U test based on the normality of data distribution. Categorical variables were compared using Chi-square and Fisher's exact tests were employed. To determine the optimal cutoff value for distinguishing between favorable and poor outcomes for the 3-month mRS score, a receiver operating characteristic (ROC) curve analysis was performed and the Youden Index was computed. A p-value of <0.05 was used to determine statistical significance.

RESULTS

We included 69 patients (37 females, 53.6%) in the study with a mean age of 69.06 ± 13.48 years (Table I). The most common comorbidities identified in the study cohort were hypertension (n=27, 39.13%), coronary artery disease (n=16, 23.19%), atrial fibrillation (n=9, 13.04%), diabetes mellitus (n=9, 13.04%), and heart failure (n=7, 10.14%). Table II presents a summary of the different comorbidities observed in the cohort.

The mean pre-stroke mRS score and the median (IQR) NIHSS score at admission of the study cohort were 0.072 ± 0.312 (range: 0–2; median 0) and 15 (5–24), respectively. The occlusion was located in the ICA-T in 13 patients (18.8%) one of which was a tandem occlusion, the M1 segment in 41 patients (59.4%), the M2 segment in 12 patients (17.4%), the BA trunk in two patients (2.9%), and the BA tip in one patient (1.5%). Seven of the 13 ICA occlusions were on the right side, while 25 out of the 41 M1 occlusions were right-sided; out of the 12 M2 occlusions, eight cases were left-sided. The median (IQR) ASPECT score on initial imaging was 8 (4–10). The median (IQR) time from last "known well" status to hospital arrival was 3 hours (0–6 hours), while the median (IQR) door-to-puncture time was 1 hour (1–5 hours) (Table I).

Regarding treatment methodologies, MT was performed in nine patients (13%), MT plus TA in 39 patients (56.5%), and TA alone in 21 patients (30.5%). Additionally, two patients received intraarterial tPA, carotid stenting was done in two patients, and balloon angioplasty in six patients (Table I). Final nearly complete reperfusion (mTICI grade ≥2b) was achieved in 54 of the 69 patients (78.3%), while complete reperfusion (mTICI grade 3) was noted in 41 patients (59.4%).

Treatment-related complications were observed in 15 patients (21.7%) (Table I) – nine patients experienced subarachnoid hemorrhage (SAH), while six patients had sICH. DC was performed in 12 patients (including four cases of external ventricular drainage, EVD), and EVD alone was performed in two patients.

At the third-month follow-up, the median (IQR) mRS score of the study cohort was 4 (0–6). Statistically significant differences were observed between patients with favorable (0–2) and poor (3–6) mRS scores regarding age, baseline NIHSS score, ASPECT score, complication rates, and use of DC ($p < 0.05$ each). The average age of patients with poor mRS scores was 71.96 ± 11.04 years compared to 61.95 ± 16.37 years for those with favorable mRS scores. Likewise, patients with poor mRS had significantly higher baseline NIHSS scores, whereas those with favorable mRS had higher ASPECT scores. None of the patients with complications had a favorable mRS score at the 3-month follow-up, whereas 37% of those without complications had a favorable mRS. Additionally, none of the patients who underwent DC had a favorable mRS, compared to 35.1% of those who did not undergo DC (Table I).

Table I: Baseline Demographic and Clinical Characteristics of the Study Patients Stratified Based on the mRS Score at the Third-Month Follow-Up (n=69)

Variables		mRS Score			p-value
		Overall	Poor	Favorable	
Age (years)	Mean ± SD	69.06 ± 13.48	71.96 ± 11.04	61.95 ± 16.37	**0.010[b]**
	Median (Min–Max.)	71.00 (19.00–90.00)	73.00 (41.00–90.00)	67.00 (19.00–81.00)	
Gender, n (%)	Female	37 (53.6)	25 (67.6)	12 (32.4)	0.497[c]
	Male	32 (46.4)	24 (75.0)	8 (25.0)	
Comorbidity, n (%)	No	6 (8.7)	2 (33.3)	4 (66.7)	0.054[d]
	Yes	63 (91.3)	47 (74.6)	16 (25.4)	
Myocard Infractus, n (%)	No	67 (97.1)	48 (71.6)	19 (28.4)	0.499[d]
	Yes	2 (2.9)	1 (50.0)	1 (50.0)	
Premorbid oral anticoagulants, n (%)	No	20 (29.0)	14 (70.0)	6 (30.0)	0.906[c]
	Yes	49 (71.0)	35 (71.4)	14 (28.6)	
Current smoker, n (%)	No	65 (94.2)	47 (72.3)	18 (27.7)	0.574[d]
	Yes	4 (5.8)	2 (50.0)	2 (50.0)	
Time from the last “known well” to hospital arrival (h)	Mean ± SD	3.14 ± 1.50	3.08 ± 1.67	3.28 ± 0.99	0.328[b]
	Median (Min.-Max.)	3.00 (0.00–6.00)	3.00 (0.00–6.00)	3.00 (1.00–5.50)	
Door to puncture time (h)	Mean ± SD	1.57 ± 0.86	1.68 ± 0.94	1.28 ± 0.53	0.096[b]
	Median (Min–Max.)	1.00 (1.00–5.00)	1.00 (1.00–5.00)	1.00 (1.00–3.00)	
Baseline NIHSS score	Mean ± SD	15.23 ± 4.69	16.69 ± 4.27	11.65 ± 3.69	**<0.001[a]**
	Median (Min–Max.)	15.00 (5.00–24.00)	17.00 (8.00–24.00)	12.00 (5.00–20.00)	
ASPECT Score	Mean ± SD	7.34 ± 1.78	7.00 ± 1.88	8.25 ± 1.06	**0.017[b]**
	Median (Min–Max.)	8.00 (4.00–10.00)	7.00 (4.00–10.00)	8.50 (6.00–10.00)	
tPA, n (%)	No	66 (95.7)	47 (71.2)	19 (28.8)	1.000[d]
	Yes	3 (4.3)	2 (66.7)	1 (33.3)	
Occlusion site, n (%)	BA	3 (4.3)	2 (66.7)	1 (33.3)	0.486[d]
	ICA	13 (18.8)	11 (84.6)	2 (15.4)	
	MCA	53 (76.9)	36 (67.9)	17 (32.1)	
Treatment, n (%)	MT	10 (14.5)	7 (70.0)	3 (30.0)	0.061[c]
	TA	21 (30.4)	11 (52.4)	10 (47.6)	
	MT+TA	38 (55.1)	31 (81.6)	7 (35.0)	
Complication, n (%)	No	54 (78.3)	34 (63.0)	20 (37.0)	**0.003[d]**
	Yes	15 (21.7)	15 (100.0)	0 (0.0)	
Decompressive Hemicraniectomy, n (%)	No	57 (82.6)	37 (64.9)	20 (35.1)	**0.014[d]**
	Yes	12 (17.4)	12 (100.0)	0 (0.0)	
TICI Score, n (%)	TICI < 2b	15 (21.7)	14 (93.3)	1 (6.7)	0.051[d]
	TICI ≥2b	54 (78.3)	35 (64.8)	19 (35.2)	

Mean: *Average,* ***SD:*** *Standard Deviation,* ***Min:*** *Minimum,* ***Max:*** *Maximum,* ***mRS:*** *Modified Rankin Scale,* ***TICI:*** *Thrombolysis in Cerebral Infarction,* ***tPA:*** *Tissue Plasminogen Activator,* ***ASPECT:*** *Alberta Stroke Program Early CT Score,* ***NIHSS:*** *National Institutes of Health Stroke Scale,* ***BA:*** *Basilar Artery,* ***MCA:*** *Middle Cerebral Artery,* ***ICA:*** *Internal Carotid Artery,* ***MT:*** *Mechanical Thrombectomy,* ***TA:*** *Thromboaspiration.*
[a]Student’s t-test, [b]Mann-Whitney U test, [c]Chi-Square test, [d]Fisher’s exact test

Table II: Summary of the Different Comorbidities Observed in the Cohort

Comorbidity	n (%)
Hypertension	27 (39.13)
Coronary artery disease	16 (23.19)
Atrial fibrillation	9 (13.04)
Diabetes mellitus	9 (13.04)
Heart failure	7 (10.14)
Chronic obstructive pulmonary disease	4 (5.80)
Coronary bypass surgery	5 (7.25)
Stenting	3 (4.35)
Mitral valve replacement	2 (2.90)
Rectum cancer	1 (1.45)
Schizophrenia	1 (1.45)
Hypertrophic cardiomyopathy	1 (1.45)
Epilepsy	1 (1.45)
Pneumonia	1 (1.45)
Hypothyroidism	1 (1.45)
Anxiety disorder	1 (1.45)
Parkinsonism	1 (1.45)
Breast cancer	1 (1.45)
Lung cancer	1 (1.45)
Nephrotic syndrome	1 (1.45)

Similarly, at the third-month follow-up, patients with favorable and poor mRS scores showed statistically significant differences concerning blood glucose and creatinine levels ($p < 0.05$), that is, those with a poor mRS score had significantly higher mean blood glucose and creatinine levels (Table III). The pre-stroke mRS values were favorable for all patients; however, by the third month, 71% of the patients experienced a deterioration in their mRS scores, while 29% maintained the same score.

Figure 1 presents the ROC curves for different variables affecting the mRS score at the 3-month follow-up. We did not find any significant area under the curve (AUC) value for SBP and WBC count in the ROC analysis. However, the ROC curve analyses for blood glucose levels and creatinine at 3 months for different mRS scores revealed statistically significant AUC values – blood glucose: cutoff=127.50 mg/dL (p=0.013; sensitivity=0.755; specificity=0.600); creatinine: cutoff=0.80 mg/dL (p<0.001; sensitivity=0.755; specificity=0.800) (Table IV).

DISCUSSION

Stroke is a critical global public health issue because of the high associated rates of morbidity and mortality (20,25). This initial stroke study exploring the effects of establishing dedicated stroke centers in Türkiye revealed that younger age, lower NIHSS scores at admission, and higher ASPECT scores were associated with favorable mRS outcomes three months after the stroke. The majority of patients (78.3%) achieved successful recanalization, and 29% of patients had a 3-month mRS score of ≤2. However, a significant proportion of patients (21.7%) developed complications. While these results may reflect low success rates compared to other studies (3,17,21,30), it is noteworthy that this is the first study

Table III: A Comparison of Different Parameters Affecting Outcomes (mRS scores) at the Third-Month Follow-up (n=69)

Parameter		mRS Score			
		Overall	Poor	Favorable	p-value
Systolic Blood Pressure (mmHg)	Mean ± SD	179.39 ± 30.94	177.72 ± 30.16	173.65 ± 28.51	0.529[a]
	Median (Min–Max)	180.00 (120.00–240.00)	180.00 (110.00–240.00)	180.00 (110.00–210.00)	
Blood Glucose (mg/dL)	Mean ± SD	168.06 ± 58.67	159.39 ± 55.73	138.15 ± 41.82	**0.013[a]**
	Median (Min–Max)	151.00 (100.00–362.00)	136.00 (96.00–362.00)	124.00 (96.00–245.00)	
White Blood Cell Count (K/uL)	Mean ± SD	11.82 ± 14.45	11.05 ± 12.30	9.14 ± 2.95	0.547[a]
	Median (Min–Max)	9.50 (0.78–106.00)	9.50 (0.78–106.00)	8.95 (4.76–14.50)	
Serum Creatinine (mg/dL)	Mean ± SD	1.17 ± 1.15	1.04 ± 0.99	0.73 ± 0.11	**<0.001[a]**
	Median (Min–Max)	1.01 (0.50–8.65)	0.87 (0.50–8.65)	0.73 (0.56–0.95)	

Mean: *Average,* ***SD:*** *Standard Deviation,* ***Min:*** *Minimum,* ***Max:*** *Maximum,* ***mRS:*** *Modified Rankin Scale.* [a]*Mann-Whitney U test*

reflecting the endovascular stroke treatment experiences of Turkish neurosurgeons.

In this study, TA was predominantly selected as the initial treatment method, as recommended in the existing literature (19). While a recent meta-analysis stated that there are no significant differences between MT and TA, they highlighted the inadequacy of current evidence to definitively determine the optimal surgical approach (31). Interestingly, the combined application of stent retrievers and TA as a first-line strategy yielded higher recanalization rates (mTICI grades 2b/3 and 3) but also presented a greater risk of SAH within 24 hours compared to direct aspiration alone. However, due to the limited number of cases in our study, we could not directly compare the effectiveness of the MT and combined methods. Despite significant technological advancements and high success rates, several randomized controlled trials have reported 4% to 29% complication rates associated with devices or procedures (5,6,14,15), which is comparable to the complication rates observed in our study (21.7%). Our complication rate of 21.7% aligns with ranges reported in landmark trials such as THRACE (5), where procedure-related complications ranged from 12% (excluding vasospasm) to 35% (including vasospasm), underscoring that our findings are within acceptable limits for an initial multicenter experience. The reported complication rate reflects the heterogeneity of experience across centers, ranging from those with emerging endovascular programs to those with more established expertise, providing a comprehensive snapshot of the national learning curve.

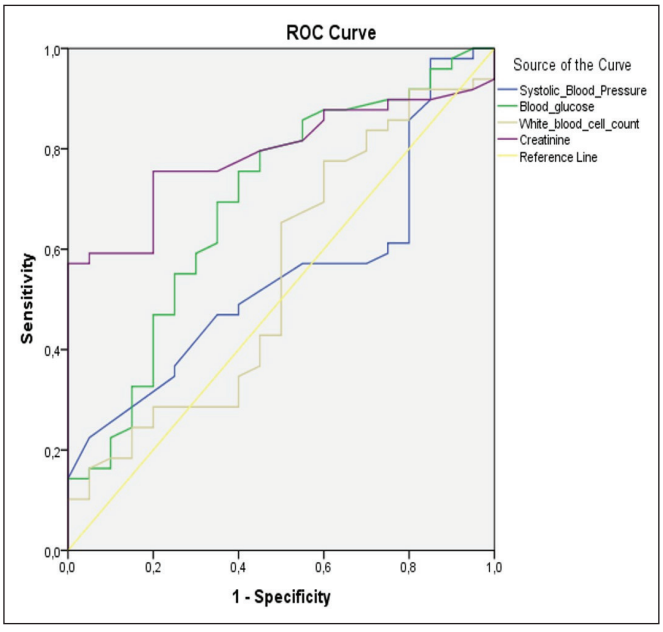

Figure 1: Receiver operating characteristic (ROC) curve for variables related to the Modified Rankin Scale (mRS) score at 3 months after stroke.

Table IV: A Comparison of Pre-Stroke Versus Third-Month mRS Scores

mRS Score		3rd Month		p-value
		Poor	Favorable	
Pre-stroke, n (%)	**Favorable**	49 (71.0)	20 (29.0)	-

mRS: *Modified rankin scale.*

Of 392 AIS patients assessed across the three centers from June 2023 to June 2024, 69 (17.6%) were eligible for MT. This included 57 patients with LVO (14.5%) and 12 with MVO (3%), proportions slightly higher than literature estimates of 11% for LVO and 9% for MVO (26). Current MT procedures in our series accounted for 5% of all AIS cases, 27% of all vascular occlusions (LVO + MVO), and 38% of LVO and M2 occlusions (26). These findings highlight the critical need for dedicated stroke centers to efficiently identify and treat this subgroup in Türkiye.

The key factors influencing favorable outcomes with posterior MT at discharge and the third-month follow-up include NIHSS scores, time to MT, and leukocytosis (4). A recent study comparing patients with anterior and posterior circulation strokes who underwent MT found that the latter had significantly lower NIHSS scores upon admission and at 24-hour post-MT (4); however, our analysis did not differentiate between anterior and posterior circulation strokes. Elevated WBC counts are associated with an increased risk of subsequent vascular events and mortality (33), whereas high SBP has been linked to unfavorable clinical outcomes. In our study, leukocytosis did not affect the three-month mRS scores, and we did not

Table V: Results of the Receiver Operating Characteristic (ROC) Curve Analysis for Variables Related to the mRS Score at Three Months After Stroke

Variables	Area	SE	p-value	95% CI for AUC (Lower-Upper)	Sensitivity	Specificity	Cut-off
Systolic Blood Pressure	0.548	0.073	0.530	0.406–0.691	0.224	0.950	205.00
Blood Glucose	0.692	0.072	**0.013**	0.551–0.833	0.755	0.600	127.50
White Blood Cell Count	0.546	0.079	0.547	0.393–0.700	0.766	0.400	7.35
Serum Creatinine	0.789	0.053	**<0.001**	0.685–0.893	0.755	0.800	0.80

SE: *Standard Error,* ***CI:*** *Confidence Interval,* ***mRS:*** *Modified Rankin Scale,* ***AUC:*** *Area Under the Curve.*

find any statistically significant correlation between WBC counts, SBP, and patient outcomes.

There is substantial evidence indicating that pre-stroke elevated glucose levels are linked to adverse effects in the acute phase of stroke, serving as an independent predictor of increased infarct size, poor clinical outcomes, and higher mortality risk (12,23). Additionally, indicators of renal function, specifically serum creatinine and estimated glomerular filtration rate, also serve as significant predictors of mortality and functional outcomes in individuals with acute stroke (27). In our study, both elevated glucose and creatinine levels correlated significantly with the three-month mRS score, consistent with the literature and indicating their contribution to poor outcomes.

An ASPECT score of ≤5 is linked to having a large infarct in the literature. A previous study on acute stroke patients found that thrombectomy combined with medical care resulted in improved functional outcomes and reduced mortality rates compared with medical care alone; however, it was also associated with a higher incidence of sICH (9). In our study, no additional assessments were performed for the group with an ASPECT score of ≤5.

Training standards, competency assessments, and credentialing requirements are essential for practitioners involved in stroke interventions (10,29). A Turkish study published educational standards for neuro-interventional procedures related to endovascular treatment of acute ischemic stroke and secondary endovascular protection, which were developed by interventional neurologists (22). As neurosurgeons, we aim to establish a similar level of educational standardization which may be disseminated nationwide through multidisciplinary approaches. At present, the Turkish Neurosurgery Society organizes biannual courses that incorporate models and simulation devices for teaching neuroendovascular treatments to stroke interventionists. Additionally, post marketing studies are available for various aspiration catheters and stent retrievers from different brands (1,28,34,36); however, there is a lack of comparative data regarding the effectiveness of thrombectomy and TA tools from different brands, primarily due to insufficient sample sizes.

Limitations

The retrospective design is a significant limitation of this study, which may introduce potential bias, as well as the small number of patients, which is less than ideal. Additionally, the varying learning curves and experiences of surgeons across different clinics represent further limitations that may have influenced the study's outcomes. Furthermore, due to the small number of posterior circulation strokes in our series, we were unable to compare the effectiveness of thrombectomy between anterior and posterior circulation strokes.

CONCLUSION

As stroke continues to be a significant public health concern, adopting a multidisciplinary approach is fundamental to its treatment. Over the past two decades, Turkish neurosurgeons have increasingly engaged in endovascular therapies for stroke treatment, evolving the treatment strategies from DC to hybrid surgery. Although the clinical and radiological outcomes presented in this study may not be as favorable as those reported in other recent studies, the current study represents a preliminary attempt to understand the effects of establishing dedicated stroke centers across Türkiye. Within this framework, we should train young neurosurgeons to become proficient in interventional therapies.

Declarations

Funding: Preparation for publication of this article is partly supported by Turkish Neurosurgical Society.

Availability of data and materials: The datasets generated and/or analyzed during the current study are available from the corresponding author by reasonable request.

Disclosure: The authors declare no competing interests.

AUTHORSHIP CONTRIBUTION

Study conception and design: SC, CT, EK, FY, ET

Data collection: CE, GU, MSG, ISD, MN, RF, NC, MA, NDE

Analysis and interpretation of results: BB

Draft manuscript preparation: SC, FY

Critical revision of the article: CT, MET, MEC

All authors (SC, CT, EK, CE, GU, MSG, BB, ISD, MN, RF, ET, NC, MA, NDE, MEC, MET, FY) reviewed the results and approved the final version of the manuscript.

REFERENCES

1. Akmangit I, Sayin B, Karaman A, Daglioglu E, Arli B, Sahin MH, Orhan G: Endovascular stroke therapy focused on direct clot aspiration using the SOFIATM catheter for acute ischemic stroke. Turk Neurosurg 32: 720-726, 2022. https://doi.org/10.5137/1019-5149.JTN.34409-21.3
2. Amaral S, Duloquin G, Béjot Y: Symptomatic Intracranial Hemorrhage after Ischemic Stroke Treated with Bridging Revascularization Therapy. Life (Basel) 13: 1593, 2023. https://doi.org/10.3390/life13071593
3. Berkhemer OA, Fransen PS, Beumer D, van den Berg LA, Lingsma HF, Yoo AJ, Schonewille WJ, Vos JA, Nederkoorn PJ, Wermer MJ, van Walderveen MA, Staals J, Hofmeijer J, van Oostayen JA, Lycklama à Nijeholt GJ, Boiten J, Brouwer PA, Emmer BJ, de Bruijn SF, van Dijk LC, Kappelle LJ, Lo RH, van Dijk EJ, de Vries J, de Kort PL, van Rooij WJ, van den Berg JS, van Hasselt BA, Aerden LA, Dallinga RJ, Visser MC, Bot JC, Vroomen PC, Eshghi O, Schreuder TH, Heijboer RJ, Keizer K, Tielbeek AV, den Hertog HM, Gerrits DG, van den Berg-Vos RM, Karas GB, Steyerberg EW, Flach HZ, Marquering HA, Sprengers ME, Jenniskens SF, Beenen LF, van den Berg R, Koudstaal PJ, van Zwam WH, Roos YB, van der Lugt A, van Oostenbrugge RJ, Majoie CB, Dippel DW; MR CLEAN Investigators: A randomized trial of intraarterial treatment for acute ischemic stroke. N Engl J Med 372: 11-20, 2015. https://doi.org/10.1056/NEJMoa1411587

4. Borończyk M, Kuźniak M, Borończyk A, Żak A, Binek Ł, Wagner-Kusz A, Lasek-Bal A: Efficacy and safety of mechanical thrombectomy in the posterior cerebral circulation-a single center study. Sci Rep 14: 7700, 2024. https://doi.org/10.1038/s41598-024-57963-6
5. Bracard S, Ducrocq X, Mas JL, Soudant M, Oppenheim C, Moulin T, Guillemin F; THRACE Investigators: Mechanical thrombectomy after intravenous alteplase versus alteplase alone after stroke (THRACE): A randomised controlled trial. Lancet Neurol 15: 1138-1147, 2016. https://doi.org/10.1016/S1474-4422(16)30177-6
6. Campbell BC, Mitchell PJ, Kleinig TJ, Dewey HM, Churilov L, Yassi N, Yan B, Dowling RJ, Parsons MW, Oxley TJ, Wu TY, Brooks M, Simpson MA, Miteff F, Levi CR, Krause M, Harrington TJ, Faulder KC, Steinfort BS, Priglinger M, Ang T, Scroop R, Barber PA, McGuinness B, Wijeratne T, Phan TG, Chong W, Chandra RV, Bladin CF, Badve M, Rice H, de Villiers L, Ma H, Desmond PM, Donnan GA, Davis SM; EXTEND-IA Investigators: Endovascular therapy for ischemic stroke with perfusion-imaging selection. N Engl J Med 372: 1009-1018, 2015. https://doi.org/10.1056/NEJMoa1414792
7. Cheang MY, Manning N, Churilov L, Mitchell P, Dowling R, Yan B: Recanalisation success is associated with good clinical outcome despite advanced age and stroke severity in patients treated with the Solitaire stentriever. J Clin Neurosci 21: 401-405, 2014. https://doi.org/10.1016/j.jocn.2013.05.005
8. Chen X, Liu H, Ye H, Bian Z, Peng Y: Systolic blood pressure trajectories after acute ischemic strokes and clinical outcomes: A systematic review. J Clin Hypertens (Greenwich) 24: 963-970, 2022. https://doi.org/10.1111/jch.14537
9. Costalat V, Jovin TG, Albucher JF, Cognard C, Henon H, Nouri N, Gory B, Richard S, Marnat G, Sibon I, Di Maria F, Annan M, Boulouis G, Cardona P, Obadia M, Piotin M, Bourcier R, Guillon B, Godard S, Pasco-Papon A, Eker OF, Cho TH, Turc G, Naggara O, Velasco S, Lamy M, Clarençon F, Alamowitch S, Renu A, Suissa L, Brunel H, Gentric JC, Timsit S, Lamy C, Chivot C, Macian-Montoro F, Mounayer C, Ozkul-Wermester O, Papagiannaki C, Wolff V, Pop R, Ferrier A, Chabert E, Ricolfi F, Béjot Y, Lopez-Cancio E, Vega P, Spelle L, Denier C, Millán M, Arenillas JF, Mazighi M, Houdart E, Del Mar Freijo M, Duhamel A, Sanossian N, Liebeskind DS, Labreuche J, Lapergue B, Arquizan C; LASTE Trial Investigators: Trial of thrombectomy for stroke with a large infarct of unrestricted size. N Engl J Med 390: 1677-1689, 2024. https://doi.org/10.1056/NEJMoa2314063
10. Day AL, Siddiqui AH, Meyers PM, Jovin TG, Derdeyn CP, Hoh BL, Riina H, Linfante I, Zaidat O, Turk A, Howington JU, Mocco J, Ringer AJ, Veznedaroglu E, Khalessi AA, Levy EI, Woo H, Harbaugh R, Giannotta S: Training standards in neuroendovascular surgery: Program accreditation and practitioner certification. Stroke 48: 2318-2325, 2017. https://doi.org/10.1161/STROKEAHA.117.016560
11. ElHabr AK, Katz JM, Wang J, Bastani M, Martinez G, Gribko M, Hughes DR, Sanelli P: Predicting 90-day modified Rankin Scale score with discharge information in acute ischaemic stroke patients following treatment. BMJ Neurol Open 3: e000177, 2021. https://doi.org/10.1136/bmjno-2021-000177
12. Fuentes B, Ntaios G, Putaala J, Thomas B, Turc G, Díez-Tejedor E; European Stroke Organisation: European Stroke Organisation (ESO) guidelines on glycaemia management in acute stroke. Eur Stroke J 3: 5-21, 2018. https://doi.org/10.1177/2396987317742065
13. GBD 2016 Stroke Collaborators: Global, regional, and national burden of stroke, 1990-2016: A systematic analysis for the Global Burden of Disease Study 2016. Lancet Neurol 18: 439-458, 2019. https://doi.org/10.1016/S1474-4422(19)30034-1
14. Goyal M, Demchuk AM, Menon BK, Eesa M, Rempel JL, Thornton J, Roy D, Jovin TG, Willinsky RA, Sapkota BL, Dowlatshahi D, Frei DF, Kamal NR, Montanera WJ, Poppe AY, Ryckborst KJ, Silver FL, Shuaib A, Tampieri D, Williams D, Bang OY, Baxter BW, Burns PA, Choe H, Heo JH, Holmstedt CA, Jankowitz B, Kelly M, Linares G, Mandzia JL, Shankar J, Sohn SI, Swartz RH, Barber PA, Coutts SB, Smith EE, Morrish WF, Weill A, Subramaniam S, Mitha AP, Wong JH, Lowerison MW, Sajobi TT, Hill MD; ESCAPE Trial Investigators: Randomized assessment of rapid endovascular treatment of ischemic stroke. N Engl J Med 372: 1019-1030, 2015. https://doi.org/10.1056/NEJMoa1414905
15. Jovin TG, Chamorro A, Cobo E, de Miquel MA, Molina CA, Rovira A, San Román L, Serena J, Abilleira S, Ribó M, Millán M, Urra X, Cardona P, López-Cancio E, Tomasello A, Castaño C, Blasco J, Aja L, Dorado L, Quesada H, Rubiera M, Hernandez-Pérez M, Goyal M, Demchuk AM, von Kummer R, Gallofré M, Dávalos A; REVASCAT Trial Investigators: Thrombectomy within 8 hours after symptom onset in ischemic stroke. N Engl J Med 372: 2296-2306, 2015. https://doi.org/10.1056/NEJMoa1503780
16. Kleindorfer DO, Towfighi A, Chaturvedi S, Cockroft KM, Gutierrez J, Lombardi-Hill D, Kamel H, Kernan WN, Kittner SJ, Leira EC, Lennon O, Meschia JF, Nguyen TN, Pollak PM, Santangeli P, Sharrief AZ, Smith SC Jr, Turan TN, Williams LS: 2021 Guideline for the prevention of stroke in patients with stroke and transient ischemic attack: A guideline from the American Heart Association/American Stroke Association. Stroke 52: e364-e467, 2021. https://doi.org/10.1161/STR.0000000000000375
17. Kuntze Söderqvist A, Kaijser M, Söderman M, Holmin S, Wahlgren N, Andersson T: Mechanical thrombectomy in acute ischemic stroke-experience from 6 years of practice. Neuroradiology 56: 477-486, 2014. https://doi.org/10.1007/s00234-014-1353-z
18. McGuire LS, Theiss P, Tshibangu M, Madapoosi A, Alaraj A: Radial artery mechanical thrombectomy for transradial approach in neurointerventions: A step-by-step technical report. Neuroradiology 2024. https://doi.org/10.1007/s00234-024-03528-3
19. Meder G, Żuchowski P, Skura W, Płeszka P, Dura M, Rajewski P, Nowaczewska M, Meder M, Alexandre AM, Pedicelli A: Mechanical thrombectomy in stroke-retrospective comparison of methods: Aspiration vs. stent retrievers vs. combined method-is aspiration the best starting point? J Clin Med 13: 1477, 2024. https://doi.org/10.3390/jcm13051477

20. Nguyen TN, Abdalkader M, Fischer U, Qiu Z, Nagel S, Chen HS, Miao Z, Khatri P: Endovascular management of acute stroke. Lancet 404: 1265-1278, 2024. https://doi.org/10.1016/S0140-6736(24)01410-7
21. Nogueira RG, Andersson T, Haussen DC, Yoo AJ, Hanel RA, Zaidat OO, Hacke W, Jovin TG, Fiehler J, De Meyer SF, Brinjikji W, Doyle KM, Kallmes DF, Liebeskind DS, Virmani R, Kokoszka MA, Inoa V, Humphries W, Woodward KB, Jabbour PM, François O, Levy EI, Bozorgchami H, Boor S, Cohen JE, Dashti SR, Taqi MA, Budzik RF, Schirmer CM, Hussain MS, Estrade L, De Leacy RA, Puri AS, Chitale RV, Brekenfeld C, Siddiqui AH: EXCELLENT registry: A prospective, multicenter, global registry of endovascular stroke treatment with the EMBOTRAP device. Stroke 55: 2804-2814, 2024. https://doi.org/10.1161/STROKEAHA.124.047324
22. Özdemir AÖ, Giray S, Gürkaş E: Training standards for neurointerventional procedures regarding endovascular treatment and secondary endovascular protection of acute ischemic stroke. Türk Beyin Damar Hastalıkları Dergisi 29: 106-114, 2023. https://doi.org/10.5505/tbdhd.2023.29053
23. Piironen K, Putaala J, Rosso C, Samson Y: Glucose and acute stroke: Evidence for an interlude. Stroke 43: 898-902, 2012. https://doi.org/10.1161/STROKEAHA.111.631218
24. Powers WJ, Rabinstein AA, Ackerson T, Adeoye OM, Bambakidis NC, Becker K, Biller J, Brown M, Demaerschalk BM, Hoh B, Jauch EC, Kidwell CS, Leslie-Mazwi TM, Ovbiagele B, Scott PA, Sheth KN, Southerland AM, Summers DV, Tirschwell DL: Guidelines for the early management of patients with acute ischemic stroke: 2019 update to the 2018 guidelines for the early management of acute ischemic stroke: A guideline for healthcare professionals from the American Heart Association/American Stroke Association. Stroke 50: e344-e418, 2019. https://doi.org/10.1161/STR.0000000000000211
25. Raha O, Hall C, Malik A, D'Anna L, Lobotesis K, Kwan J, Banerjee S: Advances in mechanical thrombectomy for acute ischaemic stroke. BMJ Med 2: e000407, 2023. https://doi.org/10.1136/bmjmed-2022-000407
26. Rai AT, Link PS, Domico JR. Updated estimates of large and medium vessel strokes, mechanical thrombectomy trends, and future projections indicate a relative flattening of the growth curve but highlight opportunities for expanding endovascular stroke care. J Neurointerv Surg 15(e3):e349-e355, 2023 https://doi.org/ 10.1136/jnis-2022-019777.
27. Reddy Y D, Thyagaraj V, Shetty V, Rizwanullah, Djeagou A, Tahir S, Gill SK, Khan MU, Ahmad A, Patel H: Renal function as a predictor of mortality and functional outcomes in acute stroke: A prospective study. Cureus 16: e73176, 2024. https://doi.org/ 10.7759/cureus.73176
28. Sallustio F, Pampana E, Davoli A, Merolla S, Koch G, Alemseged F, Panella M, D'Agostino VC, Mori F, Morosetti D, Konda D, Fabiano S, Diomedi M, Gandini R: Mechanical thrombectomy of acute ischemic stroke with a new intermediate aspiration catheter: Preliminary results. J Neurointerv Surg 10: 975-977, 2018. https://doi.org/10.1136/neurintsurg-2017-013679
29. Schirmer CM, Siddiqui AH, Frid I, Khalessi AA, Mocco J, Griessenauer CJ, Goren O, Dalal S, Weiner G, Arthur AS: Modern training and credentialing in neuroendovascular acute ischemic stroke therapy. Neurosurgery 85: S52-S57, 2019. https://doi.org/10.1093/neuros/nyz014
30. Scopelliti G, Pero G, Macera A, Quilici L, Cervo A, Platania G, Tadeo CS, Prelle AC, Muscia F, Riggio MG, Zilioli A, Agostoni EC, Piano M, Pantoni L: Outcome of a real-world cohort of patients subjected to endovascular treatment for acute ischemic stroke. J Stroke Cerebrovasc Dis 31: 106511, 2022. https://doi.org/10.1016/j.jstrokecerebrovasdis.2022.106511
31. Texakalidis P, Giannopoulos S, Karasavvidis T, Rangel-Castilla L, Rivet DJ, Reavey-Cantwell J: Mechanical thrombectomy in acute ischemic stroke: A meta-analysis of stent retrievers vs direct aspiration vs a combined approach. Neurosurgery 86: 464-477, 2020. https://doi.org/10.1093/neuros/nyz258
32. Turc G, Bhogal P, Fischer U, Khatri P, Lobotesis K, Mazighi M, Schellinger PD, Toni D, de Vries J, White P, Fiehler J: European Stroke Organisation (ESO)- European Society for Minimally Invasive Neurological Therapy (ESMINT) guidelines on mechanical thrombectomy in acute ischemic stroke. J Neurointerv Surg 15: e8, 2023. https://doi.org/10.1136/neurintsurg-2018-014569
33. Vo TP, Kristiansen MH, Hasselbalch HC, Wienecke T: Elevated white blood cell counts in ischemic stroke patients are associated with increased mortality and new vascular events. Front Neurol 14: 1232557, 2023. https://doi.org/10.3389/fneur.2023.1232557
34. Vogt ML, Kollikowski AM, Weidner F, Strinitz M, Feick J, Essig F, Neugebauer H, Haeusler KG, Pham M, Maerz A: Safety and effectiveness of the new generation aperio® hybrid stent-retriever device in large vessel occlusion stroke. Clin Neuroradiol 32: 141-151, 2022. https://doi.org/10.1007/s00062-021-01122-1
35. Yin C, Ding Y, Chang H: Direct carotid artery puncture for acute ischemic stroke: Local experience and systematic review. Interv Neuroradiol 2022. https://doi.org/10.1177/15910199221125094
36. Zaidat OO, Castonguay AC, Nogueira RG, Haussen DC, English JD, Satti SR, Chen J, Farid H, Borders C, Veznedaroglu E, Binning MJ, Puri A, Vora NA, Budzik RF, Dabus G, Linfante I, Janardhan V, Alshekhlee A, Abraham MG, Edgell R, Taqi MA, Khoury RE, Mokin M, Majjhoo AQ, Kabbani MR, Froehler MT, Finch I, Ansari SA, Novakovic R, Nguyen TN: TREVO stent-retriever mechanical thrombectomy for acute ischemic stroke secondary to large vessel occlusion registry. J Neurointerv Surg 10: 516-524, 2018. https://doi.org/10.1136/neurintsurg-2017-013328

Turk Neurosurg 35(4):546-552, 2025
DOI: 10.5137/1019-5149.JTN.46902-24.2

Original Investigation

Cerebrovascular-Endovascular

Received: 19.05.2024
Accepted: 27.10.2024
Published Online: 25.06.2025

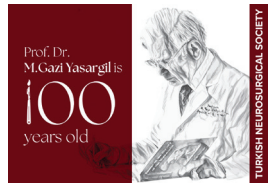

Comparison of Pre-Operative and Post-Operative Mean Transit Time Delay in Ipsilateral and Contralateral Hemispheres in Moyamoya Disease Using DSC Perfusion

Nishtha YADAV[1], Hima PENDHARKAR[2], Arun Kumar GUPTA[3], Chandrajit PRASAD[2], Dhaval SHUKLA[4], K. THENNARASU[5], Sonia BANSAL[6]

[1]NSCB Medical College, School of Excellence in Neurosurgery, Super Speciality Hospital, Department of Neuroradiology, Jabalpur, India
[2]National Institute of Mental Health and Neurosciences, Department of Neuroimaging and Interventional Radiology, Bengaluru, Karnataka, India
[3]Paras Hospital, Department of Neurointervention, Delhi, India
[4]National Institute of Mental Health and Neurosciences, Department of Neurosurgery, Bengaluru, Karnataka, India
[5]National Institute of Mental Health and Neurosciences, Department of Biostatistics, Bengaluru, Karnataka, India
[6]National Institute of Mental Health and Neurosciences, Department of Neuroanaesthesia, Bengaluru, Karnataka, India

Corresponding author: Hima PENDHARKAR ✉ himasp2@gmail.com

ABSTRACT

AIM: To perform comparison of preoperative and postoperative mean transit time (MTT) delay in ipsilateral, and contralateral hemispheres in Moyamoya disease using dynamic susceptibility contrast (DSC) perfusion.

MATERIAL and METHODS: Preoperative images were obtained within 1 week before surgery and postoperative images were taken 3 months after surgery. Cerebral perfusion was assessed in bilateral middle cerebral artery territories with 3 Region Of Interest (ROI) on each side (ipsilateral and contralateral to surgery side). Two ROI were also drawn in bilateral cerebellar hemisphere. MTT delay at each middle cerebral artery (MCA) region was calculated by subtracting MCA territory ROI MTT value from ipsilateral cerebellar ROI MTT value. Non-normally distributed measurement data are expressed as the median [interquartile range (IQR)] and compared using Wilcoxon's rank-sum test. $p<0.05$ was considered statistically significant.

RESULTS: Median ipsilateral MTT delay values (in seconds) before surgery were 2.4, Interquartile Range (IQR) 4.95; and after surgery was 1, IQR 2.1 We noted a significant decrease in postoperative MTT delay values on ipsilateral side compared with preoperative values ($p=0.008$). Contralateral MTT delay values did not show this trend. Median contralateral MTT delay values (in seconds) before surgery were 0.6, IQR 3.7; and after surgery was 1.6, IQR 3.65 We noted no significant difference in preoperative and postoperative MTT delay values on contralateral side ($p=0.12$).

CONCLUSION: DSC perfusion analysis of MTT delay in follow up imaging after revascularization surgery can be helpful in deciding success of surgery. Evaluation of contralateral hemisphere perfusion can be helpful to guide regarding need of contralateral side surgery. Future studies to evaluate contralateral perfusion characteristics are necessary to understand the complex hemodynamic changes which occur post revascularization surgery.

KEYWORDS: Moyamoya disease, Perfusion, MTT delay, Revascularization surgery, DSC perfusion

ABBREVIATIONS: MTT: Mean transit time, **DSC:** Dynamic susceptibility contrast, **ROI:** Region of interest, **MCA:** Middle cerebral artery, **IQR:** Interquartile range, **ICA:** Internal carotid artery, **MRI:** Magnetic resonance ımaging, **CBF:** Cerebral blood flow, **CBV:** Cerebral blood volume, **TTP:** Time to peak, **EDAMS:** Encephalo-duro-arterio-myo-synangiosis, **STA-MCA:** Superficial temporal artery- middle cerebral artery, **CT:** Computed tomography, **SPECT:** Single photon emission computed tomography, **O-15 PET:** Oxygen-15 photon emission tomography, **CVR:** Cerebrovascular reserve

Nishtha YADAV : 0000-0001-5239-816X
Hima PENDHARKAR : 0000-0002-8711-7708
Arun Kumar GUPTA : 0000-0003-4664-6088
Chandrajit PRASAD : 0000-0001-6944-0926
Dhaval SHUKLA : 0000-0001-7613-1929
K. THENNARASU : 0000-0001-8797-8834
Sonia BANSAL : 0000-0003-2872-8629

INTRODUCTION

Moyamoya disease (MMD) is a chronically progressive cerebrovascular disease that is associated with narrowing of supraclinoid internal carotid arteries (ICAs) along with basal fine net-like vascular network, which is known as "moyamoya" vessels (16). It presents with ischemic or hemorrhagic symptoms.

Surgical revascularization procedures aim to improve the state of the cerebral circulation to decrease the risk of future strokes and are categorized into direct, indirect, and combined bypass. Postoperative imaging usually includes magnetic resonance imaging (MRI) to evaluate the parenchyma and angiography to assess revascularization development. Postoperative revascularization is graded on angiography with the Matsushima and Inaba grading (14). However, it is invasive and does not provide hemodynamic and cross-sectional information. Thus, adding perfusion imaging is useful in the follow-up of patients after surgical revascularization. Mean transit time (MTT) is a crucial parameter to assess parenchymal perfusion because a delay in MTT helps diagnose ischemic areas. We conducted preoperative and postoperative perfusion analysis in seven patients with MMD to identify its use in postoperative imaging.

MATERIAL and METHODS

This was a prospective observational study. The study was done after ethical committee approval (letter number NIMH/DO/ETHICS SUB-COMMITTEE {BS & NS} 7TH MEETING/ 2017 dated 22/11/2017), and patient consent was taken. Patient's demographic, clinical information and biochemical investigation reports were collected from the patient's outpatient / inpatient file and e-hospital portal of the institute. Information about symptoms and their duration and other demographic profile was taken in a predesigned proforma.

Confirmation of diagnosis of moyamoya disease was based on MR angiography/cerebral angiography diagnostic criteria (based on Guidelines for Diagnosis and Treatment of moyamoya disease). Cooperative patients were taken up for MRI examination without sedation, for children <10 years, imaging/DSA procedure was done under anaesthesia.

MRI was performed on 1.5T Aera (Siemens) or 1.5T Optima MR450w (GE) system.

Preoperative images were obtained within 1 week before surgery and postoperative images were taken 3 months after surgery. DSC perfusion images were analyzed quantitatively using IntelliSpace Portal 9.0 workstation (Philips Healthcare) and gamma variate processing was used to generate perfusion maps and maps of cerebral blood flow (CBF), cerebral blood volume (CBV), mean transit time (MTT) and time to peak (TTP) were generated and values of these parameters were estimated.

Cerebral perfusion was assessed in bilateral middle cerebral artery territories with 3 ROI on each side (ipsilateral and contralateral to surgery side): MCA^{1}- ROI involving cortical MCA territory at level of centrum semiovale, MCA^{2}: ROI involving cortical MCA territory at level of thalamus and MCA^{bg}- ROI drawn at basal ganglia). These ROI were drawn in reference to previous studies (4,17). Two ROI were also drawn in bilateral cerebellar hemisphere at level of middle cerebellar peduncles for cerebellar perfusion assessment. ROI are shown in Figure 1. MTT delay at each MCA region was calculated by subtracting MCA territory ROI MTT value from ipsilateral cerebellar ROI MTT value. Non-normally distributed measurement data are expressed as the median (interquartile range [IQR]) and compared using Wilcoxon's rank-sum test. $p<0.05$ was considered statistically significant.

RESULTS

A total of 7 patients were recruited for the study. The demographic, clinical and preoperative morphologic MRI data of these patients are given in Table I. Details of management, follow up symptoms and follow up MRI is given in Table II. Three patients underwent Encephalo-duro-arterio-myo-synangiosis (EDAMS) and 4 patients underwent superficial temporal artery - middle cerebral artery (STA-MCA) bypass. STA-MCA bypass has been found to be superior to EDAMS for secondary stroke prevention and was preferred for the symptomatic hemisphere (8). However, if the caliber of the donor or the recipient vessel was not found suitable either during the preoperative evaluation or during surgery, then EDAMS was done.

We analysed the MTT delay values of hemispheres ipsilateral to operative side and contralateral to it.

Median ipsilateral MTT delay values (in seconds) before surgery were 2.4, Interquartile Range 4.95; and after surgery was 1, Interquartile Range 2.1 We noted a significant difference in preoperative and postoperative MTT delay values on ipsilateral side, with postoperative MTT showing a significant decrease in values compared to preoperative values ($p=0.008$).

Contralateral MTT values did not show this trend. Median contralateral MTT delay values (in seconds) before surgery were 0.6, Interquartile Range 3.7; and after surgery was 1.6, Interquartile Range 3.65 We noted no significant difference in preoperative and postoperative MTT delay values on contralateral side ($p=0.12$). Comparison of preoperative and postoperative ipsilateral and contralateral MTT delay values are shown in Figure 2, 3.

Postoperatively, all patients had ipsilateral benefit with no new symptoms and/or improvement in ipsilateral symptoms. 4 patients had contralateral symptoms in postoperative period. All four of these patients developed increase in MTT delay in one or more of MCA territories on perfusion imaging analysis, corresponding with their symptoms.

Examples of comparison of preoperative and postoperative MTT analysis are shown in Figure 4 and Figure 5.

DISCUSSION

Postoperative evaluation after revascularization surgery in MMD is usually performed by angiographic assessment with the Matsushima grading (14). However, it is invasive and does not provide hemodynamic information. Dynamic susceptibility

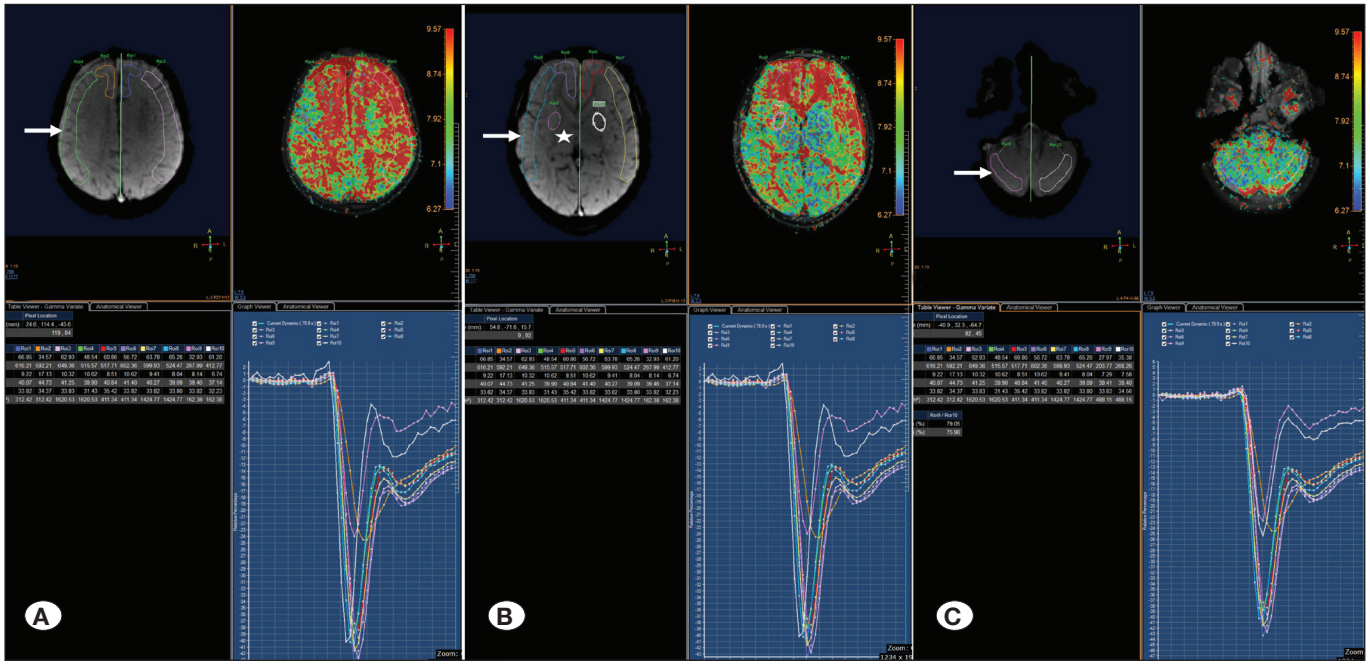

Figure 1: A) Arrow shows region of interest (ROI) drawn in cortical middle cerebral artery (MCA) territory (M^1) at level of centrum semivale. **B)** Arrow shows ROI drawn in cortical MCA territory (M^2) at level of thalamus. Marked Star (*) shows ROI drawn at basal ganglia (M^{bg}). **C)** Arrow shows ROI drawn involving cerebellar hemisphere.

Table I: Demographic, Clinical and Preoperative Morphologic MRI Data of Patients

No	Age (Years)	Sex	Ischemic/ Hemorrhagic	Symptoms	Stroke/ TIA Symptom	Infarct in MRI	IVY Sign
1	2	Female	Ischemic	Seizures, b/l limb weakness	Stroke	Infarcts bilateral (b/l) watershed cortical and deep watershed	No
2	24	Female	Ischemic	Headache, cognitive dysfunction, right weakness	Stroke	Infarcts b/l watershed cortical and deep watershed	No
3	4	Male	Ischemic	Left weakness	Stroke	Right mca cortical and deep lacunar	Yes
4	11	Female	Ischemic	Right weakness	Stroke	Left mca cortical infarct	Yes
5	14	Female	Ischemic	Left weakness	Stroke	Infarcts b/l watershed cortical, cortical watershed and deep watershed	Yes
6	9	Male	Ischemic	Left weakness	TIA	No infarct	Yes
7	6	Male	Ischemic	Right weakness	TIA	No infarct	Yes

TIA: *Transient Ischemic Attack,* ***IVY Sign:*** *Refers to sulcal hyperintensities noted on Fluid Attenuated Inversion Recovery Sequence (FLAIR), denoting presence of collaterals in Moyamoya disease.*

contrast-enhanced (DSC) perfusion imaging on MRI is one of the important modalities used to evaluate hemodynamic changes.

We observed a significant difference in the preoperative and postoperative MTT values on the ipsilateral side, with the postoperative MTT demonstrating a significant decrease in values compared to the preoperative values (p=0.03). This is similar to the results of multiple studies exhibiting a decrease in MTT of the MCA territory on the ipsilateral side after unilateral surgical revascularization on computed tomography (CT) and MRI perfusion analysis (2,7,8,10-12,18-20) cerebral blood volume (CBV with MTT delay changes described as

Table II: Details of Management, Complications, Follow up Symptoms and Follow up MRI Findings

No	Surgery	Postoperative complication	Follow up symptoms	Follow up MRI	Contrlateral symptoms
1	EDAMS	None	Seizures frequency reduced	No fresh infarct	None
2	STA-MCA Bypass	None	Lower limb weakness persisting, upper limb weakness improved, no fresh symptoms	No fresh infarct	None
3	EDAMS	None	Weakness improved, no fresh ipsilateral symptoms	No fresh infarct	Yes
4	STA-MCA Bypass	None	Weakness improved, no fresh ipsilateral symptoms	No fresh infarct	Yes
5	EDAMS	None	Weakness improved, no fresh ipsilateral symptoms	No fresh infarct	None
6	STA-MCA Bypass	None	Weakness improved, no fresh ipsilateral symptoms	No fresh infarct	Yes
7	STA-MCA Bypass	None	Weakness improved, no fresh ipsilateral symptoms	No fresh infarct	Yes

EDAMS: *Encephalo-duro-arterio-myo-synangiosis,* ***STA:*** *Superficial temporal artery,* ***MCA:*** *Middle cerabral artery,* ***MRI:*** *Magnetic resonance imaging.*

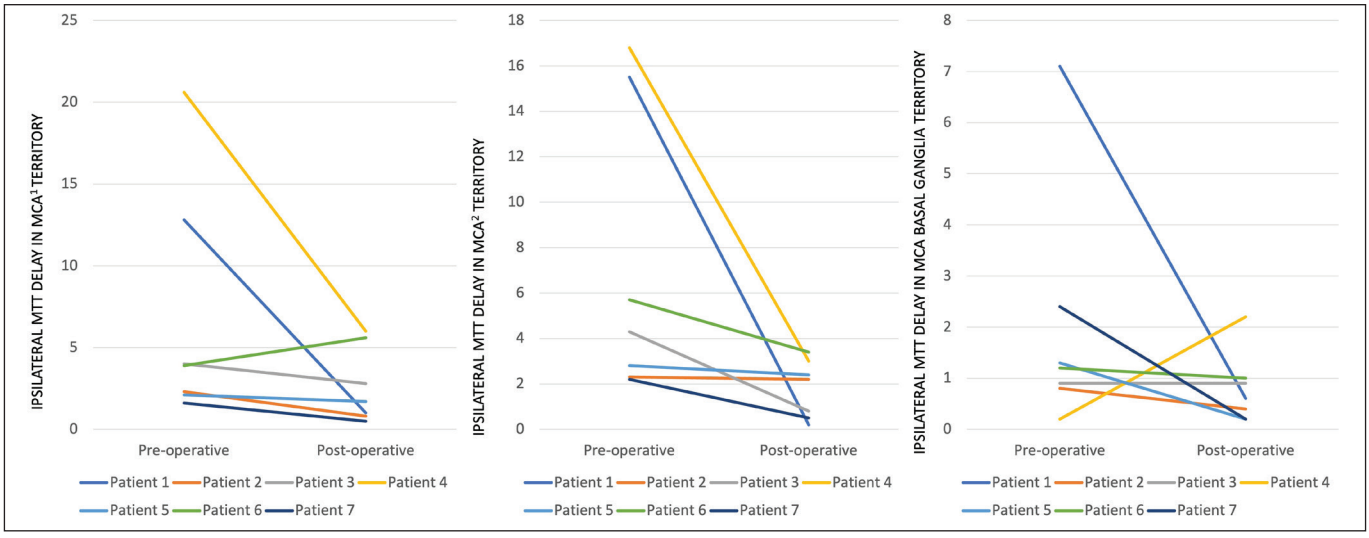

Figure 2: Graph showing preoperative vs postoperative mean transit time (MTT) delay changes in middle cerabral artery (MCA) territory in MCA[1], MCA[2] and MCA[bg] territory in ipsilateral hemisphere with significant reduction in MTT delay (p=0.008).

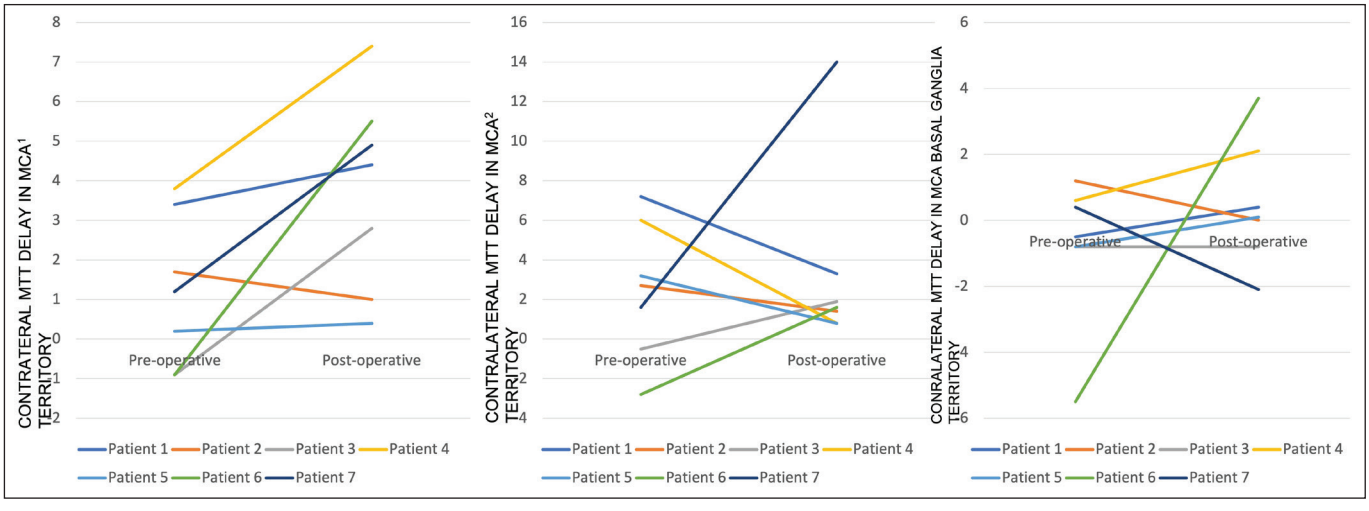

Figure 3: Graph showing preoperative vs postoperative mean transit time (MTT) delay changes in middle cerabral artery (MCA) territory in MCA[1], MCA[2] and MCA[bg] territory in contralateral hemisphere with no significant changes in MTT delay (p=0.12).

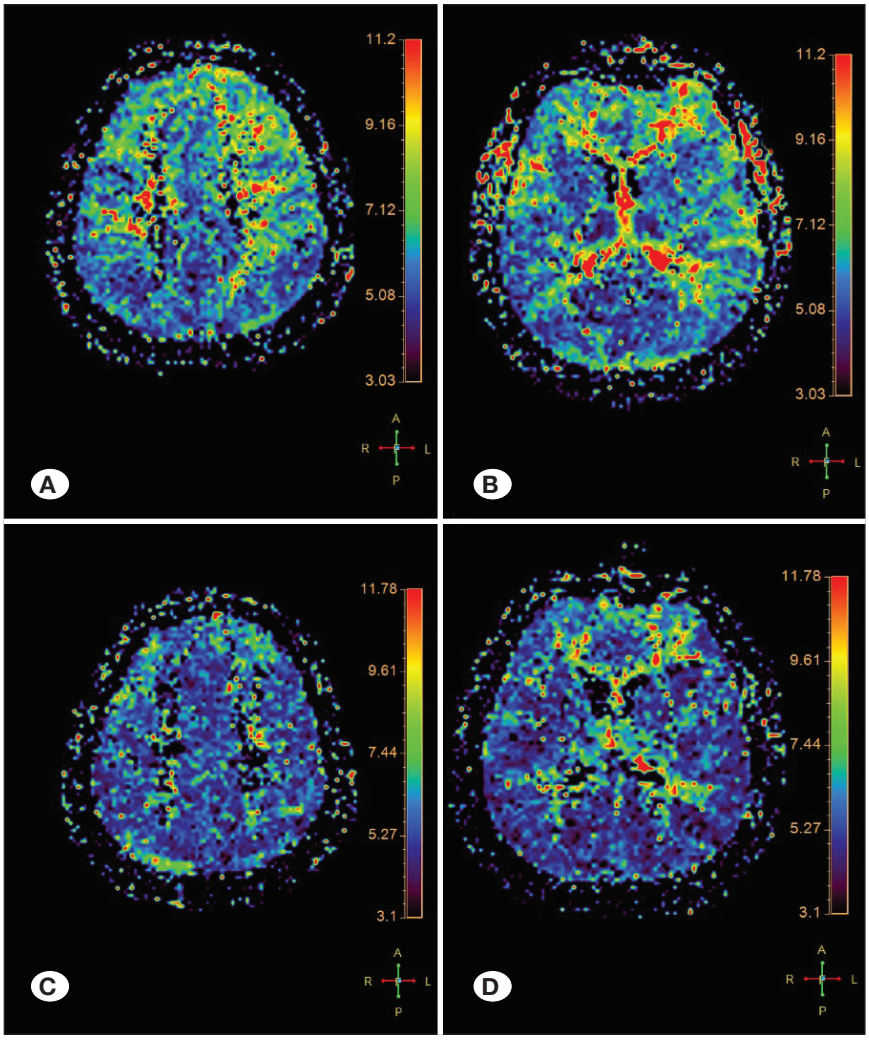

Figure 4: A 24-year-old female patient presented with history of headache and cognitive dysfunction for 2 years and recent onset of right sided weakness. Preoperative mean transit time (MTT) maps **(A,B)** showing raised MTT in bilateral hemispheres involving anterior circulation (left>right). Patient was operated on left side. Postoperative MTT maps **(C,D)** show decreased MTT following surgery on ipsilateral side (left hemisphere) as well as contralateral side (right hemisphere).

early as 2–4 weeks postoperatively (8). We revealed that MTT delay reduction correlated with symptom resolution in the postoperative period in all our patients.

In most centers, especially in developing countries, other postoperative imaging modalities, such as SPECT and O-15 PET, may not be readily available. Additionally, CT perfusion is not very readily available and most machines exhibit a limited coverage slab for CT perfusion, and whole brain perfusion analysis may not be readily available. Thus, follow-up MTT delay reduction on DSC perfusion imaging helps determine the success of surgery and should be routinely performed as a follow-up imaging.

All of the seven operated patients developed improvement in ipsilateral hemispheric symptoms postoperatively, whereas four patients developed contralateral hemispheric symptoms on follow-up. All four patients demonstrated an increase in MTT delay in one or more MCA territories. This observation is similar to a study by Ma et al. who revealed their experience in the perfusion evaluation of contralateral (nonoperated and asymptomatic) hemispheres in 15 MMD cases in whom unilateral direct bypass surgery of the symptomatic hemisphere was conducted. They demonstrated rCBF and cerebrovascular reserve (CVR) improvement on the ipsilateral side with decreased rCBF and CVR developing on the contralateral side on follow-up. The authors concluded that unilateral (symptomatic side) direct surgical revascularization for patients with MMD caused CVR impairment in the contralateral asymptomatic hemisphere (13). However, this study did not perform an angiographic follow-up of these patients who developed impaired CVR on the contralateral side, which could be caused by disease progression itself. We also did not conduct an angiographic follow-up of these patients who developed worsening of the contralateral MTT postoperatively on follow-up and developed symptoms on the contralateral side. Thus, disease progression may cause the development of contralateral perfusion worsening in these four patients.

In contrast, the recent literature shows a contralateral hemodynamic benefit (3). Bacigaluppi et al. revealed a contralateral hemodynamic improvement after unilateral direct bypass surgical revascularization, as demonstrated by improved CVR on postoperative quantitative MRI (1). Other perfusion studies in patients with MMD revealed a beneficial effect in the nontreat-

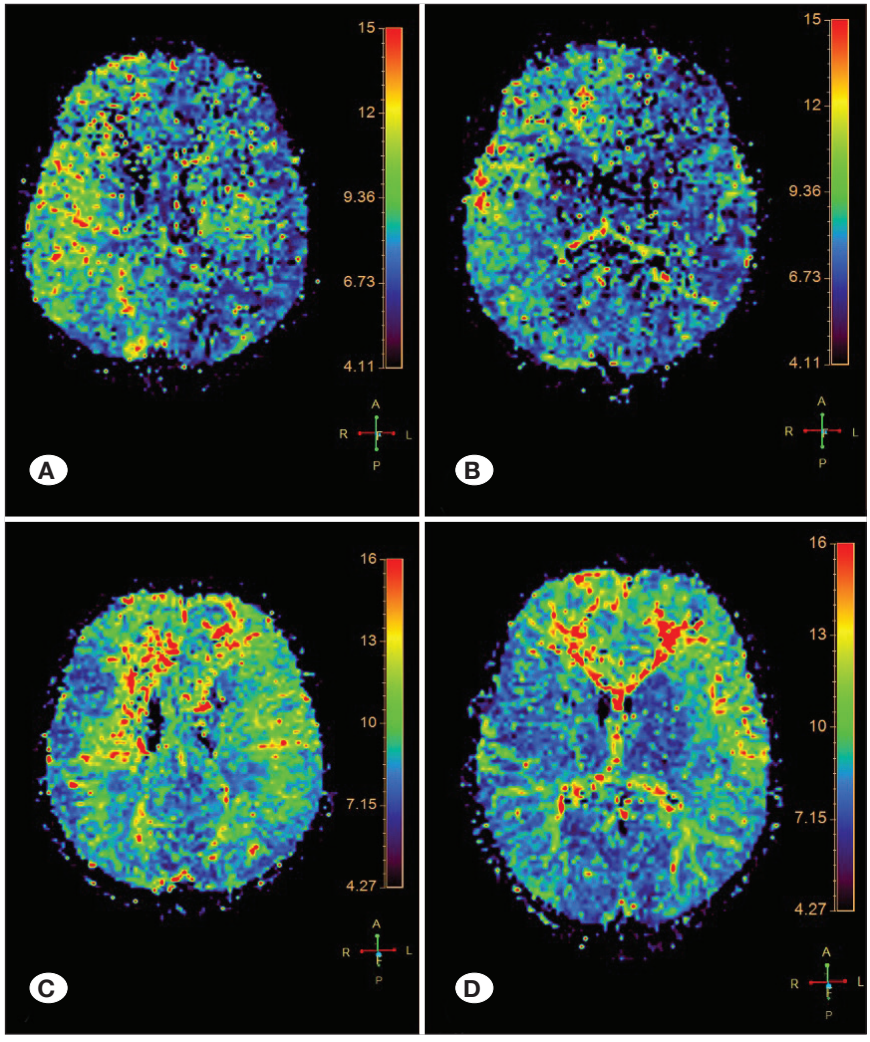

Figure 5: A 4-year-old male patient presented with a history of episodic left sided weakness for 4 months [recurrent transient ischemic attack (TIA)]. Preoperative mean transit time (MTT) maps **(A,B)** showing raised MTT in right cerebral hemispheres involving anterior circulation with mildly raised MTT in left cerebral hemisphere (anterior circulation). Patient was operated on right side. Postoperative MTT maps **(C,D)** show decreased MTT following surgery in MCA territory on ipsilateral side (right hemisphere) with marked increase in MTT on contralateral side (left hemisphere) postoperatively.

ed hemisphere after unilateral surgery (6,15). We exhibited that other patients who underwent surgery and did not develop contralateral symptoms and for whom DSC parameters were available for preoperative and postoperative comparison (n=3) demonstrated MTT improvement on the ipsilateral as well as the contralateral side. These incongruities are explained by the complex cerebral hemodynamic rearrangement that occurs postoperatively and the inherent underlying challenge in understanding these complex dynamic changes (3).

Huang et al. evaluated the hemodynamic difference between symptomatic and nonsymptomatic cerebral hemispheres in patients with symptomatic MMD using CT perfusion (5). They concluded that rCBF and rMTT were more sensitive than rTTP for assessing hemodynamic changes in patients with symptomatic bilateral MMS. Additionally, we observed that the increase in postoperative contralateral hemisphere MTT delay corresponded to the development of patient symptoms corresponding to the contralateral hemisphere. This observation emphasizes the importance of perfusion MRI, especially MTT analysis, which helps guide the decision for the side of surgery in case of bilateral symptoms.

CONCLUSION

DSC perfusion analysis of MTT delay in follow up imaging after revascularization surgery can be helpful in deciding success of surgery. Also evaluation of contralateral hemisphere perfusion can be helpful to guide regarding need of contralateral side surgery. Future studies to evaluate contralateral perfusion characteristics are necessary to understand the complex hemodynamic changes which occur post revascularization surgery.

Declarations

Funding: This research did not receive any specific grant from funding agencies in the public, commercial, or not-for-profit sectors.

Availability of data and materials: The datasets generated and/or analyzed during the current study are available from the corresponding author by reasonable request.

Disclosure: The authors declare no competing interests.

AUTHORSHIP CONTRIBUTION

Study conception and design: NY, HP
Data collection: NY, HP, AKG, CP, DS, SB
Analysis and interpretation of results: NY, HP, KT
Draft manuscript preparation: NY, HP
Critical revision of the article: NY, HP, AKG, CP, DS, SB
Other (study supervision, fundings, materials, etc...): NY, HP
All authors (NY, HP, AKG, CP, DS, KT, SB) reviewed the results and approved the final version of the manuscript.

REFERENCES

1. Bacigaluppi S, Dehdashti AR, Agid R, Krings T, Tymianski M, Mikulis DJ: The contribution of imaging in diagnosis, preoperative assessment, and follow-up of moyamoya disease: A review. Neurosurg Focus 26:E3, 2009. https://doi.org/10.3171/2009.01.FOCUS08296
2. Chen Y, Xu W, Guo X, Shi Z, Sun Z, Gao L, Jin F, Wang J, Chen W, Yang Y: CT perfusion assessment of Moyamoya syndrome before and after direct revascularization (superficial temporal artery to middle cerebral artery bypass). Eur Radiol 26:254–261, 2016. https://doi.org/10.1007/s00330-015-3802-4
3. Esposito G, Fierstra J, Kronenburg A, Regli L: A comment on "Contralateral cerebral hemodynamic changes after unilateral direct revascularization in patients with moyamoya disease." Neurosurg Rev 35:141-143, 2012. https://doi.org/10.1007/s10143-011-0367-9
4. Goetti R, O'Gorman R, Khan N, Kellenberger CJ, Scheer I: Arterial spin labelling MRI for assessment of cerebral perfusion in children with moyamoya disease: Comparison with dynamic susceptibility contrast MRI. Neuroradiol 55: 639-647, 2013. https://doi.org/10.1007/s00234-013-1155-8
5. Huang S, Gao L, Chen Y, Guo X, Liu D, Wang J, Shi Z, Sun Z, Jin F, Chen W, Yang Y: Application of CT perfusion to assess hemodynamics in symptomatic Moyamoya syndrome: focus on affected side and parameter characteristic. Childs Nerv Syst 34:1189-1197, 2018. https://doi.org/10.1007/s00381-018-3727-8
6. Ikezaki K, Matsushima T, Kuwabara Y, Suzuki SO, Nomura T, Fukui M: Cerebral circulation and oxygen metabolism in childhood moyamoya disease: A perioperative positron emission tomography study. J Neurosurg 81:843-850, 1994. https://doi.org/10.3171/jns.1994.81.6.0843
7. Ishii Y, Nariai T, Tanaka Y, Mukawa M, Inaji M, Maehara T, Ohno K: Practical clinical use of dynamic susceptibility contrast magnetic resonance imaging for the surgical treatment of moyamoya disease. Neurosurgery 74:302-309, 2014. https://doi.org/10.1227/NEU.0000000000000266
8. Ishii Y, Tanaka Y, Momose T, Yamashina M, Sato A, Wakabayashi S, Maehara T, Nariai T: Chronologic evaluation of cerebral hemodynamics by dynamic susceptibility contrast magnetic resonance imaging after indirect bypass surgery for moyamoya disease. World Neurosurgery 108:427-435, 2017. https://doi.org/10.1016/j.wneu.2017.09.001
9. Jeon JP, Kim JE, Cho WS, Bang JS, Son YJ, Oh CW: Meta-analysis of the surgical outcomes of symptomatic moyamoya disease in adults, 2017. Available from: https://thejns.org/view/journals/j-neurosurg/128/3/article-p793.xml. https://doi.org/10.3171/2016.11.JNS161688
10. Kwon WK, Kwon TH, Park DH, Kim JH, Ha SK: Efficacy of superficial temporal artery-middle cerebral artery bypass in cerebrovascular steno-occlusive diseases: Hemodynamics assessed by perfusion computed tomography. Asian J Neurosurg 12:519, 2017. https://doi.org/10.4103/1793-5482.153497
11. Lee SK, Kim DI, Jeong EK, Kim SY, Kim SH, In YK, Kim DS, Choi JU: Postoperative evaluation of moyamoya disease with perfusion-weighted MR imaging: Initial experience. Am J Neuroradiol 24:741-747, 2003.
12. Lin YH, Kuo MF, Lu CJ, Lee CW, Yang SH, Huang YC, Liu HM, Chen YF: Standardized MR perfusion scoring system for evaluation of sequential perfusion changes and surgical outcome of moyamoya disease. AJNR Am J Neuroradiol 40: 260-266, 2019. https://doi.org/10.3174/ajnr.A5945
13. Ma Y, Li M, Jiao LQ, Zhang HQ, Ling F: Contralateral cerebral hemodynamic changes after unilateral direct revascularization in patients with moyamoya disease. Neurosurg Rev 34:347-354, 2011. https://doi.org/10.1007/s10143-011-0312-y
14. Matsushima Y, Inaba Y: Moyamoya disease in children and its surgical treatment. Introduction of a new surgical procedure and its follow-up angiograms. Childs Brain 11:155-170, 1984. https://doi.org/10.1159/000120172
15. Nair AK, Drazin D, Yamamoto J, Boulos AS: Computed tomographic perfusion in assessing postoperative revascularization in moyamoya disease. World Neurosurg 73:93-99; discussion e13, 2010. https://doi.org/10.1016/j.surneu.2009.06.023
16. Suzuki J, Takaku A: Cerebrovascular moyamoya disease: Disease showing abnormal net-like vessels in base of brain. Arch Neurol 20:288-299, 1969. https://doi.org/10.1001/archneur.1969.00480090076012
17. Tatu L, Moulin T, Bogousslavsky J, Duvernoy H: Arterial territories of the human brain: Cerebral hemispheres. Neurology 50:1699-1708, 1998. doi: 10.1212/wnl.50.6.1699.
18. Teng MMH, Jen SL, Chiu FY, Kao YH, Lin CJ, Chang FC: Change in brain perfusion after extracranial–intracranial bypass surgery detected using the mean transit time of computed tomography perfusion. J Chinese Med Assoc 75: 649-653, 2012. https://doi.org/10.1016/j.jcma.2012.08.008
19. Yuan X, Yu H, Sun Z, Wu J, Gao L, Chong Z, Jin F, Chen Y, Liu D: Evaluation of surgical revascularization procedure outcomes for adult Moyamoya disease: A computed tomography perfusion-based study. Insights Imaging 14:184, 2023. https://doi.org/10.1186/s13244-023-01519-1
20. Zhang J, Wang J, Geng D, Li Y, Song D, Gu Y: Whole-brain CT perfusion and CT angiography assessment of Moyamoya disease before and after surgical revascularization: Preliminary study with 256-slice CT. PLoS One 8:e57595, 2013. https://doi.org/10.1371/journal.pone.0057595

Turk Neurosurg 35(4):553-560, 2025
DOI: 10.5137/1019-5149.JTN.47812-24.2

Original Investigation

Cerebrovascular-Endovascular

Received: 16.10.2024
Accepted: 02.12.2024
Published Online: 25.06.2025

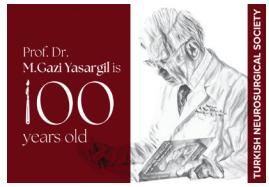

Neuroendoscopic Surgical Treatment of Hypertensive Brainstem Hemorrhage

Zhi-Lin YİN[1], Long ZHOU[2], Qiang CAI[2]

[1]Hubei Provincial Hospital of Integrated Chinese and Western Medicine, Department of Neurosurgery, Wuhan, China
[2]People's Hospital of Wuhan University, Department of Neurosurgery, Wuhan, China

All authors contributed equally to this article.

Corresponding author: Qiang CAI ✉ cqno@sina.com

To watch the surgical videoclip, please visit https://www.turkishneurosurgery.org.tr/submit/pdf-files/in/48176-JTN-case3.rev-1.mp4

ABSTRACT

AIM: To investigate the clinical effect of neuroendoscopic surgery on 15 patients with hypertensive brainstem hemorrhage (HBSH).

MATERIAL and METHODS: A retrospective analysis was conducted on the clinical data collected from 15 patients with HBSH and treated with neuroendoscopy between January 2021 and March 2023. Prior to surgery, head computed tomography (CT) data were imported into 3D-slicer software to reconstruct the hematoma in three dimensions, allowing for the calculation of hematoma volume. During surgery, neuroendoscopy was used to clear the hematoma, after which the hematoma clearance rate, along with 30-day and 90-day mortality rates, was calculated. Three months after surgery, the Glasgow Outcome Scale (GOS) was used to evaluate patient prognosis, calculate the good recovery rate, and assessed surgical efficacy.

RESULTS: Re-examination of head CT images within 24 hours post-surgery revealed a hematoma clearance rate of > 90% in 11 cases and over 80–90% in four cases, with a mean hematoma clearance rate of 90.52±3.85%. There were no complications associated with postoperative rebleeding, intracranial infection, or the leakage of cerebrospinal fluid. Mortality rates on days 30 and 90 post-surgery were 26.7% (4/15) and 40% (6/15), respectively. After a 3-month follow-up period, GOS prognostic scoring revealed that one case had recovered well and could live a normal life, two cases had mild disability, and two cases had severe disability. Four patients survived in a vegetative state while six patients died; the good prognostic rate was 20% (3/15).

CONCLUSION: Neuroendoscopic technology is safe and effective for the treatment of HBSH. This method has a high hematoma clearance rate and a good clinical treatment effect with few postoperative complications.

KEYWORDS: Neuroendoscopy, Hypertension, Brainstem hemorrhage, Surgical treatment, Endoport technology

ABBREVIATIONS: HBSH: Hypertensive brainstem hemorrhage, **CT:** Computed tomography, **GOS:** Glasgow outcome scale, **GCS:** Glasgow coma scale, **CTA:** Computed tomography angiography

INTRODUCTION

Hypertensive brainstem hemorrhage (HBSH) is an acute cerebrovascular disease characterized by rapid onset, rapid progression, high mortality and disability rates, and an extremely poor prognosis (6,11,14). Due to the complex anatomical structure of the brainstem and the difficulty associated with performing surgery after hemorrhage, there is still considerable debate regarding whether surgical treatment can improve the prognosis of patients with brainstem hemor-

Zhi-Lin YIN : 0009-0004-0572-8526 Long ZHOU : 0000-0001-9559-2501 Qiang CAI : 0000-0003-4280-0770

rhage (17). Therefore, from a global perspective, conservative treatment is normally provided to patients with HBSH. With the continuous improvement of surgical techniques, some patients with HBSH have achieved symptom improvement following surgical treatment (7,8), although the safety and efficacy of such surgery have yet to be fully determined. In the present study, we retrospectively analyzed the clinical data of 15 patients with HBSH who admitted to our hospital between January 2021 and March 2023. For each patient, we used neuroendoscopic technology to remove the hematoma and then determined the specific clinical efficacy of this technique.

MATERIAL and METHODS

The research has been approved (Ethics Review Number: WDRY2022-KS002, Date: January 10, 2022)

Study Population

We retrospectively analyzed the clinical data of 15 patients with HBSH who had been admitted to the Department of Neurosurgery at our institution between January 2021 and March 2023. Detailed information related to the patient cohort is provided in Table I. The inclusion criteria were as follows: 1) a clear history of hypertension and surgery performed within 24 hours of onset; 2) parenchymal hemorrhage of the brainstem indicated by head CT; 3) hematoma volume ≥5 mL; and 4) progressive neurological dysfunction with a Glasgow coma scale (GCS) score <8 points. The exclusion criteria were as follows: 1) late cerebral hernia due to bilateral pupil dilation; 2) bleeding caused by other factors such as tumors, trauma, vascular malformations, and aneurysms; 3) abnormal coagulation function; and 4) inability to tolerate anesthesia or surgery. The study protocol conformed to the ethical guidelines of the Declaration of Helsinki, and was approved by the Ethics Committee of our hospital. All patients underwent surgery with informed consent signed by their families.

Acquisition of Three-dimensional (3D) Images

Following hospital admission, we first performed head CT examination. Data acquired by head CT were then imported into 3D-Slicer system in DICOM format (The version 3D Slicer 4.10.2. link: https://slicer.org). Segment Editor, Threshold, Island, Volume Rendering, Segment Statistics and other functional modules were run sequentially in 3D-Slicer software to reconstruct the brainstem hematoma and calculate hematoma volume.

Neuroendoscopic Hematoma Evacuation

We selected the appropriate surgical approach for each patient in accordance with the different shapes and locations of the hematoma, as reconstructed by 3D-Slicer software: the subtemporal transtentorial approach (suitable for posterolateral pontine hematomas), and the suboccipital posterior median approach (suitable for medulla bulbar and inferior dorsal pontine hematomas). Of the 15 patients, the subtemporal transtentorial approach was selected for nine patients, the suboccipital posterior median approach for two patients, the frontal approach for one patient, and the retrosigmoid sinus approach for three patients. Two patients with acute obstructive hydrocephalus underwent external ventricular drainage initially. In these cases, cerebrospinal fluid was fully released during routine craniotomy. Once cerebral pressure had fallen, we used the advantages of neuroendoscopy (good deep illumination, and a clear visual field) to reveal the rupture of brainstem hematomas. A bespoke transparent working sheath (Endoport) was then inserted into the hematoma cavity and the hematoma was removed by neuroendoscopy. In cases of obvious and active bleeding, we applied weak bipolar electrocoagulation for hemostasis, and the surgical area was irrigated with warm physiological saline. When there was no evidence of obvious active bleeding, we placed a drainage tube into the hematoma cavity, sutured the dural membrane, and closed the cranium using a routine method.

Observation and Evaluation Indicators

Head CT was re-examined within 24 hours of surgery, and 3D-Slicer software was used to calculate the residual hematoma volume and the hematoma clearance rate. The hematoma clearance rate was calculated as follows: (preoperative hematoma volume – postoperative residual hematoma volume) ÷ preoperative hematoma volume × 100%. We also calculated the incidence of postoperative complications, including rebleeding, intracranial infection and the leakage of cerebrospinal fluid. In addition, we calculated the 30- and 90-day survival rates. Patients were followed up for three months post-surgery and the GOS was used to evaluate patient prognosis (Table II); a GOS score greater than or equal to 4 indicated a good prognosis, while a GOS score <4 indicated a poor prognosis.

RESULTS

Postoperative Clinical Results

All patients underwent head CT re-examination within 24 hours of surgery. Hematoma clearance rates were > 90% in 11 cases and > 80%–90% in four cases, with a mean hematoma clearance rate of 90.52 ± 3.85%. There were no complications associated with intracranial rebleeding, intracranial infection, or cerebrospinal fluid leakage. The 30- and 90-day mortality rates were 26.7% (4/15) and 40% (6/15), respectively. All patients were followed up for three months after surgery. Of the 15 patients, six died and nine survived. The prognosis of the nine surviving patients was evaluated according to GOS. One case had recovered well and could live a normal life, two cases had mild disability, two cases had severe disability, and four cases survived in a vegetative state. The overall good prognosis rate was 20% (3/15).

Typical Cases of Brainstem Hemorrhage

Case 1

A 60-year-old male patient was admitted to our hospital due to a sudden disturbance of consciousness for five hours. Physical examination revealed that the patient was unconscious and in a state of tracheal intubation. Bilateral pupil size was 2 mm with absent light reflexes. Furthermore, the patient exhibited quadriplegia with bilateral Babinski sign positivity. Emergency head CT examination revealed pontine hemorrhage; the largest level of hematoma was predominantly

Table I: Basic Information Relating to the 15 Patients

Patient	Gender	Age (Years)	Preoperative GCS score	Preoperative bilateral pupil size (mm)	Hematoma location	Preoperative hematoma volume (ml)	Combined hydrocephalus (Yes/No)	Surgical approach	Hematoma clearance rate (%)	Postoperative GOS score
1	Female	57	3	5	Whole brainstem	12.3	N	Subtemporal	90.2	1
2	Male	39	3	2	Whole brainstem	12	N	Retrosigmoid	82.5	2
3	Male	52	3	5	Whole brainstem	15	Y	Frontal	84.7	1
4	Male	58	4	2	Mesencephalon-pontine	8	N	Retrosigmoid	91.3	2
5	Male	60	5	2	Pontine-medulla oblongata	14.8	N	Subtemporal	91.2	4
6	Male	54	5	1.5	Pontine	10.3	N	Subtemporal	85.4	3
7	Male	46	4	1	Pontine	8.4	N	Subtemporal	96.4	2
8	Male	68	3	3	Whole brainstem	13.8	N	Retrosigmoid	91.3	1
9	Male	48	3	2	Whole brainstem	14.5	N	Subtemporal	90.3	1
10	Male	40	3	Left 3 Right 5	Whole brainstem	12.7	N	Subtemporal	91.3	1
11	Male	47	5	Left 2 Right 1.5	Pontine	7.9	Y	Subtemporal	93.8	4
12	Female	44	4	Left 3 Right 3.5	Mesencephalon-pontine	11.6	N	Posterior median	88.8	2
13	Male	64	4	1.5	Pontine	9.7	N	Subtemporal	91.8	3
14	Male	64	3	2	Pontine	8	N	Subtemporal	93.8	3
15	Male	64	5	1.5	Mesencephalon-pontine	6	N	Posterior median	95	4

GCS: *Glasgow coma scale,* ***GOS:*** *Glasgow outcome scale,* ***N:*** *No,* ***Y:*** *Yes.*

Table II: Glasgow Outcome Scale (GOS) (3,16)

Score	Grade	Description
5	Good recovery	Able to return to normal life, despite mild defects
4	Moderate disability	Disabled but able to live independently and work under protection
3	Severe disability	Daily life cannot be independent and needs care
2	Vegetative state	Unable to interact with environment, unresponsive
1	Dead	Dead

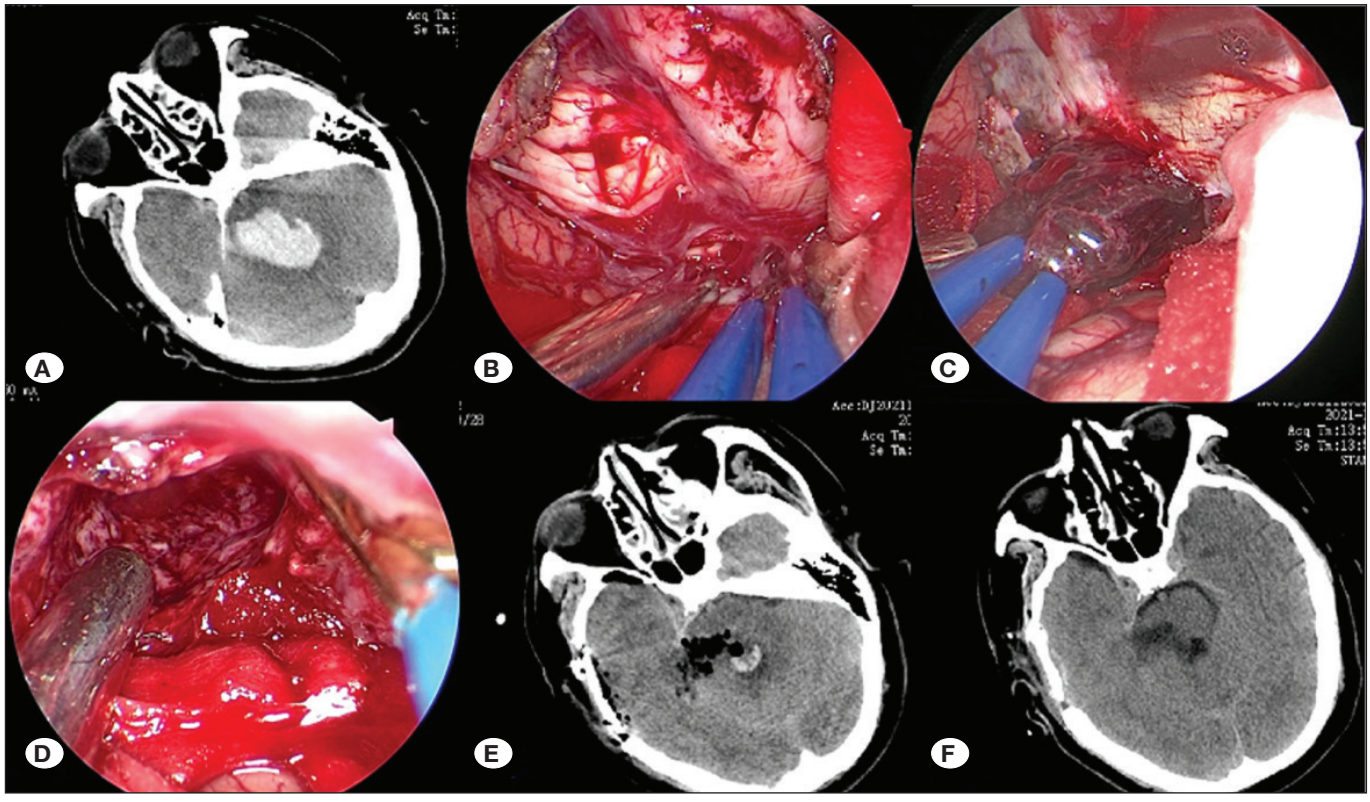

Figure 1: Preoperative head computed tomography (CT) showing that the largest level of the hematoma was located in the right pontine region **(A)**. The tentorium of the cerebellum was cut and the brainstem structure was exposed **(B)**. The hematoma was removed by neuroendoscopy **(C)**. Examination of the hematoma cavity showed no obvious active bleeding **(D)**. CT examination of the head within 24 hours revealed satisfactory brainstem hematoma clearance after surgery **(E)**. CT examination of the head one month after surgery **(F)**.

located in the right region of the pontine. The volume of the hematoma was calculated by 3D-slicer software before surgery (14.8 mL). Head computed tomography angiography (CTA) showed no significant abnormalities. The hematoma was subsequently removed by the right subtemporal approach and neuroendoscopic technology. Repeat head CT examination revealed that the hematoma had been completely removed during surgery. The patient was subsequently transferred to the rehabilitation department one month after surgery. After three months of follow-up, the GOS score of the patient was 4 points (Figure 1).

Case 2

A 47-year-old male patient was admitted to our hospital due to a sudden consciousness disorder that lasted for three hours. Physical examination revealed that the patient was in a state of coma, with unequal pupil sizes on both sides, with a left pupil diameter of 2 mm and a right pupil diameter of 1.5 mm. The light reflex had disappeared, and the limbs were paralyzed with low muscle tone. There was a positive Babinski sign on both sides. Emergency head CT examination revealed a left pontine hemorrhage. The volume of the hematoma was calculated by 3D-slicer software before surgery (7.9 mL). Head CTA showed no significant abnormalities. The hematoma was removed by the left subtemporal approach and neuroendoscopic

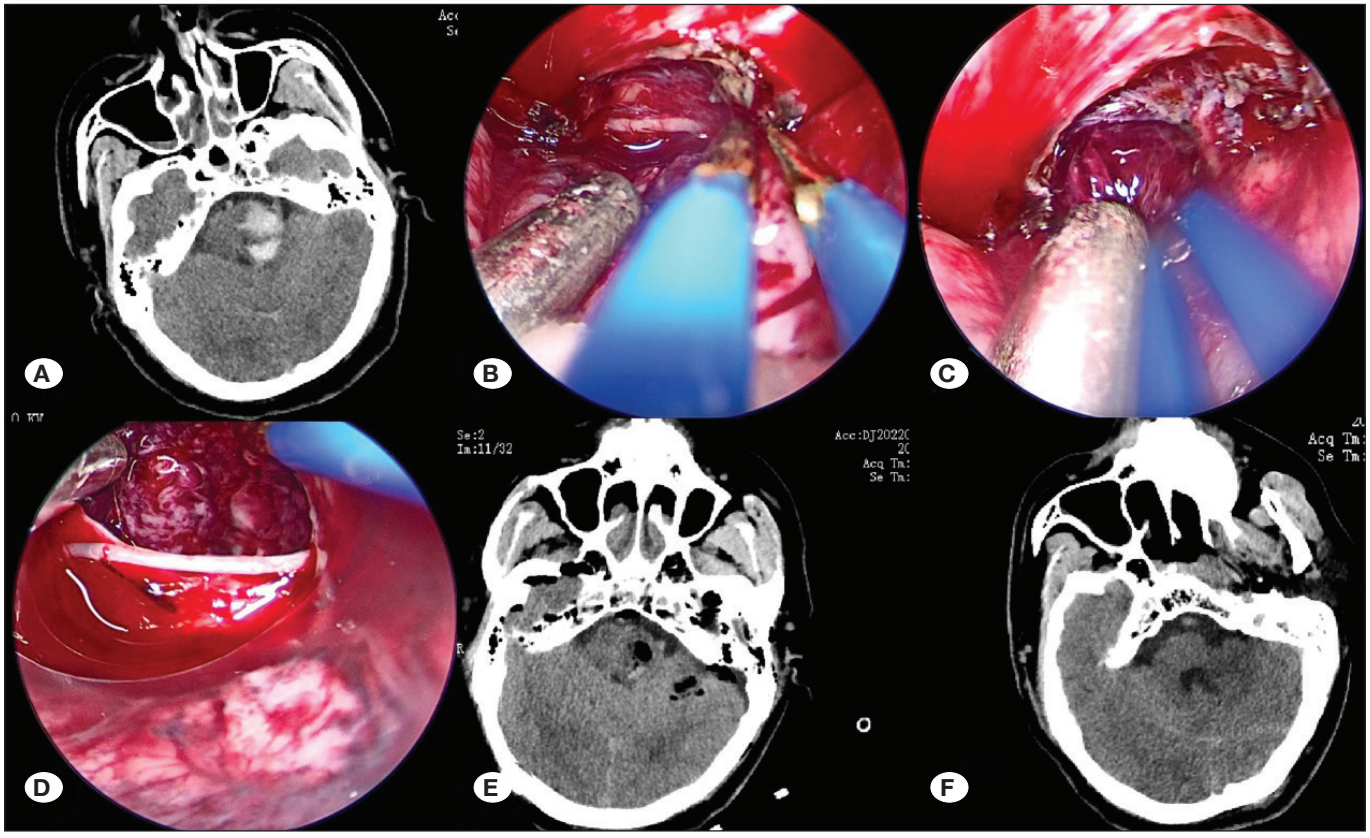

Figure 2: Preoperative head computed tomography (CT) showed that the largest level of the hematoma was located in the left pontine region **(A)**. The tentorium of the cerebellum was cut and the brainstem structure was exposed **(B)**. The hematoma was removed by neuroendoscopy **(C)**. Examination of the hematoma cavity showed no obvious active bleeding **(D)**. CT examination of the head within 24 hours revealed satisfactory hematoma clearance after surgery **(E)**. CT examination of the head one month after surgery **(F)**.

technology. Repeat head CT examination showed that the hematoma had been completely removed during surgery. the patient was transferred to the rehabilitation department one month after surgery. After three months of follow-up, the GOS score of the patient was 4 points (Figure 2).

Case 3

A 64-year-old male patient was admitted to our hospital due to a sudden disturbance of consciousness for two hours. Physical examination revealed that the patient was comatose with irregular breathing. Bilateral pupil size was 1.5 mm with absent light reflexes, and the patient displayed quadriplegia with bilateral Babinski sign positivity. Emergency head CT examination revealed a hematoma located in the dorsal pontine. The volume of the hematoma was calculated by 3D-slicer software before surgery (6 mL). Head CTA revealed no significant abnormalities. The hematoma was removed by the membranous medullary velum approach and neuroendoscopic technology. Repeat head CT examination revealed that the hematoma had been completely removed during surgery. The patient was transferred to the rehabilitation department one month after surgery. After three months of follow-up, the GOS score of the patient was 5 points (Figure 3). The patient's surgical video can be found in Video 1.

DISCUSSION

HBSH is the deadliest form of cerebral hemorrhage, accounting for 6 to 10% of all cases of hypertensive cerebral hemorrhage (4). HBSH most commonly occurs in the pontine region. Due to its special anatomical location, corrective surgery is difficult, the surgical risk is significant, and the patient prognosis is poor (1,12). Previously, the surgical treatment of HBSH was considered to be of limited value, and conservative medical treatment was mainly adopted. American Heart Association/American Stroke Association(AHA/ASA) guidelines clearly prohibit surgical intervention for brainstem hematoma, although the effect of conservative treatment remains extremely poor (4). Over recent years, surgeons have adopted various surgical methods to treat HBSH in order to reduce patient mortality and improve their survival rate and quality-of-life. The symptoms of some HBSH patients were improved after surgical treatment, and the prognosis of surgery was better than that of conservative treatment; furthermore, clinical experience led to greater surgical effect (2,5,18).

Many surgical methods have been applied for HBSH, including craniotomy hematoma removal, stereotactic hematoma puncture, and drainage. Each of these methods has its own advantages and disadvantages (2,9). Neuroendoscopy is one of

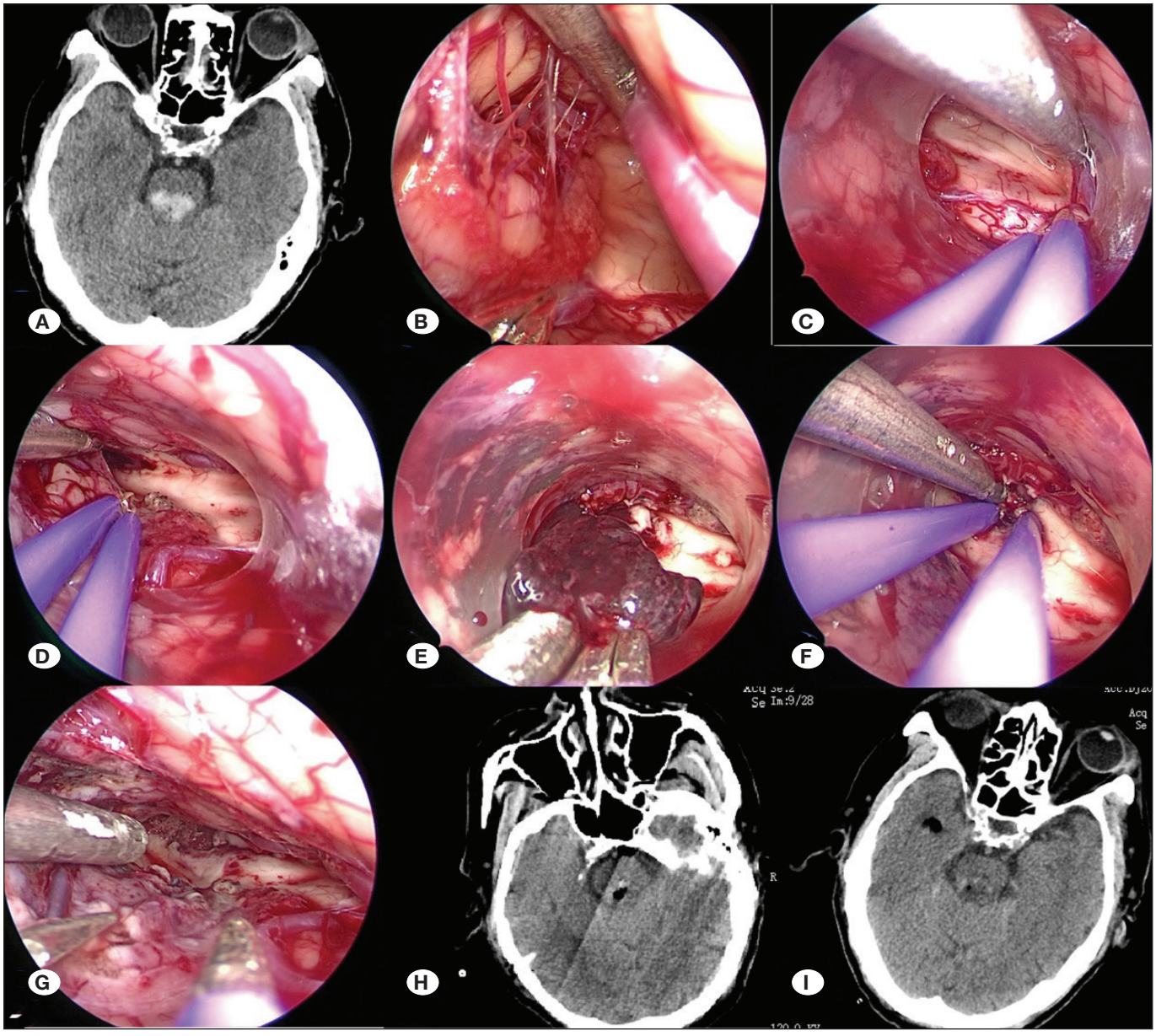

Figure 3: Preoperative CT examination of the head showed that the hematoma was located in the dorsal pontine region **(A)**. The membrane medullary velum structure was opened **(B)**. A micro-sheath (Endoport) was then implanted to explore the bottom of the fourth ventricle **(C)**. Hematoma rupture was observed at the upper end of the fourth ventricle **(D)**. The hematoma was removed by neuroendoscopy **(E)**. Complete hemostasis **(F)**. There was no obvious active bleeding **(G)**. CT examination of the head within 24 hours revealed satisfactory brainstem hematoma clearance after surgery **(H)**. CT examination of the head three days after surgery **(I)**.

the surgical methods for brainstem hemorrhage, but has been rarely used. Oertel et al. used neuroendoscopy to resect 19 patients with brainstem cavernous malformations, and reported good clinical effects and no postoperative complications related to neuroendoscopy (13). Takimoto et al. were the first to remove a brainstem hematoma by neuroendoscopy, making neuroendoscopic technology as a viable alternative for the surgical treatment of brainstem lesions (15). In another study, Zhou et al. used neuroendoscopy technology to treat brain stem and fourth ventricle lesions via the posterior sigmoid sinus approach, including three cases of pontine arm cavernous hemangioma and two cases of brain stem and fourth ventricle tumors. The enhanced maneuverability of neuroendoscopy during surgery effectively compensated for the limitations of a microscope, made the operation more minimally invasive, and achieved good surgical results (19). Liu et al. reported a successful case of neuroendoscopy for brainstem hemorrhage in a man with severe HBSH. One month after surgery, his GCS score improved from 3 to 11, and his symptoms improved significantly (10). Huang et al. used neuroendoscopy to treat 14 patients with primary brainstem hemorrhage; nine of these patients achieved satisfactory functional recovery. This tech-

nique caused minimal levels of damage to important brainstem structures, and achieved satisfactory clinical results (5). However, the safety and efficacy of this procedure has yet to be demonstrate in a large study cohort.

Over recent years, we have used neuroendoscopic technology to treat 15 cases of HBSH, and achieved good clinical results. Neuroendoscopy has several advantages for the treatment of brainstem hemorrhage. First, there is no need to overpull the brain tissue during the operation, there is minimal damage to the brain tissue, and only mild edema occurs in the brain tissue following surgery, especially in the brainstem. Secondly, neuroendoscopy can visualize important nerves and blood vessels in the brainstem and surrounding areas, thus reducing iatrogenic injury. Third neuroendoscopy can be used in a narrow space in multiple directions and angles, thus improving the hematoma clearance rate. In addition, when using this method, it is easy to identify small bleeding points during surgery. This means that it is possible to stop bleeding in good time and ensure hemostasis with only a low probability of postoperative rebleeding. Finally, neuroendoscopy results in a shorter surgical duration, less intraoperative bleeding, and fewer postoperative complications.

There are several key points to emphasize from our research. First, when a hematoma breaks through the cortex of the brainstem, the hematoma can be gradually removed along the break. When the hematoma does not break through the surface of the brainstem, the site of the hematoma can be determined under the guidance of neural navigation, and the non-vascular area on the surface of the brain stem can be selected, while avoiding the location of important nerve nuclei for corticostomy. Secondly, removal of the hematoma should be carried out in the hematoma cavity as far as possible and not exceeding the edge of the hematoma cavity. To avoid damage to normal brain tissue, the suction force should not be too excessive. Third, when there is active bleeding, low-power bipolar electrocoagulation can be used for accurate hemostasis, and the surgical area can be repeatedly rinsed with normal saline to reduce thermal damage. Areas of active bleeding can be covered by a hemostasis gauze or cotton sheet without the need for bipolar electrocoagulation. Finally, the midbrain aqueduct should be opened during surgery to establish an unobstructed cerebrospinal fluid circulation pathway to prevent postoperative hydrocephalus.

There are some limitations to this study that need to be considered. First, we only included a small number of patients. Second, this was a retrospective study performed in a single-center with a short follow-up time. Multi-center, large-sample, case-randomized and controlled studies are still needed to further confirm the clinical efficacy of this technique.

CONCLUSION

Neuroendoscopy-assisted treatment of HBSH is safe and effective, offering a high hematoma clearance rate, fewer postoperative complications, and favorable surgical outcomes. However, this study has some limitations. The sample size of patients in this group is small, it is a single-center retrospective study, and the follow-up period is relatively short. To further validate the clinical efficacy of this technique, multi-center, large-sample, case-randomized controlled studies are needed, which should be covered in future studies.

ACKNOWLEDGMENTS

We thank the patients who participated in this study.

Declarations

Funding: This work was supported by National Natural Science Foundation of China (81671306; 81971158; 82271518), Wuhan Science and Technology project (2019020701011470).

Availability of data and materials: The datasets generated and/or analyzed during the current study are available from the corresponding author by reasonable request.

Disclosure: The authors declare no competing interests.

AUTHORSHIP CONTRIBUTION

Study conception and design: ZLY, QC

Data collection: ZLY

Analysis and interpretation of results: ZLY, LZ

Draft manuscript preparation: ZLY

Critical revision of the article: LZ, QC

Other (study supervision, fundings, materials, etc...): QC

All authors (ZLY, LZ, QC) reviewed the results and approved the final version of the manuscript.

REFERENCES

1. Behrouz R: Prognostic factors in pontine haemorrhage: A systematic review. Eur Stroke J 3:101-109, 2018. https://doi.org/10.1177/2396987317752729.
2. Chen D, Tang Y, Nie H, Zhang P, Wang W, Dong Q, Wu G, Xue M, Tang Y, Liu W, Pan C, Tang Z: Primary brainstem hemorrhage: A review of prognostic factors and surgical management. Front Neurol 12:727962, 2021. https://doi.org/10.3389/fneur.2021.727962
3. Chen LH, Li FJ, Zhang HT, Chen WJ, Sun K, Xu RX: The microsurgical treatment for primary hypertensive brainstem hemorrhage: Experience with 52 patients. Asian J Surg 44:123-130, 2021. https://doi.org/10.1016/j.asjsur.2020.04.016
4. Hemphill JC 3rd, Greenberg SM, Anderson CS, Becker K, Bendok BR, Cushman M, Fung GL, Goldstein JN, Macdonald RL, Mitchell PH, Scott PA, Selim MH, Woo D; American Heart Association Stroke Council; Council on Cardiovascular and Stroke Nursing; Council on Clinical Cardiology: Guidelines for the management of spontaneous intracerebral hemorrhage: A guideline for healthcare professionals from the American Heart Association/American Stroke Association. Stroke 46:2032-2060, 2015. https://doi.org/10.1161/STR.0000000000000069
5. Huang C, Liu X, Zhao G, Qian W, Zhang Y, Zhang W, Zhu Y, Zou Y: Neuroendoscopic surgery for brainstem hemorrhage: Technical notes and preliminary clinical results.Clin Neurol Neurosurg 246:108576, 2024. https://doi.org/10.1016/j.clineuro.2024.108576

6. Huang K, Ji Z, Sun L, Gao X, Lin S, Liu T, Xie S, Zhang Q, Xian W, Zhou S, Gu Y, Wu Y, Wang S, Lin Z, Pan S: Development and validation of a grading scale for primary pontine hemorrhage. Stroke 48:63-69, 2017. https://doi.org/10.1161/STROKEAHA.116.015326
7. Ichimura S, Bertalanffy H, Nakaya M, Mochizuki Y, Moriwaki G, Sakamoto R, Fukuchi M, Fujii K: Surgical treatment for primary brainstem hemorrhage to improve postoperative functional outcomes. World Neurosurg 120:e1289-e1294, 2018. https://doi.org/10.1016/j.wneu.2018.09.055
8. Konovalov AN, Spallone A, Makhmudov UB, Kukhlajeva JA, Ozerova VI: Surgical management of hematomas of the brain stem. J Neurosurgery 73:181-186,1990. https://doi.org/10.3171/jns.1990.73.2.0181.
9. Li Y, Shang FJ, Xu Z, Wu DX, Li CH, Liu JF, Li YX, Zhang WH, Zhang WC: Comparison of stereotactic aspiration surgery and conventional treatment for primary brainstem haemorrhage. Clin Neurol Neurosurg 234:108008, 2023. https://doi.org/10.1016/j.clineuro.2023.108008.
10. Liu B, Zheng T, Mao Y, Bian K, He S, Lv W: Endoscopic endonasal transclival approach to spontaneous hypertensive brainstem hemorrhage. J Craniofac Surg 31:e503-506, 2020. https://doi.org/10.1097/SCS.0000000000006599.
11. Meguro T, Kuwahara K, Tomita Y, Okuma Y, Tanabe T, Muraoka K, Terada K, Hirotsune N, Nishino S: Primary pontine hemorrhage in the acute stage: Clinical features and a proposed new simple scoring system. J Stroke Cerebrovasc Dis 24:860-865, 2015. https://doi.org/10.1016/j.jstrokecerebrovasdis.2014.12.006.
12. Morotti A, Jessel MJ, Brouwers HB, Falcone GJ, Schwab K, Ayres AM, Vashkevich A, Anderson CD, Viswanathan A, Greenberg SM, Gurol ME, Romero JM, Rosand J, Goldstein JN: CT angiography spot sign, hematoma expansion, and outcome inprimary pontine intracerebral hemorrhage. Neurocrit Care 25:79-85, 2016. https://doi.org/10.1007/s12028-016-0241-2.
13. Oertel J, Fischer G, Linsler S, Huelser M, Sippl C, Teping F. Endoscope-assisted resection of brainstem cavernous malformations. Neurosurg Rev 45:2823-2836, 2022. https://doi.org/10.1007/s10143-022-01793-5.
14. Takeuchi S, Suzuki G, Takasato Y, Masaoka H, Hayakawa T, Otani N, Yatsushige H, Shigeta K, Momose T, Wada K, Nawashiro H: Prognostic factors in patients with primary brainstem hemorrhage. Clin Neurol Neurosurg 115:732-735, 2013. https://doi.org/10.1016/j.clineuro.2012.08.022
15. Takimoto H, Iwaisako K, Kubo S, Yamanaka K, Karasawa J, Yoshimine T: Transaqueductal aspiration of pontine hemorrhage with the aid of a neuroendoscope. Technical note. J Neurosurg 98:917-919, 2003. https://doi.org/10.3171/jns.2003.98.4.0917
16. Teasdale G, Jennett B: Assessment and prognosis of coma after head injury. Acta Neurochir 34:45-55,1976. https://doi.org/10.1007/BF01405862.
17. Wang SS, Yang Y, Velz J, Keller E, Luft AR, Regli L, Neidert MC, Bozinov O: Management of brainstem hemorrhages. Swiss Med Wkly 149:w20062, 2019. https://doi.org/10.4414/smw.2019.20062.
18. Zhang HT, Chen LH, Bai MC, Xu RX: Anterior subtemporal approach for severe upper pontine hematomas: A report of 28 surgically treated cases. J Clin Neurosci 54:20-24, 2018. https://doi.org/10.1016/j.jocn.2018.04.063
19. Zhou L, Wei H, Li Z, Zhang H, Song P, Cheng L, Wang W, Lei P, Chen Q, Liu Z, Ye H, Sun D, Cai Q: Treatment of brainstem and fourth ventricle lesions by the full neuroendoscopic telovelar approach. Eur J Med Res 28:564, 2023. https://doi.org/10.1186/s40001-023-01460-5.

Turk Neurosurg 35(4):561-569, 2025
DOI: 10.5137/1019-5149.JTN.47590-24.3

Original Investigation

Cerebrovascular-Endovascular

Received: 09.09.2024
Accepted: 25.10.2024
Published Online: 25.06.2025

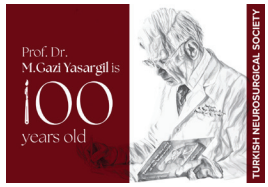

Endovascular Occlusion of Intracranial Pial Arteriovenous Fistula: Technical Aspects

Celal CINAR[1], Mahmut KUSBECI[1], Alperen ELEK[1], Egemen OZTURK[2], Ismail ORAN[1]

[1]Ege University, Faculty of Medicine, Department of Interventional Radiology, Izmir, Türkiye
[2]Usak Training and Research Hospital, Department of Radiology, Usak, Türkiye

Corresponding author: Ismail ORAN ✉ ismailoran@gmail.com

ABSTRACT

AIM: To evaluate pial arteriovenous fistulas (AVFs), focusing on the radio-anatomic architecture and contemporary endovascular devices and techniques.

MATERIAL and METHODS: Sixteen patients with congenital pial AVFs who underwent endovascular treatment between 2002 and 2023 at a single institution were included in this review. This retrospective study was approved by the Institutional Review Board. The study was descriptive and involved no statistical comparisons.

RESULTS: The study included 16 patients (6 female patients, 10 male patients) with a mean age of 19.93 ± 21.1 years (range: 1–63 years). Nine (56.25%) were pediatric patients, six (37.5%) of whom were younger than 5 years. Five patients (31.25%) had more than one feeding artery, whereas 11 (68.75%) had a single feeding artery. One patient had two separate fistulas. All fistulas were successfully occluded without complications. Four patients (25%) were treated with glue alone, four (25%) with coils alone, five (31.25%) with a non-adhesive liquid agent alone, and three (18.75%) with a combination of coils and a non-adhesive liquid agent. Venous sinus thrombosis occurred in two patients (12.5%) in the early postoperative period; both cases resolved without permanent deficits.

CONCLUSION: Pial AVF is a rare intracranial vascular malformation. Endovascular treatment using liquid embolic agents, coils, or a combination of these techniques is effective.

KEYWORDS: Glue, Coils, Non-adhesive liquid agent, Arteriovenous fistula, Pial AVF

ABBREVIATIONS: AVF: Arteriovenous fistula, **CT:** Computed tomography, **MR:** Magnetic resonance, **AVM:** Arteriovenous malformation, **SAH:** Subarachnoid hemorrhage, **EVOH:** Ethylene-vinyl alcohol, **DMSO:** Dimethyl sulfoxide

INTRODUCTION

A pial arteriovenous fistula (AVF) is a rare vascular disorder, accounting for approximately 1.6% of all intracranial vascular malformations. Pial AVFs differ from both pial and dural arteriovenous malformations (AVMs); the latter are characterized by vascular nidi (tangled vascular networks) in the parenchyma and meningeal layers, respectively. Although pial AVFs share some radiological features with pial AVMs, they are now recognized as distinct vascular anomalies (8). The defining characteristics of a pial AVF include pial arterial feeders, a direct arteriovenous fistula without an intervening nidus, and an aneurysmal varix with lobulated, serpiginous venous drainage.

We reviewed a series of patients with pial AVFs, focusing on the radio-anatomic architectures and the utility of contemporary endovascular devices and techniques.

Celal CINAR : 0000-0002-3237-9268
Mahmut KUSBECI : 0000-0002-7583-1170
Alperen ELEK : 0000-0001-5414-6548
Egemen OZTURK : 0000-0002-1167-9990
Ismail ORAN : 0000-0002-3546-7773

MATERIAL and METHODS

This retrospective study was approved by Ege University Faculty of Medicine, Institutional Review Board (protocol number 24-6.1T/37). The Board waived the requirement for informed patient consent due to the retrospective and observational nature of the study. All patient details were anonymized during data collection and analysis to ensure confidentiality.

Between 2002 and 2023, 16 patients with pial AVFs were treated using endovascular methods. Patient demographics, clinical presentations, endovascular management strategies, follow-up data, and outcomes were recorded. All patients underwent computed tomography (CT)/CT angiography and magnetic resonance (MR) imaging/MR angiography, which revealed the characteristics and anatomy of the vascular lesions. MR angiography was generally preferred for follow-up. Clinical outcomes were defined as "excellent" when neurological findings returned to normal and as "good" when no additional neurological deficit was observed postoperatively. Modified Rankin scores from the most recent neurological examinations were also recorded.

No statistical comparisons were performed in this descriptive study. Continuous variables are presented as medians with standard deviations (SDs) and ranges; categorical variables are presented as frequencies with percentages.

RESULTS

There were 10 male (62.5%) and 6 female patients (37.5%) of mean age 19.93 ± 21.1 years and median age 8.5 years (range 1 to 63 years). Nine patients (56.25%) were pediatric, six (37.5%) of whom were younger than 5 years. Patient data are summarized in Table I. Six patients (37.5%) presented with acute ictus, and imaging suggested pial AVF hemorrhages. Five patients (31.25%) had more than one feeding artery, whereas the remainder had single feeding arteries. One patient (case #11) had two distinct fistulas with separate drainage routes; all others had single fistulas and drainage routes. Nine patients (56.25%) exhibited aneurysmal venous varices associated with the pial AVFs; five (31.25%) of these patients were pediatric. Thrombosed varicose aneurysms were observed in three of these nine patients (18.75%).

All embolization procedures were successful, and no complications occurred. Four fistulas (25%) were occluded using glue alone, four (25%) with coils alone, five (31.25%) with a non-adhesive liquid agent alone, and the remaining three (18.75%) with combinations of coils and the non-adhesive liquid agent. Simple embolization (either coils or a liquid agent) was used in 13 patients (81.25%). The double microcatheter technique was utilized in two patients (12.5%) (Figures 1-4), and the flow arrest technique with a double microcatheter was used in another two patients (12.5%) (Figures 5 and 6).

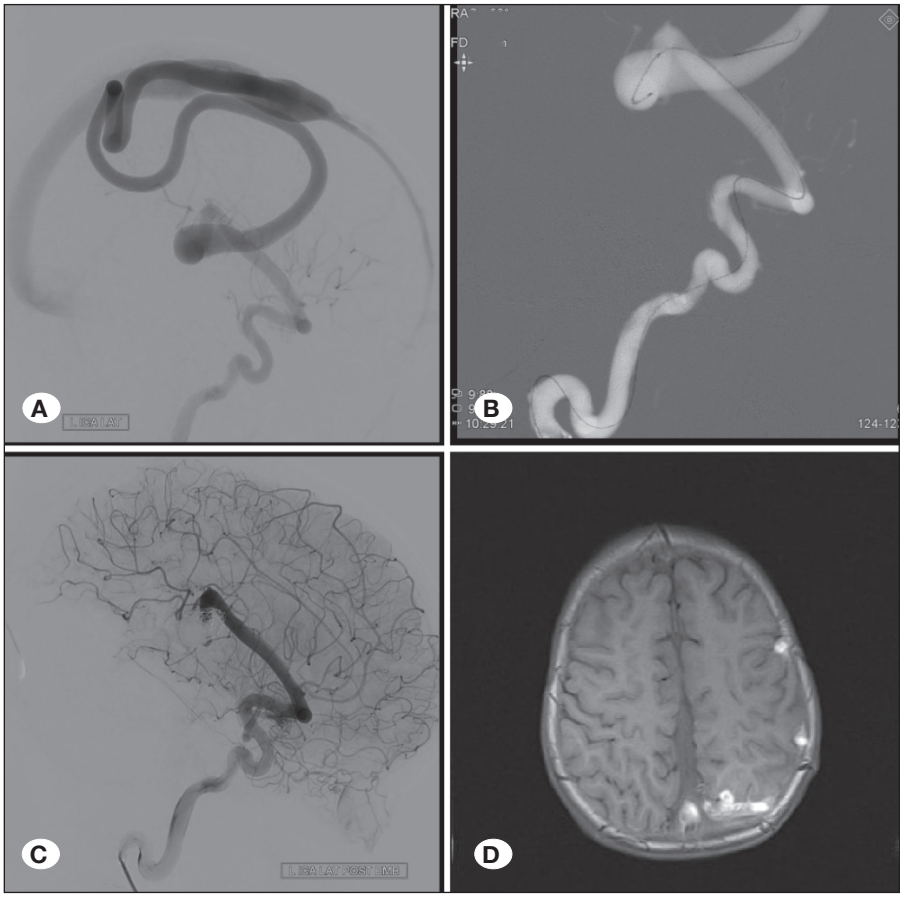

Figure 1: A 1-year-old male patient presented with macrocrania and hydrocephalus. **A)** Left internal carotid angiography lateral projection. There is a single-hole high-flow fistula fed by the M2 branch of left middle cerebral artery which drains to a superficial serpiginous dilated vein, then superior sagittal sinus. **B)** Although the proximal venous part of the fistula site has relatively dilated, deploying coils without migration would be difficult. This anatomy is ideal for using the double-microcatheter technique. **C)** Control angiography shows total occlusion with coils only. **D)** MR imaging 15 days later demonstrates subacute thrombosis in the fistula's serpiginous vein which also extends up to the superior sagittal sinus.

Table I: Summary of 16 Patients with Pial AVF

Case No/ Sex/Age (year)	Presentation	Bleeding	Feeding Artery	Draining Sinus	Venous Varix	Embolization Material / Technique	Follow-up	Clinical Outcome (mRS)
1/M/1	Macrocrania, Hydrocephalus		R AICA R PICA R SCA	Occipital	Yes (thrombosed)	Glue /Simple	6 months	Good (0)
2/M/55	Headache		L PCA L MCA	Superior sagittal	Yes	Glue /Simple	6 months	Excellent (0)
3/F/35	Headache		L MCA L PCA	Transverse	Yes	Glue /Simple	2 years	Excellent (0)
4/M/24	Syncope	Hematoma	R PCA	Transverse	No	Glue /Simple	6 months	Excellent (0)
5/F/2	Incidental (PHACE Syndrome)		R ACA	Transverse	No	Coil/ Simple	2 years	Excellent (0)
6/M/28	Headache		R MCA	Superior sagittal	Yes (thrombosed)	Coil /Simple	15 years	Excellent (0)
7/F/1	Incidental (PHACE syndrome)		L PCA	Rectus	Yes	Coil/ Simple	6 years	Excellent (0)
8/M/1	Macrocrania, Hydrocephalus		L MCA	Superior sagittal	Yes	Coil /Double catheter	6 months	Good (1)
9/M/32	Syncope	Hematoma	L PCA	Transverse	No	Onyx /Simple	2 years	Excellent (0)
10/M/5	Syncope, Paresia	Hematoma	R MCA	Superior sagittal	No	Onyx /Simple	2 years	Good (1)
11/F/1	Seizure	SAH	R PCA R ACA	Superior sagittal	Yes (thrombosed)	Onyx /Simple	4 years	Good (1)
12/M/63	Incidental		R MCA	Superior sagittal	No	Onyx /Simple	2 years	Excellent (0)
13/M/9	Headache	SAH	R ACA	Rectus	No	Onyx /Simple	6 months	Excellent (0)
14/M/8	Headache		R PCA	Rectus	No	Coil + Onyx/ Double-catheter	4 years	Excellent (0)
15/F/47	Headache Seizure		L ACA	Superior sagittal	Yes	Coil + Onyx/ Double-catheter flow arrest	2 years	Excellent (0)
16/F/7	Syncope	SAH	R, L PICA	Marginal	Yes	Coil + Onyx/ Double-catheter flow arrest	3 months	Excellent (0)

mRS: *Modified Rankin Scale,* ***M:*** *Male,* ***F:*** *Female,* ***R:*** *Right,* ***L:*** *Left.* ***AICA:*** *Anterior Inferior Cerebellar Artery,* ***PICA:*** *Posterior Inferior Cerebellar Artery,* ***SCA:*** *Superior Cerebellar Artery,* ***MCA:*** *Middle Cerebral Artery,* ***PCA:*** *Posterior Cerebral Artery,* ***ACA:*** *Anterior Cerebral Artery,* ***SAH:*** *Subarachnoid Hemorrhage.*

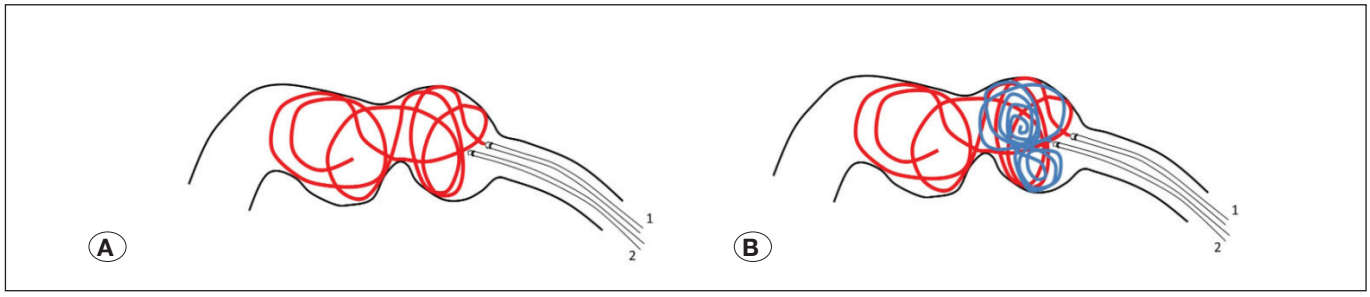

Figure 2: Schematic representation of coiling with the double-microcatheter technique. **A)** Two microcatheters are placed in the fistula, extending to the very proximal part of the venous route. The oversized first coil was deployed through the first microcatheter. **B)** Subsequent smaller coils were deployed in the nest of first coil through the second microcatheter, while the first coil remains undetached.

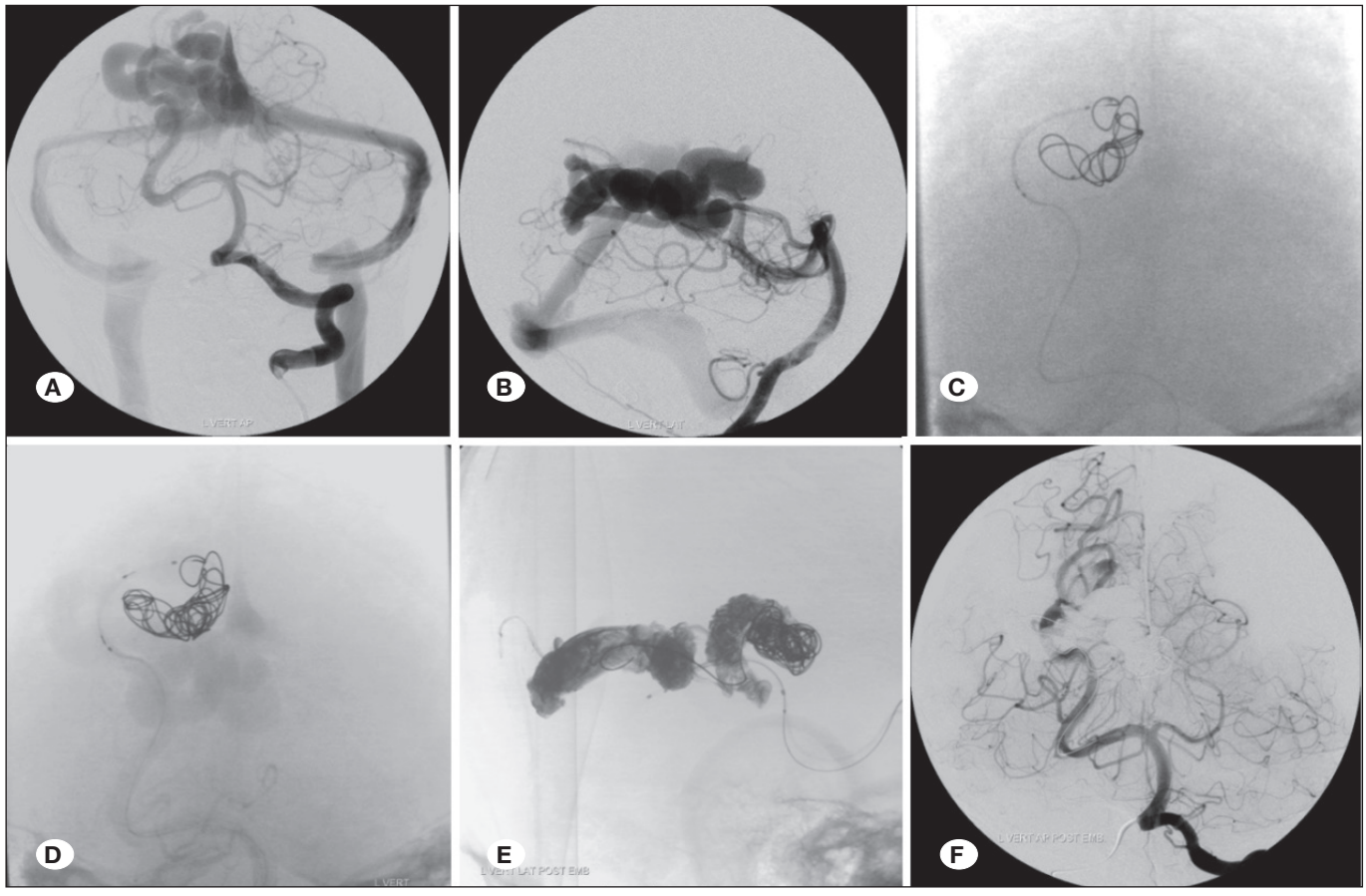

Figure 3: An 8-year-old male patient presented with headaches. Left vertebral artery angiography, frontal **(A)** and lateral **(B)** projection. There is a single hole high-flow fistula fed by the right posterior cerebral artery which drains to superficial serpiginous dilated vein and then ipsilateral Rosenthal vein, and sinus rectus. **C)** First coil is deployed through the first microcatheter and kept undetached. **D)** The second coil is deployed in the nest of the first coil through the second microcatheter. This is an example of the double-microcatheter technique. **E)** Lateral image. After blood flow is markedly reduced by coil packing, liquid is injected in front of the coil pack to achieve total occlusion of the fistula. Note the unintentional migration of coil pack in the distal venous segment. Also, note that coil nest successfully holds the proximal liquid cast without fragmentation. **F)** Control angiography frontal projection reveals total occlusion of the fistula.

In the early postoperative period, lethargy and drowsiness occurred in a 1-year-old patient (case #8), and an adult (case #15) experienced worsening headaches. MR imaging revealed the development of venous and/or dural sinus thrombosis in both cases, and both patients responded well to appropriate medical treatment. MR venography performed 6 months later showed complete recanalization of the thrombosed sinuses in case #8. Endovascular treatment and shunt surgery for hydrocephalus were performed simultaneously in two pediatric patients (cases #1 and #8). In a third patient (case #11), hydrocephalus developed later, attributed to a subarachnoid hemorrhage, and a shunt was placed after endovascular treatment. Aside from early thrombotic complications in two patients, the remaining 14 (87.5%) experienced no worsening of their clinical conditions. Symptoms improved over time; all hemorrhages were reabsorbed, and hydrocephalus resolved after shunt placement.

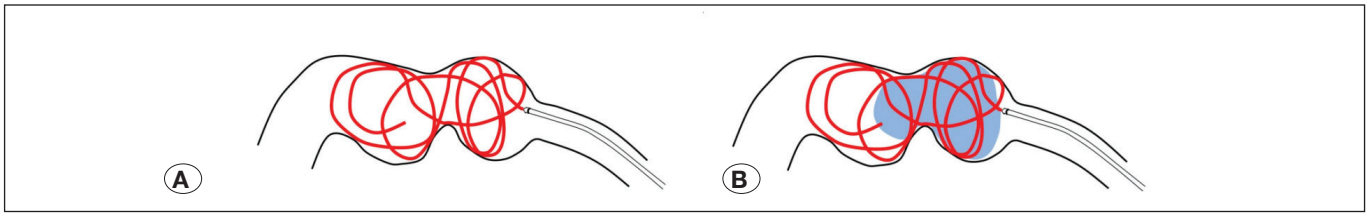

Figure 4: Schematic representation of the combined usage of coils and non-adhesive liquid embolization agent. **A)** Appropriate coil packing is initially achieved. **B)** To obtain stable and absolute occlusion, the spaces within the coil nest are filled with a liquid embolization agent using the same microcatheter.

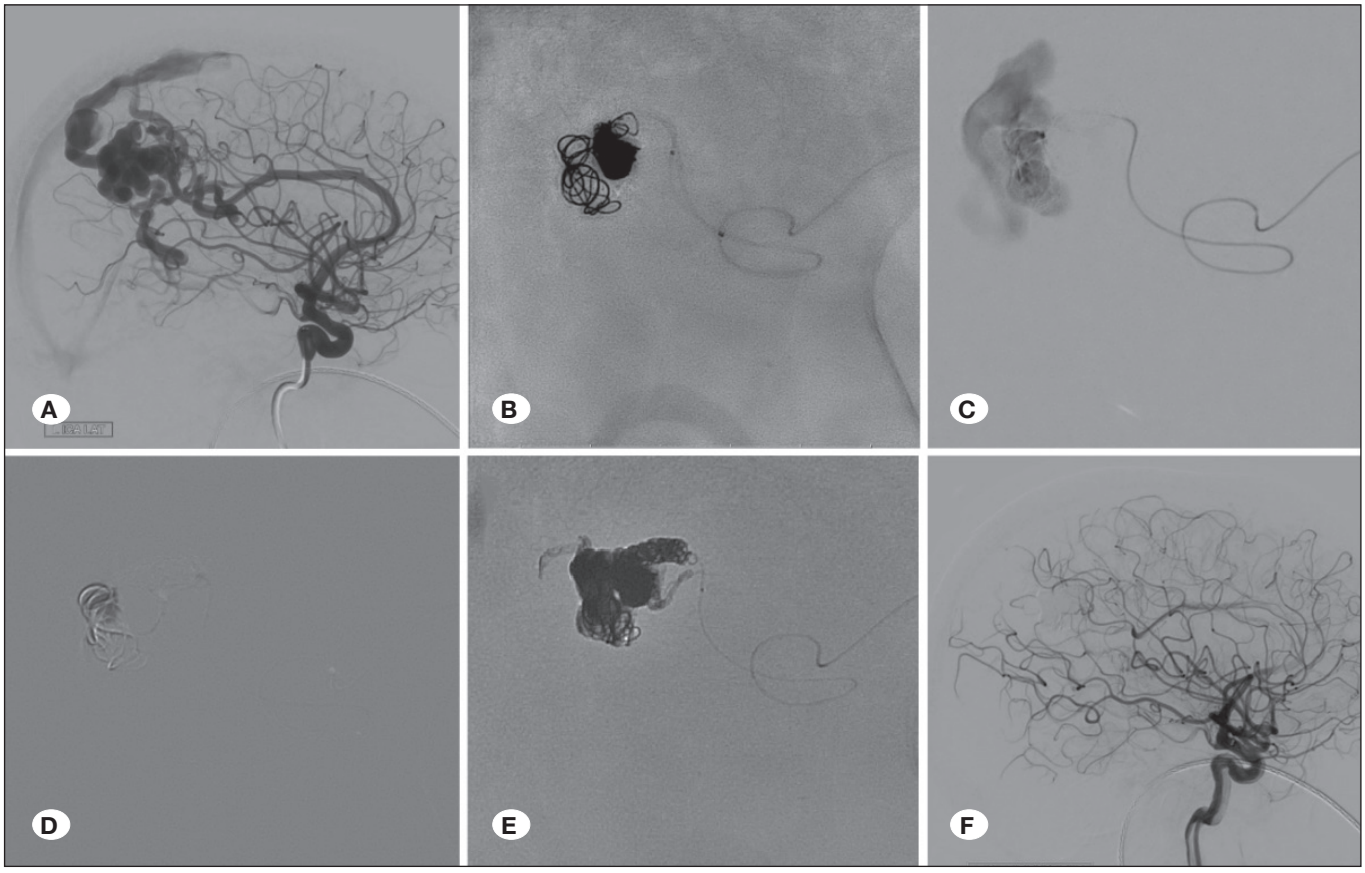

Figure 5: An 8-year-old male patient presented with headaches. **A)** Left internal carotid angiography lateral projection. There is a single-hole high-flow fistula fed by the left anterior cerebral artery, which drains to a superficial serpiginous dilated vein with multiple varicose aneurysms and then sinus rectus and superior sagittal sinus. **B)** Double-microcatheter flow-arrest technique. While one microcatheter is placed at the fistula point, the second microcatheter is placed 1-2 cm distal. Coils are deployed through the first microcatheter. **C)** Contrast injection through the second microcatheter reveals markedly diminished but still flowing blood. **D)** Slow non-adhesive liquid embolization injection through the second microcatheter on the roadmap image. **E)** Final embolic cast ensuring firm occlusion, consisting of coils and liquid. **F)** Final angiography confirming total occlusion of the fistula.

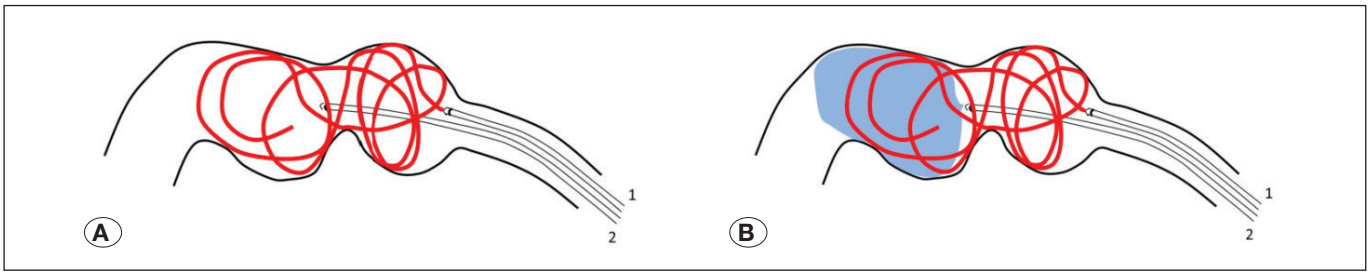

Figure 6: Schematic representation of double-microcatheter flow-arrest technique, combining the usage of coils and non-adhesive liquid embolization agent. **A)** Appropriate coil packing is achieved through the first microcatheter. The coil package diminishes markedly dragging force of blood flow. **B)** To obtain stable and

DISCUSSION

This study demonstrated that endovascular treatment is effective for pial AVF; all 16 patients underwent successful procedures without immediate complications. Aneurysmal venous varices were present in 56.25% of patients, particularly in the pediatric group. Multiple arterial feeders were observed in 31.25% of patients, and one patient had two distinct fistulas. Simple embolization was sufficient in most cases; complex techniques, such as the double microcatheter approach, rarely were required. Postoperative thrombotic complications occurred in two patients but resolved with medical management. Favorable clinical outcomes were achieved in 87.5% of cases.

Pial AVFs are generally characterized by single-hole arteriovenous connections with single feeding arteries and ectatic, serpiginous venous drainage; no nidus is present. A venous aneurysmal varix is another distinctive feature, especially in patients with high-flow pial AVFs. Low-flow pial AVFs may lack this varix, which can lead to confusion with pial AVMs. The typical subpial location, near the cortex, helps to differentiate pial AVFs from pial AVMs. Multiple feeding arteries with several venous routes (i.e., multiple fistulas) and multiple feeding arteries with single venous routes are rare in pial AVFs.

As of September 2024, 231 pediatric cases of pial AVF have been reported in the literature (16). Most pial AVF patients are diagnosed in childhood, typically before the age of 5 years (10,13,16,18). In these patients, the primary presenting symptoms include hydrocephalus, developmental delay, enlarged head circumference, cardiac failure, and seizures. Coubes et al. reported a potential association between pial AVF and Rendu-Osler-Weber disease, a rare autosomal-dominant disorder (3). In older children and adults, headaches, seizures, and neurological deficits are more common, often due to mass effects from venous varices and hemorrhages (9,10,13). Hydrocephalus was observed in three of our pediatric patients, all of whom required shunt placement. However, hydrocephalus may improve after endovascular treatment alone (11). Spontaneous thrombosis of a pial AVF has also been reported; three of our 16 patients displayed acute thrombosis of venous aneurysmal varices. Some patients may present with intracranial bleeding; three of our patients exhibited intraparenchymal hemorrhages, and two presented with subarachnoid hemorrhages at diagnosis.

The endovascular treatment strategy for pial AVF is similar to that for other intracranial fistulas: the fistula should be occluded, extending to the proximal drainage vein when possible. Adhesive agents (cyanoacrylates), non-adhesive liquids (12), and metallic endovascular implants (coils, stents) are used to achieve this occlusion.

Cyanoacrylate monomers undergo exothermic polymerization upon contact with blood, ensuring rapid adhesion and immediate occlusion of the injected vessel. Various intravascular acrylic agents are available, differing in both molecular structure and specific additives. Common N-butyl cyanoacrylate-based agents include Histoacryl (B. Braun, Melsungen, Germany), Glubran 2 (GEM SRL, Viareggio, Italy), and TruFill (Cerenovus, Irvine, CA, USA). Magic Glue (Balt, Montmorency, France) is an N-hexyl cyanoacrylate-based agent, whereas Fuaile (Beijing, China) is a combination of N-butyl and 2-octyl cyanoacrylates. Cyanoacrylates are typically mixed with Lipiodol (Guerbet, Villepinte, France) to slow polymerization and adhesion in a concentration-dependent manner (17).

Neurointerventional non-adhesive liquid embolization agents include Onyx (Medtronic, Irvine, CA, USA), Squid (Balt, Montmorency, France), and PHIL (MicroVention, Tustin, CA, USA) (17). These agents are permanent, non-absorbable, and non-adhesive. Onyx, one of the most widely used liquids, is an elastic polymer (ethylene-vinyl alcohol [EVOH]) dissolved in dimethyl sulfoxide (DMSO); micronized tantalum powder provides radiopacity. Squid is also based on EVOH/DMSO; its low-viscosity variant enhances distal penetration. PHIL contains an iodinated material bound to the copolymer, ensuring radiopacity and preventing CT artifacts caused by tantalum (17).

Since Guglielmi et al. first used detachable coils in 1991 (5), many manufacturers have developed coils with various distinct features; notably, the basic operating principle remains unchanged. Coils are both easy to use and effective for endovascular occlusion; they have numerous neurovascular applications. Considering the extensive literature, the specific types and features of detachable coils will not be discussed in detail here.

Despite advances in endovascular devices and techniques, neurointerventionalists still face two key challenges. First, it can be difficult to ensure that occlusive implants remain at a fistula site, given the relatively dilated and serpiginous vascular

bed associated with high-flow blood. High-concentration glue (Lipiodol: cyanoacrylate ratio of 1:2 or a cyanoacrylate concentration above 65% v/v) has been successfully used to treat high-flow fistulas with techniques similar to those utilized for Galenic fistulas (10,18). In the present study, four patients were successfully treated with high-concentration glue alone. However, the use of glue has decreased with the development of alternative embolization agents and techniques; fewer operators today have sufficient experience with this method. Detachable coils offer more controlled embolization relative to that achieved using glue. Four of our patients were treated with coils alone. The enlarged venous side of a pial AVF contains vascular structures folded over each other, often exhibiting sharp bends and/or venous varices. An experienced neurointerventionalist can anchor detachable coils within these anatomic structures, ultimately achieving total occlusion of the fistula.

Non-adhesive liquid embolization agents have been in use for approximately 15 years. Compared with glue, they are easier to handle and less thrombogenic (17). However, they are soft, pliable, and persistently remain in fluid form, making them unsuitable for treating AVFs, except in cases of low-flow AVFs.

Using the standard endovascular techniques described above, most pial AVFs can be treated successfully. In more complex cases, where challenging anatomy or high-flow blood is present, advanced endovascular techniques may be necessary.

Coiling Using Double Microcatheters

The 6-Fr access systems routinely used today allow for the simultaneous placement of two microcatheters within a fistula. If ideal coil anchor sites are absent, an oversized initial coil can be placed without detachment, creating a barrier. Subsequent coils are then delivered into the nest of the first coil via the second microcatheter (Figures 1-3). This technique has been used to coil large-necked intracranial aneurysms (15). Additionally, the Solitaire endovascular device (Medtronic, Irvine, CA, USA), a detachable stent, may serve as an initial nest (19).

Combinations of Coils and Non-adhesive Liquid Embolization Agents

Coiling alone may not always achieve fistula occlusion, particularly in high-flow cases. Sometimes, the anatomy prevents dense coil packing. In such situations, complete occlusion can be achieved by filling the spaces between the coils with a liquid embolization agent using the same microcatheter. Non-adhesive liquid agents, rather than glue, should be preferred. These agents can be safely injected into an already-placed coil pack, even in high-flow fistulas. Controlled, fractionated, slow injection under roadmap guidance is essential when using non-adhesive liquids for embolization. Coil and liquid combinations have been employed for transvenous obliteration of cerebral and dural AVFs. This approach enhances venous sinus obliteration, as the liquid fills the entire vascular bed (1), and can even penetrate the arterial fistula. The already-placed coil pack acts as a nest for the liquid, preventing fragmentation, while liquid accumulation within the coil nest ensures stable occlusion within minutes (Figures 3 and 4). More experienced operators can combine coils with glues (Lipiodol: cyanoacrylate ratios of 4:1 to 1:1, cyanoacrylate at 20-50% v/v). Operators must be aware that the catheter may adhere to the coil pack during retrieval, potentially pulling it back. When performed correctly, glue injection ensures immediate fistula occlusion.

Flow Arrest Techniques

These techniques prevent undesirable distal embolization that may occur if a liquid agent is dragged distally by proximal blood flow. Either a double-microcatheter or a dedicated double-lumen balloon catheter is required. In the double-microcatheter flow-arrest approach, one microcatheter is positioned at the fistula site, and the second is placed at the same level or 1–2 cm proximally. When coils are deployed through the second microcatheter, the blood flow in the arterial feeder is largely or completely stopped. This stopped flow reduces the blood's dragging force, allowing the liquid agent to be safely injected through the first catheter to achieve permanent occlusion of the feeding artery (Figures 5 and 6). In the dual-lumen balloon technique, a balloon is inflated via one lumen near the fistula, arresting flow in the feeding artery. The liquid agent is then safely injected through the second lumen of the balloon catheter. Currently, four double-lumen balloon catheters from three manufacturers are available: Ascent (Codman Neurovascular, Raynham, MA, USA), Scepter (MicroVention Terumo), Copernic 2L (Balt Extrusion), and Eclipse (Balt Extrusion). These intracranial dual-lumen balloon catheters may not be compatible with Lipiodol (i.e., glue) (14); therefore, non-adhesive liquid embolization agents should be used. To ensure stable occlusion, the fistula and proximal vein must be completely filled, and the balloon should remain inflated for some time (Figure 7).

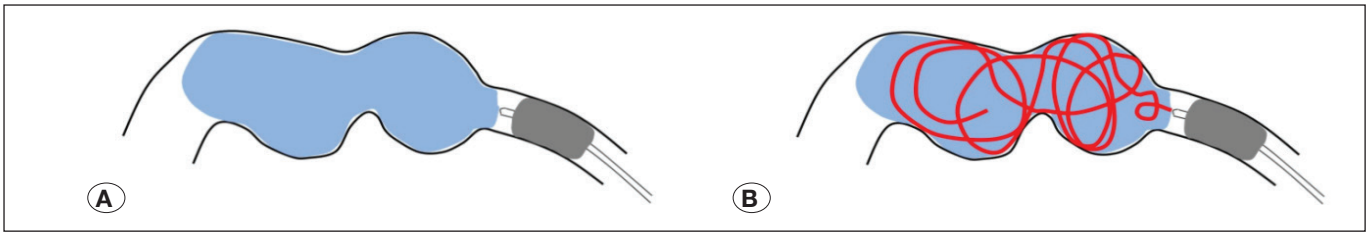

Figure 7: Schematic representation of dual-lumen balloon flow-arrest technique. **A)** After inflating the balloon to arrest flow in the feeding artery, a non-adhesive liquid agent is injected to occlude the fistula site and the proximal venous part. **B)** Coils and liquid can also be injected sequentially under balloon flow-arrest.

Coil-Liquid Embolization with Flow-arrest by a Dual-lumen Balloon

This is a variant of the "flow arrest by dual-lumen balloon" technique. All modern dual-lumen balloon catheters are DMSO-compatible and accommodate a 0.014-inch guidewire (2). After the balloon is inflated in an appropriate location and flow arrest is achieved, both coil placement and non-adhesive fluid injection can be safely performed, either separately or sequentially, through the second lumen (Figure 7). The safest approach during balloon flow arrest, even in high-flow pial AVFs, is to first create a coil pack, followed by gap-filling with a liquid agent (4).

Another challenge is the potential for hemorrhagic complications following successful obliteration of pial AVFs. The risk of new intracranial bleeding after surgical or endovascular treatment is 10–15% (10). The clinical phenomenon known as "normal perfusion pressure breakthrough hemorrhage" may occur due to the sudden occlusion of a high-flow fistula. Acute thrombosis, resulting from stagnant blood flow in the ectatic, serpiginous venous outflow or even in major dural sinuses, is not uncommon after successful embolization (9,13). Some patients with successfully occluded pial AVFs develop dural AVFs during follow-up, which may be related to post-embolization acute venous thrombosis (6,9). Previous dural sinus thrombosis is known to trigger acquired cranial dural AVF (7). However, objective evidence of "pressure breakthrough" is lacking. Nonetheless, it is reasonable to suggest that hemorrhage occurring after pial AVF occlusion is secondary to acute thrombosis of cerebral veins and/or sinuses. In our study, two of 16 patients experienced symptomatic acute thrombosis without hemorrhagic complications; one thrombosis was confined to the serpiginous draining vein of the fistula, whereas the other extended into the dural sinuses (Figure 1). Thus, post-embolization heparin therapy is strongly recommended for patients with high-flow fistulas and varicose veins (13).

The primary limitations of this study were its retrospective design and small sample size, both of which limit the discriminatory power.

CONCLUSION

Congenital pial AVF is rare. However, endovascular treatments using modern materials and techniques are highly effective.

ACKNOWLEDGMENTS

The English in this document has been checked by at least two professional editors, both native speakers of English. For a certificate, please see: http://www.textcheck.com/certificate/cv4Avs.

Declarations

Funding: This research did not receive any specific grant from funding agencies in the public, commercial, or not-for-profit sectors.

Availability of data and materials: The datasets generated and/or analyzed during the current study are available from the corresponding author by reasonable request.

Disclosure: The authors declare no competing interests.

AUTHORSHIP CONTRIBUTION

Study conception and design: CC, MK, EO, AE, IO
Data collection: CC, IO
Analysis and interpretation of results: AE, IO
Draft manuscript preparation: CC, AE, IO
Critical revision of the article: CC, IO
Other (study supervision, fundings, materials, etc...): CC, IO
All authors (CC, MK, AE, EO, IO) reviewed the results and approved the final version of the manuscript.

REFERENCES

1. Abaunza-Camacho JF, Vergara-Garcia D, Perez F, Benavides C, Portilla F, Riveros WM, Caballero A: Direct transcranial coil and Onyx embolization of a dural arteriovenous fistula: Technical note and brief literature review. J Clin Neurosci 80:232-237, 2020. https://doi.org/10.1016/j.jocn.2020.08.021
2. Arslan M, Cinar C, Oran I: Embolization of spinal dural arteriovenous fistulae using a nonadhesive liquid embolic agent delivered via a dual-lumen balloon catheter. In: Lv X (ed), Intracranial and Spinal Dural Arteriovenous Fistulas. Springer, 2022:257-264. https://doi.org/10.1007/978-981-19-5767-3_17
3. Coubes P, Humbertclaude V, Rodesch G, Lasjaunias P, Echenne B, Frerebeau P: Total endovascular occlusion of a giant direct arteriovenous fistula in the posterior fossa in a case of Rendu-Osler-Weber disease. Childs Nerv Syst 12:785-788, 1996. https://doi.org/10.1007/BF00261599
4. Feng L, Liu Y, Liu J, Lv C, Su C: Pial arteriovenous fistulas: Two pediatric cases and. Int J Clin Exp Med 9:7855-7862, 2016.
5. Guglielmi G, Vinuela F, Sepetka I, Macellari V: Electrothrombosis of saccular aneurysms via endovascular approach. Part 1: Electrochemical basis, technique, and experimental results. J Neurosurg 75:1-7, 1991. https://doi.org/10.3171/jns.1991.75.1.0001
6. Hetts SW, Keenan K, Fullerton HJ, Young WL, English JD, Gupta N, Dowd CF, Higashida RT, Lawton MT, Halbach VV: Pediatric intracranial nongalenic pial arteriovenous fistulas: Clinical features, angioarchitecture, and outcomes. AJNR Am J Neuroradiol 33:1710-1719, 2012. https://doi.org/10.3174/ajnr.A3194
7. Huang X, Shen H, Fan C, Chen J, Meng R: Clinical characteristics and outcome of dural arteriovenous fistulas secondary to cerebral venous sinus thrombosis: A primary or secondary event? BMC Neurol 23:131, 2023. https://doi.org/10.1186/s12883-023-03141-6
8. Lasjaunias P, Manelfe C, Chiu M: Angiographic architecture of intracranial vascular malformations and fistulas--pretherapeutic aspects. Neurosurg Rev 9:253-263, 1986. https://doi.org/10.1007/BF01743632
9. Li J, Ji Z, Yu J, Ren J, Yang F, Bian L, Zhi X, Li G, Zhang H: Angioarchitecture and prognosis of pediatric intracranial pial arteriovenous fistula. Stroke Vasc Neurol 8:292-300, 2023. https://doi.org/10.1136/svn-2022-001979

10. Madsen PJ, Lang SS, Pisapia JM, Storm PB, Hurst RW, Heuer GG: An institutional series and literature review of pial arteriovenous fistulas in the pediatric population: Clinical article. J Neurosurg Pediatr 12:344-350, 2013. https://doi.org/10.3171/2013.6.PEDS13110
11. Morales-Gómez JA, Garza-Oyervides VV, Arenas-Ruiz JA, Mercado-Flores M, Guillermo Elizondo-Riojas C, Boop FA, de León AMP: Hydrocephalus in a patient with an unruptured pial arteriovenous fistula: Hydrodynamic considerations, endovascular treatment, and clinical course. J Neurosurg Pediatr 19:307-311, 2017. https://doi.org/10.3171/2016.9.PEDS16458
12. Newman CB, Hu YC, McDougall CG, Albuquerque FC: Balloon-assisted Onyx embolization of cerebral single-channel pial arteriovenous fistulas. J Neurosurg Pediatr 7:637-642, 2011. https://doi.org/10.3171/2011.4.PEDS10577
13. Paramasivam S, Toma N, Niimi Y, Berenstein A: Development, clinical presentation and endovascular management of congenital intracranial pial arteriovenous fistulas. J Neurointerv Surg 5:184-190, 2013. https://doi.org/10.1136/neurintsurg-2011-010241
14. Park S, Hwang SM, Lim OK, Hwang C, Lee DH: Compliant neurovascular balloon catheters may not be compatible with liquid embolic materials: Intraprocedural rupture of the protecting balloon during tumor embolization using n-butyl cyanoacrylate and lipiodol mixture. J Neurointerv Surg 7:740-743, 2015. https://doi.org/10.1136/neurintsurg-2014-011331
15. Starke RM, Durst CR, Evans A, Ding D, Raper DM, Jensen ME, Crowley RW, Liu KC: Endovascular treatment of unruptured wide-necked intracranial aneurysms: Comparison of dual microcatheter technique and stent-assisted coil embolization. J Neurointerv Surg 7:256-261, 2015. https://doi.org/10.1136/neurintsurg-2014-011159
16. Thrash GW, Hale AT, Feldman MJ, Saccomano BW, Barrett DJ, Malenkia PD, Das S, Tsemo GB, Blount JP, Rocque BG, Rozzelle CJ, Johnston JM, Jones JG: Pediatric non-galenic pial arteriovenous fistula's characteristics and outcomes: A systematic review. Childs Nerv Syst 40:1721-1729, 2024. https://doi.org/10.1007/s00381-024-06352-5
17. Vollherbst DF, Chapot R, Bendszus M, Mohlenbruch MA: Glue, Onyx, Squid or PHIL? Liquid embolic agents for the embolization of cerebral arteriovenous malformations and dural arteriovenous fistulas. Clin Neuroradiol 32:25-38, 2022. https://doi.org/10.1007/s00062-021-01066-6
18. Yu J, Shi L, Lv X, Wu Z, Yang H: Intracranial non-galenic pial arteriovenous fistula: A review of the literature. Interv Neuroradiol 22:557-568, 2016. https://doi.org/10.1177/1591019916653934
19. Zhou Y, Li Q, Li JN, Xu Y, Liu JM: Embolization of a non-galenic pial arteriovenous fistula with assistance of a SolitaireTM stent: Case report. Turk Neurosurg 34:362-366, 2024. https://doi.org/10.5137/1019-5149.JTN.29642-20.2

Turk Neurosurg 35(4):570-576, 2025
DOI: 10.5137/1019-5149.JTN.48257-24.3

Original Investigation

Cerebrovascular-Endovascular

Received: 17.12.2024
Accepted: 25.04.2025
Published Online: 25.06.2025

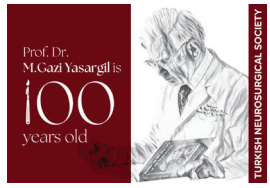

Syringic Acid Reduces Subarachnoid Hemorrhage–Induced Oxidative Damage in Rats

Veysel KIYAK[1], Ozgur DEMIR[1], Fikret GEVREK[2], Osman DEMIR[3], Muzaffer KATAR[4]

[1]Tokat Gaziosmanpasa University, Faculty of Medicine, Department of Neurosurgery, Tokat, Türkiye
[2]Tokat Gaziosmanpasa University, Faculty of Medicine, Department of Histology and Embryology, Tokat, Türkiye
[3]Tokat Gaziosmanpasa University, Faculty of Medicine, Department of Biostatistics, Tokat, Türkiye
[4]Tokat Gaziosmanpasa University, Faculty of Medicine, Department of Biochemistry, Tokat, Türkiye

Corresponding author: Veysel KIYAK ✉ vyslkyk86@gmail.com

ABSTRACT

AIM: To investigate the neuroprotective effects of various amounts of syringic acid (SA) on cerebral damage resulting from experimentally induced subarachnoid hemorrhage (SAH) in rats, utilizing both histological and biochemical analyses.

MATERIAL and METHODS: In total, 40 male Wistar albino rats were randomly and equally assigned to four groups: Control, SAH, SAH + 50 mg/kg/day SA (po), and SAH + 250 mg/kg/day SA (po). The rats in the SAH, SAH + 50 mg/kg/day SA, and SAH + 250 mg/kg/day SA groups were induced with SAH by administering 0.15 mL of autologous blood, collected from each rat's heart, into the subarachnoid space through the foramen magnum. On day 10th, the rats were sacrificed, and their blood and brain tissues were collected for biochemical, and histological analyses.

RESULTS: Glutathione peroxidase levels were considerably elevated in the SAH + 250 mg/kg/day SA group compared to both the control and SAH groups. Although not statistically significant, IL-6 levels were lower in the SAH + 250 mg/kg/day SA group compared with those in the control group. In the SAH + 250 mg/kg/day SA group, the histological and cellular damages in the cortical brain tissue reduced significantly.

CONCLUSION: SA (250 mg/kg/day) ameliorated the oxidative and histopathological changes in blood profile and cerebral tissue of rats when exposed to experimentally induced SAH. Thus, SA can reduce secondary cerebral damage in an SAH-induced rat model.

KEYWORDS: Syringic acid, subarachnoid hemorrhage, oxidative stress, rat

ABBREVIATIONS: CAT: Catalase, **FORs:** Free oxygen radicals, **Gpx:** Glutathione peroxidase, **GSH:** Glutathione, **IL:** Interleukin, **MDA:** Malondialdehyde, **SAH:** Subarachnoid hemorrhage, **SA:** Syringic acid, **SOD:** Superoxide dismutase, **TNF-α:** Tumor necrosis factor alpha

INTRODUCTION

Subarachnoid hemorrhage (SAH) is a severe form of hemorrhagic stroke with high morbidity and mortality rates (24). Current treatment guidelines for SAH still do not provide a definitive solution (7). In patients with SAH, cerebral damage often occurs due to delayed complications, most commonly associated with cerebral ischemia caused by hemorrhage (1). During ischemia, impaired glucose and oxygen supply leads to calcium influx, which in turn triggers apoptosis by activating mitochondrial permeability transition (30).

Veysel KIYAK : 0000-0002-4371-0155
Ozgur DEMIR : 0000-0002-9450-3906
Fikret GEVREK : 0000-0002-3722-2542
Osman DEMIR : 0000-0002-1322-2716
Muzaffer KATAR : 0000-0002-6296-2390

The free oxygen radicals (FORs) produced by mitochondria initiate apoptotic pathways (9). The increase in neuronal apoptosis induced by free oxygen radicals (FORs) underlies the pathogenesis of chronic neurodegeneration and acute central nervous system trauma (26). Cellular defensive potential functions as a critical protective system against oxidative damage triggered by FORs (15). Malondialdehyde (MDA), a byproduct of lipid peroxidation, is a key marker of oxidative damage (32). Antioxidant enzymes such as superoxide dismutase (SOD), catalase (CAT), glutathione (GSH), and glutathione peroxidase (GPx) help protect tissues against FORs and lipid peroxidation (5). Previous studies have shown elevated levels of reactive oxygen species (ROS) and MDA, alongside significantly reduced in antioxidant activity, in a rat model of cerebral ischemia (21,22). Impairment of the protective mechanisms against oxidation induces oxidative harm to neural lipids, proteins, and genetic material, eventually culminating in nerve cell death (33). Proinflammatory cytokines such as interleukin-1β (IL-1β), tumor necrosis factor alpha (TNF-α), and interleukin-6 (IL-6) play a central role in inflammation (10). These small-scale molecular compounds are secreted by cellular entities when triggered by pro-inflammatory signals (14). Evaluating levels of MDA, CAT, GSH, GPx, SOD, TNF-α, IL-1β, and IL-6 is therefore essential to assess SAH-induced oxidative and inflammatory damage (19).

In recent years, there has been a growing focus on reducing secondary cerebral damage, with several pharmacological agents such as curcumin and nitric oxide under investigation (11,20). Phenolic acid derivatives are of particular interest owing to their ability to scavenge free radicals and suppress oxidative stress (6). Syringic acid (SA), a phenolic acid derivative with no observed toxicity up to 1,000 mg/kg/day (22,23), has antioxidant, antiproliferative (16), antiendotoxic (34), and anticarcinogenic properties (10). It has been shown to reduce inflammation and oxidative stress in various neurodegenerative disease models (29). However, no study has yet evaluated the effect of SA on SAH-induced brain damage. Therefore, this study aims to biochemically and histologically explore the neuroprotective effects of different SA doses on oxidative damage in rats after experimentally inducing SAH. This is the first study to investigate the effect of SA in SAH-induced oxidative brain damage.

MATERIAL and METHODS

Ethics Statement

The research was executed in alignment with the protocols for the handling and welfare of lab animals established by the National Institutes of Health. The investigation received sanction from our institution's Animal Research Ethics Board. (No: 2023 HADYEK-13/51879863-41; Dated: August 17, 2023).

Animals

Forty male Wistar albino rats (aged 8–10 weeks; weighing 230–250 g) were procured from the Laboratory Animal Research Center of Tokat Gaziosmanpaşa University. They were fed standard commercial pellet feed and allowed ad libitum access to water. The rats were housed at a temperature of 22°C ± 1°C, with a relative humidity of 55% ± 5%, under a 12-h light/dark cycle.

Procedure

Overall, 40 male Wistar albino rats were randomly and equally assigned to the following four groups: Group 1, Control; Group 2, SAH; Group 3, SAH + 50 mg/kg/day SA; and Group 4, SAH + 250 mg/kg/day SA. After the rats were anesthetized using xylazine/ ketamine, SAH was induced in the rats in Groups 2, 3, and 4 by injecting 0.15 cc of autologous blood, collected from each rat's heart, into the subarachnoid space via the foramen magnum (18). Following the protocol, the rats were tracked throughout the investigation. A total of 10 rats died during the monitoring period (Group 2, n = 4; Group 3, n = 3; and Group 4, n = 3). In Groups 3 and 4, SA was administered orally once daily via a nasogastric tube. To control for handling stress, rats in the other groups received physiological saline via the same method. The rats were sacrificed on the 10th day after the procedure for biochemical analysis and histopathological evaluations.

Biochemical Analysis

Immunological methods were employed to evaluate oxidative stress markers within the rodent blood plasma. Reduced GSH levels were assessed using the competitive (inhibition) enzyme immunoassay (EIA) technique. It was measured at 450 nm and expressed in ng/mL. The CAT, GPx, and SOD levels (ng/mL) were determined using the sandwich EIA technique at 450 nm. The level of MDA (pg/mL), an end-product of the peroxidation of polyunsaturated fatty acids, was measured at 450 nm using the competitive (inhibition) EIA technique. The level of IL-1β (ng/mL), which is crucial in regulating the immune response and inflammation, was measured using the sandwich EIA. The level of IL-6 (pg/mL) was measured at 450 nm using the sandwich EIA. Similarly, the level of TNF-α (ng/mL), another key proinflammatory cytokine, was assessed using a double-antibody sandwich enzyme linked immunosorbent assay.

Histological Procedures

Hematoxylin–eosin staining

The tissue sections from the brain, including the cerebellum, were fixed in formalin and embedded in paraffin blocks. The sections were deparaffinized, rehydrated, and immersed in hematoxylin solution. After rinsing the hematoxylin-stained sections under running water, they were immersed in acid alcohol, rinsed with distilled water, and immersed in eosin solution. Subsequently, the sections were washed with distilled water and processed through a series of alcohol solutions (80%, 90%, 95%, and 99%) followed by xylene. Finally, coverslips were applied to the sections.

Histopathological analysis

Hematoxylin–eosin-stained slices of brain and cerebellum samples were examined via light microscopy (ECLIPSE TS-200; Nikon, Tokyo, Japan). The severity of injury in the brain and cerebellum specimens was evaluated semi-quantitatively, graded as normal, mild, moderate, or severe (Table I) (18). All

microscopic tissue examinations were conducted by a skilled histopathologist (FG) utilizing a blinded coding protocol.

Statistical Analysis

The general characteristics of the groups were descriptively analyzed. Continuous variables are expressed as means with standard deviations. One-way analysis of variance was used to compare the means of quantitative variables between the study groups. Statistical significance was defined as $p<0.05$. All statistical analyses were performed using SPSS (version 22.0; Chicago, IL, USA).

RESULTS

Biochemical Results

The levels of GSH, GPX, IL-1 β, IL6, CAT, MDA, SOD, and TNF-α in the four study groups are presented in Table II.

Histopathological Results

In the control group, neurons in the cortical brain tissue exhibited a typical histological appearance (Figure 1A). In Group 2, severe structural degeneration were observed, including intraparenchymal hemorrhage, shrinkage of cerebral cortex neurons, and densely darkly stained heterochromatic pyknotic nuclei. In Group 3, these damages had decreased to some extent. In Group 4, histological and cellular damage in the cortical brain tissue was significantly decreased (Figure 1B–D).

In the control group, the Purkinje cells and granular layer of the cerebellar cortex showed a normal histological structure (Figure 2A). In Group 2, the Purkinje cells were deformed, with shrunken cytoplasm and pyknotic nuclei densely stained with heterochromatin. Furthermore, there was a reduction in Purkinje cells, thinning of the granular layer, and pronounced congestion and hemorrhage in the molecular layer. Group 3 showed slight improvement, while Group 4 demonstrated a significant reduction in degenerative tissue and cellular damage (Figure 2B–D).

Table I: Cerebral and Cerebellar Tissue Damage Scoring Criteria (18)

Grades	Criteria
0	Normal
1	Mild
2	Moderate
3	Severe

DISCUSSION

SA has been used effectively in several neurodegenerative diseases (12). In a study conducted on rats using an experimental ischemia-reperfusion model, SA administered at four doses significantly reduced oxidative stress by increasing the antioxidant enzyme level of cell damage in hippocampal neuronal cells and had strong neuroprotective effects (4). In another rat study, SA (25 mg/kg/day) improved neuronal damage via its antioxidant and antiapoptotic activity in a study evaluating neurotoxicity induced by the insecticide deltamethrin (25). In this study, we investigated the antioxidant effects of SA at different doses for treating SAH-induced brain damage. Our findings indicate that in a SAH rat model, daily dose of 250 mg/kg SA significantly increased GPx levels, suggesting enhanced antioxidant activity and a reduction in oxidative damage. Furthermore, its therapeutic effect on the histopathological changes in the brain tissue were also observed.

Previous studies reported model-related mortality rates of up to 47% in experimental SAH models (31). In our study, considering that model-related mortality may occur at specified rates, the study was started with 10 rats per group. A total of 10 rats died in all groups during the experimental period. However, power analysis conducted before the experiment

Table II: Blood Oxidant, Antioxidant, and Proinflammatory Cytokines Values

Variables	Overall	Groups				p-value
		Control	SAH	SAH + SA-50	SAH + SA-250	
GSH	99.87 ± 29.8	98.94 ± 23.72	114.77 ± 8.78	105.34 ± 21.42	85.72 ± 48.35	0.490
GPX	36.47 ± 6.01	31.64 ± 3.46^{a}	33.07 ± 3.65^{ab}	39.36 ± 3.07^{bc}	41.47 ± 6.74^{c}	**0.003**
IL-1 β	26.65 ± 0.16	26.7 ± 0.15	26.55 ± 0.05	26.61 ± 0.18	26.69 ± 0.2	0.400
IL6	22.59 ± 11.93	22.15 ± 13.86	14.8 ± 10.55	29.25 ± 13.07	21.7 ± 6.73	0.320
CAT	4.94 ± 0.96	5.05 ± 0.92	5.29 ± 0.74	5.05 ± 1.44	4.44 ± 0.45	0.531
MDA	125.34 ± 53.55	151.49 ± 55.73	96.79 ± 15.58	104.62 ± 68.22	130.24 ± 41.86	0.272
SOD	0.36 ± 0.08	0.39 ± 0.13	0.38 ± 0.07	0.35 ± 0.05	0.31 ± 0.02	0.407
TNF-α	106.96 ± 14.96	98.4 ± 12.97	109.47 ± 17.99	113.73 ± 19.33	109.93 ± 6.16	0.248

SAH: *Subarachnoid hemorrhage;* ***SA:*** *Syringic acid;* ***GSH:*** *Glutathione;* ***GPx:*** *Glutathione peroxidase;* ***IL-1β:*** *İnterleukin-1β;* ***IL-6:*** *İnterleukin-6;* ***CAT:*** *Catalase;* ***MDA:*** *Malondialdehyde;* ***SOD:*** *Superoxide dismutase;* ***TNF-α:*** *Tumor necrosis factor alpha.*
One-way analysis of variance was used. a, b, and c, means with common letters in the same row did not differ significantly.

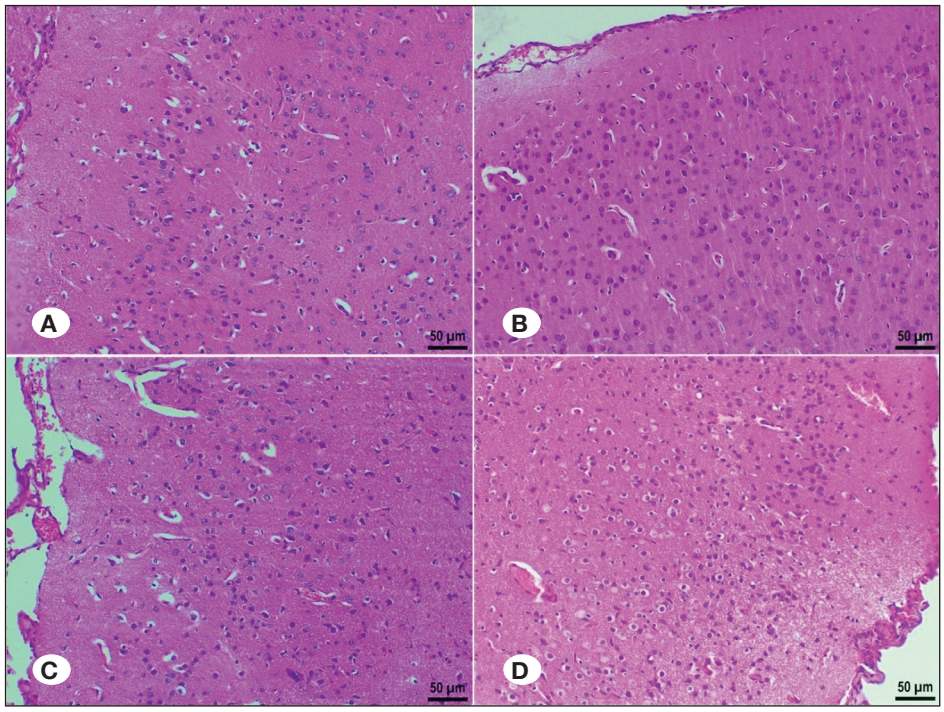

Figure 1: Representative microscopic images of cerebral tissue from the study groups. **A (control):** Normal histological appearance. **B (SA-250):** Marked reduction in histological and cellular damage in the cerebral tissue. **C (SA-50):** Mild reduction in the histological and cellular damage. **D (SAH):** Congestion and hemorrhagic areas as well as neuronal degenerative damage in the cortical tissue (hematoxylin–eosin staining; scale bar: 50 µm).

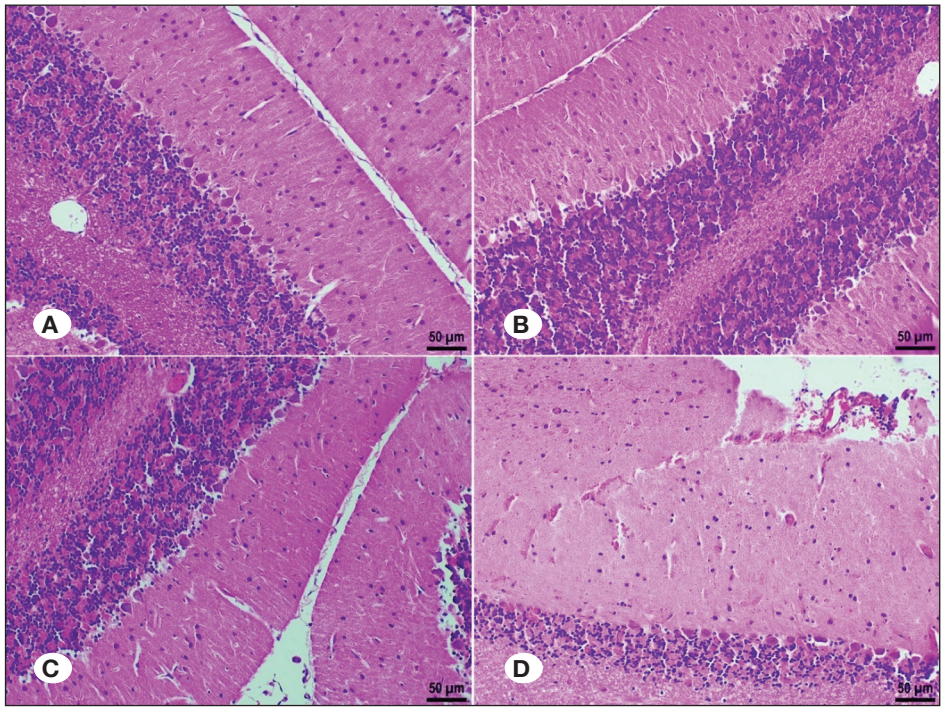

Figure 2: Representative microscopic images of cerebellar tissues from the study groups. **A (control group):** Normal histological appearance. **B (SA-250):** Pronounced decrease in the damage, resulting in an appearance similar to normal cerebellar tissue. **C (SA-50):** Moderate tissue and cellular damage. **D (SAH):** Purkinje cells with shrunken cytoplasm, dense heterochromatin-stained pyknotic nuclei, and reduced granular cell layer. Furthermore, the molecular layer exhibits intense tissue damage characterized by inflammatory cells, congestion, and hemorrhagic areas (hematoxylin–eosin staining; scale bar: 50 µm).

Table III: Molecules Used in Subarachnoid Hemorrhage Studies in Rats

Molecule	Article
Nimodipine, (2)	Biondi A, Ricciardi GK, Puybasset L, Abdennour L, Longo M, Chiras J, Van Effenterre R. (2004). Intra-arterial nimodipine for the treatment of symptomatic cerebral vasospasm after aneurysmal subarachnoid hemorrhage: preliminary results. American Journal of Neuroradiology, 25(6), 1067-1076.
Curcumin, (19)	Kuo CP, Lu CH, Wen LL, Cherng CH, Wong CS, Borel CO, Ju DT, Chen CM, Wu CT. (2011). Neuroprotective effect of curcumin in an experimental rat model of subarachnoid hemorrhage. Anesthesiology, 115(6), 1229-1238. https://doi.org/10.1097/aln.0b013e31823306f0
Secukinumab, (17)	Kiyak V, Gevrek F, Demir O, Katar M (2024). Secukinumab Ameliorates Oxidative Damage Induced by Subarachnoid Hemorrhage. World Neurosurgery, 190, e158-e164. https://doi.org/10.1016/j.wneu.2024.07.080

determined that a minimum of five rats per group were required for statistical significance. The number of rats that remained healthy in our study exceeded this number. Therefore, the observed mortality did not affect the statistical reliability of our results.

Numerous therapeutic agents have been used to reduce SAH-induced brain damage (Table III). In a study using an experimental SAH model in rats, Secukinumab significantly reduced oxidative stress and played a crucial role in the recovery of resulting brain damage (17). In another rat study, curcumin was reported to have antioxidant effects and reduced mortality in the SAH group (19). In a study on patients with SAH, intra-arterial administration of nimodipine reduced vasoconstriction, thereby decreasing brain damage secondary to SAH (2).

Antioxidant enzymes like, CAT, GSH, SOD, and GPx are vital for counteracting the effects of ROS in tissues. FORs interact with unsaturated fatty acids in cell membranes, triggering lipid peroxidation. Lipid peroxides decompose into secondary products like MDA (27,28). These products induce oxidative damage in DNA and other tissues, which are directly or indirectly responsible for cell death in brain tissue (28). FORs released following SAH and subsequent brain damage reduce the levels of various endogenous antioxidant enzymes, such as SOD, GSH, GPx and CAT, altering their activities (27). In one study, stanniocalcin-1 decreased oxidative stress and reduced the associated brain dysfunction (3). In another study, quercetin increased SOD and GPx levels and significantly decreased MDA levels in an experimental SAH model (8). These studies demonstrated that oxidative stress is involved in the pathogenesis of secondary brain damage, and agents that help increase the effectiveness of antioxidant systems may decrease brain damage by reducing oxidative stress. In our study, the levels of SOD, GSH, CAT, GPx, MDA, IL-6, TNF-α, and IL-1β were analyzed to identify secondary brain damage after SAH. Our results revealed that SAH induced changes in the levels of antioxidant enzymes—such as GPx, GSH, CAT, and SOD —and markers of oxidative stress—such as MDA. We found that the GPx level was significantly higher in the SAH group receiving 250 mg/kg/day SA than in the control and SAH groups (Table I). These results suggest that SA may help decrease FORs by enhancing the levels of the antioxidant enzyme GPx. This may contribute to the alleviation of cerebral damage by hindering lipid peroxidation.

IL-6, IL-1β, and TNF-α are proinflammatory cytokines, and their blood levels increase during inflammation. This increase may induce neurotoxic effects, leading to brain tissue damage (33). Elevated IL-6 levels are also associated with delayed cerebral ischemia (9). In our study, although not statistically significant, we observed a reduction in IL-6 levels in the SAH group receiving 250 mg/kg/day SA compared with that in the control group. This indicates that SA may suppress inflammation and contribute to reducing potential brain damage.

SAH-induced microscopic tissue injury in neural tissue stems from a disruption in the balance between oxidative stress and antioxidant defenses. Experimental studies using cysteamine and sodium orthovanadate have shown that reducing SAH and oxidative stress, which are responsible for subsequent damage, also helps protect against histopathological changes (13,35). In our study, histological and cellular damage decreased slightly in the SAH group treated with 50 mg/kg/day of SA (Figure 1). However, in the SAH group treated with 250 mg/kg/day of SA, histological and cellular damage in the cortex had remarkably reduced. Marked programmed cell death is observed in the brain neuronal cells of rats due to SAH and its accompanying alterations (15). In a study that examined the effects of SA in an ischemic rat model, oxidative stress and neuronal degeneration decreased after SA administration (11). In our study, the SAH group treated with 50 mg/kg/day SA exhibited moderate tissue and cellular damage. However, in the SAH group treated with 250 mg/kg/day SA, the cerebellar tissue appeared almost normal. These results indicate that SA reduces the histological damage to brain tissue caused by oxidative stress. Therefore, a daily dose of 250 mg/kg SA plays a crucial role in minimizing SAH-induced brain damage and preventing histopathological alterations in brain tissue.

CONCLUSION

SA treatment (250 mg/kg/day) effectively reduced oxidative stress and neuronal degeneration in a rat experimental model of SAH. Our biochemical and histopathological findings suggest that SA is an alternative treatment modality for SAH due to its antioxidant and neuroprotective properties. There are certain limitations in our study. Although our results suggest that

SA has neuroprotective benefits in mitigating brain damage induced by SAH, additional pharmacokinetic studies and investigations into the safe-dose range are required before it can be incorporated into human treatment protocols. Another limitation is the death of 10 rats during the study.

ACKNOWLEDGMENTS

We thank Tokat Gaziosmanpaşa University's Scientific Research Projects Unit.

The authors would like to thank Enago (www.enago.com) for the English language review.

Declarations

Funding: This study was supported by Tokat Gaziosmanpaşa University's Scientific Research Projects Unit (Grant No: 2023/92).

Availability of data and materials: The datasets generated and/or analyzed during the current study are available from the corresponding author by reasonable request.

Disclosure: The authors declare no competing interests.

AUTHORSHIP CONTRIBUTION

Study conception and design: VK, OD
Data collection: FG, OD, MK
Analysis and interpretation of results: VK, OD, FG, OD, MK
Draft manuscript preparation: VK
Critical revision of the article: VK, OD
Other (study supervision, fundings, materials, etc...): VK
All authors (VK, OD, FG, OD, MK) reviewed the results and approved the final version of the manuscript.

REFERENCES

1. Arpa A, Ozturk PA: Histopathological effects of nimodipine and pentoxifylline on the vessel wall in end-to-end anastomoses in rat carotid arteries. J Exp Clin Med 39:879–883, 2022. https://doi.org/10.52142/omujecm.39.3.54
2. Biondi A, Ricciardi GK, Puybasset L, Abdennour L, Longo M, Chiras J, Van Effenterre R: Intra-arterial nimodipine for the treatment of symptomatic cerebral vasospasm after aneurysmal subarachnoid hemorrhage: Preliminary results. Am J Neuroradiol 25:1067-1076, 2004
3. Bonfante S, Della Giustina A, Danielski LG, Denicol T, Joaquim L, Biehl E, Scopel G, de Carli RJ, Hubner M, Cardoso T, Tuon T, Generoso J, Barichello T, Terra S, Petronilho F: Stanniocalcin-1 ameliorates cerebral ischemia by decrease oxidative stress and blood brain barrier permeability. Microvasc Res 128: 103956, 2020. https://doi.org/10.1016/j.mvr.2019.103956
4. Cao Y, Zhang L, Sun S, Yi Z, Jiang X, Jia D: Neuroprotective effects of syringic acid against OGD/R-induced injury in cultured hippocampal neuronal cells. Int J Mol Med 38:567–573, 2016. https://doi.org/10.3892/ijmm.2016.2623
5. Ciftci O, Vardi N, Ozdemir I: Effects of quercetin and chrysin on 2,3,7,8-tetrachlorodibenzo-p-dioxin induced hepatotoxicity in rats. Environ Toxicol 28:146-154, 2013. https://doi.org/10.1002/tox.20707
6. Di Meo S, Venditti P: Evolution of the knowledge of free radicals and other oxidants. Oxid Med Cell Longev 2020: 9829176, 2020. https://doi.org/10.1155/2020/9829176
7. Diringer M.N, Bleck TP, Claude Hemphill J 3rd, Menon D, Shutter L, Vespa P, Bruder N, Connolly ES, Jr Citerio G, Gress D, Hänggi D, Hoh BL, Lanzino G, Le Roux P, Rabinstein A, Schmutzhard E, Stocchetti N, Suarez JI, Treggiari M, Tseng MY, Vergouwen MDI, Wolf S, Zipfel G, Neurocritical Care Society: Critical care management of patients following aneurysmal subarachnoid hemorrhage: Recommendations from the Neurocritical Care Society's multidisciplinary consensus conference. Neurocrit Care 15:211-240, 2011. https://doi.org/10.1007/s12028-011-9605-9
8. Dong YS, Wang JL, Feng DY, Qin HZ, Wen H, Yin ZM, Gao GD, Li C: Protective effect of quercetin against oxidative stress and brain edema in an experimental rat model of subarachnoid hemorrhage. Int J Med Sci 11:282–290, 2014. https://doi.org/10.7150/ijms.7634
9. Gong L, Tang Y, An R, Lin M, Chen L, Du J: RTN1-C mediates cerebral ischemia/reperfusion injury via ER stress and mitochondria-associated apoptosis pathways. Cell Death Dis 8:e3080, 2017. https://doi.org/10.1038/cddis.2017.465
10. Guimarães CM, Gião MS, Martinez SS, Pintado AI, Pintado ME, Bento LS, Malcata FX: Antioxidant activity of sugar molasses, including protective effect against DNA oxidative damage. J Food Sci 72:C039–C043, 2007. https://doi.org/10.1111/j.1750-3841.2006.00231.x
11. Guven M, Aras AB, Topaloglu N, Ozkan A, Sen HM, Kalkan Y, Okuyucu A, Akbal A, Gokmen F, Cosar M: The protective effect of syringic acid on ischemia injury in rat brain. Turk J Med Sci 45:233-240, 2015. https://doi.org/10.3906/sag-1402-71
12. Guzelad O, Ozkan A, Parlak H, Sinen O, Afsar E, Ogut E, Yildirim FB, Bulbul M, Agar A, Aslan M: Protective mechanism of syringic acid in an experimental model of Parkinson's disease. Metab Brain Dis 36:1003–1014, 2021. https://doi.org/10.1007/s11011-021-00704-9
13. Hasegawa Y, Suzuki H, Altay O, Zhang JH: Preservation of tropomyosin-related kinase B (TrkB) signaling by sodium orthovanadate attenuates early brain injury after subarachnoid hemorrhage in rats. Stroke 42:477-483, 2011. https://doi.org/10.1161/STROKEAHA.110.597344
14. Islekel S, Islekel H, Guner G, Ozdamar N: Alterations in superoxide dismutase, glutathione peroxidase and catalase activities in experimental cerebral ischemia-reperfusion. Research in experimental medicine. Zeitschrift fur die gesamte experimentelle Res Exp Med (Berl) 199:167-176, 1999. https://doi.org/10.1007/s004330050121
15. Jing CH, Wang L, Liu PP, Wu C, Ruan D, Chen G: Autophagy activation is associated with neuroprotection against apoptosis via a mitochondrial pathway in a rat model of subarachnoid hemorrhage. Neuroscience 213:144-153, 2012. https://doi.org/10.1016/j.neuroscience.2012.03.055
16. Kampa M, Alexaki VI, Notas G, Nifli AP, Nistikaki A, Hatzoglou A, Bakogeorgou E, Kouimtzoglou E, Blekas G, Boskou D, Gravanis A, Castanas E: Antiproliferative and apoptotic effects of selective phenolic acids on T47D human breast cancer cells: Potential mechanisms of action. Breast Cancer Res BCR 6:R63–R74, 2004. https://doi.org/10.1186/bcr752

17. Kiyak V, Gevrek F, Demir O, Katar M: Secukinumab ameliorates oxidative damage induced by subarachnoid hemorrhage. World Neurosurg 190:e158–e164, 2024. https://doi.org/10.1016/j.wneu.2024.07.080
18. Kiyak V, Oztanir MN, Turkmen NB, Tasdemir A, Ciftci O: Assessment of sertraline activity in a vasospasm model following experimental subarachnoid haemorrhage. Med Sci 9:817–822, 2020. https://doi.org/10.5455/medscience.2020.08.158
19. Kuo CP, Lu CH, Wen LL, Cherng CH, Wong CS, Borel CO, Ju DT, Chen CM, Wu CT: Neuroprotective effect of curcumin in an experimental rat model of subarachnoid hemorrhage. Anesthesiology 115:1229-1238, 2011. https://doi.org/10.1097/ALN.0b013e31823306f0
20. Li R, Li X, Wu H, Yang Z, Fei L, Zhu J: Theaflavin attenuates cerebral ischemia/reperfusion injury by abolishing miRNA1283pmediated Nrf2 inhibition and reducing oxidative stress. Mol Med Rep 20:4893-4904, 2019. https://doi.org/10.3892/mmr.2019.10755
21. Mirza AC, Panchal SS: Safety evaluation of syringic acid: Subacute oral toxicity studies in Wistar rats. Heliyon 5: e02129, 2019. https://doi.org/10.1016/j.heliyon.2019.e02129
22. Muthukumaran J, Srinivasan S, Venkatesan RS, Ramachandran V, Muruganathan U: Syringic acid, a novel natural phenolic acid, normalizes hyperglycemia with special reference to glycoprotein components in experimental diabetic rats. J Acute Dis 2:304-309, 2013. https://doi.org/10.1016/S2221-6189(13)60149-3
23. Neifert SN, Chapman EK, Martini ML, Shuman WH, Schupper AJ, Oermann EK, Mocco J, Macdonald R: Aneurysmal subarachnoid hemorrhage: The last decade. Transl Stroke Res 12:428–446, 2021. https://doi.org/10.1007/s12975-020-00867-0
24. Nita DA, Nita V, Spulber S, Moldovan M, Popa DP, Zagrean AM, Zagrean L: Oxidative damage following cerebral ischemia depends on reperfusion - a biochemical study in rat. J Cell Mol Med 5:163–170, 2001. https://doi.org/10.1111/j.1582-4934.2001.tb00149.x
25. Ogut E, Sekerci R, Akcay G, Yildirim FB, Derin N, Aslan M, Sati L: Protective effects of syringic acid on neurobehavioral deficits and hippocampal tissue damages induced by sub-chronic deltamethrin exposure. Neurotoxicol Teratol 76: 106839, 2019. https://doi.org/10.1016/j.ntt.2019.106839
26. Oguz F, Ciftci O, Aydın M, Timurkaan N, Beytur A, Altıntas R, Parlakpinar H: Aminoguanidine prevents testicular damage-induced-2,3,7,8-tetrachlorodibenzo-p-dioxin (TCDD) in male rats. Andrologia 45:225–231, 2013. https://doi.org/10.1111/j.1439-0272.2012.01334.x
27. Orellana-Urzúa S, Claps G, Rodrigo R: Improvement of a novel proposal for antioxidant treatment against brain damage occurring in ischemic stroke patients. CNS Neurol Disord Drug Targets 20:3-21, 2021. https://doi.org/10.2174/1871527319666200910153431
28. Puyal J, Ginet V, Clarke PG: Multiple interacting cell death mechanisms in the mediation of excitotoxicity and ischemic brain damage: A challenge for neuroprotection. Prog Neurobiol 105:24-48, 2013. https://doi.org/10.1016/j.pneurobio.2013.03.002
29. Shan HM, Zang M, Zhang Q, Shi RB, Shi XJ, Mamtilahun M, Liu C, Luo LL, Tian X, Zhang Z, Yang GY, Tang Y, Pu J, Wang Y: Farnesoid X receptor knockout protects brain against ischemic injury through reducing neuronal apoptosis in mice. J Neuroinflamm 17:164, 2020. https://doi.org/10.1186/s12974-020-01838-w
30. Simon M, Grote A: Interleukin 6 and aneurysmal subarachnoid hemorrhage. A narrative review. Int J Mol Sci 22:4133, 2021. https://doi.org/10.3390/ijms22084133
31. Vatter H, Weidauer S, Konczalla J, Dettmann E, Zimmermann M, Raabe A, Preibisch C, Zanella FE, Seifert, V: Time course in the development of cerebral vasospasm after experimental subarachnoid hemorrhage: Clinical and neuroradiological assessment of the rat double hemorrhage model. Neurosurgery 58:1190–1197, 2006. https://doi.org/10.1227/01.NEU.0000199346.74649.66
32. Wang M, Li YJ, Ding Y, Zhang HN, Sun T, Zhang K, Yang L, Guo YY, Liu SB, Zhao MG, Wu YM: Silibinin prevents autophagic cell death upon oxidative stress in cortical neurons and cerebral ischemia-reperfusion injury. Mol Neurobiol 53:932–943, 2016. https://doi.org/10.1007/s12035-014-9062-5
33. Wilms H, Sievers J, Rickert U, Rostami-Yazdi M, Mrowietz U, Lucius R: Dimethylfumarate inhibits microglial and astrocytic inflammation by suppressing the synthesis of nitric oxide, IL-1beta, TNF-alpha and IL-6 in an in-vitro model of brain inflammation. J Neuroinflamm 7:30, 2010. https://doi.org/10.1186/1742-2094-7-30
34. Wu X, Liu Y, Sheng W, Sun J, Qin G: Chemical constituents of Isatis indigotica. Planta Med 63:55–57, 1997. https://doi.org/10.1055/s-2006-957604
35. Zhang ZY, Yang MF, Wang T, Li DW, Liu YL, Zhang JH, Sun BL: Cysteamine alleviates early brain injury via reducing oxidative stress and apoptosis in a rat experimental subarachnoid hemorrhage model. Cell Mol Neurobiol 35:543–553, 2015. https://doi.org/10.1007/s10571-014-0150-x

Turk Neurosurg 35(4):577-579, 2025
DOI: 10.5137/1019-5149.JTN.46931-24.1

Technical Note

Cerebrovascular-Endovascular

Received: 15.05.2024
Accepted: 13.09.2024
Published Online: 25.06.2025

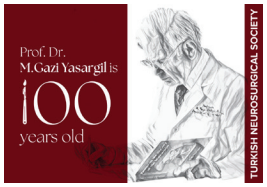

Basilar Artery Stenosis: Technical Tips to Prevent and Treat Hemorrhage during Angioplasty

Zeferino DEMARTINI Jr[1,2], Renato Fedatto BERALDO[2], Adriane CARDOSO-DEMARTINI[1]

[1]Complexo Hospital de Clinicas – Universidade Federal do Parana –Curitiba, PR, Brazil
[2]Hospital Pequeno Principe – Curitiba, PR, Brazil

Corresponding author: Zeferino DEMARTINI ✉ demartiniz@gmail.com

ABSTRACT

To describe the strategies and techniques to improve the outcomes in intracranial hemorrhage during endovascular procedures, a case of a 60-year-old male with symptomatic basilar artery stenosis who underwent balloon angioplasty procedure following an iatrogenic basilar artery hemorrhage, is presented. Hemorrhage control and vessel wall reconstruction were achieved with heparin reversal, intermittent balloon inflation, and telescoping stents. In addition, immediate external ventricular drainage was able to control the intracranial hypertension. In conclusion, the ruptured of intracranial vessels is usually challenging to treat. Intermittent balloon inflation with telescoping stents can help stop bleeding.

KEYWORDS: Balloon angioplasty, Basilar artery, Endovascular procedures, Intracranial arteriosclerosis, Intracranial hemorrhages, Intraoperative complications

ABBREVIATIONS: BMT: Best medical therapy, **CT:** Computed tomography, **EVD:** External ventricular drain, **ICAS:** Intracranial atherosclerosis, **PTA:** Percutaneous transluminal angioplasty

INTRODUCTION

Intracranial atherosclerosis (ICAS) is increasingly recognized as a cause of ischemic stroke. The involvement of posterior circulation and eloquent brain areas is associated with high morbidity and mortality (1). The best medical therapy (BMT) for initial treatment of symptomatic ICAS, recommended as the result of large randomized controlled trials, consists of statin therapy, dual antiplatelet agents (usually aspirin and clopidogrel), reduction of cardiovascular risk, and smoking cessation (1). In addition, an increased risk of stroke has been associated with percutaneous transluminal angioplasty (PTA) and stenting, mainly related to distal embolization, arterial dissection, or hemorrhage (1). This article describes a basilar rupture associated with PTA and discusses technical tips to increase treatment effectiveness, prevent complications, and treat the feared intraoperative hemorrhage.

ILLUSTRATIVE CASE

This study was conducted ethically in accordance with the World Medical Association Declaration of Helsinki**.** Ethics approval was not required from Institutional Review Board in accordance with local guidelines concerning single patient reports. Written informed consent for publication of data and images was provided and signed by the patient's guardian.

Clinical Presentation

A 60-year-old male with a history of vertigo and ataxia was diagnosed with vertebrobasilar insufficiency due to basilar artery stenosis, being treated with combined antiplatelet therapy (clopidogrel 75 mg and aspirin 100 mg). Despite one year of treatment followed by six months of anticoagulation therapy with warfarin, his condition progressed with recurrent episodes of syncope, leading to a referral for PTA and

Zeferino DEMARTINI Jr : 0000-0002-0683-5418
Renato Fedatto BERALDO : 0000-0001-8892-1493
Adriane CARDOSO-DEMARTINI : 0000-0002-6772-1940

stenting. Digital subtraction angiography revealed a 90% basilar stenosis.

Surgical Technique

A Neuron 6F (Penumbra Inc., Alameda, CA, USA) catheter was positioned into the left vertebral artery. Suboptimal PTA using a 3.5mm×18mm PRO-Kinetic (Biotronik Berlin, Germany) coronary stent over 0.010-inch microguidewire (Silverspeed®, Medtronic, Minneapolis, MN, USA) was performed by inflating the balloon to a sub-nominal pressure of 7 atm (nominal pressure 8 atm). The postoperative angiogram revealed active contrast extravasation in the proximal basilar artery (Figure 1). Balloon was then immediately re-inflated for five minutes, and heparin was reversed with protamine. However, as the contrast leakage persisted after balloon deflation, a similar overlapping 3.0 mm×18 mm stent was rapidly deployed through the same microwire to provide a flow-diverter effect. The balloon was kept inflated for an additional five minutes and achieved bleeding control. An external ventricular drain (EVD) was placed in the angio-suite for intracranial pressure monitoring.

Postoperative Course

A CT scan confirmed posterior fossa subarachnoid hemorrhage. The patient was sedated for 48 hours, and the follow-up CT scan showed a left cerebellar ischemic stroke. The patient was discharged eight days later with mild ataxia and dysmetria and was able to walk assisted. He showed good functional recovery and could walk independently at a one-year follow-up.

DISCUSSION

The use of PTA and stenting for symptomatic ICAS refractory to BMT remains a matter of debate (2). It has been associated with higher stroke and death rates than BMT, but these risks have decreased with devices improvement and increased use of endovascular techniques (1). A recent meta-analysis involving 777 patients found that submaximal angioplasty for ICAS reduced the stroke and death rate, supporting its combination with BMT as a viable treatment option (7). Although decreasing the radial force reduces the risk of vessel rupture, the diseased vessel wall is still vulnerable to injury. In addition, the use of preoperative antiplatelets plus intraoperative anticoagulation can fatally exacerbate the hemorrhage. The role of endovascular therapy for iatrogenic vessel laceration or perforation injuries to intracranial vessels is not fully elucidated and usually involves vessel sacrifice (1).

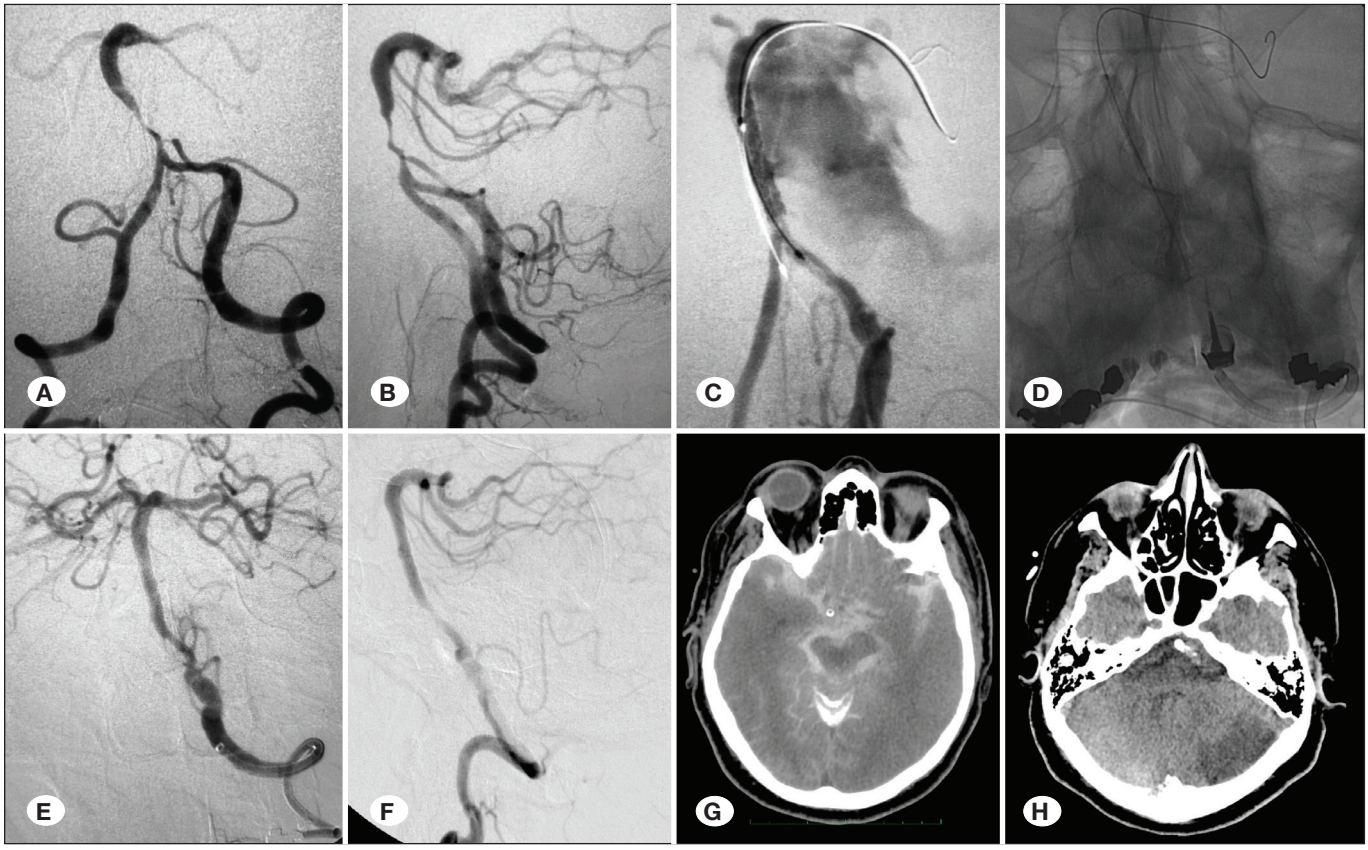

Figure 1: Left vertebral angiogram in frontal **(A)** and lateral view **(B)** shows subocclusive stenosis of the proximal basilar artery, with additional stenosis at the origin of the left anteroinferior cerebellar artery; after submaximal balloon angioplasty there is active contrast extravasation from the basilar artery **(C)**; the balloon is re-inflated **(D)**, the heparin is reversed and another stent is telescoped, ultimately being able to stop the bleeding **(E,F)**; the immediate postoperative CT-scan shows subarachnoid hemorrhage **(G)**, while late CT-scan shows cerebellar infarct **(H)**; the patient has good recovery.

More recently, flow-diverter stents have been successfully deployed to reconstruct the vessel wall and achieved hemorrhage control (1). In this case of iatrogenic injury to the basilar artery, telescoping stents were enough to cover the rupture point and stop bleeding. Telescoping stents achieved similar flow reduction compared with flow diverters; thus, they may be a viable treatment alternative when flow diverters are not a possibility (5). Additionally, coronary stents are usually more available and cheaper than flow diverters, and the attached balloon provides temporary flow occlusion, providing an interesting alternative as a rescue treatment. The tortuosity of the posterior cerebral circulation can present a challenge for endovascular therapy (3). Associated vertebral stenosis below 70% may also affect asymmetric flow, contributing to basilar artery tortuosity (6). Using shorter balloons and paying attention to arterial curves can avoid straightening the basilar artery, causing eventual detachment of perforators. Paying attention to the insufflated balloon period for damage control is another important matter of concern because it may cause brainstem ischemia with catastrophic outcomes. Therefore, fast covering with another stent and transient occlusion may be better tolerated than prolonged balloon inflation. Although an ischemic cerebellar injury occurred in this case, it was probably related to anteroinferior cerebellar artery occlusion, as evidenced by Wang et al. (8); the risk of postoperative ischemic stroke is higher for PTA patients with perforator artery involvement than those with distal hypoperfusion or embolic symptomatology.

CONCLUSION

PTA and stenting for symptomatic ICAS may be safe and effective in properly selected cases (3,4). Although it is extremely difficult to successfully manage periprocedural bleeding, fast intervention with intermittent balloon inflation, heparin reversal, telescoping stents, and immediate EVD can be lifesaving option. Further experience is necessary to define the optimal management of these patients and improve their outcomes.

Declarations

Funding: This research did not receive any specific grant from funding agencies in the public, commercial, or not-for-profit sectors.

Availability of data and materials: All data generated or analyzed during this study are included in this article. Further enquiries can be directed to the corresponding author.

Disclosure: The authors declare no competing interests.

AUTHORSHIP CONTRIBUTION

Study conception and design: ZDJ, RFB
Data collection: ZDJ, RFB
Analysis and interpretation of results: ZDJ, ACD
Draft manuscript preparation: ZDJ, RFB
Critical revision of the article: RFB, ACD
Other (study supervision, fundings, materials, etc...): ZDJ, RFB, ACD
All authors (ZDJ, RFB, ACD) reviewed the results and approved the final version of the manuscript.

REFERENCES

1. Johnson RM, Young M, Guglielmi GN, Farhat H: Proximal basilar artery hemorrhage after submaximal angioplasty for intracranial atherosclerotic disease presenting as a large vessel occlusion treated with pipeline embolization device. J Cerebrovasc Endovasc Neurosurg 23:145-151, 2021. https://doi.org/10.7461/jcen.2021.E2020.11.005
2. Machado M, Borges de Almeida G, Sequeira M, Pedro F, Fior A, Carvalho R, Fragata I, Reis J, Nunes AP: Percutaneous transluminal angioplasty and stenting in acute stroke caused by basilar artery steno-occlusive disease: The experience of a single stroke centre. Interv Neuroradiol 28:547-555, 2022. https://doi.org/10.1177/15910199211051830
3. Palmisciano P, Hoz SS, Algburi HA, Ventre G, Street S, Agyeman N, Robinson MW, Smith MS, Shirani P, Grossman AW, Prestigiacomo CJ: Percutaneous transluminal angioplasty and/or stenting for the treatment of basilar artery stenosis: A systematic review and meta-analysis. Neuroradiology 65: 985-1000, 2023. https://doi.org/10.1007/s00234-023-03124-x
4. Piano M, Milonia L, Cervo A, Modello B, Macera A, Pero G, Quilici L, Boccardi E, Valvassori L: Endovascular treatment of symptomatic intracranial vertebrobasilar stenosis: A 10-year single centre experience using balloon-expandable coronary artery stents. J Stroke Cerebrovasc Dis 30:105431, 2021. https://doi.org/10.1016/j.jstrokecerebrovasdis.2020.105431
5. Roszelle BN, Gonzalez LF, Babiker MH, Ryan J, Albuquerque FC, Frakes DH: Flow diverter effect on cerebral aneurysm hemodynamics: An in vitro comparison of telescoping stents and the Pipeline. Neuroradiol 55:751-758, 2013. https://doi.org/10.1007/s00234-013-1169-2
6. Sahin H, Gokce M: The effect of the vertebral artery stenosis on the basilar artery tortuosity. Turk Neurosurg 33:156-161, 2023. https://doi.org/10.5137/1019-5149.JTN.40980-22.2
7. Seyedsaadat SM, Yolcu YU, Neuhaus A, Rizvi A, Alzuabi M, Murad MH, Brinjikji W, Bydon M, Kallmes DF: Submaximal angioplasty in the treatment of patients with symptomatic ICAD: A systematic review and meta-analysis. J Neurointerv Surg 12:380-385, 2020. https://doi.org/10.1136/neurintsurg-2019-015451
8. Wang G, Cheng T, Niu H, Ma J, Wang J, Li W: Risk prediction of CISS classification in endovascular treatment of basilar artery stenosis. Heliyon 10:e23747, 2023. https://doi.org/10.1016/j.heliyon.2023.e23747

Turk Neurosurg 35(4):580-586, 2025
DOI: 10.5137/1019-5149.JTN.47419-24.2

Original Investigation

Stereotactic and Functional

Received: 14.08.2024
Accepted: 20.10.2024
Published Online: 25.06.2025

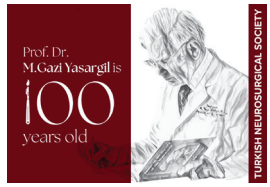

Accuracy of Deep Brain Stimulation Lead Placement Using a Cranial Robotic Guidance Platform: A Preliminary Cadaveric Study

Huseyin BICEROGLU[1], Bilal Bahadir AKBULUT[1], Okan DERIN[2], Ozde Senol AKBULUT[1], Mustafa Serdar BOLUK[1], Nevhis AKINTURK[1], Kadri Emre CALISKAN[1], Cenk ERASLAN[3], Servet CELIK[2], Ahmet ACARER[4], Taskin YURTSEVEN[1]

[1]Ege University, Faculty of Medicine, Department of Neurosurgery, Izmir, Türkiye
[2]Ege University, Faculty of Medicine, Department of Anatomy, Izmir, Türkiye
[3]Ege University, Faculty of Medicine, Department of Radiology, Izmir, Türkiye
[4]Ege University, Faculty of Medicine, Department of Neurology, Izmir, Türkiye

Corresponding author: Bilal Bahadır AKBULUT ✉ b.bahadirakbulut@gmail.com

ABSTRACT

AIM: To measure the deviation rate of a custom 3D-printed Deep Brain Stimulation (DBS) lead holder assisted electrode placements from their intended targets, providing a benchmark for the system's accuracy and paving the way for its use in standard DBS workflows.

MATERIAL and METHODS: The study was conducted in an experimental lab using a cadaver obtained according to local regulations. Planned electrode trajectories, designed with Medtronic's DBS surgery planning system, were transferred to the StealthStation Autoguide. A 3D-printed DBS lead holder with integrated navigation fiducials was used to place six electrodes in the targeted brain regions. Pre-operative CT and MRI scans were used for planning, and post-operative imaging confirmed electrode placement. Deviation from planned trajectories was analyzed using Python to assess accuracy.

RESULTS: Following a 30-minute registration and draping process, the median electrode placement time was 22.5 minutes (range: 15-120). The total surgical time for all six electrodes was approximately 5 hours, including imaging, adjustments, and confirmation. The median difference was 1.73 mm (0.03-5.45) on the X-axis, 1.86 mm (0.46-2.74) on the Y-axis, and 1.95 mm (0.73-4.4) on the Z-axis. The median vectorial difference was 2.68 mm (2.3-6.71), while the median trajectory difference was 3.01 mm (1.64-6.63).

CONCLUSION: Despite 50% of leads having a vectorial difference exceeding 4 mm, most had a trajectory difference of less than 3 mm, which could be attributed to the inability to measure the length of the electrode precisely. These results suggest that with minor adjustments, the StealthStation Autoguide could be a cost-effective alternative to similar systems, though further cadaveric studies are necessary to address potential learning curves and random factors.

KEYWORDS: Deep brain stimulation, Electrode placement, Parkinson's disease, Placement accuracy, Robot-assisted

ABBREVIATIONS: 3D: Three-Dimensional, **CNC:** Computer Numerical Control, **CT:** Computed Tomography, **DBS:** Deep Brain Stimulation, **FDM:** Fused Deposition Modeling, **GPi:** Globus Pallidus Interna, **MRI:** Magnetic Resonance Imaging, **PLA:** Polylactic Acid, **SPSS:** Statistical Package for the Social Sciences, **STL:** Stereolithography, **STN:** Subthalamic Nucleus, **TPU:** Thermoplastic Polyurethane, **Vim:** Ventral Intermediate Nucleus

Huseyin BICEROGLU : 0000-0003-2306-0826
Bilal Bahadir AKBULUT : 0000-0002-7983-5056
Okan DERIN : 0000-0002-6076-5844
Ozde SENOL AKBULUT : 0000-0002-6024-1899
Mustafa Serdar BOLUK : 0000-0002-9406-4114
Nevhis AKINTURK : 0000-0002-0938-1810
Kadri Emre CALISKAN : 0000-0002-5281-9347
Cenk ERASLAN : 0000-0002-5762-6149
Servet CELIK : 0000-0002-1102-4417
Ahmet ACARER : 0000-0003-1194-3971
Taskin YURTSEVEN : 0000-0001-7982-8115

INTRODUCTION

Deep brain stimulation (DBS) is a widely used procedure for various movement disorders. However, its treatment efficacy is dependent on the accuracy of the electrodes. While effective, traditional stereotactic methods are less comfortable for the patient, as the patient has to be placed in a frame to obtain an MRI and then brought back to the operating room and have a longer duration (both overall and per electrode) than frameless methods (8,10,18,26).

Frameless placement of the DBS electrodes is a proven procedure used since 2019 (5,8,10,15,21,26). These systems either use highly specialized platforms that, after the navigation system specifies the insertion point, allow controlled drive into the target location (e.g., Nexframe® DB2040; Medtronic Neurological Division, Dublin, Ireland) or use a robot with a freely moving arm (e.g., now discontinued Mazor Robotics Renaissance® system (Mazor Robotics Ltd, Caesarea, Israel) and ROSA® robot (Zimmer Biomet, Warsaw, Indiana, USA). These systems may require more investment than compact systems such as StealthStation Autoguide (Medtronic, Dublin, Ireland).

Beyond DBS, robotic surgery has been increasingly adopted in various neurosurgical procedures, offering enhanced precision, reduced operative times, and improved patient outcomes. The integration of robotic systems into neurosurgery facilitates minimally invasive approaches, enhances surgical accuracy, and improves overall workflow efficiency, thereby expanding the capabilities and applications of neurosurgical interventions (1,3,4,6).

However, no studies explore the possibility of utilizing custom-made lead holders with the StealthStation Autoguide system in DBS placement. This study seeks to measure the deviation of the placed electrodes from their intended targets on a cadaveric model, providing a benchmark for the system's accuracy and reliability. It also serves as a preliminary study to justify further research.

MATERIAL and METHODS

Cadaver Preparation

This study was conducted at the Ege University Faculty of Medicine, utilizing a cadaver obtained following Turkish Law No. 2238. The local institutional review board approved the research protocol, ensuring adherence to ethical standards for using human cadaveric material in research (Decision no: 24-3.1T/40, Date: 21.03.2024).

A single cadaver with an intact calvarium was obtained from the Ege University Faculty of Medicine, Department of Anatomy. The cadaver was imaged pre-operatively to plan the trajectories for electrode placement. We used computed tomography (CT) and magnetic resonance imaging (MRI) per our local protocol for DBS placement. MRI studies were performed using a 3.0 Tesla MRI system (Magnetom® Verio, Siemens, Erlangen, Germany), and a 16-channel head coil, T2 SPACE sequence, and T1-MPRAGE pulse sequence were used. The CT scan was performed on a 64 detector 128 sliced CT scanner (Siemens Somatom Definition AS, Siemens, Erlangen, Germany).

Medtronic DBS model 3389 leads with 28 cm length and 2 Medtronic DBS model 3389 leads with 40 cm leads were available and were used in this study.

Surgical Planning

Using the StealthStation S8 planning station Version 1.3.2 (Medtronic, Dublin, Ireland) for DBS surgery, trajectories for the subthalamic nucleus (STN), Globus pallidus interna (GPi), and ventral intermediate nucleus (Vim) on both hemispheres of the brain were auto-calculated and then modified by an experienced neurosurgeon and neurologist. These plans were then transferred to the StealthStation Autoguide robotic system, which was used to guide the placement of six DBS electrodes (three on each side).

Electrode Placement

Currently, the StealthStation Autoguide system does not have a holder for DBS electrodes. Thus, the biopsy module and its cannula were used to design the custom 3D-printed DBS lead holder (STL files can be found at https://github.com/AkbulutBB/DBSNav). The files were then printed using a fused deposition modeling 3D printer Ender-3 S1(Creality, Shenzen, China) with polylactic acid(PLA).

In the biopsy module, the guidance system only works within a single axis after the trajectory is locked. It requires two fiducials arranged in a single line and placed within a specific distance of each other (Figure 1A). Thus, the fiducials were placed within two cavities that were made within the holder, and a hole for the electrode to pass was placed using a drill within the fiducials.

The cadaver was positioned in the operating room (Figure 2), and the StealthStation Autoguide system was set up according to the pre-operative plans. The target distance was calculated using the provided measurement tool for biopsy cannulas (Figure 1B), and DBS electrodes were locked in the desired length using a screw-tightened system. The system's robotic arm was used to guide the DBS lead holder, ensuring precise alignment with the planned trajectories.

To guide the leads, a STar Array Lead Insertion Tube was inserted through the StealthStation Autoguide biopsy system, 5 cm proximal to the target. Then, the electrodes were inserted using the 3D printed tool to stop the leads at the correct depth (Figure 3). After placement, an X-ray image was obtained to account for any displacement when retracting the robotic system. While lead was held in place using bayonet forceps, the custom DBS holder was disengaged using the screw system, and then the robot arm was carefully retracted. After obtaining another X-ray image, ensuring the lead was not moved during this retraction process, it was locked in place by the burr hole covers provided with the leads.

After all leads were placed, the skin was approximated using silk sutures, and the cadaveric head was carefully placed in the transportation box.

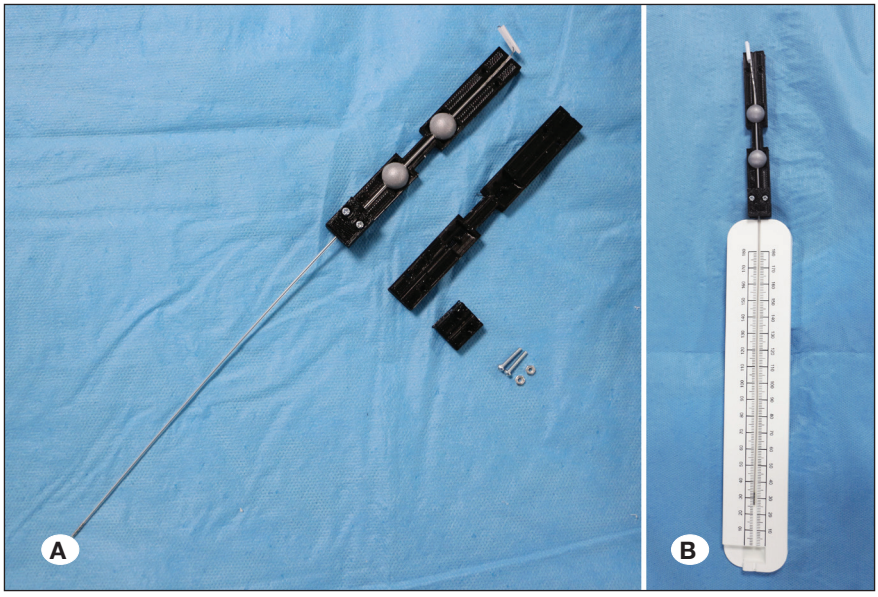

Figure 1: A) Two fiducials are arranged specifically with a DBS electrode passing through. **B)** Measuring tool with screw-tightened locking mechanism.

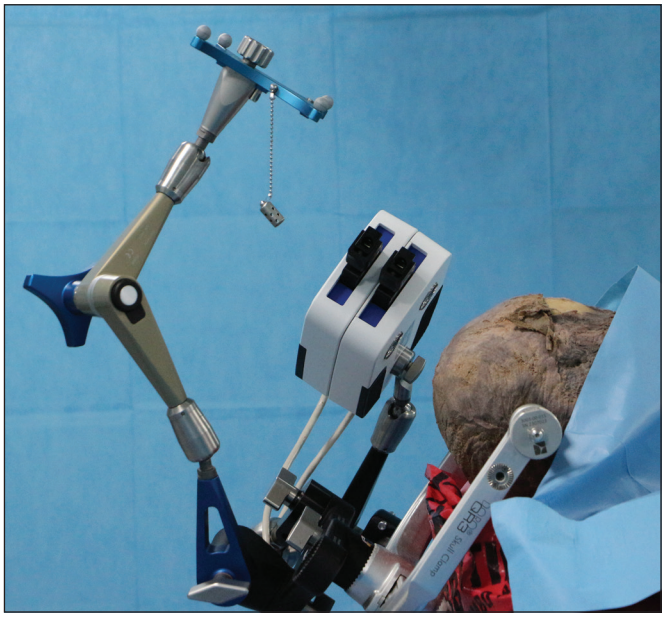

Figure 2: Cadaver with Stealth Station Autoguide in position.

Post-operative Imaging and Analysis

Following electrode placement, CT and MRI scans were repeated with the preoperative protocols to confirm the actual locations of the electrodes. Accuracy was assessed using the method proposed by Burchiel et al. (2), where the difference between the intended and actual trajectory (trajectory difference) and the difference between the intended end-point of the electrode and the actual electrode (vectorial difference) is calculated using the post-operative scans. Coordinates were obtained from the StealthStation system, the difference between intended and actual electrode coordinates was calculated, and 3D vector fields were drawn using the Python libraries Matplotlib and Numpy (12,13). Details of the code can be found in our code repository (https://github.com/AkbulutBB/DBSNav).

Statistical Analysis

The collected data were analyzed using IBM SPSS Statistics Version 27.0 (IBM Corp., Armonk, NY, USA). Descriptive statistics were calculated for each electrode placement. No comparative analysis was made as this is a preliminary study involving one cadaver.

RESULTS

After registration and the draping was complete (approximately 30 minutes), the actual electrode placement process took a median time of 22.5 minutes per electrode. The overall surgical time for placing all six electrodes was approximately 5 hours. This time includes the necessary imaging, adjustments, and confirmation steps. Details can be found in Table I.

Using coordinates obtained from StealthStation, the differences in 3 axes, vectorial, and trajectory differences were calculated (Table II). The median difference was 1.73 mm on the X-axis, 1.86 mm on the Y-axis, and 1.95 mm on the Z-axis. The median vectorial difference was 2.68 mm, while the median trajectory difference was 3.01 mm. Figures 4, 5, and 6 provide visual representations of the planned trajectories and the actual placements.

DISCUSSION

The preliminary results of our study demonstrate the potential of the StealthStation Autoguide system for DBS lead placement in a cadaveric model, warranting further research to improve upon our design and possibly match the accuracy of more specialized robotic platforms.

We created and employed a specialized 3D-printed DBS lead holder due to the lack of a commercially accessible holder for DBS electrodes compatible with the StealthStation Autoguide.

Table I: Placement Time and Coordinates of Electrodes

No	Electrode	Time (min)	I-X	I-Y	I-Z	A-X	A-Y	A-Z
1	L STN	120	135.56	135.72	145.93	135.37	134.89	143.31
2	L Gpi	45	146.38	130.16	148.81	140.93	129.7	152.69
3	L Vim	25	137.08	138.39	149.61	136.91	139.07	147.11
4	R STN	20	111.56	135.46	145.93	113.48	133.66	142.72
5	R Gpi	15	100.86	129.67	148.82	100.89	127.49	148.09
6	R Vim	20	109.98	138.1	149.61	111.69	135.36	145.21

The X-axis is the medial-lateral axis, The Y-axis is the anterior-posterior axis, and the Z-axis is the superior-inferior axis in this context. "I" stands for intended, and the "A" stands for the actual coordinates. ***Abbreviations: STN:*** *Subthalamic Nucleus,* ***GPi:*** *Globus Pallidus Interna,* ***Vim:*** *Ventralis Intermediate Nucleus*

Table II: Differences in Different Axes in the Actual Electrode Position and the Planned Coordinates

No	Electrode	Delta-X (mm)	Delta-Y (mm)	Delta-Z (mm)	Vectorial Difference (mm)	Trajectory Difference (mm)
1	L STN	0.19	0.83	2.62	2.75	1.91
2	L Gpi	5.45	0.46	-3.88	6.71	6.63
3	L Vim	0.17	-0.68	2.5	2.6	1.64
4	R STN	-1.92	1.8	3.21	4.15	3.16
5	R Gpi	-0.03	2.18	0.73	2.3	2.08
6	R Vim	-1.71	2.74	4.4	5.46	2.86

Vectorial difference and trajectory difference are calculated through the process provided in the methods. ***STN:*** *Subthalamic Nucleus,* ***GPi:*** *Globus Pallidus Interna,* ***Vim:*** *Ventralis Intermediate Nucleus.*

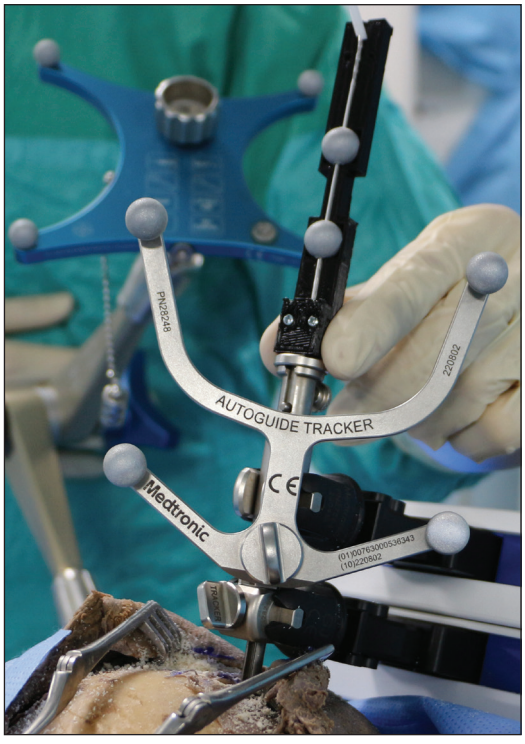

Figure 3: The 3D-printed tool stops the lead at the correct depth.

Although our custom holder allowed the electrode placement, future versions could be enhanced to overcome the limitations of StealthStation's biopsy length calculation tool. This could enable lead advancement by 0.1 mm intervals, similar to traditional insertion systems, potentially leading to improved lead placement accuracy.

It should also be noted that fused deposition modeling, which has been used to print the DBS holder, has a reported 0.08-3.14% manufacturing accuracy (19). This means some deviations from the target may have been caused by warping and deformation during the printing process. This may be reduced by using computer numerical control (CNC) machining and industrial-grade calibration techniques.

While there is no clear literature on what constitutes a malposition, most authors report their vectorial difference is less than 3mm and consider revision when it is more than 3 mm. In comparison, 4 mm can be considered unacceptable by all accounts (2,5,7,9,16,17,22,23,27). In our experiment, while half of the leads had a high vectorial difference (more than 4 mm), the majority of the leads had a trajectory difference of less than 3 mm, possibly explained by the inability to measure the length of the electrode precisely, and extended the electrode deeper than planned. This was also partially caused by challenges in visualizing the real-time trajectory of the electrodes on the StealthStation Autoguide screen. This difficulty

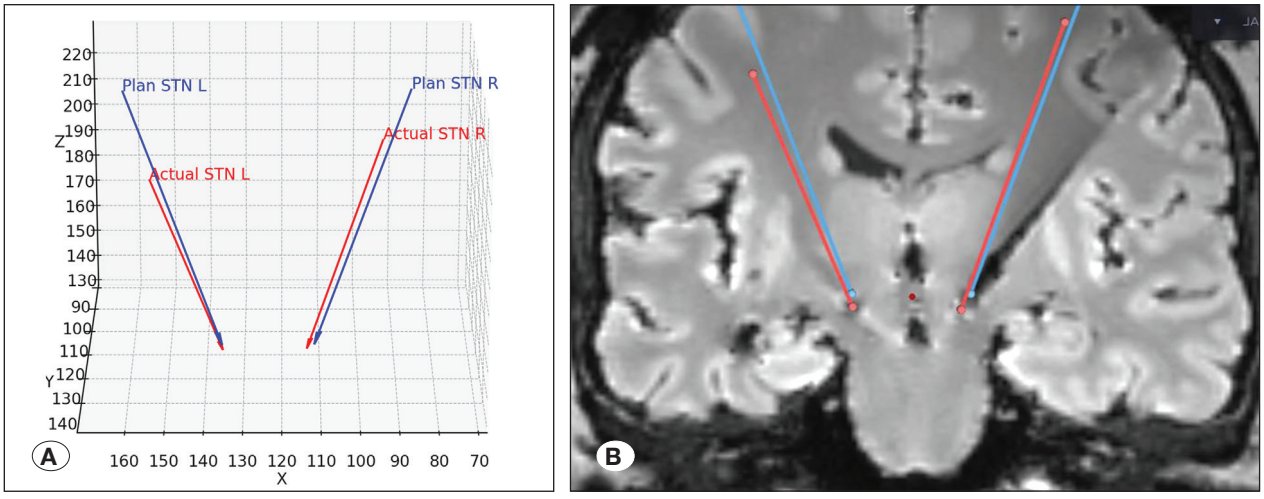

Figure 4: 3D vector field **(A)** and the StealthStation images **(B)** for intended electrode vectors (blue arrows) and the electrodes placed for the STN (red arrows).

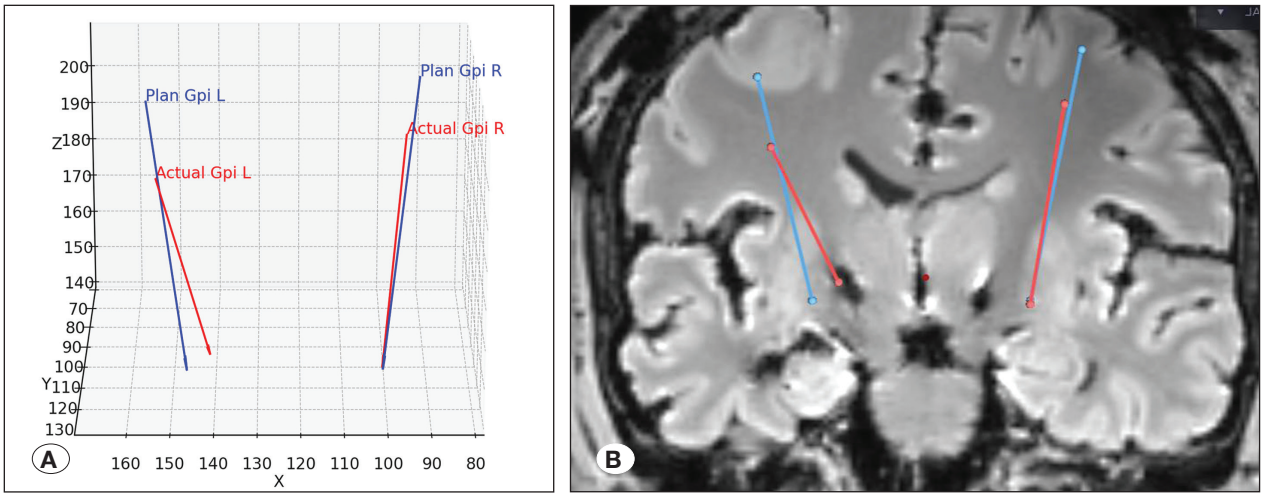

Figure 5: 3D vector field **(A)** and the StealthStation images **(B)** for intended electrode vectors (blue arrows) and the electrodes placed for the Gpi (red arrows).

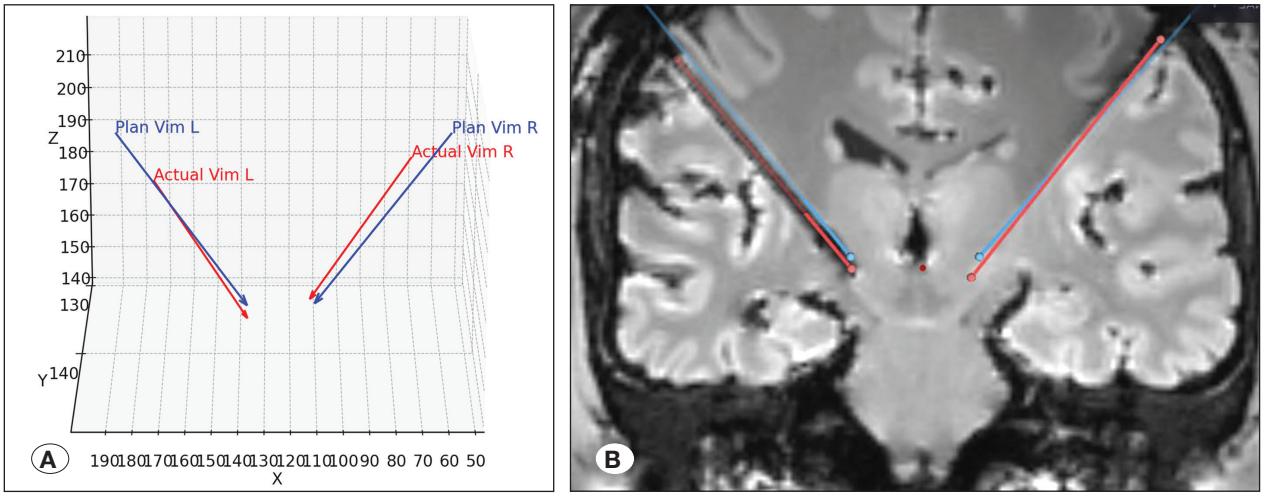

Figure 6: 3D vector field **(A)** and the StealthStation images **(B)** intended electrode vectors (blue arrows) and the electrodes placed for the Vim (red arrows).

arose because the targets for DBS placement were located further from the biopsy cannula, which the system is primarily designed for. Enhancing the system's capabilities to provide real-time feedback for our specialized DBS lead holder could improve accuracy and operator confidence in further research.

An interesting observation is that the duration of the surgery significantly reduced as the primary surgeon felt more at ease with the design. Although the learning curve of the Autoguide platform may have contributed to this, the primary surgeon had ample expertise in both DBS insertion and the utilization of the robotic platform before this. Hence, this occurrence can likely be attributed to the incorporation of our recently developed 3D-printed fiducial holder into the workflow. More cadaveric specimens would be required to minimize the potential variability caused by this.

So, while platforms such as Mazor Robotics Renaissance® system and ROSA® robot offer high-accuracy placement of the DBS leads, their cost may be a barrier for some healthcare organizations, particularly in developing countries, as while their prices are not publicly listed, StealthStation Autoguide is approximately $^{1}/_{5}$ of the price of the Renaissance, and ¼ of the ROSA robotic platform (24). This study serves as an initial exploration of Autoguide's feasibility for DBS lead placement, and future research should investigate its cost-effectiveness compared to other robotic and frame-based systems.

An important constraint of this study is the utilization of only one cadaver. Anatomical variability between specimens can affect the generalizability of our findings. Preliminary studies are crucial for justifying additional research and funding, but bigger sample sizes are required to validate and expand upon these findings. Additionally, the biomechanical properties of a cadaver brain differ significantly from those of a living human brain. The rigidity and fragility of a cadaver brain can potentially impact the precision of electrode positioning. During this study, the increased resistance encountered when inserting the electrodes may have caused bending, resulting in deviations from the intended trajectories (11,20).

Furthermore, the absence of physiological fluids in a cadaver brain may affect its stability and lead to brain tissue displacement during transport as the fixative fluids drain out of the severed cadaveric head. While this phenomenon is not explored in the literature, there are reports of increased brain displacement in patients with CSF over drainage (14,25). This displacement may further contribute to the discrepancies between planned and actual electrode positions. Addressing these differences in future studies by simulating more realistic brain conditions (e.g., fresh frozen cadavers or whole-body cadavers) could improve the findings' relevance to clinical practice.

The precision of the StealthStation Autoguide system's biopsy length calculation tool is a notable limitation. Traditional DBS frames operate with a precision of approximately 0.1 mm, whereas the StealthStation's biopsy calculation tool has a resolution of 1 mm. This issue has not been addressed in the literature, but we believe this lower resolution may have contributed to the observed deviations in electrode placement. Modifying the 3D-printed DBS lead holder for each plan could address this limitation by bypassing the measurement tool's constraints and enhancing placement accuracy.

CONCLUSION

This preliminary study serves as the first step in the implementation of the StealthStation Autoguide cranial robotic guidance platform for DBS surgery. By demonstrating its ability to perform this surgery using a custom 3D-printed DBS holder, our research paves the way for the clinical application of this technology. The potential to shorten surgical times, reduce patient discomfort, and its affordability compared to its counterparts makes Autoguide an appealing option and warrants further research into this topic. Future studies should focus on repeating this work after addressing the technical issues we have encountered and with larger sample sizes. Such research will help refine the technique and build upon our findings, ultimately improving the safety, accuracy, and accessibility of frameless DBS surgery using the StealthStation Autoguide.

ACKNOWLEDGMENTS

The authors sincerely thank those who donated their bodies to science so that anatomical research could be performed. Results from such research can potentially increase mankind's overall knowledge that can then improve patient care. Therefore, these donors and their families deserve our highest gratitude.

Declarations

Funding: This research did not receive any specific grant from funding agencies in the public, commercial, or not-for-profit sectors.

Availability of data and materials: The datasets generated and/or analyzed during the current study are available from the corresponding author by reasonable request.

Disclosure: The authors declare no competing interests.

AUTHORSHIP CONTRIBUTION

Study conception and design: HB, SC, AA, TY
Data collection: BBA, OD, OSA, MSB
Analysis and interpretation of results: NA, KEC, CE
Draft manuscript preparation: HB, BBA, MSB
Critical revision of the article: HB, MSB, NA, KEC
All authors (HB, BBA, OD, OSA, MSB, NA, KEC, CE, SC, AA, TY) reviewed the results and approved the final version of the manuscript.

REFERENCES

1. Ahmed SI, Javed G, Mubeen B, Bareeqa SB, Rasheed H, Rehman A, Phulpoto M, Samar SS, Aziz K Robotics in neurosurgery: A literature review. J Pak Med Assoc 68:258-263, 2018
2. Burchiel KJ, McCartney S, Lee A, Raslan AM: Accuracy of deep brain stimulation electrode placement using intraoperative computed tomography without microelectrode recording. J Neurosurg 119:301-306, 2013. https://doi.org/10.3171/2013.4.JNS122324
3. Cossetto TL, Zareinia K, Sutherland GR: Robotics for Neurosurgery. Medical Robotics. Elsevier, 2012:59-77. https://doi.org/10.1533/9780857097392.59

4. De Benedictis A, Trezza A, Carai A, Genovese E, Procaccini E, Messina R, Randi F, Cossu S, Esposito G, Palma P, Amante P, Rizzi M, Marras CE: Robot-assisted procedures in pediatric neurosurgery. Neurosurg Focus 42:E7, 2017. https://doi.org/10.3171/2017.2.FOCUS16579
5. Eleopra R, Rinaldo S, Devigili G, Mondani M, D'Auria S, Lettieri C, Ius T, Skrap M: Frameless deep brain stimulation surgery: A single-center experience and retrospective analysis of placement accuracy of 220 electrodes in a series of 110 patients. Stereotact Funct Neurosurg 97:337-346, 2019. https://doi.org/10.1159/000503335
6. Eroglu U, Meco C, Caglar S, Ugur HC: Pure robotic surgery for odontoid tumor: first case. World Neurosurg 116:299-304, 2018. https://doi.org/10.1016/j.wneu.2018.05.105
7. Fiegele T, Feuchtner G, Sohm F, Bauer R, Anton JV, Gotwald T, Twerdy K, Eisner W: Accuracy of stereotactic electrode placement in deep brain stimulation by intraoperative computed tomography. Parkinsonism Relat Disord 14:595-599, 2008. https://doi.org/10.1016/j.parkreldis.2008.01.008
8. Furlanetti L, Ellenbogen J, Gimeno H, Ainaga L, Narbad V, Hasegawa H, Lin JP, Ashkan K, Selway R: Targeting accuracy of robot-assisted deep brain stimulation surgery in childhood-onset dystonia: a single-center prospective cohort analysis of 45 consecutive cases. J Neurosurg Pediatr 27:677-687, 2021. https://doi.org/10.3171/2020.10.PEDS20633
9. Girgis F, Zarabi H, Said M, Zhang L, Shahlaie K, Saez I: Comparison of intraoperative computed tomography scan with postoperative magnetic resonance imaging for determining deep brain stimulation electrode coordinates. World Neurosurg 138:e330-e335, 2020. https://doi.org/10.1016/j.wneu.2020.02.108
10. Giridharan N, Katlowitz KA, Anand A, Gadot R, Najera RA, Shofty B, Snyder R, Larrinaga C, Prablek M, Karas PJ, Viswanathan A, Sheth SA: Robot-assisted deep brain stimulation: high accuracy and streamlined workflow. Oper Neurosurg (Hagerstown) 23:254-260, 2022. https://doi.org/10.1227/ons.0000000000000298
11. Hackett MJ, McQuillan JA, El-Assaad F, Aitken JB, Levina A, Cohen DD, Siegele R, Carter EA, Grau GE, Hunt NH, Lay PA: Chemical alterations to murine brain tissue induced by formalin fixation: Implications for biospectroscopic imaging and mapping studies of disease pathogenesis. Analyst 136:2941-2952, 2011. https://doi.org/10.1039/c0an00269k
12. Harris CR, Millman KJ, van der Walt SJ, Gommers R, Virtanen P, Cournapeau D, Wieser E, Taylor J, Berg S, Smith NJ, Kern R, Picus M, Hoyer S, van Kerkwijk MH, Brett M, Haldane A, Del Río JF, Wiebe M, Peterson P, Gérard-Marchant P, Oliphant TE: Array programming with NumPy. Nature 585:357-362, 2020. https://doi.org/10.1038/s41586-020-2649-2
13. Hunter JD: Matplotlib: A 2D graphics environment. Comput Sci Eng 9:90-95, 2007. https://doi.org/10.1109/MCSE.2007.55
14. Kim YS, Kim SH, Jung SH, Kim TS, Joo SP: Brain stem herniation secondary to cerebrospinal fluid drainage in ruptured aneurysm surgery: A case report. Springerplus 5:247, 2016. https://doi.org/10.1186/s40064-016-1875-4
15. Liu L, Mariani SG, De Schlichting E, Grand S, Lefranc M, Seigneuret E, Chabardès S: Frameless ROSA® robot-assisted lead implantation for deep brain stimulation: Technique and accuracy. Oper Neurosurg 19:57-64, 2020. https://doi.org/10.1093/ons/opz320
16. Lumsden DE, Ashmore J, Charles-Edwards G, Lin JP, Ashkan K, Selway R: Accuracy of stimulating electrode placement in paediatric pallidal deep brain stimulation for primary and secondary dystonia. Acta Neurochir 155:823-836, 2013. https://doi.org/10.1007/s00701-013-1629-9
17. McClelland S, Ford B, Senatus PB, Winfield LM, Du YE, Pullman SL, Yu Q, Frucht SJ, McKhann GM, Goodman RR: Subthalamic stimulation for Parkinson disease: Determination of electrode location necessary for clinical efficacy. Neurosurg Focus 19:E12, 2005. https://doi.org/10.3171/foc.2005.19.5.13
18. Neudorfer C, Hunsche S, Hellmich M, El Majdoub F, Maarouf M: Comparative study of robot-assisted versus conventional frame-based deep brain stimulation stereotactic neurosurgery. Stereotact Funct Neurosurg 96:327-334, 2018. https://doi.org/10.1159/000494736
19. Petropolis C, Kozan D, Sigurdson L: Accuracy of medical models made by consumer-grade fused deposition modelling printers. Plast Surg 23:91-94, 2015. https://doi.org/10.4172/plastic-surgery.1000912
20. Schulz G, Crooijmans HJA, Germann M, Scheffler K, Müller-Gerbl M, Müller B: Three-dimensional strain fields in human brain resulting from formalin fixation. J Neurosci Methods 202:17-27, 2011. https://doi.org/10.1016/j.jneumeth.2011.08.031
21. Sharma M, Rhiew R, Deogaonkar M, Rezai A, Boulis N: Accuracy and precision of targeting using frameless stereotactic system in deep brain stimulator implantation surgery. Neurol India 62:503-509, 2014. https://doi.org/10.4103/0028-3886.144442
22. Singer A, Zhang C, Wang T, Qiu S, Li D, Du Y, Liang Z-P, Herman P, Sun B, Feng Y: Post-operative electrode placement prediction in deep brain stimulation using support vector regression. proceedings of the third international symposium on image computing and digital medicine. ISICDM 2019: Proceedings of the Third International Symposium on Image Computing and Digital Medicine 202-207, 2019. https://doi.org/10.1145/3364836.3364876
23. Starr PA, Martin AJ, Ostrem JL, Talke P, Levesque N, Larson PS: Subthalamic nucleus deep brain stimulator placement using high-field interventional magnetic resonance imaging and a skull-mounted aiming device: Technique and application accuracy. J Neurosurg 112:479-490, 2010. https://doi.org/10.3171/2009.6.JNS081161
24. Tay AS-MS, Menaker SA, Chan JL, Mamelak AN: Placement of stereotactic electroencephalography depth electrodes using the stealth autoguide robotic system: Technical methods and initial results. Oper Neurosurg (Hagerstown) 22:e150-e157, 2022. https://doi.org/10.1227/ONS.0000000000000110
25. Tsutsumi S, Ono H, Yasumoto Y: Immobile cerebral veins in the context of positional brain shift: an undescribed risk factor for acute subdural hemorrhage. Surg Radiol Anat 39:1063-1067, 2017. https://doi.org/10.1007/s00276-017-1837-8
26. VanSickle D, Volk V, Freeman P, Henry J, Baldwin M, Fitzpatrick CK: Electrode placement accuracy in robot-assisted asleep deep brain stimulation. Ann Biomed Eng 47:1212-1222, 2019. https://doi.org/10.1007/s10439-019-02230-3
27. Xu Y, Qin G, Tan B, Fan S, An Q, Gao Y, Fan H, Xie H, Wu D, Liu H, Yang G, Fang H, Xiao Z, Zhang J, Zhang H, Shi L, Yang A: Deep brain stimulation electrode reconstruction: Comparison between lead-DBS and surgical planning system. J Clin Med 12:1781, 2023. https://doi.org/10.3390/jcm12051781

Turk Neurosurg 35(4):587-591, 2025
DOI: 10.5137/1019-5149.JTN.46394-24.2

Original Investigation
Stereotactic and Functional

Received: 06.02.2024
Accepted: 29.11.2024
Published Online: 25.06.2025

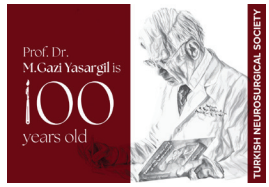

Non-Root Exit Zone Exploration during Facial Nerve Microvascular Decompression: A Discussion of the Pathogenesis in Atypical Cases of Hemifacial Spasm

Gaochao SONG[1,2]*, Yuanyang WU[1]*, Qi YAO[1], Guiping NI[1], Jianhong SHEN[1]

[1]Affiliated Hospital of Nantong University, Department of Neurosurgery, Nantong, Jiangsu Province, China
[2]Second Affiliated Hospital of Nanjing Medical University, Department of Neurosurgery, Nanjing, Jiangsu Province, China

*Gaochao Song and Yuanyang Wu contributed equally to this work

Corresponding author: Jianhong SHEN ✉ ntdxsjh@163.com

ABSTRACT

AIM: To summarise atypical cases of hemifacial spasm (HFS) found during microvascular decompression (MVD), and to investigate its pathogenesis and range of exploration.

MATERIAL and METHODS: We retrospectively analysed cases of HFS performed in our department in recent years and summarised the intraoperative electrophysiological monitoring findings, vascular and nerve exploration, and postoperative symptoms. We then discussed the pathogenesis of and treatment for atypical HFS.

RESULTS: In total, 85 cases of facial nerve MVD were performed in the past 3 years, of which 77 (90.6%) were responsible factors in the root exit zone (REZ) and eight (9.4%) in the non-REZ. For patients without vascular compression of the REZ, the compression factors outside the REZ were separated, and the arachnoid band around the facial nerve was released; subsequently, the amplitude of the abnormal muscle response of the facial nerve diminished or disappeared. Facial twitch symptoms disappeared or improved significantly after surgery. Most symptoms disappeared after 3 months of postoperative follow-up.

CONCLUSION: Factors responsible for non-REZ observed during MVD of the facial nerve are not rare. It is suggested that full-length exploration should be performed during facial nerve MVD under electrophysiological monitoring.

KEYWORDS: Hemifacial spasm, Microvascular decompression, Intraoperative electrophysiology, Abnormal muscle response

ABBREVIATIONS: HFS: Hemifacial spasm, **MVD:** Microvascular decompression, **REZ:** Root exit zone, **AMR:** Abnormal muscle response, **MRTA:** Magnetic resonance tomographic angiography, **AICA:** Anterior inferior cerebellar artery, **PICA:** Posterior inferior cerebellar artery, **VA:** Vertebral artery, **BA:** Basilar artery, **SCA:** Superior cerebellar artery

INTRODUCTION

Hemifacial spasm (HFS) is a common neurosurgical condition. The pathogenesis of HFS is generally believed to be vascular compression of the facial nerve root exit zone (REZ), resulting in changes in the local neural structure and involuntary twitching of the orbicularis oculi and orbicularis oris muscles due to similar abnormal discharges (2). This is known as the microvascular compression theory, and based on this theory, microvascular decompression (MVD) has become the standard surgery for treating HFS; however, symptoms commonly fail to improve after MVD. In some cases, this failure may be related to incomplete surgical decompression, whereas in others, it may involve understanding the pathogenesis.

Gaochao SONG : 0000-0003-0092-8776
Yuanyang WU : 0009-0000-0199-1393
Qi YAO : 0000-0001-9445-0384
Guiping NI : 0000-0003-2231-0897
Jianhong SHEN : 0000-0003-2270-8555

Our department has performed 85 HFS procedures in the past 3 years, including some atypical cases. In this paper, we analyse the surgical effects and particular characteristics observed intraoperatively in these patients and discuss the pathogenesis and surgical exploration methods of atypical cases.

MATERIAL and METHODS

This study has been approved by the Ethics Committee of the Affiliated Hospital of Nantong University (NO. 2024-K075).

Patient Data

The study included 85 patients aged 24 to 80 years (median, 55 years) with a disease course ranging from 1 month to 20 years (median, 3 years). Thirty-three were male (18 affected on the left, 15 on the right), and 52 were female (27 affected on the left, 25 on the right). Before the operation, neurotrophic medications were administered to 17 patients, carbamazepine to 28 patients, acupuncture to 13 patients (which proved beneficial in five cases), botulinum toxin injections to eight patients, and no treatment to 19 patients. All patients underwent facial nerve magnetic resonance tomography (MRTA) angiography before surgery.

Surgical Indications

The surgical indications were as follows: 1) a clear diagnosis of primary HFS; 2) MRTA revealing closely related blood vessels surrounding the facial nerve; 3) exclusion of history of facial nerve injury; 4) obvious symptoms that significantly impacted the quality of life and did not improve with conservative treatment; and 5) tolerance to general anaesthesia.

Surgical Material

Recently, China has been regulating the management of human implants. Teflon cannot be used for MVD surgery because it is not registered or accessible in China. Polyester is permitted for MVD surgery, and a medical gasket resembling Teflon is made entirely of polyester fibres. The safety and efficacy of MVD have been thoroughly confirmed after several years of clinical use. Follow-up findings were satisfactory.

Surgical Strategy

In the lateral recumbent position under general anaesthesia, a straight incision was created approximately 6 cm behind the affected side. A small bone window was opened behind the transverse sinus and sigmoid sinus. The blood vessels close to it were explored from the facial nerve REZ and separated with polyester. The operation was performed under a microscope or neuroendoscope. Furthermore, 80 patients were operated on under electrophysiological monitoring.

Atypical Cases

Case 1: Female, 51 years old, with paroxysmal convulsions of the left cheek and corner of the eye for 10 years. During the operation, the anterior inferior cerebellar artery (AICA) was shown to pass through the facial and auditory nerves, wherea the posterior inferior cerebellar artery (PICA) was ventral to the facial nerve immediately adjacent to the REZ; thus, the PICA and AICA formed a clamp in the REZ (Figure 1A). The facial nerve was separated from the two blood vessels using polyester; however, the AMR did not disappear. We continued to explore the facial nerve until the AMR disappeared before entering the inner ear foramen; however, no blood vessels were observed. Here, the AMR disappeared following the separation of the facial and auditory nerves using polyester (Figure 1B); it reappeared after withdrawal and disappeared after re-insertion.

Case 2: Female, 55 years old, with paroxysmal convulsions on the left side of the face for 3 months. During surgery, the PICA from the vertebral artery was found to oppress the initial segment of the facial nerve instead of the normal REZ. The AMR disappeared after the PICA was separated from the facial nerve, revealing that the AICA passed through the REZ of the facial and auditory nerve (Figure 2A). The PICA was carefully pushed away from the facial nerve with polyester, and the AICA was separated from the facial nerve (Figure 2B).

Case 3: Female, 53 years old, had paroxysmal convulsions on the left face for 9 years. During the operation, the facial and auditory nerves were found to be in close proximity, without gaps, seemingly merging into one branch. Electrophysiological

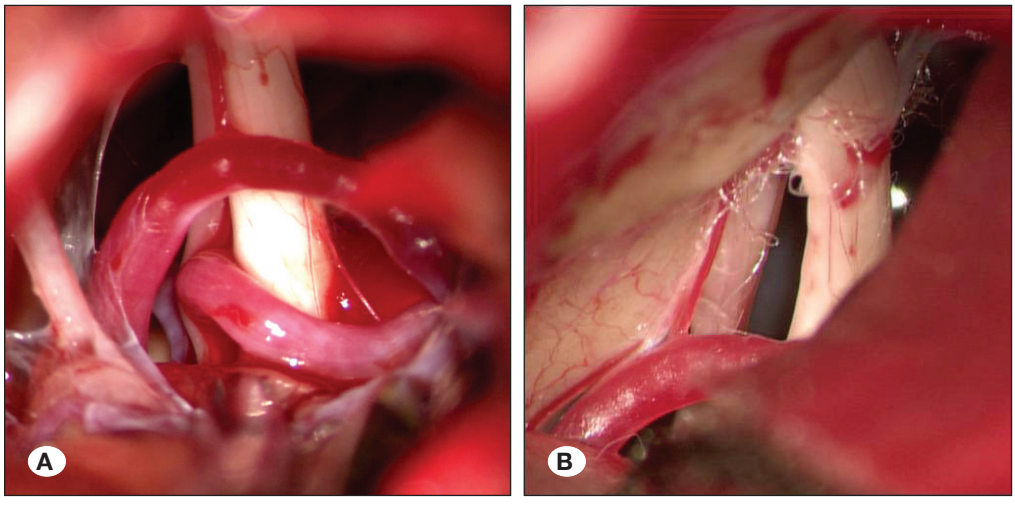

Figure 1: Vascular compression in the facial nerve root exit zone (REZ); however, the abnormal muscle response (AMR) did not disappear after treatment. **A)** The anterior inferior cerebellar artery (AICA) passed between the facial and auditory nerve, and the posterior inferior cerebellar artery (PICA) was ventral to the facial nerve immediately adjacent to the REZ. **B)** Near the inner ear foramen, the AMR disappeared after separating the facial nerve and auditory nerve.

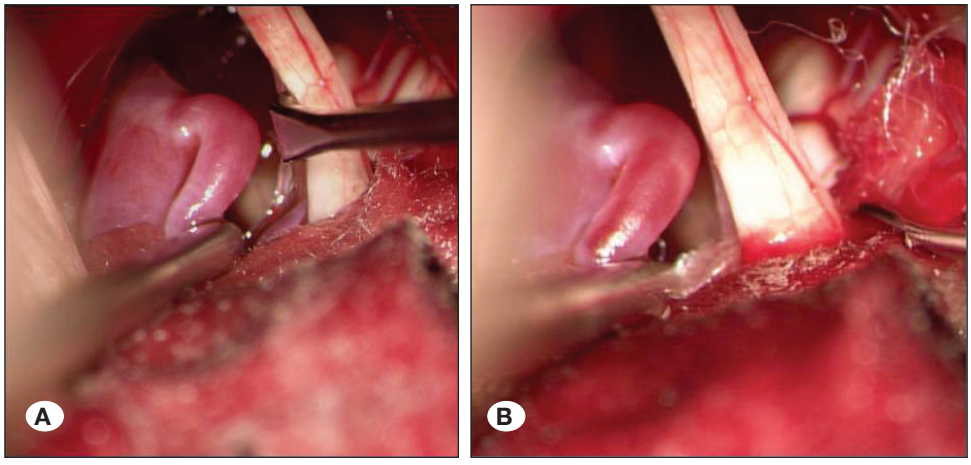

Figure 2: The posterior inferior cerebellar artery (PICA) from the vertebral artery oppressed the initial segment of the facial nerve and superimposed the anterior inferior cerebellar artery (AICA), forming a compression series. **A)** The PICA from the vertebral artery oppressed the initial segment of the facial nerve; the abnormal muscle response (AMR) disappeared after the PICA was pushed away. **B)** Separating the AICA passing between the root exit zone (REZ) of the facial nerve and the auditory nerve.

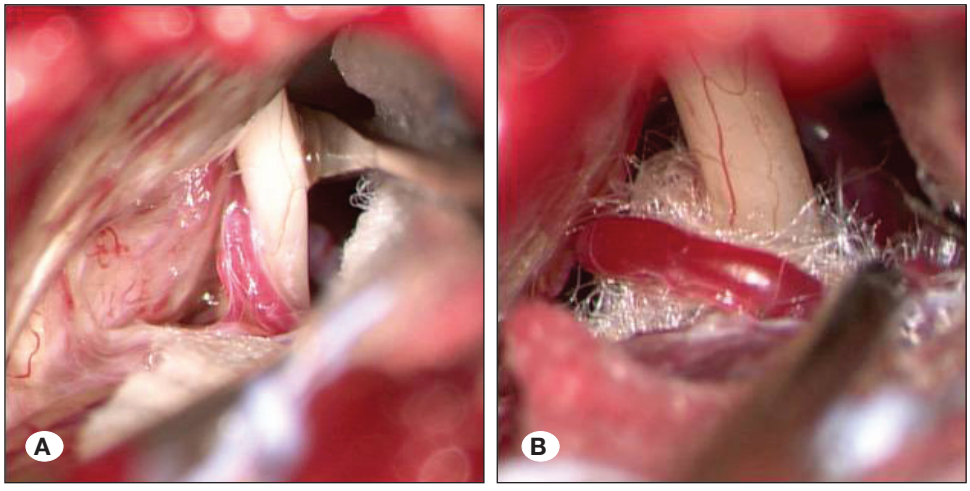

Figure 3: The intracranial segment of the facial nerve and auditory nerve are in close proximity and seem to merge into one branch. **A)** The anterior inferior cerebellar artery (AICA) hovered from the auditory nerve root exit zone (REZ) to the deep place. **B)** The abnormal muscle response (AMR) disappeared after separating the AICA from the facial nerve.

monitoring confirmed that the deep surface was the facial nerve fibre. The AICA hovered from the REZ of the auditory nerve to the middle of the facial nerve (Figure 3A). The AICA was separated from the facial nerve fibres with polyester (Figure 3B), and the AMR disappeared.

Case 4: Male, 56 years old, with paroxysmal convulsions of the left face for 2 years. During the operation, the AICA compressed the distal segment of the facial nerve. The AMR in the orbicularis oris muscle area disappeared after separating the AICA from the facial nerve with polyester (Figure 4A). There was no change in the AMR in the orbicularis oculi muscle area. After further exploration, a pulsatile great blood vessel was observed dorsal to the facial nerve REZ, which was confirmed as the vertebral artery (VA). Electrophysiological observations showed that the amplitude of the AMR in the orbicularis oculi muscle area decreased after the facial nerve was separated from the VA using polyester (Figure 4B).

RESULTS

In most cases, one or two close vessels were found near the facial nerve REZ, including the basilar artery (BA) (n = 2), VA (n = 21), superior cerebellar artery (SCA) (n = 2), AICA (n = 41), PICA (n = 24), and the petrosal vein and its branches (n = 4). The remaining vessels were branched arterioles.

Of the 85 patients, 63 resolved after surgery, 13 showed clear relief, four had mild facial paralysis, and five had mild hearing loss. Twelve of the 13 patients who improved postoperatively no longer experienced convulsions at the 3-month follow-up. The four patients with mild facial paralysis fully recovered, and the five with mild hearing loss improved.

Four atypical cases were observed under the microscope, and all postoperative symptoms of facial convulsions vanished; however, in Case 4, convulsions recurred 4 days after the operation, although less than those before the operation, and vanished once more 9 days later. No postoperative effects on hearing were observed in any of the four cases.

DISCUSSION

HFS is a common functional disorder in neurosurgery, and understanding its pathogenesis directly affects the treatment. Since Jannetta proposed that vascular compression in the REZ is the main pathogenic factor for HFS, MVD has become the standard modality for the aetiology of HFS, with definite curative effects (3,7,8).

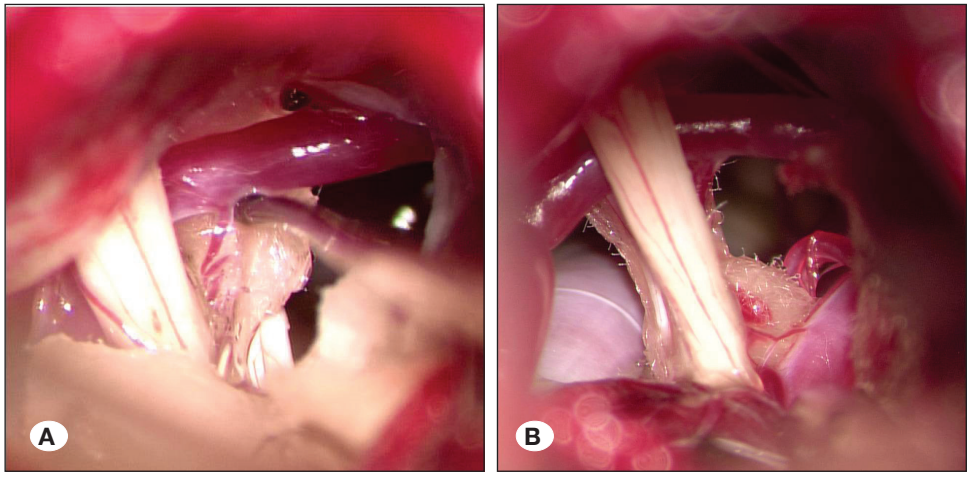

Figure 4: Vascular compression of the distal segment of the facial nerve. After treatment, there was no change in the abnormal muscle response (AMR) of the orbicularis oculi muscle area. **A)** The anterior inferior cerebellar artery (AICA) compressed the distal segment of the facial nerve. After separation, the AMR of the orbicularis oris muscle area disappeared. **B)** Vertebral artery compression was seen dorsal to the facial nerve root exit zone (REZ), and the AMR amplitude of the orbicularis oculi muscle area decreased after separation.

In the clinic, there are some instances where the conventional REZ has no clear accountable vessel during MVD, or electrophysiological alterations in the REZ are not immediately apparent following vascular separation. By summarising these cases, we propose novel ideas regarding the aetiology of therapeutic approaches for HFS.

The traditional theory of peripheral vascular compression suggests that local demyelination caused by vascular compression of the facial nerve REZ is the pathological basis for developing HFS, explaining the postoperative symptom relief and delayed remission in some cases where the intraoperative AMR did not disappear. However, the demyelination explanation could not account for symptoms that disappeared immediately after surgery in a significant percentage of patients, including 63 of the 85 patients included in our study. Zheng et al. proposed the sympathetic bridge hypothesis (12), which suggests that the facial nerve REZ is compressed and abraded by blood vessels over an extended period, thereby breaking the vascular wall. Consequently, the exposed sympathetic fibres of the vessel wall come in contact with the exposed facial nerve fibres after demyelination, and sympathetic excitation releases neurotransmitters that act on the damaged facial nerve and cause it to produce impulses, leading to clinical symptoms. Although the sympathetic bridge hypothesis explains the immediate postoperative disappearance of symptoms, it is still considered a peripheral theory.

Treatment strategies for the blood vessels in the REZ have always been the focus of research on facial nerve MVD. Park et al. categorised the vessels responsible for vascular loop compression into arachnoid, perforating arterial, vascular clamping, and series compression types; however, the actual situation of MRTA examination is that even on the healthy side, there is a high probability of the presence of closely related small blood vessels around the facial nerve, which leads to confusion regarding how to accurately identify the responsible vessels (9). Can completion of the treatment of vessels that compress the REZ be used as a criterion for the end of the operation? AMR is a delayed response to stimulation of one branch of the facial nerve motor branch, recorded in muscles innervated by other branches. It was first described in 1986, and its disappearance has been positively correlated with the clinical results of MVD (6). Although the exact mechanism of AMR is unclear, similar to that of HFS, there are peripheral (demyelination of the facial nerve) and central hypotheses (4) (increased excitability of the facial nucleus). Microvascular decompression for HFS is now frequently accompanied by changes in AMR, and the dependability and efficacy of decompression can be assessed (13). Several studies have analysed such cases and concluded that AMR could be used as a "biomarker" for HFS, which is helpful for diagnosis and monitoring during MVD (10,13).

It was not unusual for AMR to disappear following non-REZ treatment in several instances, including Cases 1–4. In Case 1, the AICA and PICA clamped the facial nerve REZ, but the AMR persisted even after decompression. If decompression of the REZ was taken as the standard, the operation could be terminated. However, recent literature has also explained that the pathogenic factors causing HFS may include vascular and non-vascular factors outside the REZ (11), such as bony stenosis of the internal auditory meatus (5), and strangulation of the arachnoid band (1). In this case, the AMR disappeared after separating the facial and auditory nerves at the internal auditory meatus, which proved that the appearance of AMR may also be related to compression outside the REZ and illustrated that the disappearance of an AMR is an important indicator of surgical efficacy. The disappearance of AMR following the separation of the facial and auditory nerves may be due to the displacement of the facial nerve at the internal auditory meatus to avoid bony entrapment.

Intraoperative observations in Case 2 showed the PICA compressing the distal segment of the facial nerve REZ. The AMR disappeared after pushing the PICA away. Further, exploration showed that only the AICA passed through the facial nerve REZ. This may be due to cascade compression of the REZ by the PICA superimposed on the AICA. The pathogenesis of this case may be explained by the theory of peripheral vascular compression in the REZ; however, the compression of the distal segment of the facial nerve REZ by the PICA and the immediate disappearance of the AMR after separation of the two are inconsistent with the theory of compression in the REZ.

In Case 3, the AICA was seen hovering closely to the middle segment of the facial nerve, and the disappearance of the AMR after treatment was not consistent with the REZ compression theory. Similarly, the intraoperative disappearance of AMR in the orbicularis oris region in Case 4 did not result from treatment of the REZ; however treatment of the AICA in the non-REZ did not attenuate AMR in the orbicularis oculi region. Therefore, it is necessary to explore the blood vessels outside the REZ. The above cases show that the persistence of AMR after treatment of the REZ does not mean it does not disappear at the end of MVD. Many surgeons have also proposed the necessity for a full-length exploration of facial nerve root areas I–IV.

In summarising our data and combining our findings with those in the literature, we believe that vascular factors, bone compression, fibre adhesion, and nerve demyelination caused by peripheral factors involving the entire length of the facial nerve form an important pathological basis for HFS. The central factors (excitatory "igniting" of the facial nucleus) are indispensable for typical clinical symptoms. Full-length exploration of facial nerve MVD is necessary to improve the intraoperative disappearance rate of AMR and the postoperative negative rate of HFS. Of course, if the compression and traction factors have been removed, there is no need to worry about whether the AMR disappears, avoiding excessive perturbation of the facial and auditory nerves which may lead to increased complications.

CONCLUSION

The theory of vascular compression in the REZ cannot explain all the incidences of HFS. There is great uncertainty in the intraoperative identification of the responsible factors and the prediction of surgical effects. A full-length exploration of the facial nerve should be performed during MVD. For atypical HFS, electrophysiological monitoring of AMR is of great help in identifying the causative factors.

Declarations

Funding: This study was supported by the following grants: Jiangsu Provincial Medical Innovation Center (CXZX202212); Jiangsu Provincial Research Hospital (YJXYY202204); Medical Innovation Team Project of the "14th Five-Year Plan" Science Education and Health Project (NTCXTD48).

Availability of data and materials: The datasets generated and/or analyzed during the current study are available from the corresponding author by reasonable request.

Disclosure: The authors declare no competing interests.

AUTHORSHIP CONTRIBUTION

Study conception and design: GS, JS
Data collection: GS, YW, QY, GN
Analysis and interpretation of results: GS, JS
Draft manuscript preparation: GS, JS
Critical revision of the article: GS, YW, JS
All authors (GS, YW, QY, GN, JS) reviewed the results and approved the final version of the manuscript.

REFERENCES

1. El Refaee E, Marx S, Rosenstengel C, Baldauf J, Schroeder HWS: Arachnoid bands and venous compression as rare causes of hemifacial spasm: Analysis of etiology in 353 patients. Acta Neurochirurgica 162:211-219, 2019. https://doi.org/10.1007/s00701-019-04119-5.
2. Han IB, Chang JH, Chang JW, Huh R, Chung SS: Unusual causes and presentations of hemifacial spasm. Neurosurgery 65:130-137; discussion 137, 2009. https://doi.org/10.1227/01.NEU.0000348548.62440.42.
3. Jannetta PJ, Abbasy M, Maroon JC, Ramos FM, Albin MS: Etiology and definitive microsurgical treatment of hemifacial spasm. J Neurosurgery 47:321-328, 1977. https://doi.org/10.3171/jns.1977.47.3.0321.
4. Kameyama S, Masuda H, Shirozu H, Ito Y, Sonoda M, Kimura J: Ephaptic transmission is the origin of the abnormal muscle response seen in hemifacial spasm. Clin Neurophysiol 127:2240-2245, 2016. https://doi.org/10.1016/j.clinph.2016.02.004.
5. Ligas B, Khatri D, Higbie C, Wagner K, Langer D: Hemifacial spasm due to bony stenosis of the internal auditory meatus: Look beyond the loop. World Neurosurgery 137:179-182, 2020. https://doi.org/10.1016/j.wneu.2020.01.196.
6. Liu MX, Zhong J, Xia L, Dou NN, Sun H, Li B, Visocchi M, Li ST: The significance of abnormal muscle response monitoring during microvascular decompression for hemifacial spasm. Trends in reconstructive neurosurgery. Acta Neurochir Suppl 124:297-301, 2017. https://doi.org/10.1007/978-3-319-39546-3_43.
7. Ma Q, Zhang W, Li G, Zhong W, Yang M, Zheng X, Yang X, Li S: Analysis of therapeutic effect of microvascular decompression surgery on idiopathic hemifacial spasm. J Craniofac Surg 25:1810-1813, 2014. https://doi.org/10.1097/SCS.0000000000000990.
8. Park CK, Lee SH, Park BJ: Surgical outcomes of revision microvascular decompression for persistent or recurrent hemifacial spasm after surgery: Analysis of radiologic and intraoperative findings. World Neurosurg 131:e454-e459, 2019. https://doi.org/10.1016/j.wneu.2019.07.191.
9. Park JS, Kong DS, Lee JA, Park K: Hemifacial spasm: Neurovascular compressive patterns and surgical significance. Acta Neurochir 150:235-241, 2008. https://doi.org/10.1007/s00701-007-1457-x.
10. Sen CN, Møller AR: Signs of hemifacial spasm created by chronic periodic stimulation of the facial nerve in the rat. Exp Neurol 98:336-349, 1987. https://doi.org/10.1016/0014-4886(87)90246-9.
11. Son BC, Ko HC, Choi JG: Hemifacial spasm caused by vascular compression in the cisternal portion of the facial nerve: Report of two cases with review of the literature. Case Rep Neurol Med 2019:8526157, 2019. https://doi.org/10.1155/2019/8526157.
12. Zheng X, Hong W, Tang Y, Wu Z, Shang M, Zhang W, Zhong J, Li S: Sympathetic nerves bridge the cross-transmission in hemifacial spasm. Neurosci Lett 517:52-55, 2012. https://doi.org/10.1016/j.neulet.2012.04.023.
13. Zhu W, Sun C, Zhang Y, Xu J, Wu S: AMR monitoring in microvascular decompression for hemifacial spasm: 115 cases report. J Clin Neurosci 73:187-194, 2020. https://doi.org/10.1016/j.jocn.2019.10.008.

Turk Neurosurg 35(4):592-602, 2025
DOI: 10.5137/1019-5149.JTN.46820-24.4

Original Investigation

Stereotactic and Functional

Received: 08.05.2024
Accepted: 01.05.2025
Published Online: 25.06.2025

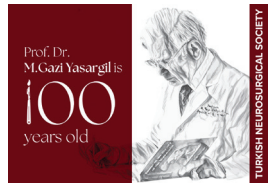

Not to Wait Too Long After Failed Surgery for Intractable Mesial Temporal Lobe Epilepsy: Results of Reoperation at a Tertiary Hospital

Seyda ERDOGAN[1], Serdar SOLMAZ[2], Murat ZAIMOGLU[2], Atilla ERDEM[2]

[1]Ankara University School of Medicine, Ibn-i Sina Hospital, Department of Neurology, Ankara, Türkiye
[2]Ankara University School of Medicine, Ibn-i Sina Hospital, Department of Neurosurgery, Ankara, Türkiye

Corresponding author: Seyda ERDOGAN; Serdar SOLMAZ ✉ dr_seyda@yahoo.com; serdar-solmaz@hotmail.com

ABSTRACT

AIM: To evaluate the causes and risk factors of seizure recurrence, as well as the outcomes of reoperation in patients who did not achieve sufficient seizure control following surgery for mesial temporal lobe epilepsy (MTLE).

MATERIAL and METHODS: We retrospectively reviewed the hospital charts of patients with medically refractory MTLE who were operated between 1990 and 2021.

RESULTS: A total of 240 patients (127 females and 113 males) with medically refractory mesial temporal lobe epilepsy underwent resective epilepsy surgery. Of these, 12 (5%) required reoperation due to seizure recurrence after the initial surgery. Six out of the 12 patients with available seizure outcome data were included in the study. The cause of seizure recurrence in all patients was remnant tissue. The age at reoperation ranged from 17 to 59 years, and the time between the initial and final surgery ranged from 2 to 20 years. The seizure outcome was Engel Class I in all patients, with follow-up periods ranging from 4 to 21 years.

CONCLUSION: Surgical failure is still prevalent in patients with MTLE, with inadequate resection frequently serving as the primary cause. Reoperation can considerably improve the seizure outcome. Delaying the opportunity for a second surgical intervention should be avoided.

KEYWORDS: Epilepsy, Intractable epilepsy, Reoperation, Surgery, Surgery failure, Temporal lobe epilepsy

ABBREVIATIONS: TLE: Temporal lobe epilepsy, **MTLE:** Mesial temporal lobe epilepsy, **FIASs:** Focal impaired awareness seizures, **FBTCSs:** Focal to bilateral tonic-clonic seizures, **EEG:** Electroencephalography, **MRI:** Magnetic resonance imaging, **ASDs:** Antiseizure drugs, **ATL:** Anterior temporal lobectomy, **DNET:** Dysembryoplastic neuroepithelial tumor

INTRODUCTION

The majority of surgically treated patients diagnosed with medically intractable seizures have temporal lobe epilepsy (TLE). The seizure-free rates following resective surgery range from 60% to 80% in temporal lobe epilepsy (4,5,19,21). However, up to 30% of patients may not benefit from surgical treatment and may continue to experience seizures following surgery (18). The results of studies investigating the outcomes of reoperation in patients with failed epilepsy surgery are encouraging, prompting epileptologists to re-evaluate these patients (2,9,13,14,17,20).

Several studies have reported the outcomes of reoperation for recurring TLE (1,5,10,12). These studies found that more

Seyda ERDOGAN : 0000-0003-2759-9562
Serdar SOLMAZ : 0000-0001-7889-3396
Murat ZAIMOGLU : 0000-0001-5330-1251
Atilla ERDEM : 0000-0001-9942-3174

complete resection of the mesiobasal structures can prevent seizure recurrence and need for reoperation (7). However, in the case of resective surgeries which provide the best results in terms of seizure-free rate and neuropsychological outcome, the approach and size of the resection remain debatable (18).

The primary aim of this study is to investigate the surgical outcomes in patients with mesial TLE (MTLE) who were re-operated due to seizure recurrence. Additionally, we examine the causes of seizure recurrence after the initial surgery and discuss the surgical tips related to seizure recurrence.

MATERIAL and METHODS

This study is a retrospective consecutive case series from a single center. The study protocol was reviewed and approved by the local ethics committee. The ethical approval was obtained from the Ankara University School of Medicine, Human Research Ethics Committee (Decision No: I2-121-20).

We retrospectively reviewed the hospital charts of patients with medically refractory MTLE who were operated on at the Department of Neurosurgery between 1990 and 2021. Patients who underwent reoperation owing to seizure recurrence after their initial surgical treatment, as well as those patients with postoperative follow-ups and available seizure outcomes, were included in the study. Before the second surgery, all patients had been thoroughly evaluated by an experienced epilepsy center. These evaluations included video-electroencaphalography (EEG) monitoring with seizure recording, 1.5 or 3T epilepsy protocol magnetic resonance imaging (MRI), detailed neuropsychological assessment and, when necessary, positron emission tomography (PET) or functional MRI.

We collected data on the demographic features, risk factors for epilepsy, age at seizure onset, seizure types, brain MRI findings before and after the initial surgery, any changes in the frequency and type of seizures post-surgery, pathological findings, time to seizure recurrence after the initial surgery, and seizure outcomes after both the initial and second surgeries. The primary outcome was seizure status following surgery. Seizure outcome was evaluated according to the Engel classification (3).

RESULTS

Between the years 1990 and 2021, 240 patients (127 female and 113 male) with medically refractory MTLE underwent resective epilepsy surgery at our institution. All patients underwent anterior temporal lobectomy (ATL). Of the 240 patients, 12 (5%) underwent reoperation owing to seizure recurrence after the initial surgical treatment. Six of the 12 patients were excluded from the study due to the absence of documented seizure outcomes. We present the data of six patients with MTLE who underwent reoperation owing to seizure recurrence after the initial surgical treatment. The demographic and clinical data of these patients are summarized in Table I. There was no reduction or discontinuation of drug therapy in any of the patients for at least 24 months after the initial surgery.

Recurrent seizures occurred in the first 6 months after the initial surgery in five of the six patients. Patient #6 (see below) had a single seizure at the 6th month, however, recurrent seizures occurred at the 30th month of the initial surgery. Patients #1 and #2 experienced frequent seizures in the early period, shortly after the first surgery (<1 month). The histopathological findings indicated focal cortical dysplasia and DNET in these patients, respectively.

The recurrent seizures were semiologically identical to the preoperative seizures in all patients. Exceptionally, patient #3 had frequent focal seizures and rare, focal to bilateral tonic clonic seizures (FBTCS) before the initial surgery; however, all seizures after the initial surgery were FBTCSs. In all patients, based on video-EEG monitoring, brain imaging results, and evaluations made during patient management conferences, it was concluded that the cause of seizure recurrence after the initial surgery was the residual tissue observed on the brain MRI, specifically in the mesial temporal region. All patients underwent reoperation to complete anterior temporal lobectomy with resection of residual tissues. The patient's age at reoperation ranged from 17 to 59 years. The time from the initial to the last surgery, in terms of reoperation, ranged from 2 to 20 years (Table I).

The follow-up duration after the repeat surgery ranged from 4 to 21 years. The median follow-up time was 15 years. The seizure outcome at last follow-up was Engel Class I (Ia and Ib) with no disabling seizures since surgery.

The histopathological findings showed neoplasms in three patients (patients #2, 3, and 5) and nonneoplastic conditions in the others (patients #1, 4, and 6). In three patients, the diagnosis changed after the second surgery (patient #2: from gliosis to dysembryoplastic neuroepithelial tumor, patient #3: from astrocytoma to grade 1 ganglioglioma; and patient #5: from nonspecific changes to glioneuronal tumor), all of whom were diagnosed with a neoplastic pathology. After the repeat surgery, there were no serious complications. Preoperative and postoperative neuropsychological test results were only available for patient #6, while the results for the other patients could not be retrieved. However, during outpatient evaluations and follow-up phone calls (carried out in previous and recent follow-ups), neither the patients nor their relatives reported any complaints regarding the new onset of memory or language deficits following the most recent surgery.

Detailed examination of each patient is presented below:

Patient #1

The patient was a 41-year-old female with a 17-year history of focal impaired awareness seizures (FIAS) and focal to bilateral tonic-clonic seizures (FBTCS). Regarding her medical history, she had febrile convulsions at the age of 6 months. Brain MRI showed increased hyperintensity in the left mesial temporal lobe structures. She underwent left amygdalohippocampectomy for mesial temporal lobe epilepsy at another hospital at the age of 30 years. In the postoperative follow-up, the frequency of seizures increased by more than 50% in the first month after surgery. Eleven years after the first surgery, the patient was re-evaluated. Interictal electroencephalography revealed epileptiform discharges in the left temporal region. Focal onset seizures with impaired awareness, which were

Table I: The Demographic and Clinical Features of MTLE Patients Re-Operated Due to Failure From Initial Surgical Intervention

	Patient #1	**Patient #2**	**Patient #3**	**Patient #4**	**Patient #5**	**Patient #6**
Gender	F	M	F	M	F	M
Risk factors for epilepsy	FS	TBI	Negative	FS	Negative	FS
Age at seizure onset (years)	24	11	5	10	27	13
Type of seizures before 1st operation	Aura>> FIA>> FBTCS	FIA>> FBTCS	Aura>> FIA>> FBTCS	Aura>> FIA	FIA	Aura>> FIA>> FBTCS
MRI findings before 1st operation	Increased hyperintensity in the left mesial temporal lobe structures	Mass lesion in the right temporal region	Mass lesion in the left temporal region	Atrophy and increased hyperintensity in the right mesial temporal lobe structures	Mass lesion in the right temporal region	Atrophy and increased hyperintensity in the left mesial temporal lobe structures
Age at 1st operation (years)	30	16	12	1st: 18 2nd:23	33	39
Side of operation	Left	Right	Left	Right	Right	Left
Type of 1st operation	sAH	GTR+sAH	GTR+sAH	ATL	STR	ATL
Pathology after 1st operation	Cortical dysplasia type 1	Gliosis	Astrocytoma (Grade 1)	HA/S	Non-specific	Glial tissue showing degenerative changes
Outcome after 1st operation. (l-year follow up)	Engel 5	Engel 5	Engel 4	Engel 5	Engel 5	Engel 1
Time of Seizure Recurrence After 1st operation (months)	<1	<1	<2	<6	<6	First seizure: 6th month Recurrent seizures: 30th month
Any change in frequency and type of seizures after 1st operation	No change	No change	No change except all seizures were focal to bilateral tonic clonic seizures	No change	No change	No change
MRI findings before 2nd operation	Remnant tissue on left mesial temporal region	Remnant tissues and encephalomalastic changes in right temporal region	Remnant tissues in left temporal region	Residual tissues in the right mesial temporal region	Residual tissues in the right mesial temporal region	Remnant tissue on left anteromesial temporal region
Concordance of semiology, EEG and MRI before 2nd operation	All	All	All	All	All	All
Age at 2nd operation (years)	41	18	19	30	49	59

Table I: Cont.

	Patient #1	Patient #2	Patient #3	Patient #4	Patient #5	Patient #6
Time to 2nd operation (years)	11	2	7	12	16	20
Type of 2nd operation	ATL	ATL	ATL	ATL	ATL	Resection of remnant tissues seen on MRI
Pathology after 2nd operation	Cortical dysplasia type 1	DNET (grade 1)	Ganglioglioma (grade 2)	HA/S	Mixed glioneuronal tumor	Non-specific gliosis
FU period after 2nd operation (years)	17	17	18	21	10	4
Outcome after 2nd operation (at last FU)	Engel I	Engel I	Engel I	Engel I	Engel I	Engel 1

***F:** Female; **M:** Male; **FS:** Febrile seizure; **TBI:** Traumatic brain injury; **FIA:** Focal impaired awareness; **FBTCS:** Focal to bilateral tonic clonic seizure; **sAH:** Selective amygdalo-hippocampectomy; **GTR:** Gross tumor resection; **STR:** Subtotal tumor resection; **ATL:** Anterior temporal lobectomy; **HA/S:** Hippocampal atrophy/sclerosis; **m:** months; **y:** years.*

semiologically identical to the preoperative seizures arising from the left hemisphere, were recorded during long-term video-EEG monitoring. Remnant tissue in the left mesial temporal region detected on brain MRI (Figure 1A, B) was thought to be responsible for seizure recurrence after the previous surgery. Anterior temporal lobectomy was performed, and the residual tissue in the mesial temporal region was resected at the age of 41 years. The histopathological findings were compatible with cortical dysplasia type 1. After the second surgery, the patient remained seizure-free for 2 years, at which point antiseizure drugs (ASDs) were gradually discontinued during follow-up. The patient has now been seizure-free for 17 years.

Patient #2

This is an 18-year-old male who had FIASs characterized by unresponsiveness, oral automatisms and FBTCS for 6 years. He had intractable seizures despite using multiple anti-seizure drugs. Brain MRI showed a mass lesion in the right temporal region involving the mesial structures. Consequently, the patient underwent right temporal mass resection via stereotactic surgery at the age of 16 years at another hospital. The histopathological findings of the surgical specimen indicated gliosis. After the initial surgery, the seizures continued and the seizure frequency increased by > 100%. Thus, the patient was re-evaluated. In long-term video EEG monitoring, interictal EEG showed focal epileptiform discharges at the right temporal region, and generalized spike-waves. Additionally, three seizures (two FIASs and one FBTCS) with right hemisphere ictal onset were recorded. Remnant tissues and encephalomalacia were detected in the mesial temporal region on brain MRI (Figure 2A). In the second surgery performed two years after the first operation, ATL was combined with gross total tumor resection. (Figure 2B). The specimen was histopathologically identified as a dysembryoplastic neuroepithelial tumor (DNET). In the postoperative follow-up, the patient has remained seizure-free for 17 years.

Patient #3

The third case is that of a 19-year-old female who had been followed with a diagnosis of focal epilepsy for 13 years. She was diagnosed with intractable left MTLE based on the results of presurgical evaluation, so the patient underwent left-sided amygdalohippocampectomy at the age of 12 years at another hospital. After the surgery, the surgical specimen was histopathologically identified as an astrocytoma (grade I). Two months after the initial surgery, she began to experience seizures. Preoperatively, she had FIASs that rarely progressed to bilateral tonic-clonic seizures. However, postoperatively, all seizures evolved into bilateral tonic-clonic seizures. The patient was monitored in the video EEG monitoring unit, where two FBTCSs with left temporal region onset were recorded. Remnant tissue was detected in the mesial temporal region on MRI (Figure 3A). Gross total tumor resection, along with ATL, was performed at our institution (Figure 3B). The histopathological findings were consistent with a grade 2 ganglioglioma. In the postoperative follow-up, the patient has remained seizure-free for 18 years.

Patient #4

The fourth case, which was previously reported, is that of a 30-year-old male with a >10-year history of focal seizures (6). He was diagnosed with HS-related mesial temporal lobe epilepsy based on the video-EEG and brain MRI results. His seizures were resistant to medical treatment; therefore, he underwent surgery first at the age of 18 and second at the age of 23 years for right temporal lobe epilepsy at two different centers. After both surgeries, the patient began experiencing seizures approximately 6 months later. The semiology of the seizures remained unchanged. The patient was re-evaluated for possible surgical treatment. Long-term scalp video-EEG monitoring was not informative regarding the lateralization of the seizures, so invasive monitoring with subdural strip electrodes was performed. During invasive video EEG monitoring,

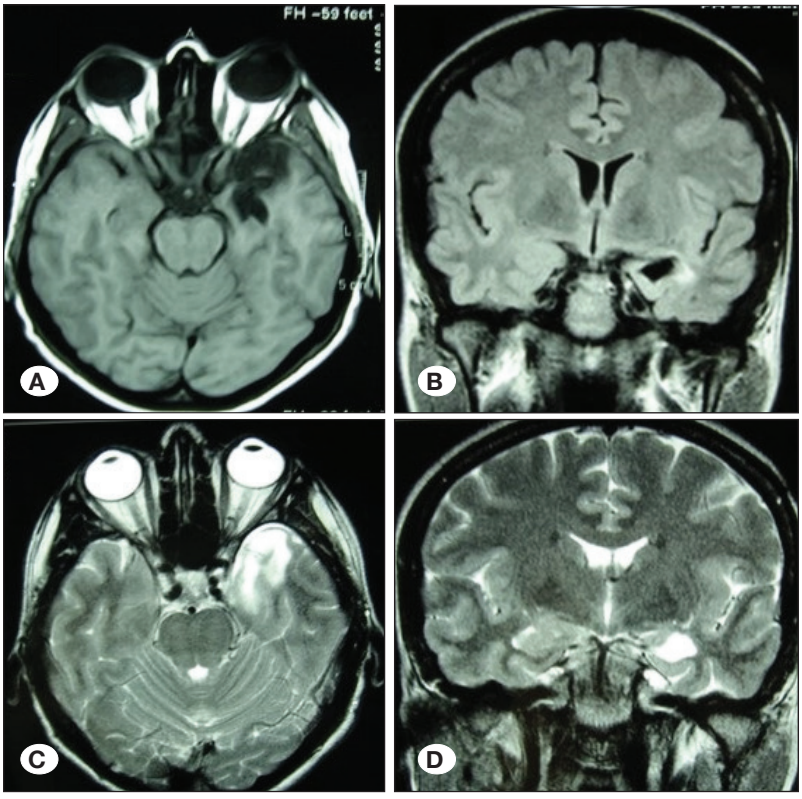

Figure 1: T1 (**A:** axial, **B:** coronal) and T2 (**C:** axial, **D:** coronal)-weighted brain magnetic resonance imagings of patient #1 show remnant tissues in the anteromesial regions of the left temporal lobe after the first surgery.

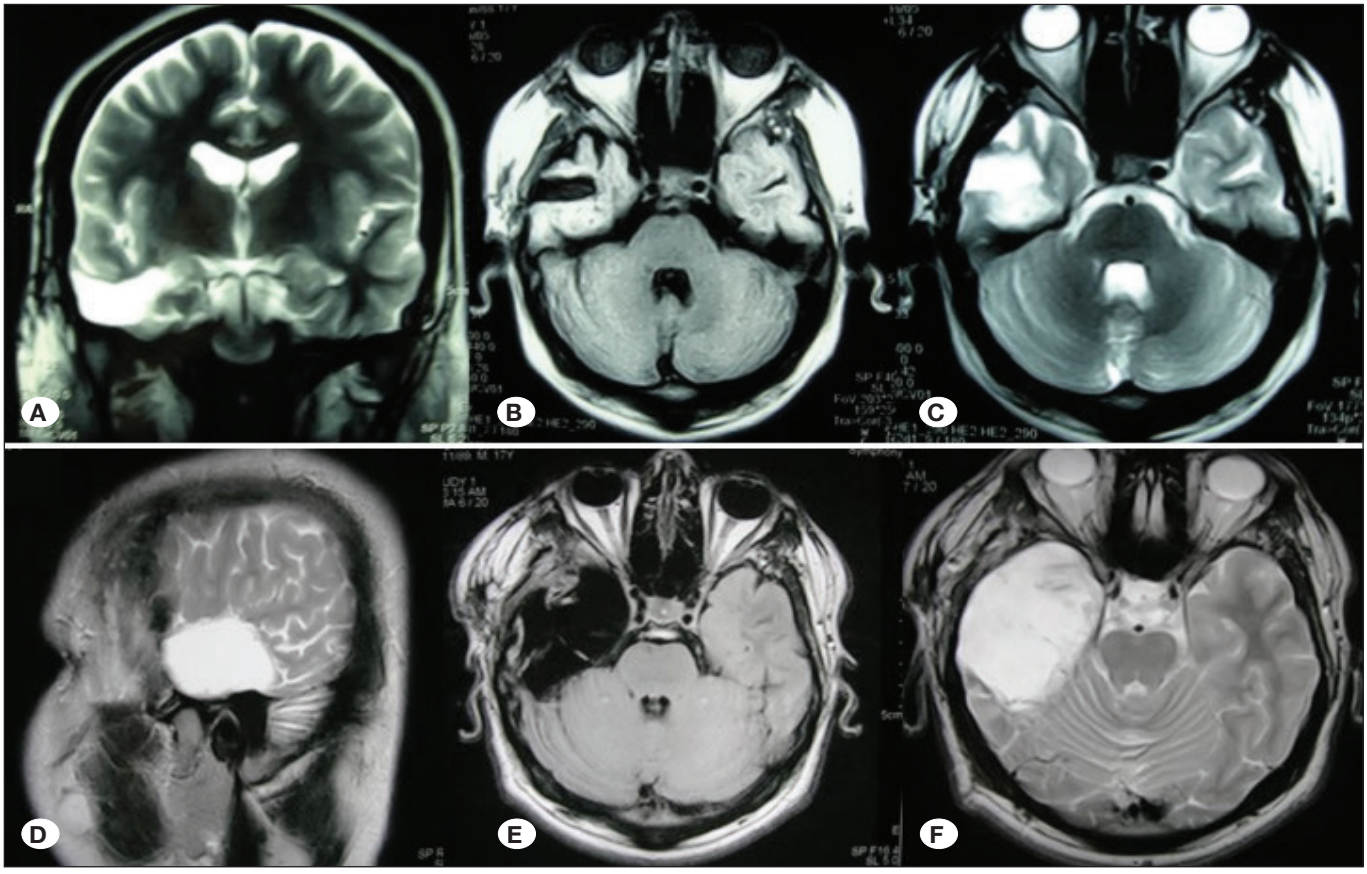

Figure 2: A-C) Preoperative brain magnetic resonance imaging (MRI) sections of patient #2; **D-F)** brain MRIs (**D:** T2W coronal, **E:** T1W axial, **F:** T2W axial) after the second surgical treatment of the patient.

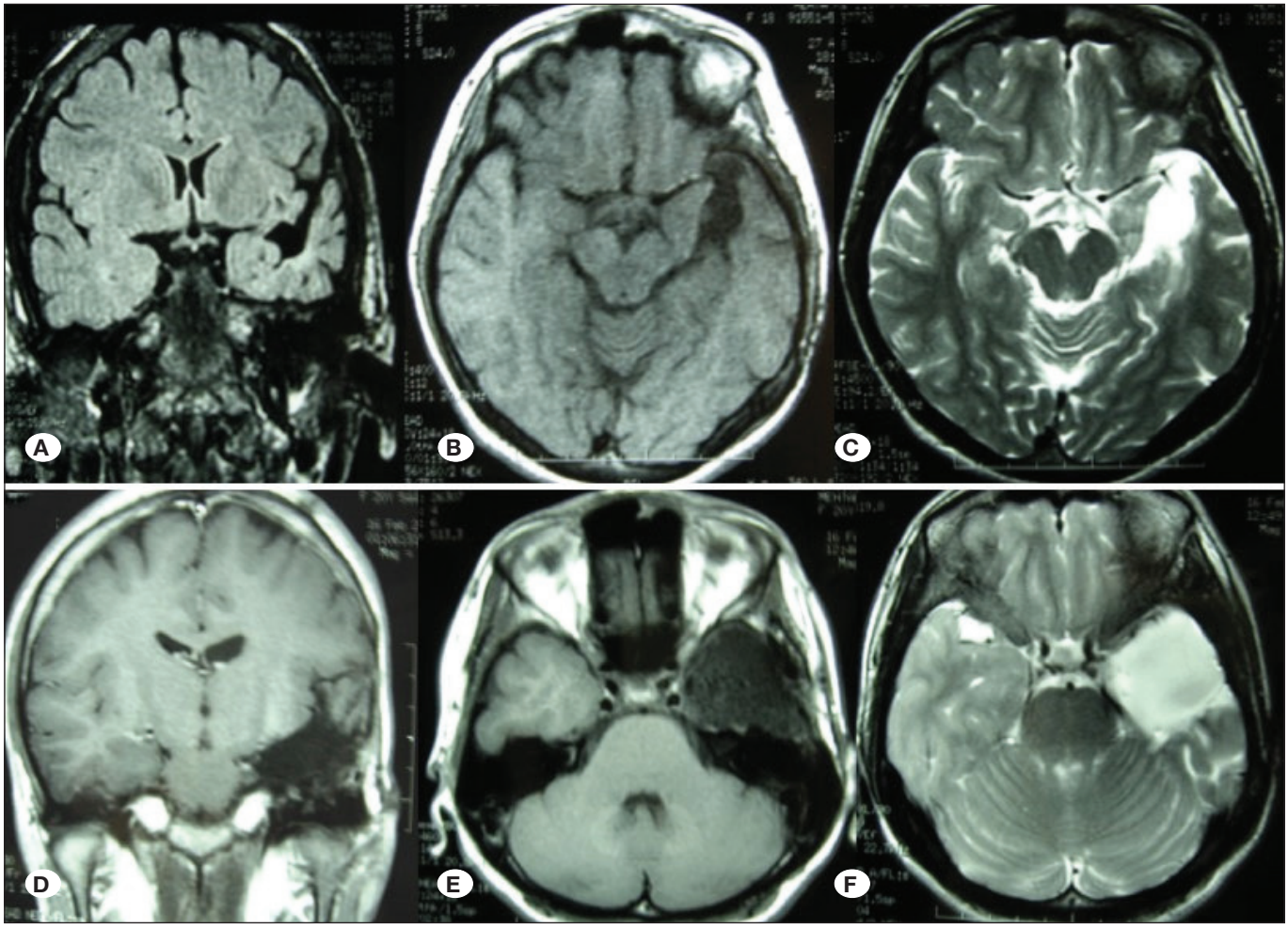

Figure 3: A-C) Preoperative brain magnetic resonance imaging (MRI) sections (**A:** T1W coronal, **B:** T1W axial, **C:** T2W axial) of patient #3; **D-F)** Postoperative MRI sections (**D:** T1W coronal, **E:** T1W axial, **F:** T2W axial) of patient #3.

three FIASs (two with right temporal and one with left temporal onset) were recorded. Remnant tissue was identified in the right temporal region on brain MRI (Figure 4A). After discussing all the risks with the patient, including the possibility of not achieving seizure freedom after an additional surgery, and with the patient's consent, the third surgery was performed. Right ATL, including the resection of the residual tissue in the right mesial temporal region, was performed (Figure 4B). The histopathological findings indicated hippocampal sclerosis. In the postoperative follow-up, the patient has been seizure-free for 21 years.

Patient #5

The fifth case is that of a 49-year-old female with a 22-year history of FIAS. She was diagnosed with right MTLE because of an extensive mass lesion involving the mesial temporal structures seen on MRI (Figure 5A). Therefore, the patient underwent surgery due to intractable seizures at 33 years of age at another hospital. However, in the postoperative period, the patient continued to have frequent seizures, which were semiologically identical to the preoperative seizures. The mass lesion similar to the one seen in the previous MRI was detected in the mesial temporal region (Figure 5A). The patient underwent right ATL with resection of the neoplastic tissue (Figure 5B). The specimen was identified as a low-grade mixed glioneuronal tumor. In the postoperative follow-up, the patient has been seizure-free for 10 years.

Patient #6

The last patient was a 59-year-old male with a history of left MTLE for more than 40 years. He was diagnosed with medically refractory MTLE and evaluated for surgical treatment. Brain MRI findings supported left mesial temporal sclerosis. The interictal and ictal EEG findings also pointed to the left mesial temporal region. Therefore, the patient underwent ATL at the age of 39 years. Six months after the surgery, the patient had his typical seizure once. No change was made to the medical treatment. However, 30 months after the surgery, he started to have recurrent seizures. The frequency of the seizures increased over time, despite adjustments to drug treatments. The seizures were the same as before the first surgery, including the aura. The patient asked for a second surgical treatment if possible. The interictal and ictal EEG findings pointed to the left temporal region. The neuropsychological

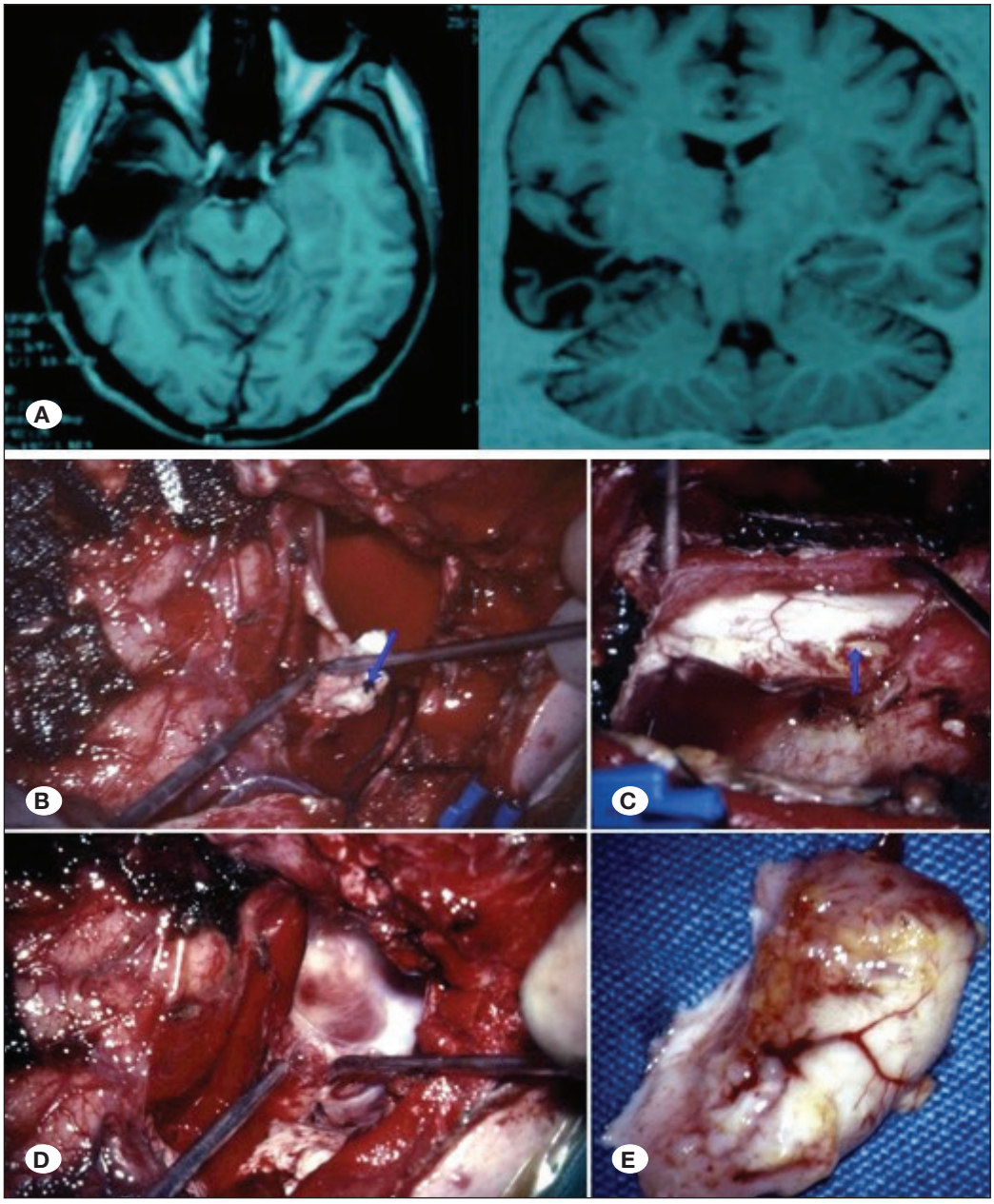

Figure 4: A) Preoperative brain magnetic resonance imaging (MRI) sections (left: T1W axial, right: double inversion recovery coronal) of patient #4; **B-E)** Intraoperative surgical view and remnant tissue (blue arrow) in mesial temporal region **(B, C)**, surgical view of mesial temporal region after resection **(D)**, and hippocampal remnant **(E)**.

tests revealed a mild verbal memory deficit. Remnant tissues were identified in the left temporal region on MRI (Figure 6). The patient underwent a second surgery involving resection of residual structures 4 years ago. He has been seizure-free ever since the second surgery, and the neuropsychological assessment performed at the first-year follow-up showed no changes compared to the preoperative evaluation.

DISCUSSION

The first randomized controlled trial of surgical treatment for epilepsy in 2001 showed the superiority of surgical treatment over optimal medical treatment in patients with refractory TLE (21). However, 20%–30% of medically refractory TLE patients who undergo surgical treatment might continue to have seizures. There may be multiple factors contributing to surgical failure. Najm et al. pointed to the possible relationship between the timing of seizure recurrence and the cause of surgical failure (16). The authors emphasized the importance of distinction between “early” and “late” failures. Various studies, have shown that there is an initial period in which seizure recurrence is common, and the relapse rate is 2%–5% per year for 5 years after TLE surgery (15,16). Therefore, 6–12 postop-

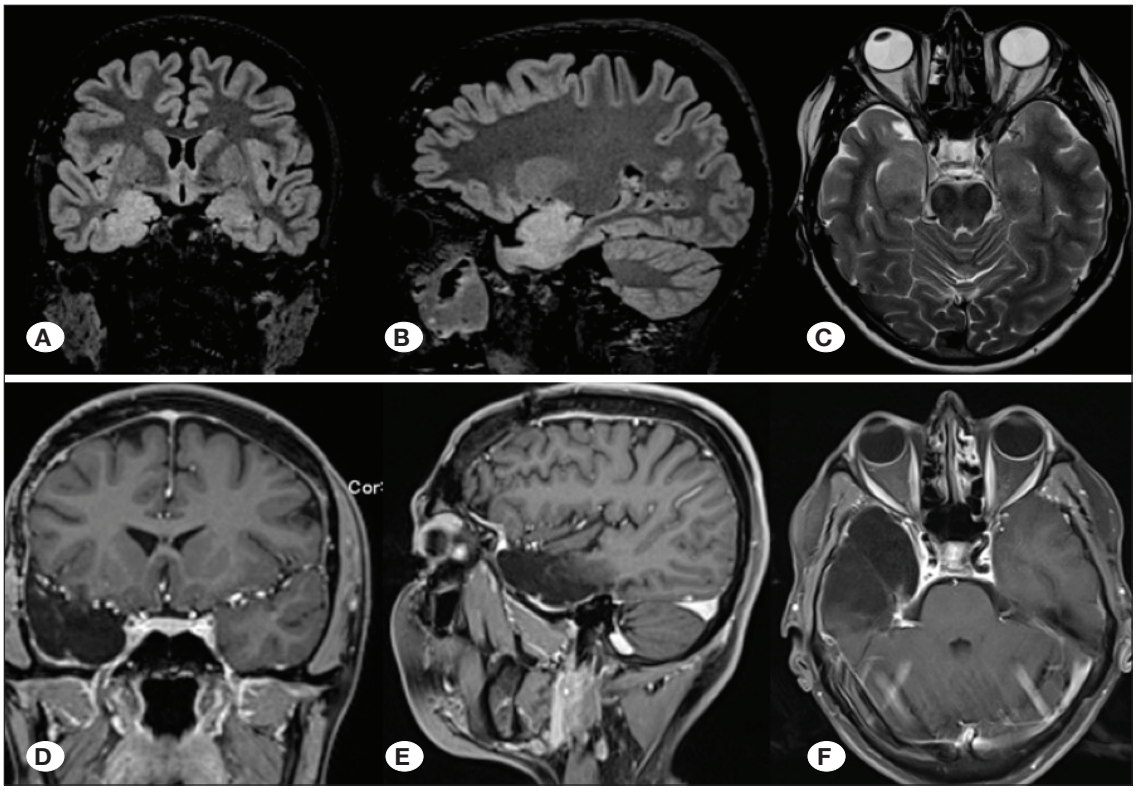

Figure 5: A-C) Preoperative brain magnetic resonance imaging (MRI) sections (**A:** double inversion recovery coronal, **B:** double inversion recovery sagittal, **C:** T2W axial) of patient #5; **D-F)** Postoperative T1-weighted contrast-enhanced MRIs (**D:** coronal, **E:** sagittal, **F:** axial) of patient #5.

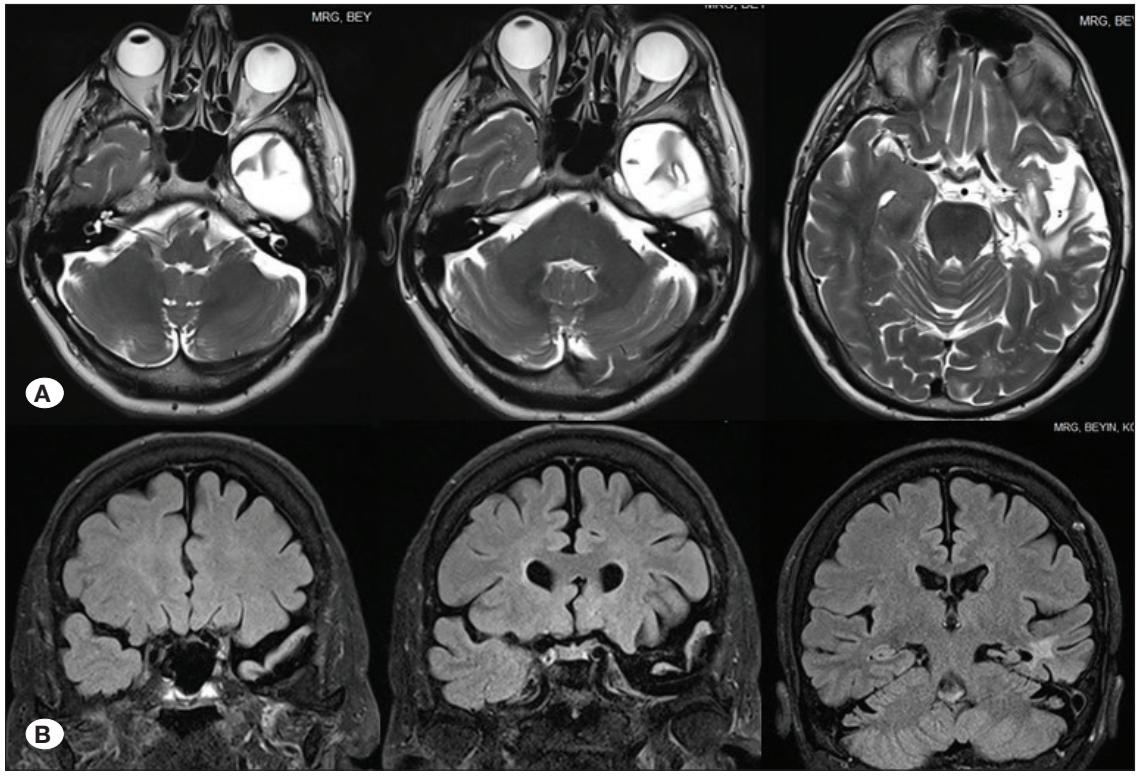

Figure 6: A) Preoperative axial T2-weighted magnetic resonance imaging (MRI) sections of patient #6; **B)** Preoperative T1-weighted coronal MRI sections of patient #6.

erative months are suggested as the cutoff for the distinction between early and late seizure recurrence. For late recurrence, the semiology of recurrent seizures is likely to be different from that of previous seizures, suggesting "new" epilepsy, and they are easier to control with ASDs and have a location contiguous to the resection bed (13,16). The existing clinical and animal data point to "de novo" epileptogenesis as the potential mechanism of late recurrence (16).

Early recurrent seizures are more similar to previous seizures, and are unfortunately more likely to be resistant to medical treatment. The location of recurrence may be distant or contiguous to the resection bed. Thus, the proposed mechanism for early recurrence is mainly incomplete resection, which may be caused by mislocation of the epileptogenic area, multiple epileptogenic lesions, and overlap of the functional cortex with the epileptic focus (16). When examined specifically for TLE surgery, the causes of recurrence include insufficient resection of mesial structures, insufficient resection of the temporal neocortex, dual pathology (coexistence of mesial temporal sclerosis and a neocortical lesion), relapse at the contralateral mesial temporal lobe, and extratemporal or temporal plus epilepsy (10,11,15,16).

In this study, all patients, except one (patient #6), had "early" seizure recurrence within the first 6 months postoperatively.

The recurrent seizures were at least as frequent as those in the preoperative period in our patients and could not be controlled with medical treatment. Patient #6 had a single seizure at 6 months after the first surgery and was seizure-free for about 2 years; however, medically intractable seizures subsequently occurred, and we may need to question the timing of recurrence. The patient's recurrent seizures were identical to the seizures prior to the initial surgery, a finding consistent with all of our patients. Additionally, brain MRI showed remnant tissues in the mesial temporal region, and the interictal and ictal EEG findings were concordant in all our reoperated patients. Therefore, we believe that the reason for surgical failure in our patients was insufficient resection. Indeed, the most common cause of surgical failure in TLE was thought to be insufficient resection (9). Although dual pathology, underlying pathology, and extratemporal epileptogenic zones have recently gained importance among the causes of surgical failure in TLE, inadequate resection is still one of the major causes (11). A recent study analyzed the outcomes of patients who had undergone a second resection surgery for intractable epilepsy (10). Most of the patients (77%) had TLE, and the most common cause of failure was incomplete resection (59%). Freedom from seizures was achieved in 70% of the reoperated patients. One of the most striking results of this study was the neuropsychological outcome after the second surgery. Repeated losses in the same cognitive domain were rare, and if they occurred, improvement was noted with time, likely as a consequence of the successful seizure outcome. Nevertheless, the risk of permanent postoperative neurological deficit should be considered when consulting for reoperation.

We included 240 patients who underwent ATL for medically refractory MTLE at our institution. Of these patients, 12 (5%) had undergone surgery previously on the same side at least once for the same indication. We presented six of the 12 reoperated patients whose data regarding the seizure outcome was available. In all of our patients, the reason for seizure recurrence was insufficient resection, and further resection provided a good seizure outcome. In our observation, patients experiencing frequent seizures tend to accept the risk of a second or even third resection surgery. The age of the patient may not make a difference in this regard. Our oldest patient was 59 years, and this patient requested a second surgery to treat his frequent seizures. Another noteworthy point is the long duration before patients are evaluated for a second surgery after a failed surgical treatment. After seizure recurrence, our patients continued to experience frequent seizures for up to 20 years. The literature highlights the delay in referring patients with medically refractory epilepsy to epilepsy centers for evaluation regarding surgical treatment. Nevertheless, the same situation appears also to apply to patients who experience surgical failure.

In our opinion, the favorable outcome in our patient series is due to the surgical technique and extensive resection adopted (6). The main reason for surgical failure was the remnant tissue specifically in the mesial temporal region in our patients. The anatomy of the mesial temporal region is inherently complex, and neurosurgeons will need to face a more complex anatomy in previously operated patients. Microanatomical knowledge of the region and the surgical technique may determine the clinical outcome (8). Surgical techniques may vary across institutions; for example, in patient #2, stereotactic technology was utilized. We explained the surgical technique, which we apply in detail, in a previous publication, which can be broadly summarized as follows (6):

1. Anterior temporal pole resection is performed while leaving the residual tissue of the superior temporal gyrus medially.
2. Subpial removal of the superior temporal gyrus remnant is performed, and it is used as a guide to reach the inferolateral part of the circular sulcus of the insula.
3. Incision of the circular sulcus is performed just lateral to the M2 segment of the middle cerebral artery and the circular sulcus vein. This incision is extended anteriorly to complete the cutting of the temporal stem and to enter the temporal horn of the lateral ventricle. Moreover, the uncus is removed subpially and posteriorly to gain access to the collateral trigone in order to remove the hippocampal tail.
4. The choroid plexus is reflected upward, and the tenia fimbriae are opened in order to enter the ambient cistern.
5. The uncal sulcus is opened anteriorly, and the hippocampal sulcus is opened posteriorly. The hippocampal feeding arteries and drainage veins are coagulated within these sulci while staying away from the parent vessels.
6. The hippocampal head and body, anterior part of the hippocampal tail, and subiculum remnant are removed.
7. The amygdala is a nuclear complex composed of six different nuclei (lateral, basal, accessory basal, cortical, medial, and central nuclei), and total resection is not possible.

Its medial components are not included in the resection as they are located inferior to the basal ganglia.

The limitations of our study include its single-center and retrospective nature, as well as the small sample size. In addition, the study has the possibility of bias owing to the single center, and the same surgical procedure.

CONCLUSION

Surgical failure remains common among patients with MTLE, with inadequate resection often being the primary cause. However, failure after the initial surgery does not necessarily mark the end of the road for these patients. The opportunity for a second surgical treatment should not be delayed. When given a second chance, many patients may choose to take the risk of reoperation rather than continue living with frequent seizures. This opportunity for seizure freedom can be realized through the expertise and awareness of neurologists and neurosurgeons who manage epilepsy patients.

Declarations

Funding: This research did not receive any specific grant from funding agencies in the public, commercial, or not-for-profit sectors.

Availability of data and materials: The datasets generated and/or analyzed during the current study are available from the corresponding author by reasonable request.

Disclosure: The authors declare no competing interests.

AUTHORSHIP CONTRIBUTION

Study conception and design: SS, AE

Data collection: SE, SS, MZ

Analysis and interpretation of results: SE, SS, MZ, AE

Draft manuscript preparation: SE, SS

Critical revision of the article: SE, SS, AE

Other (study supervision, fundings, materials, etc...): SE, AE

All authors (SE, SS, MZ, AE) reviewed the results and approved the final version of the manuscript.

REFERENCES

1. Awad IA, Nayel MH, Luders H: Second operation after the failure of previous resection for epilepsy. Neurosurgery 28:510-518, 1991. https://doi.org/10.1227/00006123-199104000-00005
2. El Tahry R, Wang IZ: Failed epilepsy surgery: Is this the end? Acta Neurol Belg 117:433-440, 2017. https://doi.org/10.1007/s13760-017-0769-8
3. Engel J Jr: Clinical neurophysiology, neuroimaging, and the surgical treatment of epilepsy. Curr Opin Neurol Neurosurg 6:240-249, 1993. https://doi.org/10.1016/0013-4694(93)90872-S
4. Engel J Jr, McDermott MP, Wiebe S, Langfitt JT, Stern JM, Dewar S, Sperling MR, Gardiner I, Erba G, Fried I, Jacobs M, Vinters HV, Mintzer S, Kieburtz K, Early Randomized Surgical Epilepsy Trial Study G: Early surgical therapy for drug-resistant temporal lobe epilepsy: A randomized trial. JAMA 307:922-930, 2012. https://doi.org/10.1001/jama.2012.220
5. Englot DJ, Lee AT, Tsai C, Halabi C, Barbaro NM, Auguste KI, Garcia PA, Chang EF: Seizure types and frequency in patients who "fail" temporal lobectomy for intractable epilepsy. Neurosurgery 73:838-844, 2013. https://doi.org/10.1227/NEU.0000000000000120
6. Erdem A, Demirciler AK, Solmaz S, Ozgural O, Eroglu U, Wambe A, Tekneci O: Surgical treatment of temporal lobe epilepsy and micro-neuroanatomical details of the medial temporal region. Turk Neurosurg 31:422-431, 2021. https://doi.org/10.5137/1019-5149.JTN.31629-20.2
7. Erdem A, Kahilogullari G, Erbas YC, Karatas A, Bilir E: Reoperation of a recurrent temporal lobe epilepsy: A technical case report. Surg Neurol 64 Suppl 2:S102-105, 2005. https://doi.org/10.1016/j.surneu.2005.07.048
8. Erdem A, Yasargil G, Roth P: Microsurgical anatomy of the hippocampal arteries. J Neurosurg 79:256-265, 1993. https://doi.org/10.3171/jns.1993.79.2.0256
9. Germano IM, Poulin N, Olivier A: Reoperation for recurrent temporal lobe epilepsy. J Neurosurg 81:31-36, 1994. https://doi.org/10.3171/jns.1994.81.1.0031
10. Grote A, Witt JA, Surges R, von Lehe M, Pieper M, Elger CE, Helmstaedter C, Ormond DR, Schramm J, Delev D: A second chance-reoperation in patients with failed surgery for intractable epilepsy: Long-term outcome, neuropsychology and complications. J Neurol Neurosurg Psychiatry 87:379-385, 2016. https://doi.org/10.1136/jnnp-2015-310322
11. Harroud A, Bouthillier A, Weil AG, Nguyen DK: Temporal lobe epilepsy surgery failures: A review. Epilepsy Res Treat 2012:201651, 2012. https://doi.org/10.1155/2012/201651
12. Hennessy MJ, Elwes RD, Binnie CD, Polkey CE: Failed surgery for epilepsy. A study of persistence and recurrence of seizures following temporal resection. Brain 123 Pt 12:2445-2466, 2000. https://doi.org/10.1093/brain/123.12.2445
13. Jehi LE, Silveira DC, Bingaman W, Najm I: Temporal lobe epilepsy surgery failures: Predictors of seizure recurrence, yield of reevaluation, and outcome following reoperation. J Neurosurg 113:1186-1194, 2010. https://doi.org/10.3171/2010.8.JNS10180
14. Jung R, Aull-Watschinger S, Moser D, Czech T, Baumgartner C, Bonelli-Nauer S, Pataraia E: Is reoperation an option for patients with temporal lobe epilepsy after failure of surgery? Seizure 22:502-506, 2013. https://doi.org/10.1016/j.seizure.2012.11.011
15. McIntosh AM, Kalnins RM, Mitchell LA, Fabinyi GC, Briellmann RS, Berkovic SF: Temporal lobectomy: Long-term seizure outcome, late recurrence and risks for seizure recurrence. Brain 127:2018-2030, 2004. https://doi.org/10.1093/brain/awh221
16. Najm I, Jehi L, Palmini A, Gonzalez-Martinez J, Paglioli E, Bingaman W: Temporal patterns and mechanisms of epilepsy surgery failure. Epilepsia 54:772-782, 2013. https://doi.org/10.1111/epi.12152
17. Reed CM, Dewar S, Fried I, Engel J Jr, Eliashiv D: Failed epilepsy surgery deserves a second chance. Clin Neurol Neurosurg 163:110-115, 2017. https://doi.org/10.1016/j.clineuro.2017.10.023

18. Schramm J: Temporal lobe epilepsy surgery and the quest for optimal extent of resection: A review. Epilepsia 49:1296-1307, 2008. https://doi.org/10.1111/j.1528-1167.2008.01604.x
19. Spencer S, Huh L: Outcomes of epilepsy surgery in adults and children. Lancet Neurol 7:525-537, 2008. https://doi.org/10.1016/S1474-4422(08)70109-1
20. Surges R, Elger CE: Reoperation after failed resective epilepsy surgery. Seizure 22:493-501, 2013. https://doi.org/10.1016/j.seizure.2013.04.020
21. Wiebe S, Blume WT, Girvin JP, Eliasziw M, Effectiveness, Efficiency of Surgery for Temporal Lobe Epilepsy Study G: A randomized, controlled trial of surgery for temporal-lobe epilepsy. N Engl J Med 345:311-318, 2001. https://doi.org/10.1056/NEJM200108023450501

Turk Neurosurg 35(4):603-608, 2025
DOI: 10.5137/1019-5149.JTN.47393-24.2

Original Investigation

Pediatrics

Received: 20.08.2024
Accepted: 16.10.2024
Published Online: 25.06.2025

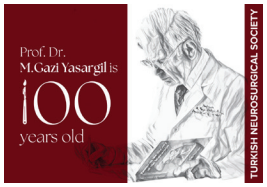

Epilepsy in Children with Myelomeningocele: A Single-Center Retrospective Cohort Study and Review of the Literature

Esra ULGEN TEMEL[1], Deniz MENDERES[2], Ayse SERDAROGLU[3], Ebru ARHAN[3]

[1]Duzce Atatürk State Hospital, Division of Child Neurology, Duzce, Türkiye
[2]University of Health Sciences, Etlik City Training and Research Hospital, Division of Child Neurology, Ankara, Türkiye
[3]Gazi University Faculty of Medicine, Department of Child Neurology, Ankara, Türkiye

This study has been presented as a poster presention at the 6th Spring Pediatrics Days between 10 and 12 March 2022, Adana, Türkiye

Corresponding author: Ebru ARHAN ✉ petekarhan@yahoo.com.tr

ABSTRACT

AIM: To examine the prevalence of epilepsy and other associated cortical abnormalities in patients with Myelomeningocele (MMC), and to present our findings along with a review of the literature.

MATERIAL and METHODS: A retrospective chart review was conducted with MMC patients followed in our pediatric neurology outpatient clinic between 2015 and 2020.

RESULTS: The study included a total of 23 patients ranging in age from 7 months to 19 years with a median follow-up period of 36 months. The frequency of epilepsy was 43.5% (n=10). Hydrocephalus was present in 20 patients (87%) patients, and 18 patients (78.3%) had concomitant central nervous system anomalies. Epilepsy was diagnosed in 52.6% of the patients with a ventriculoperitoneal shunt but none of those without a shunt.

CONCLUSION: Our study revealed a high incidence of epilepsy among patients with MMC, in contrast to the available literature. As the life expectancy of patients with MMC continues to increase, secondary clinical manifestations such as epilepsy may become more evident. Furthermore, most research on the prevalence of epilepsy and seizures among individuals with MMC was conducted approximately two decades ago. Further studies should examine the changing incidence.

KEYWORDS: Myelomeningocele, Epilepsy, Hydrocephalus, Ventriculoperitoneal shunt, Children

INTRODUCTION

Spinal dysraphism is a term used to describe a wide range of anomalies in which the neural, vertebral, and mesenchymal tissues of the spine fail to close to varying degrees. Myelomeningocele (MMC) and myeloschisis are examples of open spinal dysraphisms not covered by skin (9). The incidence of MMC is approximately 1 in 1000 live births. Although the exact mechanism of their formation is unknown, the etiology is believed to be multifactorial, and most cases are sporadic. Possible risk factors include folate metabolism disorders (maternal folate deficiency, *MTFHR* mutation), certain genetic disorders (trisomy 18, Meckel-Gruber syndrome, Lehman syndrome), maternal diabetes, family history, and certain teratogenic agents (valproic acid, carbamazepine, vitamin A) (9,25).

Approximately 85% of patients with MMC have concomitant hydrocephalus. Hydrocephalus may not always be evident at birth, but a shunt is usually required within the first week of life. The prevalence of shunt placement due to hydrocephalus in patients with MMC was reported to be 81% (24). Many factors are involved in the development of hydrocephalus in these patients. The most important of these is Chiari type II malformation (CM-II), which is present in approximately 80% of children with MMC (3,13). CM-II is characterized by cer-

Esra ULGEN TEMEL : 0000-0002-0841-5935
Deniz MENDERES : 0000-0002-0485-0593
Ayse SERDAROGLU : 0000-0002-2180-0213
Ebru ARHAN : 0000-0001-8950-8588

ebellar vermis and herniation of the fourth ventricle through the foramen magnum, brainstem kinking, tectal beaking, and a small posterior cranial fossa. CM-II may also be accompanied by cerebral abnormalities such as polymicrogyria, cortical heterotopia, corpus callosum dysgenesis, and large massa intermedia (17).

Children with MMC may also develop seizures during follow-up, and accompanying cortical abnormalities are implicated as the etiology of seizures in approximately 20% of these children (9). The reported prevalence of seizures in MMC patients is 15-29% for those with shunts and 2-19.5% among those without shunts. The prevalence of epilepsy is approximately 20% (12,18).

In this study, we aimed to investigate the frequency of epilepsy and other concomitant cortical abnormalities in patients with MMC and present our findings with a review of the literature.

MATERIAL and METHODS

A retrospective chart review of all patients diagnosed with MMC between 2015 and 2020 was conducted in the pediatric neurology outpatient clinic of Gazi University Hospital, a tertiary pediatric referral in Ankara. Data extracted from the hospital records included demographic characteristics, brain imaging results, history of epilepsy, and electroencephalogram (EEG) results. Of 27 patients identified retrospectively, 4 were excluded due to missing data (Figure 1). Statistical analyses were performed using SPSS for Windows, version 23.0 software (IBM SPSS Inc., Chicago, IL). Continuous variables were compared using the Mann-Whitney U test and categorical variables were compared using the chi-square or Fisher's exact test depending on the expected values. Results were considered statistically significant at $p<0.05$. Continuous variables were expressed as mean, standard deviation, and range, and categorical variables as number and percentage. The study was conducted in accordance with the Declaration of Helsinki. Ethics committee approval was obtained from the non-interventional clinical research ethics committee of our center (research code number 2024-541).

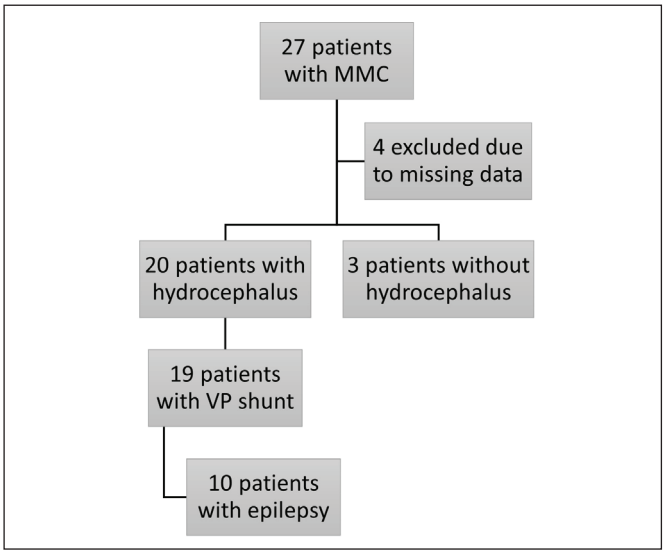

Figure 1: Flowchart of patients with myelomeningocele and epilepsy.

RESULTS

Twenty-three patients ranging in age from 7 months to 19 years (mean, 76.7 ± 71.9 months) met the inclusion criteria. Twelve (52.2%) of these patients were female, and the median follow-up time was 36 months (range, 3-216 months). The prevalence of epilepsy was 43.5% (n=10) overall. Ventriculoperitoneal (VP) shunts were required in all patients with hydrocephalus except one. The patients' data are summarized in Table I.

Central nervous system (CNS) abnormalities other than hydrocephalus included CM-II in 10 patients, corpus callosum agenesis/dysgenesis in 8 patients, periventricular gliosis in 2 patients, and cerebral atrophy in 2 patients. Other concomitant abnormalities were Chiari type I malformation, rhombencephalosynapsis, nodular gray matter heterotopia, interdigitation of the cerebral gyri, frontal encephalomalacia, interhemispheric cyst, and right cerebellar hemisphere hypoplasia.

The EEG results of the patients are presented in Table II. Of 10 patients with epilepsy, 40% were using two or more antiseizure drugs and 70% were using valproic acid as an antiseizure drug, either as polytherapy or monotherapy. Four of our patients with epilepsy required multiple shunt replacements. Two of these patients could be managed with more than one antiseizure medication. Epilepsy was not significantly associated with duration of follow-up or age.

When patients with and without VP shunt were compared in terms of the rates of concomitant CNS abnormalities and epilepsy, we noted that among patients with a shunt, 52.6% (n=10) had epilepsy and 89.5% (n=17) had concomitant CNS abnormalities (Figure 2). Of the patients without shunts, 25% had concomitant CNS abnormalities and none had epilepsy.

CNS abnormalities were significantly more common among patients with shunt and hydrocephalus ($p=0.004$ and $p<0.001$, respectively). All patients with epilepsy had VP shunt and concomitant CNS abnormalities (Figure 2).

Table I: Demographic and Clinical Data of the Patients

Characteristic	Value
Age (months) (mean ±SD)	76.7±71.9 (7-228)
Sex (female), n (%)	12 (52.2)
Follow-up period (months) (mean ±SD)	44.7±44.7 (3-216)
Epilepsy, n (%)	10 (43.5)
Hydrocephalus, n (%)	20 (87)
VP shunt, n (%)	19 (82.6)
Additional CNS abnormality, n (%)	18 (78.3)
Total, n (%)	**23 (100.0)**

***VP:** Ventriculoperitoneal, **CNS:** Central nervous system*

Table II: Electroencephalogram (EEG) Findings of the Patients

EEG Findings	n (%)
Normal	5 (38.5)
Multifocal epileptiform discharges	3 (23.1)
Focal epileptiform discharges	4 (30.8)
Cerebral dysfunction	1 (7.7)

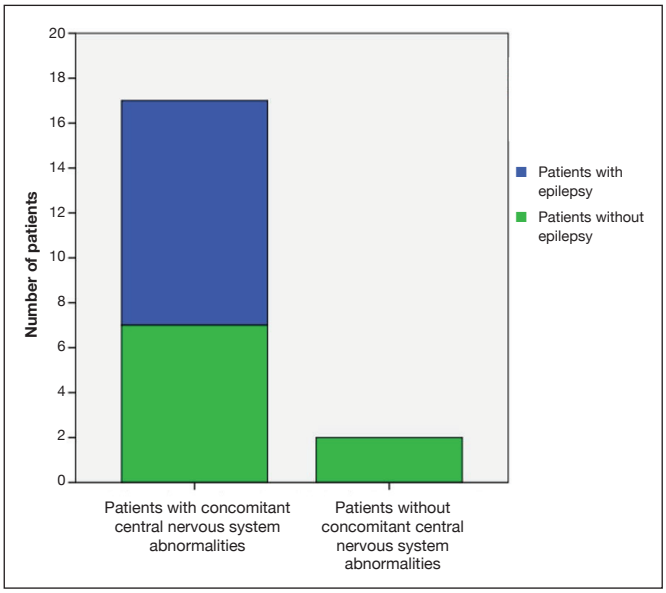

Figure 2: Distribution of shunted patients with and without epilepsy according to the presence of concomitant central nervous system abnormalities.

DISCUSSION

The most common conditions associated with MMC are CM-II and hydrocephalus (13). In previous studies, the frequency of seizures was found to be 17-48.5% in patients with hydrocephalus, regardless of the etiology (15,19). In our study, epilepsy was observed at a rate of 50% in the group with hydrocephalus. The frequency of seizures is higher in conditions associated with structural causes and cases of hydrocephalus that develop as a sequel of bacterial meningitis compared to hydrocephalus associated with MMC (15). The mere existence of a shunt raises the likelihood of seizures in individuals with MMC. This is believed to be related to minor cortical damage caused during the shunt procedures. Seizures may also be triggered by shunt infection or malfunction. Although provoked seizures are more frequently linked to shunt-related disorders, there have been reports suggesting shunt presence may be linked to the development of epilepsy (8,14,15). According to classical knowledge, a seizure provoked by a transient factor that temporarily lowers the seizure threshold in a normal brain does not contribute to a diagnosis of epilepsy (10). However, in a brain exhibiting invasive and structural changes, differentiating a provoked seizure is often challenging. In a recent study, the association of shunt-related provoking factors and epilepsy development was noted, given that preventing shunt malfunctions and infections may result in an improved long-term prognosis for seizure prevention (14).

Compared to the literature, the prevalence of epilepsy in shunted patients (52.6%) and in all patients with MMC (43.5%) was higher in our study. This may be related to the fact that seizures can now be detected more easily and in a shorter time with advances in technology and increased accessibility. Another reason may be that our center is a tertiary referral center and thus receives more complicated cases. Population studies on this subject will help determine more accurate rates. In addition, most studies on the incidence of epilepsy and seizures in patients with MMC were conducted with data collected 2-3 decades ago. Over time, patients with more severe malformations are likely to experience secondary clinical manifestations such as epilepsy more frequently as care improves and life expectancy increases.

The incidence of seizures is low in patients with MMC without VP shunt, whereas seizures and epilepsy are more common in patients with VP shunt (8). In our study, none of the patients without VP shunt were diagnosed with epilepsy. The higher frequency of epilepsy in shunted patients may be the result of adverse effects of the drainage system, such as brain damage created during the procedure, CNS infections, and increased intracranial pressure due to dysfunction (14,21). Four of our patients who were diagnosed with epilepsy required several shunt replacements. In a study conducted on patients with MMC, the overall prevalence of epilepsy was found to be 31%. This rate was 10% in patients who did not require any shunt revision and increased to 58% after one revision and 67% after two or more revisions (21). Studies in the literature (indexed in PubMed) examining the coexistence of MMC with seizures and/or epilepsy are summarized in Table III.

It is believed that in MMC patients with epilepsy, the VP shunt could not be the sole causative factor, and concomitant CNS abnormalities are also involved in epileptogenesis (14,27,30). In our study, 9 of 10 patients with epilepsy underwent cranial imaging (CT/MRI). Of those, 7 had CM-II, 3 had corpus callosum agenesis/dysgenesis, 2 had encephalomalacia/gliosis, and cerebral atrophy, interhemispheric cyst, and rhombencephalosynapsis were each detected in 1 patient. As seen in our study, not all CNS defects in MMC patients are epilepsy-related. It is clear that epilepsy in these children has a multifactorial etiology, with no single cause.

Current studies showing that the incidence of MMC has decreased over time (7,20). This may be largely due to greater awareness of modifiable causes, which resulted in increased use of folic acid during pregnancy and careful antenatal follow-up of mothers using antiseizure drugs. In addition, the life expectancy of these patients is longer due to early intervention and good care. In one study comparing MMC patients born in the periods of 1971-1981 and 1996-2006, the incidence of MMC was found to be 2.5 in 10,000 births vs. 1.1 in 10,000 births, respectively. However, one of the most striking findings reported in the study was the mortality rates, which were found to be 18% and 0%, respectively. No differenc-

Table III: Studies Evaluating the Coexistence of Epilepsy and/or Seizures in Patients with Myelomeningocele

Article Author, year	MMC (n)	Hydrocephalus (n)	VP shunt (n)	CNS malformations or disorders (n)	Seizures (n)	Epilepsy (n)
Noetzel and Blake, 1991 (18)	140	109	109	6	24 (5 with CNS malformation, 18 shunted)	N/A
Danzer et al., 2010 (8)	48	N/A	24	N/A	8 (6 shunted)	3 (shunted)
Amaral et al., 2019 (1)	15	N/A	13	N/A	6	N/A
Klepper et al., 1998 (16)	44	44	N/A	N/A	N/A	4
Spazzapan and Velnar, 2021(26)	20	N/A	13	N/A	4	N/A
Bartoshesky et al., 1985 (2)	111	106	98	14 (shunted)	25 (24 shunted)	N/A
Talwar et al., 1995 (27)	81	66	66	63	17	14 (12 with CNS pathology)
Okurowska-Zawada et al., 2007 (21)	86	70	49	N/A	N/A	27
Bowman et al., 2001 (4)	71	N/A	61	N/A	16 (all shunted)	N/A
Brown et al., 2008 (5)	35	N/A	31	18	31	N/A
Wasserman and Holmbeck, 2016 (29)	95	N/A	79	N/A	13	N/A
Chadduck and Adametz, 1988 (6)	190	N/A	144	N/A	33 (32 shunted)	N/A
Hack et al., 1990 (11)	346	346	346	N/A	51	N/A
Karakas et al., 2022 (14)	122	108	98	57 (cerebellar malformation)	24	15
Yoshida et al., 2006 (30)	6	N/A	N/A	5	N/A	0
Tully et al., 2016 (28)	78	78	67	78	N/A	5
Persson et al., 2005 (23)	84	84	N/A	N/A	N/A	8
Persson et al., 2006 (22)	44	44	N/A	N/A	N/A	5

MMC: *Myelomeningocele,* ***CNS:*** *Central nervous system,* ***N/A:*** *Not available*

es were observed in terms of hydrocephalus or CM-II (20). In our study of patients from the years 2015-2020, the proportions of patients with hydrocephalus, CNS malformations, and VP shunt were similar to those in the literature (87%, 78.3%, and 82.6%, respectively). However, the prevalence of epilepsy was higher in our patients than the literature. We attribute this to the above-mentioned fact that data on the incidence of epilepsy are generally 2-3 decades old, and the decrease in mortality is associated with an increase in the incidence of controllable morbidities such as epilepsy. Early intervention reduces early complications. Furthermore, longer life expectancy in these patients may increase complications such as VP shunt dysfunction and infections, which subsequently trigger the development of seizures and epilepsy. One of the most recent studies examining seizures in MMC included patients between 1975 and 2013. In that study, seizures were observed in 19.7% of the patients (14). However, the study covered a period of approximately 40 years, without grouping by decade. New studies examining the relationship between MMC and epilepsy according to current data are needed.

Our study has several limitations. The first is that as a single-center study, it may not reflect the actual numbers in the population. Secondly, as our center is a tertiary hospital, patients with mild findings are less likely to present. Thirdly, studies in which MRI imaging and EEG traces are available and can be evaluated together for all patients may have provided clearer results. As patients have easier access to pediatric neurologists in recent years, conducting a comprehensive study that includes MRI and EEG results as well as provoked seizures and epilepsy subgroups will yield more accurate data on this subject.

CONCLUSION

Epilepsy is less common in patients with MMC compared to other causes of hydrocephalus. Morbidity rates in these patients are likely increasing due to prolonged life expectancy resulting from medical advances. Epilepsy is one of these morbidities, and we hypothesize that the incidence of the disorder may rise as a result of potential complications caused by VP shunts. While our findings are consistent with this hypothesis, more precise results can be obtained from population-based research.

Declarations

Funding: This research did not receive any specific grant from funding agencies in the public, commercial, or not-for-profit sectors.

Availability of data and materials: The datasets generated and/or analyzed during the current study are available from the corresponding author by reasonable request.

Disclosure: The authors declare no competing interests.

AUTHORSHIP CONTRIBUTION

Study conception and design: EA, EUT

Data collection: EUT, DM

Analysis and interpretation of results: DM, EUT

Draft manuscript preparation: EUT, EA

Critical revision of the article: EA, AS

Other (study supervision, fundings, materials, etc...): AS, EA

All authors (EUT, DM, AS, EA) reviewed the results and approved the final version of the manuscript.

REFERENCES

1. Amaral C, Nardeli CS, Saito IC, Valerio JS, Filho M, Straioto FG: Myelomeningocele: Medical considerations and stomatologic aspects in the dental treatment. J Craniofac Surg 30:2517-2519, 2019. https://doi.org/10.1097/SCS.0000000000005973
2. Bartoshesky LE, Haller J, Scott RM, Wojick C: Seizures in children with meningomyelocele. Am J Dis Child 139:400-402, 1985. https://doi.org/10.1001/archpedi.1985.02140060082035
3. Beuriat PA, Szathmari A, Rousselle C, Sabatier I, Di Rocco F, Mottolese C: Complete reversibility of the chiari type II malformation after postnatal repair of myelomeningocele. World Neurosurg 108:62-68, 2017. https://doi.org/10.1016/j.wneu.2017.08.152
4. Bowman RM, McLone DG, Grant JA, Tomita T, Ito JA: Spina bifida outcome: A 25-year prospective. Pediatr Neurosurg 34:114-120, 2001. https://doi.org/10.1159/000056005
5. Brown TM, Ris MD, Beebe D, Ammerman RT, Oppenheimer SG, Yeates KO, Enrile BG: Factors of biological risk and reserve associated with executive behaviors in children and adolescents with spina bifida myelomeningocele. Child Neuropsychol 14:118-134, 2008. https://doi.org/10.1080/09297040601147605
6. Chadduck W, Adametz J: Incidence of seizures in patients with myelomeningocele: A multifactorial analysis. Surg Neurol 30:281-285, 1988. https://doi.org/10.1016/0090-3019(88)90300-x
7. Clemmensen D, Thygesen M, Rasmussen MM, Fenger-Gron M, Petersen OB, Mosdal C: Decreased incidence of myelomeningocele at birth: Effect of folic acid recommendations or prenatal diagnostics? Childs Nerv Syst 27:1951-1955, 2011. https://doi.org/10.1007/s00381-011-1473-2
8. Danzer E, Finkel R, Gerdes M, Schwartz EM, Rintoul NN, Adzick NS, Johnson MP: The relationship of seizure activity and chronic epilepsy in early infancy and short-term neurodevelopmental outcome following fetal myelomeningocele closure. Neuropediatrics 41:140-143, 2010. https://doi.org/10.1055/s-0030-1263164
9. Du Plessis AJ, Johnston MV: Fetal and neonatal neurology. In: Arzimanoglou A, O'Hare A, Johnston MV, Ouvrier R, (eds), Clinics in Developmental Medicine Aicardi's Diseases of the Nervous System in Childhood, 4th ed, Mac Keith Press 2018:8-9. https://doi.org/10.1111/dmcn.14344
10. Fisher RS, Acevedo C, Arzimanoglou A, Bogacz A, Cross JH, Elger CE, Engel J Jr, Forsgren L, French JA, Glynn M, Hesdorffer DC, Lee BI, Mathern GW, Moshe SL, Perucca E, Scheffer IE, Tomson T, Watanabe M, Wiebe S: ILAE official report: A practical clinical definition of epilepsy. Epilepsia 55:475-482, 2014. https://doi.org/ 10.1111/epi.12550
11. Hack CH, Enrile BG, Donat JF, Kosnik E: Seizures in relation to shunt dysfunction in children with meningomyelocele. J Pediatr 116:57-60, 1990. https://doi.org/10.1016/s0022-3476(05)81645-2
12. Isik U: Seizures in children with myelomeningocele. In: Ozek MM, Cinalli G, Maixner WJ, (eds), The Spina Bifida: Management and Outcome. Springer Milan Milano, 2008:297-301. https://doi.org/10.1007/978-88-470-0651-5_25
13. Januschek E, Rohrig A, Kunze S, Fremerey C, Wiebe B, Messing-Junger M: Myelomeningocele - a single institute analysis of the years 2007 to 2015. Childs Nerv Syst 32:1281-1287, 2016. https://doi.org/10.1007/s00381-016-3079-1
14. Karakas C, Fidan E, Arya K, Webber T, Cracco JB: Frequency, predictors, and outcome of seizures in patients with myelomeningocele: Single-center retrospective cohort study. J Child Neurol 37:80-88, 2022. https://doi.org/10.1177/08830738211053132
15. Keene DL, Ventureyra EC: Hydrocephalus and epileptic seizures. Childs Nerv Syst 15:158-162, 1999. https://doi.org/10.1007/s003810050359
16. Klepper J, Busse M, Strassburg HM, Sorensen N: Epilepsy in shunt-treated hydrocephalus. Dev Med Child Neurol 40:731-736, 1998. https://doi.org/10.1111/j.1469-8749.1998.tb12340.x
17. McLone DG, Dias MS: The Chiari II malformation: Cause and impact. Childs Nerv Syst 19:540-550, 2003. https://doi.org/10.1007/s00381-003-0792-3
18. Noetzel MJ, Blake JN: Prognosis for seizure control and remission in children with myelomeningocele. Dev Med Child Neurol 33:803-810, 1991. https://doi.org/10.1111/j.1469-8749.1991.tb14964.x
19. Noetzel MJ, Blake JN: Seizures in children with congenital hydrocephalus: Long-term outcome. Neurology 42:1277-1281, 1992. https://doi.org/10.1212/wnl.42.7.1277

20. North T, Cheong A, Steinbok P, Radic JA: Trends in incidence and long-term outcomes of myelomeningocele in British Columbia. Childs Nerv Syst 34:717-724, 2018. https://doi.org/10.1007/s00381-017-3685-6
21. Okurowska-Zawada B, Sobaniec W, Kulak W, Smigielska-Kuzia J, Paszko-Patej G, Sienkiewicz D, Sendrowski K: Clinical-electroencephalographic analysis of brain bioelectrical activity in children with myelomeningocele and internal hydrocephalus. Adv Med Sci 52 Suppl 1:200-203, 2007.
22. Persson EK, Hagberg G, Uvebrant P: Disabilities in children with hydrocephalus--a population-based study of children aged between four and twelve years. Neuropediatrics 37:330-336, 2006. https://doi.org/10.1055/s-2007-964868
23. Persson EK, Hagberg G, Uvebrant P: Hydrocephalus prevalence and outcome in a population-based cohort of children born in 1989-1998. Acta Paediatr 94:726-732, 2005. https://doi.org/10.1111/j.1651-2227.2005.tb01972.x
24. Rintoul NE, Sutton LN, Hubbard AM, Cohen B, Melchionni J, Pasquariello PS, Adzick NS: A new look at myelomeningoceles: Functional level, vertebral level, shunting, and the implications for fetal intervention. Pediatrics 109:409-413, 2002. https://doi.org/10.1542/peds.109.3.409
25. Shaer CM, Chescheir N, Schulkin J: Myelomeningocele: A review of the epidemiology, genetics, risk factors for conception, prenatal diagnosis, and prognosis for affected individuals. Obstet Gynecol Surv 62:471-479, 2007. https://doi.org/10.1097/01.ogx.0000268628.82123.90
26. Spazzapan P, Velnar T: Myelomeningocele in Slovenia: Results of a 10-year follow-up. J Neurosurg Sci 65:369-376, 2021. https://doi.org/10.23736/S0390-5616.18.04481-8
27. Talwar D, Baldwin MA, Horbatt CI: Epilepsy in children with meningomyelocele. Pediatr Neurol 13:29-32, 1995. https://doi.org/10.1016/0887-8994(95)00088-w
28. Tully HM, Ishak GE, Rue TC, Dempsey JC, Browd SR, Millen KJ, Doherty D, Dobyns WB: Two hundred thirty-six children with developmental hydrocephalus: Causes and clinical consequences. J Child Neurol 31:309-320, 2016. https://doi.org/10.1177/0883073815592222
29. Wasserman RM, Holmbeck GN: Profiles of neuropsychological functioning in children and adolescents with spina bifida: Associations with biopsychosocial predictors and functional outcomes. J Int Neuropsychol Soc 22:804-815, 2016. https://doi.org/10.1017/S1355617716000680
30. Yoshida F, Morioka T, Hashiguchi K, Kawamura T, Miyagi Y, Nagata S, Mihara F, Ohshio M, Sasaki T: Epilepsy in patients with spina bifida in the lumbosacral region. Neurosurg Rev 29:327-332; discussion 332, 2006. https://doi.org/10.1007/s10143-006-0035-7

Turk Neurosurg 35(4):609-617, 2025
DOI: 10.5137/1019-5149.JTN.46559-24.4

Original Investigation

Pediatrics

Received: 03.03.2024
Accepted: 13.09.2024
Published Online: 25.06.2025

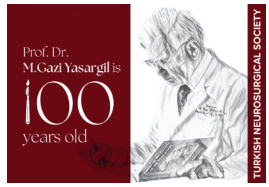

Neurosurgical Management and Follow-up of Pediatric Lumbosacral Lipomas: A Single-Center Experience with 28 Patients

Efecan CEKIC[1], Can KIVRAK[2], Adnan DAGCINAR[2]

[1]Polatli Duatepe State Hospital, Department of Neurosurgery, Ankara, Türkiye
[2]Marmara University, Faculty of Medicine, Department of Neurosurgery, Istanbul, Türkiye

This study has been presented at the Turkish Neurosurgical Society 36th Scientific Congress between 27 and 30 April, 2023 in Antalya, Türkiye

Corresponding author: Efecan CEKIC ✉ drefecancekic@gmail.com

ABSTRACT

AIM: To evaluate the efficacy of surgical interventions for pediatric lumbosacral lipomas (LSL) by focusing on preoperative symptoms, postoperative outcomes, and long-term prognosis.

MATERIAL and METHODS: The medical records and magnetic resonance images (MRI) of 28 pediatric patients (15 boys and 13 girls aged 1–17 years) who underwent LSL resection between 2018 and 2023 were retrospectively reviewed. The study assessed surgical indications, techniques (including using neuromonitoring and the extent of lipoma resection), and postoperative management. The LSLs were classified based on their location and relationship with the spinal cord, which informed the surgical approaches and prognostic predictions. Outcome measures included neurological function, as assessed by the Hoffmann grading system, and complications such as wound dehiscence and cerebrospinal fluid leakage.

RESULTS: The dorsal LSLs demonstrated a 62.5% total resection rate with 37.5% symptomatic improvement after surgery. The caudal LSLs demonstrated a lower total resection rate (46.15%), with 30.77% of the patients experiencing symptom worsening. Transitional LSLs demonstrated a 100% positive outcome after total resection. Chaotic LSLs, the most complex LSL, had a postoperative deterioration rate of 40% after subtotal resection. Overall, surgical complications were noted in 17.8% of the patients.

CONCLUSION: Surgical management of symptomatic pediatric patients with LSL yields significant benefits, with a careful balance between radical resection and preservation of neurological function. The type of lipoma significantly influences surgical planning and outcomes. Despite challenges in achieving complete resection in chaotic LSLs, tailored surgical approaches based on preoperative imaging and lipoma classification can optimize patient outcomes.

KEYWORDS: Lipomyelomeningocele, Spinal dysraphism, Neurogenic bladder, Lumbosacral lipoma

ABBREVIATIONS: LSL: Lumbosacral lipomas, **CUSA:** Cavitron ultrasonic surgical aspirator, **MRI:** Magnetic resonance imaging, **CIC:** Clean intermittent catheterization, **PFS:** Progression-free survival, **IVS:** Interactive virtual simulation, **SNS:** Split notochord syndrome, **TFTS:** Tight filum terminale syndrome, **CISS:** Constructive interference in steady state, **CSF:** Cerebrospinal fluid

INTRODUCTION

Lumbosacral lipomas (LSL) are congenital lesions of the conus medullaris and filum terminale. One of the most prevalent types of occult spinal dysraphism (spina bifida occulta) is LSL (11). The LSL (except filar lipomas) is believed to develop from the early disjunction of the neural tube from the surrounding ectoderm, resulting in a patent posterior opening of the neural plate and infiltration of mesodermal tissues, including fatty tissue and less frequently osteochondral tissues (17,24,35).

Efecan CEKIC : 0000-0003-2203-5944 Can KIVRAK : 0000-0001-6008-1285 Adnan DAGCINAR : 0000-0001-9532-7820

Although adipose tissue is a common cause of tethered cord syndrome, it is unclear whether the underlying pathology of spinal cord dysfunction is due to developmental dysplasia, growth-induced mechanical traction, or both. Tethered cord syndrome caused by LSL may cause progressive neurological deficits such as sensorimotor complications, urinary symptoms, foot deformities (14), neuropathic ulcers, neurogenic bladder (secondary renal failure), and pain (17). LSLs are believed to be associated with tethered roots, filum, and cord, and untethering these structures may prevent deterioration.

LSL can be classified into dorsal, transitional, caudal, filar, and chaotic types (2) according to the lipoma location and involvement of the cord and caudal roots. The classification is closely related to the surgical procedure chosen, residual volume, postoperative outcome, and prognosis (2,29,30,31). The criteria for surgical intervention and the most effective surgical approach for intradural spinal lipomas remain debatable (5,22).

This study aimed to present the preoperative symptoms, postoperative outcomes, and prognosis of patients with LSL, as well as the surgical technical nuances and clinical decision-making regarding lipoma type. This comprehensive analysis was performed to enhance our understanding of LSL and contribute to developing effective surgical strategies for patients with this condition.

MATERIAL and METHODS

The Institutional Review Board approved our retrospective study (No: 09.2023.900; date: 14.07.2023). Following established guidelines, all patients gave informed consent for the surgical procedures.

Patient Population and Outcome Analysis

The authors retrospectively analyzed the medical records and MRI images of pediatric patients with LSLs. From 2018 to 2023, we surgically treated 28 pediatric patients (15 boys and 13 girls). The patients' ages ranged from 1 to 17 (average, 7.1 years). The average follow-up period was one year.

The preoperative evaluations performed were neurological examination, electrophysiological studies (sensorimotor evoked potential), and urologic evaluation, including ultrasonography of the kidney and bladder, voiding cystourethrography, and urodynamic study. A lumbosacral MRI was obtained to diagnose and classify the lipoma and determine a surgical plan (Figure 1). Intraoperative neuromonitoring was performed in all the patients. A postoperative MRI was obtained to confirm that a radical excision was performed.

Dorsal and transitional LSLs were classified according to Chapman's classification, and chaotic and caudal LSLs were classified according to Arai and Pang's classification (2,6,29,30).

The indications for surgery were as follows: (i) new or progressive neurological symptoms, including sensorimotor deficits, difficulty in voiding, and/or defecation problems; (ii) aggravation of foot deformities and walking problems; (iii) development of syringes or its aggravation during follow-up; and (iv) pain.

Patients with a LSL may have intact neurology or various neurological symptoms and deficits. These symptoms include pain, changes in reflexes, sensorimotor loss, foot deformities, and urinary and sphincter issues. Hoffmann described a functional grading scheme in this study to assess treatment results (16).

If the patient complained of new symptoms or symptom progression and exhibited worsening of electrophysiological and urodynamic study results, the patient was considered to have deteriorated.

The following parameters were analyzed to determine their effect on surgical outcomes: sex, age, abnormalities on preoperative evaluation, lipoma type, presence of preoperative syrinx, amount of lipoma resected, pial reconstruction, and duraplasty.

We excluded individuals with incomplete medical records or insufficient follow-up data, essential for a comprehensive assessment of the condition's natural history and surgical outcomes.

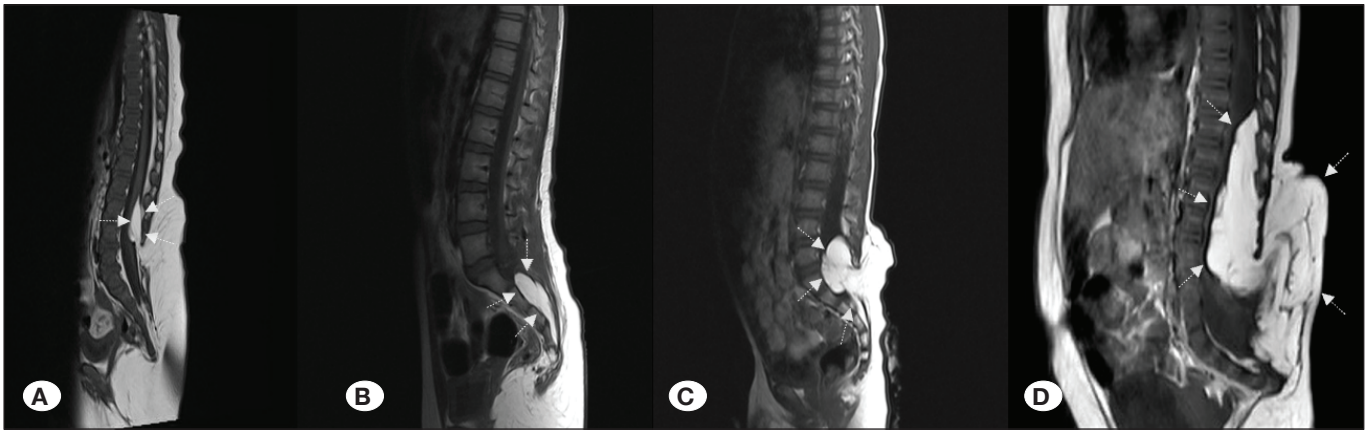

Figure 1: Lumbosacral lipoma classification using a T1-sequence magnetic resonance image. **A)** Dorsal, **B)** caudal, **C)** transitional, and **D)** chaotic.

Surgical Treatment

The authors performed untethering and total/near-total resectioning of all lipomas except chaotic ones. An ultrasonic aspirator and neuromonitoring were performed in all the patients. The skin and soft tissue were incised as one up to the subcutaneous lipoma. Frequently, lipoma removal reveals a fatty stalk connecting the subcutaneous tissue with the intraspinal lipoma via a defect in the lumbodorsal fascia or a spina bifida.

If possible, one level above the cranial end and one below the caudal end of the lipoma were exposed to ensure proper orientation. When required, a laminotomy or laminectomy was performed to access the lateral edges of the dural sac. Visualization of the normal dura rostrally and caudally allowed us to understand the anatomy of the malformation. After that, the bulk of the extradural fat was safely removed. Under microscopic magnification and illumination, the dura was opened in the midline, approximately 1 cm rostral to the lipoma. The midline incision was deepened up to the cord and lipoma adhesion level. The dura was separated just lateral to the cord, and the lipoma's adhered portions were circumferentially released with careful inspection of the roots. The free dural edge on each side was retracted with sutures to expose the cord and roots at the deepest lipoma's deepest edge. The point of fusion of the pia, spinal cord, and lipoma was identified. The roots were exposed at their exit point from the spinal cord, and microscissors were used to separate the fat cord from the root. After the lipoma was excised, the cord was shaped into a tubular form with intermittent 6/0 sutures under neuromonitoring. Subsequently, a wide duraplasty was performed to prevent retethering. In some patients, a cavitron ultrasonic surgical aspirator (CUSA) was used to shrink the lipoma tissue.

Electrophysiological determinations in chaotic lipomas are crucial to differentiate normal tissue from lipoma. Roots embedded in fat tissue may not be identified in any other way. The white plane on the dorsal side of a chaotic lipoma was handled the same way as other lipomas. However, the billows of fat on the ventral side of the placode were left alone because the dorsal part of the lipoma, unless iatrogenically invaded, is tethered to the spinal cord(28). After resection of the chaotic lipoma, the dura was closed, and a wide duraplasty was performed.

RESULTS

The medical records and MRI images of 28 pediatric patients (15 boys and 13 girls, age range 1–17 years) who underwent surgery for LSL between 2018 and 2023 were retrospectively analyzed. Among the 28 LSLs, 8 (28.5%) were dorsal, 13 (46.4%) were caudal, 2 (7.1%) were transitional, and 5 (17.8%) were chaotic (Table I).

We found distinct outcome patterns across the LSL subtypes (Table II). Among the eight treated patients with dorsal LSL, five achieved total resection (62.5%). Near-total resection was achieved in one patient, and subtotal resection was achieved in two patients. Three of the eight patients (37.5%) postoperatively exhibited symptomatic improvement. The remaining five

Table I: Comparison of LSL Types According to Resection

LSL Type	Subtotal Resection	Near- Total Resection	Total Resection	Total Patient
Dorsal Type	2	1	5	8
Caudal Type	7	0	6	13
Transitional Type	0	0	2	2
Chaotic Type	5	0	0	5

LSL: *Lumbosacral lipoma.*

Table II: Comparison of LSL Types According to Changing Neurological Symptoms Before and After Surgery

LSL Type	Worsened compared to the preoperative	Same compared to the preoperative	Better compared to the preoperative	Total resection (%)
Dorsal Type	0	5 (2 of them have no symptoms preoperatively.)	3	75.0
Caudal Type	4	4 (2 of them have no symptoms preoperatively.)	5	46.0
Transitional Type	0	1(have no symptoms preoperatively.)	1	100.0
Chaotic Type	2	3	0	0.0

LSL: *Lumbosacral lipoma.*

patients (62.5%), including two asymptomatic patients before surgery, experienced no change in neurological status.

The caudal LSL group consisted of 13 patients. Among these, total resection was achieved in six patients, and subtotal resection was achieved in seven patients. Postoperatively, four patients (30.77%) experienced worsening of symptoms, and five patients demonstrated improvement (30.77%). The condition of four patients, including two patients who were asymptomatic preoperatively, remained unchanged.

Total resection was achieved in patients with transitional LSL. Both patients demonstrated positive outcomes, with one patient improving symptoms and the other maintaining their preoperative asymptomatic status.

The chaotic LSL was the most challenging to treat, with subtotal resection being achieved on all five patients due to the condition's inherent complexity. Postoperatively, two patients (40%) experienced a decline in their condition, while three patients did not experience a significant change in their symptoms.

Among all the patients who worsened, four with voiding problems required clean intermittent catheterization (CIC). Five other patients had surgical complications, including wound dehiscence (n=3) and cerebrospinal fluid (CSF) leakage (n=2), which required revision surgery.

Hoffmann's grading score was 1.61 on average in all the patients. The average score was 2 for dorsal LSL, 1.41 for caudal LSLS, 3 for transitional LSL, and 1.4 for chaotic LSL. Syringomyelia was observed in 10 patients (35.7%) preoperatively, four patients (14.2%) exhibited diastematomyelia, and eleven study participants (39.2%) had skin problems.

DISCUSSION

In pediatric neurosurgery, managing LSL is a difficult chore. A surgeon's involvement calls for carefully assessing the pros and cons involved. Our analysis utilizing data from many studies offers a thorough overview of current approaches and their outcomes. Customizing treatment plans for every patient comes first, weighing factors such as the type of lipoma, patient age, and symptoms experienced. Our work aims to add to the present LSL management information database. We present a classification-based approach to improve understanding of surgical operations. The present work meticulously explores the possible effects of the degree of lipoma excision on long-term neurological outcomes. While our study builds on other studies, it aims to provide more thorough knowledge by focusing on the outcomes linked with several types of lipomas and surgical approaches. These points of view help neurosurgeons make better decisions and encourage more discussion in pediatric neurosurgery.

Our study demonstrates various perspectives on LSL management and highlights the importance of personalized treatment strategies. We advocate for surgery in symptomatic patients and a conservative approach with surgical intervention as needed in asymptomatic patients. Our ultimate goal is to preserve neurological function while minimizing risks. A thorough understanding of preoperative neuroimaging, lesion types, intraoperative guidance, and surgical techniques are essential for successful outcomes. Thus, objective evaluation and continuous improvement in surgical approaches, treatment strategies tailored to individual patients, and a surgeon's expertise are essential. When it comes to managing complex lipomas, we agree with the findings of Pierre-Kahn et al. that asymptomatic patients should be followed up neurologically, urologically, and orthopedically. However, symptomatic patients should be advised surgery, and the lipoma should be excised as much as possible while untethering the cord and roots. To plan a precise surgical strategy that untethers the neural tissues with minimal risk of injury, it is paramount to interpret the preoperative neuroimaging to determine the LSL type and detect any other anomalies (e.g., diastematomyelia). In patients with lipomyelomeningoceles, the lesion should be carefully excised to avoid injury of neural tissues protruding from the spinal canal (13,34). In patients with a concomitant split cord malformation, the diastematomyelia should be resected first, and the lipoma should be excised last. Although the primary surgical procedure is the same for all the lipoma types, the surgical nuances differ from one type to the other. Because the chaotic LSL engulfs the roots, total lipoma resection without worsening neurological deficits is considered nearly impossible. However, over the last decades, Pang et al. have claimed that total excision is more successful than subtotal resection (29,30). However, total lipoma resection requires much surgical experience.

In our surgical experience, we do not attempt total resection in chaotic LSLs. Instead, we perform maximal resection without attempting a hazardous approach and always perform a large duraplasty. In case of a slight decrease in intraoperative motor evoked potentials or electromyography response (a 50% decrease in amplitude or 10 % prolongation in latency) at the lipoma near the root exit zone, we discontinue the lipoma resection after untethering all the attachments to the dura and the roots. To avoid retethering, we perform a wide duraplasty to ensure the cord never touches the dura. If the patient complains of new or progressive symptoms and demonstrates worsening of electrophysiological and urodynamic study results, the patient is considered to have deteriorated, and re-surgery is considered. We believe that removing an additional small amount of fat tissue at the risk of injuring the cord is unacceptable.

The utilization of CUSA in lipoma resection presents a balanced profile of advantages and drawbacks. CUSA offers precise tissue dissection with minimal trauma and mobilization of the surrounding neural structures, essential in delicate pediatric neurosurgeries. CUSA's ability to selectively emulsify fatty tissue while preserving neural tissue helps, especially in getting more complete resections. Still, its utilization comes with challenges. By way of a steep learning curve, knowledge of this method can allow us to reduce the risk of inadvertent damage to neurovascular structures. Moreover, producing heat and the likelihood of tissue cavitation necessitate careful use to minimize thermal harm. Future studies and discussions should define CUSA's optimum use parameters and approaches for LSL resection to maximize its benefits and

reduce risks. Recently, we have been performing sharp dissections for lipoma resections instead of utilizing CUSA.

Effective long-term care and monitoring necessitate a scheduled follow-up once LSLs are removed. Three, six, and twelve months after surgery should be the times for follow-up appointments. After that, the patients should be under observation annually. During these visits, a thorough clinical neurological examination should be performed in search of any signs of tethered cord syndrome recurrence, changes in neurological function, or development of new symptoms. MRI is indicated to look for spinal cord retethering and lipoma growth both at the one-year follow-up and then every two years. Bladder performance is suggested to be checked via annual urodynamic tests. Parents and other caregivers should also be informed on the indicators of retethering or neurologic deterioration to enable fast reporting. Should postoperative problems arise to protect the quality of life, this proactive method provides rapid care. Carefully recorded long-term outcome data can direct future patient therapy and aid in understanding the success of surgical operations.

Whether patients getting LSL resections retain their quality of life depends heavily on postoperative therapy of neurogenic bladder and bowel dysfunction (18). Often using a multidisciplinary approach, this postoperative care demands gastroenterological, pediatric urological, and rehabilitative therapy. Continuity regimens are customized to the patient, usually incorporating dietary changes, a bowel schedule with planned toileting, CIC for bladder control, and regular use of stool softeners or laxatives. Cases of refractory bladder or bowel dysfunction may call for sacral neuromodulation, botulinum toxin injections, or anticholinergic drugs. Regular follow-up with urodynamic exams and bowel function evaluations lets one track development and change therapeutic plans. This whole approach systematically addresses these individuals' long-term and acute functioning issues.

In our analysis, the percentage of patients with poor outcomes and neurological impairment (17.8%) exceeded that recorded in earlier investigations (7). This suggests that even being objective about our findings, we should aim to achieve the best results. Should our findings contradict those of the literature, the signs for surgical intervention should be customized individually. Unsuccessful surgical attempts must be carefully reviewed, improved on, or corrected by someone with better results, or conservative management should be followed. Each surgeon should determine the indications for surgery according to the underlying pathology and their success rate with the lesion. By incorporating these perspectives, we aim to provide a comprehensive understanding of LSL management and contribute to developing evidence-based guidelines for clinicians.

Several authors have classified LSLs, including Chapman and Arai et al., with implications for surgical procedure selection, residual volume, postoperative outcomes, and prognosis. Asymptomatic filum lipomas and dorsal LSLs demonstrate favorable prognoses, while transitional and chaotic LSLs yield poorer outcomes (2,6,30). Our findings align with these studies, particularly regarding the outcomes of different lipoma types, where transitional and chaotic LSLs demonstrated poorer prognoses than dorsal LSLs.

Several methods besides conventional techniques have been proposed for preoperative assessment and intraoperative guidance. Kim et al. proposed the use of extended lumbosacral spine MRI instead of whole spine MRI for better image quality around the primary lesion and minimal additional time and cost (19). Some studies have demonstrated the dynamic morphological changes and clinical value of constructive interference in steady state (CISS) MR imaging in LSLs. They emphasized the need for close monitoring and timely intervention in infants to address these changes effectively (15,23). Nonaka et al. emphasized the importance of stable intraoperative neurophysiological monitoring, particularly in infants. They found the bulbocavernosus reflex more reliable than motor-evoked potentials (MEPs) in very young patients, underscoring the necessity of meticulous intraoperative monitoring to mitigate surgical risks. This is consistent with our conclusion, revealing notable postoperative improvements using modern intraoperative monitoring systems (25). Shin et al. assessed the average thickness of the filum terminale on sonography for LSL screening in young infants and proposed an acceptable cutoff value of 1.1 mm, much below the standard 2 mm threshold. For the detection of filum terminale lipomas, this new cutoff value showed great sensitivity (94%) and specificity (86%), therefore offering a more reliable diagnosis tool for early management (36). By using three-dimensional multi-fusion images applied with a haptic device for planning LSL operations, Ogura et al. presented a preoperative interactive virtual simulation (IVS). This IVS improves resection accuracy and lowers complications by enabling exact preoperative planning and intraoperative guidance. Including IVS in our surgical planning procedures would enhance our capacity to customize surgical techniques to particular patient requirements (27).

Surgical indications for symptomatic LSL patients are well established. Nevertheless, the indications in patients without symptoms are subject to debate. When analyzing the arguments favoring and against preventative surgery, Chumas observed the lack of comprehensive prospective studies that may offer a definitive answer to this matter (8). Although several studies advocate for early intervention to avoid future neurological damage, others propose a cautious strategy because of the risks associated with surgery and the potential for tethering (40). Our recommendation for asymptomatic patients who are being closely followed and monitored is to adopt a conservative approach. Surgical intervention should only be considered if there are clear signs of neurological deterioration or the appearance of new symptoms. This ensures that the benefits of intervention outweigh the risks associated with surgery.

The management of LSLs is intricate because of the diverse characteristics of these lesions and their different clinical presentations. The problems are highlighted in a recent systematic analysis conducted by Perera et al., which uncovers substantial variation in patient outcomes and therapeutic approaches among 913 cases. The study suggests that although

nearly two-thirds of patients who were treated with surgery or conservative measures maintained clinical stability, 17.6% worsened, primarily due to neuropathic bladder dysfunction. Compared to subtotal resection (10-67%), near-total excision of lipomas yielded better deterioration-free survival rates (77.2-98.4%). However, 4.5% necessitated re-do untethering operations. The study underscored the significance of using standardized terminology, evaluation instruments, and surgical procedures to enhance uniformity in results and efficiently direct management approaches (32). This aligns with our findings, emphasizing the importance of individualized treatment plans based on lipoma type and patient-specific factors, supported by comprehensive preoperative imaging and intraoperative neuromonitoring to optimize surgical outcomes.

Pierre-Kahn et al. found that unoperated asymptomatic patients with lipomyelomeningocele demonstrated better outcomes after ten years than those who underwent surgery (33). Conversely, Pang and other authors advocate for total lipoma resection, regardless of the clinical status, to prevent potential complications (12,28). La Marca et al. suggested that all spinal lipomas should be surgically excised prophylactically as early as possible. Furthermore, interdisciplinary follow-up is required postoperatively to perform a reintervention if necessary (21). Usami et al. clarified the preoperative characteristics of filum terminale lipomas and elucidated the surgical effects. They suggested that early intervention, particularly in symptomatic patients, can lead to significant improvements and prevent further deterioration (39).

De Vloo et al. and Tu et al. provided insights into the long-term outcomes of radical resection techniques and the natural history of congenital neurological deficits associated with LSL. Both studies emphasize the importance of individualized treatment strategies and suggest that observation followed by intervention upon symptom development can be an acceptable approach for managing these patients (9,38).

Kulkarni et al. and Pierre-Kahn et al. demonstrated that 33% of patients with asymptomatic conus lipomas experience worsening within nine years, and 32% of them require surgical intervention (20,33). Conservative management, followed by surgery if necessary, resulted in 88% of patients remaining neurologically intact after ten years. In contrast, only 53% of patients who underwent surgery remained neurologically intact. Insufficient evidence supports recommending prophylactic surgery for asymptomatic patients with conus lipomas, and predicting worsening in patients remains a challenge. Thus, conservative monitoring and follow-up, with surgery as needed, appears to be the most appropriate approach for asymptomatic patients with conus lipomas.

Wykes et al. analyzed 56 patients over an average of six years and found a progression-free survival (PFS) rate of 71% and an estimated 10-year PFS rate of 60%. This indicated that surgery was contemplated for the remaining 29% of patients who exhibited signs of clinical worsening. They determined that age <2 years, female sex, transitional-type lipoma, and presence of syrinx were adverse prognostic factors. Thus, these factors should be considered when determining treatment options and individualized patient management (41). Talamonti et al. analyzed 56 patients diagnosed with LSL, of whom 32 had surgical intervention and 24 received conservative treatment. Notwithstanding the absence of a statistically significant distinction among the groups, the authors advised surgical intervention for all patients diagnosed with non-transitional lipomas (37).

When combined with other rare spinal dysraphisms, such as split notochord syndrome (SNS) and tight filum terminale syndrome (TFTS), the surgical treatment of LSLs is even more difficult. Alelyani et al. successfully handled a rare instance of SNS linked with spinal cord lipoma and spinal column duplication employing microsurgical untethering. This example emphasizes the vital need for early diagnosis, knowledge of the pathophysiology of spinal cord tethering, and careful microsurgical procedures for best results (1). Likewise, Bao et al. underlined that TFTS in children can show with a typically positioned conus, challenging the diagnosis. Their research implies that clinical presentation, physical and radiological tests, MRI, and pathological abnormalities in the filum terminale should form the basis of diagnosis. Notwithstanding conus location, they support early sectioning of the filum when neurological symptoms exist (4). First, address the split cord deformity before moving on with the lipoma excision when handling LSLs related to split cord malformations and diastematomyelia. This sequential surgical method helps reduce risks and enhance surgical outcomes by precisely untethering roots before addressing the LSLs.

The results of our study on postoperative complications and the necessity for revision procedures align with the research conducted by El-Ali et al., which emphasized the requirement of a multidisciplinary approach, including neurosurgeons and plastic surgeons, to successfully address functional and aesthetic issues. Implementing this comprehensive strategy is essential for achieving the best possible patient care and tackling the complex issues raised by LSL (10).

Pang et al. conducted a thorough investigation, including patients who underwent either total or near-total lipoma resections under a 20-year follow-up (31). They discovered that patients with total and near-total resections showed a 20-year PFS rate of 88.1%. By contrast, over 10.5 years, the PFS rate among patients who solely underwent subtotal resections was much lower at 34.6%. Of the asymptomatic individuals, those with entire resections showed a PFS rate of 98.8% over 20 years; those with subtotal resections showed a PFS rate of 40% over 10.5 years. Conservative patients treated in Paris and London showed PFS rates of 67% over nine years and 60% over ten years, respectively. With rates of 96.9% for a ratio of 30 to 50, 86.2% for a ratio of 30 to 50, and 78.3% for a ratio >50, Pang et al. also noted the cord/dural sac ratio as the single independent variable influencing PFS. According to their study, the perfect patient profile is an asymptomatic younger age, less than two years, without a past surgical history, with a PFS rate of 99.2%. These results highlight the need to consider elements including the degree of lipoma resection, patient's age, symptomatology, and cord/dural sac ratio when designing surgical procedures and provide insightful analysis on managing LSLs. Pang et al. also stress the pos-

sible advantages of complete resections in particular patient groups, which might result in better long-term results (31).

Total lipoma resection achieves better long-term protection against symptomatic recurrence than partial resection (3). However, LSLs' surgical management and underlying pathology must be better understood, especially in chaotic LSLs. Because the chaotic LSL engulfs the roots, total lipoma resection is challenging without worsening neurological deficits. However, recently published studies encourage surgeons to perform total resection for chaotic LSLs (30,31).

Filar lipomas are very different from other LSLs and are, thus, not included in this study. Our policy for a growing child with filar lipomas is to advise surgery. Dorsal lipomas can be more easily treated than transitional and chaotic LSLs because of the more accessible surgical anatomy and lower risk of operational deficits. Thus, these LSLs may be excised even if they are asymptomatic.

Our study is limited by its retrospective design and the small sample size from a single institution, which may affect the generalizability of the findings. The variability in long-term follow-up and reliance on subjective assessment criteria also present challenges in evaluating surgical outcomes. In the future, prospective, multicenter studies with more extensive and diverse populations should be performed to validate our study findings. Standardizing surgical techniques and incorporating advanced intraoperative imaging and neuromonitoring tools with artificial intelligence techniques, such as deep learning algorithms, could refine surgical strategies. Additionally, long-term longitudinal studies that include quality-of-life assessments will be crucial for a more comprehensive understanding of the natural history of LSLs and the long-term impact of surgical intervention. Investigations into the molecular and genetic underpinnings of these conditions may also provide insights into predictive factors of disease progression and potential nonsurgical treatments, which may expand the scope of patient care and management (26).

CONCLUSION

Our study highlights the importance of individualized treatment strategies for LSLs. We advocate for surgery in all symptomatic patients and a conservative approach with surgical intervention as needed in asymptomatic patients with a conus lipoma. A thorough understanding of preoperative neuroimaging, lesion types, and surgical techniques, in addition to consideration of prognostic factors, is essential for achieving successful outcomes. The natural course of LSLs demonstrates a 35%–40% worsening rate, which raises questions about the need for surgery and which patients should undergo surgical intervention. Based on the available evidence, symptomatic patients should undoubtedly undergo surgery, and asymptomatic patients with filum or dorsal lipomas may be considered for surgical treatment. When possible, total resection and extensive dural sac reconstruction should be pursued for dorsal lipomas. In patients with asymptomatic transitional or chaotic LSLs, surgical intervention should be considered if the surgery yields a 10-year PFS of 60%–65% or higher. Individualized treatment planning, close monitoring, and multidisciplinary collaboration are essential in managing these patients.

ACKNOWLEDGMENTS

Preparation for publication of this article is partly supported by the Turkish Neurosurgical Society.

Declarations

Funding: This research did not receive any specific grant from funding agencies in the public, commercial, or not-for-profit sectors.

Availability of data and materials: The datasets generated and/or analyzed during the current study are available from the corresponding author by reasonable request.

Disclosure: The authors declare no competing interests.

AUTHORSHIP CONTRIBUTION

Study conception and design: EC, AD
Data collection: EC, CK
Analysis and interpretation of results: EC, CK, AD
Draft manuscript preparation: EC, AD
Critical revision of the article: EC, CK, AD
Other (study supervision, fundings, materials, etc...): EC, AD
All authors (EC, CK, AD) reviewed the results and approved the final version of the manuscript.

REFERENCES

1. Alelyani F, Aronyk K, Alghamdi H, Alnaami I: Split notochord syndrome with spinal column duplication and spinal cord lipoma: A case report. Children 9:1138, 2022. https://doi.org/10.3390/children9081138
2. Arai H, Sato K, Okuda O, Miyajima M, Hishii M, Nakanishi H, Ishii H: Surgical experience of 120 patients with lumbosacral lipomas. Acta Neurochir 143:857-864, 2001. https://doi.org/10.1007/s007010170015
3. Bai SC, Tao BZ, Wang LK, Yu XG, Xu BN, Shang AJ: Aggressive resection of congenital lumbosacral lipomas in adults: Indications, techniques, and outcomes in 122 patients. World Neurosurg 112:e331–e341, 2018. https://doi.org/10.1016/j.wneu.2018.01.044
4. Bao N, Chen ZH, Gu S, Chen QM, Jin HM, Shi CR: Tight filum terminale syndrome in children: analysis based on positioning of the conus and absence or presence of lumbosacral lipoma. Child's Nerv Syst 23:1129-1134, 2007. https://doi.org/10.1007/s00381-007-0376-8
5. Bekar A, Sahin S, Taskapiloglu O, Aksoy K, Tolunay S: Intradural spinal lipoma: Report of a thoracic case and a lumbar case. Turk Neurosurg 14:52-56, 2004
6. Chapman PH: Congenital intraspinal lipomas: Anatomic considerations and surgical treatment. Child's Brain 9:37-47, 1982
7. Chong S, Lee JY, Kim KH, Shin HI, Kim K, Park K, Kim SK, Wang KC: Radical excision of lumbosacral lipoma: An early experience of "followers." Child's Nerv Syst 35:1591-1597, 2019. https://doi.org/10.1007/s00381-019-04212-1
8. Chumas PD: The role of surgery in asymptomatic lumbosacral spinal lipomas. Br J Neurosurg 14:301-304, 2000. https://doi.org/10.1080/026886900417252

9. De Vloo P, Sharma J, Alderson L, Jankovic I, Tahir MZ, Desai D, Pang D, Thompson DNP: Radical resection of lumbosacral lipomas in children: The great ormond street hospital experience. Child's Nerv Syst 38:1113-1123, 2022. https://doi.org/10.1007/s00381-022-05483-x
10. El-Ali K, Slator R, Solanki G, Hockley A, Nishikawa H: Multidisciplinary management of spinal lipoma. J Plast Reconstr Aesthet Surg 62:964-968, 2009. https://doi.org/10.1016/j.bjps.2007.10.078
11. Finn MA, Walker ML: Spinal lipomas: clinical spectrum, embryology, and treatment. Neurosurg Focus 23:1-12, 2007. https://doi.org/10.3171/FOC-07/08/E10
12. Gao D, Bao N, Yang B, Song Y, Sun S: Preventive surgery for asymptomatic spinal lipomas in children. Turk Neurosurg 34:1-5, 2020. https://doi.org/10.5137/1019-5149.JTN.31209-20.2
13. Gao J, Kong X, Yang Y, Ma W, Wang R, Li Y: Massive lumbosacral subcutaneous exudate after surgical treatment of a large lipomyelocele. Medicine 94:e1676, 2015. https://doi.org/10.1097/MD.0000000000001676
14. Gourineni P, Dias L, Blanco R, Muppavarapu S: Orthopaedic deformities associated with lumbosacral spinal lipomas. J Pediatr Orthop 29:932-936, 2009. https://doi.org/10.1097/BPO.0b013e3181c29ce7
15. Hashiguchi K, Morioka T, Fukui K, Miyagi Y, Mihara F, Yoshiura T, Nagata S, Sasaki T: Usefulness of constructive interference in steady-state magnetic resonance imaging in the presurgical examination for lumbosacral lipoma. J Neurosurg 103:537–543, 2005. https://doi.org/10.3171/ped.2005.103.6.0537
16. Hoffman HJ, Taecholarn C, Hendrick EB, Humphreys RP: Management of lipomyelomeningoceles. J Neurosurg 62:1-8, 1985. https://doi.org/10.3171/jns.1985.62.1.0001
17. Jones V, Wykes V, Cohen N, Thompson D, Jacques TS: The pathology of lumbosacral lipomas: Macroscopic and microscopic disparity have implications for embryogenesis and mode of clinical deterioration. Histopathol 72:1136-1144, 2018. https://doi.org/10.1111/his.13469
18. Kang HS, Wang KC, Kim KM, Kim SK, Cho BK: Prognostic factors affecting urologic outcome after untethering surgery for lumbosacral lipoma. Child's Nerv Syst 22:1111–1121, 2006. https://doi.org/10.1007/s00381-006-0088-5
19. Kim KH, Lee JY, Cheon JE, Kim IO, Wang KC: A suggestion to the article "Whole spine MRI is not required in investigating uncomplicated paediatric lumbosacral lipoma: A retrospective single-institution review": Extended lumbosacral spine MRI. Child's Nerv Syst 36:7–8, 2020. https://doi.org/10.1007/s00381-019-04387-7
20. Kulkarni AV, Pierre-Kahn A, Zerah M: Conservative management of asymptomatic spinal lipomas of the conus. Neurosurgery 54:868-875, 2004. https://doi.org/10.1227/01.NEU.0000114923.76542.81
21. La Marca F, Grant JA, Tomita T, McLone DG: Spinal lipomas in children: Outcome of 270 procedures. Pediatr Neurosurg 26:8-16, 1997. https://doi.org/10.1159/000121155
22. Manoranjan B, Pozdnyakov A, Ajani O: Neurosurgical management of conus lipoma in Canada: A multi-center survey. Child's Nerv Syst 36:3041–3045, 2020. https://doi.org/10.1007/s00381-020-04641-3
23. Morioka T, Hashiguchi K, Yoshida F, Nagata S, Miyagi Y, Mihara F, Sasaki T: Dynamic morphological changes in lumbosacral lipoma during the first months of life revealed by constructive interference in steady-state (CISS) MR imaging. Child's Nerv Syst 23:415-420, 2007. https://doi.org/10.1007/s00381-006-0272-7
24. Morioka T, Murakami N, Shimogawa T, Mukae N, Hashiguchi K, Suzuki SO, Iihara K: Neurosurgical management and pathology of lumbosacral lipomas with tethered cord. Neuropathol 37:385–392, 2017. https://doi.org/10.1111/neup.12382
25. Nonaka M, Itakura T, Iwamura H, Ueno K, Naito N, Miyata M, Isozaki H, Li Y, Takeda J, Asai A: Comparison of intraoperative neurophysiological monitoring methods for lumbosacral lipoma surgery in infants. Child's Nerv Syst 39:1603-1610, 2023. https://doi.org/10.1007/s00381-023-05900-9
26. Nonaka M, Ueno K, Isozaki H, Kamei T, Takeda J, Asai A: Familial tendency in patients with lipoma of the filum terminale. Child's Nerv Syst 37:1641-1647, 2021. https://doi.org/10.1007/s00381-021-05037-7
27. Ogura R, Fujiwara H, Natsumeda M, Hiraishi T, Sano M, Oishi M: Preoperative interactive virtual simulation applying three-dimensional multifusion images using a haptic device for lumbosacral lipoma. Child's Nerv Syst 40:1129-1136, 2024. https://doi.org/10.1007/s00381-023-06234-2
28. Pang D: Total resection of complex spinal cord lipomas: How, why, and when to operate? Neurol Medico-Chir 55:695-721, 2015. https://doi.org/10.2176/nmc.ra.2014-0442
29. Pang D, Zovickian J, Oviedo A: Long-term outcome of total and near-total resection of spinal cord lipomas and radical reconstruction of the neural placode. Neurosurgery 65:511–529, 2009. https://doi.org/10.1227/01.NEU.0000350879.02128.80
30. Pang D, Zovickian J, Oviedo A: Long-term outcome of total and near-total resection of spinal cord lipomas and radical reconstruction of the neural placode, Part II. Neurosurgery 66:253-273, 2010. https://doi.org/10.1227/01.NEU.0000363598.81101.7B
31. Pang D, Zovickian J, Wong ST, Hou YJ, Moes GS: Surgical treatment of complex spinal cord lipomas. Child's Nerv Syst 29:1485-1513, 2013. https://doi.org/10.1007/s00381-013-2187-4
32. Perera D, Craven CL, Thompson D: Lumbosacral lipoma in childhood, how strong is the evidence base? A systematic review. Child's Nerv Syst 40:715-728, 2024. https://doi.org/10.1007/s00381-023-06203-9
33. Pierre-Kahn A, Zerah M, Renier D, Cinalli G, Sainte-Rose C, Lellouch-Tubiana A, Brunelle F, Merrer M Le, Giudicelli Y, Pichon J, Kleinknecht B, Nataf F: Congenital lumbosacral lipomas. Child's Nerv Syst 13:298-334, 1997. https://doi.org/10.1007/s003810050090
34. Rhodes RH: Congenital spinal lipomatous malformations. Part 1. Spinal lipomas, lipomyeloceles, and lipomyelomeningoceles. Fetal Pediatr Pathol 39:194–245, 2020. https://doi.org/10.1080/15513815.2019.1641859
35. Shimogawa T, Morioka T, Murakami N, Mukae N, Hashiguchi K, Suzuki SO, Iihara K: Bony and cartilaginous tissues in lumbosacral lipomas. Pediatr Neurosurg 53:305-310, 2018. https://doi.org/10.1159/000490391

36. Shin HJ, Kim MJ, Lee HS, Kim HG, Lee MJ: Optimal filum terminale thickness cutoff value on sonography for lipoma screening in young children. J Ultrasound Med 34:1943-1949, 2015. https://doi.org/10.7863/ultra.14.10079
37. Talamonti G, D'Aliberti G, Nichelatti M, Debernardi A, Picano M, Redaelli T: Asymptomatic lipomas of the medullary conus: Surgical treatment versus conservative management. J Neurosurg Pediatr 14:245-254, 2014. https://doi.org/10.3171/2014.5.PEDS13399
38. Tu A, Hengel R, Douglas Cochrane D: The natural history and management of patients with congenital deficits associated with lumbosacral lipomas. Child's Nerv Syst 32:667-673, 2016. https://doi.org/10.1007/s00381-015-3008-8
39. Usami K, Lallemant P, Roujeau T, James S, Beccaria K, Levy R, Di Rocco F, Sainte-Rose C, Zerah M: Spinal lipoma of the filum terminale: Review of 174 consecutive patients. Child's Nerv Syst 32:1265-1272, 2016. https://doi.org/10.1007/s00381-016-3072-8
40. Van Calenbergh F, Vanvolsem S, Verpoorten C, Lagae L, Casaer P, Plets C: Results after surgery for lumbosacral lipoma: the significance of early and late worsening. Child's Nerv Syst 15:439-442, 1999. https://doi.org/10.1007/s003810050433
41. Wykes V, Desai D, Thompson DNP: Asymptomatic lumbosacral lipomas-a natural history study. Child's Nerv Syst 28:1731-1739, 2012. https://doi.org/10.1007/s00381-012-1775-z

Turk Neurosurg 35(4):618-626, 2025
DOI: 10.5137/1019-5149.JTN.47309-24.3

Original Investigation

Pediatrics

Received: 22.07.2024
Accepted: 19.11.2024
Published Online: 25.06.2025

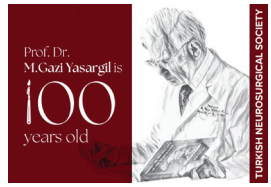

Proactive External Lumbar Drainage Use in Pediatric Idiopathic Intracranial Hypertension and Proposal of a New Treatment Algorithm

Bahattin TANRIKULU[1], Muruvvet Ayten TUZUNALP[2], Ugur ISIK[3], M. Memet OZEK[1]

[1]Acibadem University School of Medicine, Department of Neurosurgery, Division of Pediatric Neurosurgery, Istanbul, Türkiye
[2]Acibadem Altunizade Hospital, Istanbul, Türkiye
[3]Acibadem University School of Medicine, Department of Pediatrics, Division of Pediatric Neurology, Istanbul, Türkiye

Corresponding author: Bahattin TANRIKULU ✉ bahattintanrikulu@gmail.com

ABSTRACT

AIM: To determine if the concurrent use of external lumbar drainage (ELD) and oral medication will hasten the decrease in intracranial pressure (ICP) and resolution of papilledema in pediatric idiopathic intracranial hypertension (IIH).

MATERIAL and METHODS: In this retrospective study, we evaluated the outcome of pediatric patients with IIH who underwent ELD as an adjunct treatment to standard oral medications. All patients underwent ophthalmological examination, optic coherence tomography, retinal nerve fiber layer thickness assessment, and ICP measurements before and after ELD. The outcome was evaluated via serial ophthalmological examinations, optical coherence tomography to measure retinal nerve fiber layer thickness, and lumbar puncture to measure ICP.

RESULTS: Eleven pediatric patients (7 females, 4 males) were enrolled in the study. The mean age of the patients was 10.9 ± 4.4 years (range, 5.6–17.7 years). The mean cerebrospinal fluid opening pressure was 447 ± 112.5 mm H_2O before ELD. The mean post-ELD ICP was 263.1 ± 92.4 mm H_2O. The retinal nerve fiber layer thickness at the time of diagnosis was 200.9 ± 113.7 µm and 212.6 ± 123.3 µm in the right and left eyes, respectively. After ELD, the thickness was 149.4 ± 45 µm and 151.4 ± 51.3 µm in the right and left eyes, respectively. The mean duration of ELD was 8.7 ± 1.4 days (range, 7–10 days). The post-ELD cerebrospinal fluid opening pressure and retinal nerve fiber layer thickness were significantly lower than pre-ELD values. Four patients required lumboperitoneal shunt surgery during follow-up.

CONCLUSION: Proactive ELD is an effective method to achieve a rapid decrease in ICP and retinal nerve fiber layer thickness without major complications.

KEYWORDS: Papilledema, Intracranial hypertension, Lumbar drainage, Optical coherence tomography, Pediatric pseudotumor cerebri

ABBREVIATIONS: IIH: Idiopathic intracranial hypertension, **ICP:** Intracranial pressure, **CSF:** Cerebrospinal fluid, **OCT:** Optic coherence tomography, **LPS:** Lumboperitoneal shunt, **ONSF:** Optic nerve sheet fenestration, **ELD:** External lumbar drainage, **LP:** Lumbar puncture

Bahattin TANRIKULU : 0000-0002-9096-8685
Muruvvet Ayten TUZUNALP : 0009-0001-9163-4513
Ugur ISIK : 0000-0002-7327-127X
M. Memet OZEK : 0000-0002-7166-7166

INTRODUCTION

Idiopathic intracranial hypertension (IIH) is defined as an increase in intracranial pressure (ICP) in the absence of an intracranial mass lesion that is associated with normal-sized or slit ventricles and normal cerebrospinal fluid (CSF) biochemistry (8). IIH is a rare disease with an estimated incidence of 6–9 per 1,000,000 people in the pediatric population (7,9), and its incidence increases with obesity (10). The common presenting symptoms of IIH are headache, nausea, vomiting, blurred vision, double vision secondary to 6th nerve palsy, and transient visual deficits (1,17).

The most serious complication of IIH is visual loss (8-10,16), with a frequency of approximately 50% (6,27,28). Therefore, a reliable ophthalmological examination is mandatory during the diagnosis and follow-up of IIH. Fundus examination may sometimes be challenging, especially in subtle papilledema, which may be present in early-onset IIH (22). Optical coherence tomography (OCT) is a reliable and objective tool for diagnosing and monitoring optic nerve disorders, including papilledema (22). Furthermore, it is useful for measuring optic disk swelling, even in young children (7).

The pathology underlying IIH is hypothesized to be venous sinus hypertension, which decreases CSF absorption and leads to increased ICP (10). Although oral medications that decrease CSF production are widely used, surgical treatment options, such as lumbo-peritoneal shunt (LPS), optic nerve sheath fenestration (ONSF), and venous sinus stenting, are available for patients with refractory IIH (3,4). In recent studies, external lumbar drainage (ELD) has been used in pediatric patients with IIH in whom oral medications have failed (7,10,14).

In of our study, we aimed to investigate whether the combined use of ELD and oral medications at the time of diagnosis could provide a faster reduction in ICP and reduce the risk of optic nerve damage in pediatric patients with IIH. This proactive approach was designed to avoid the need for early surgical shunting, and thereby potentially reducing long-term optic nerve damage. Previous studies have demonstrated that delaying surgical intervention may increase the risk of irreversible visual damage. This justifies our approach of rapid intervention with ELD and medication. We hypothesized that the combined use of ELD and oral medication could be a more effective and less invasive first-line treatment strategy than early direct shunting.

MATERIAL and METHODS

In this retrospective study, we analyzed the medical records of pediatric patients diagnosed with IIH in our Pediatric Neurosurgery Clinic between February 2020 and February 2022. This study was approved by the institutional ethics committee, and informed consent was obtained from the legal guardians of all the patients (No: 2025-03/127). All the methods were performed in accordance with the relevant guidelines and regulations. Patients who underwent ELD during their IIH treatment were included in the study. All patients with signs and symptoms of IIH, including papilledema during a routine ophthalmological examination, visual disturbances, headache, and vomiting, were examined by the pediatric IIH study group. The group consisted of a pediatric neurologist, pediatric ophthalmologist, pediatric neurosurgeon, pediatric neuroradiologist, and nurse practitioner. All patients underwent thorough ophthalmological and neurological examinations, cranial 3T magnetic resonance imaging (MRI) to exclude hydrocephalus and any intracranial mass lesion, magnetic resonance venography with contrast to evaluate the venous sinus anatomy, OCT (Zeiss), and lumbar puncture (LP). In accordance with Friedman's criteria, an CSF opening pressure of >280 mm H_2O in obese patients or >250 mm H_2O in nonobese patients was accepted as high. All patients with an CSF opening pressure of >300 mm H_2O underwent ELD at the same time as the LP. According to our pediatric IIH treatment algorithm, all legal guardians had been informed of the concurrent ELD insertion if the CSF opening pressure was >300 mm H_2O, and informed consent was obtained (Figure 1).

All LP and ELD procedures were performed by the same neurosurgeon in an operating room under sedation (without endotracheal intubation) with anesthetic agents that did not increase the ICP (e.g., propofol and remifentanil). The obtained CSF was examined for cell count, protein and glucose levels, and bacterial growth in every patient. After the ELD was inserted, 10–15 cc/h of CSF was drained for at least 5 days. The ICP was concomitantly monitored (IntelliVue MX500; Philips) via the ELD kit, and the exact drainage amount was tailored according to the ICP. Furthermore, the retinal nerve fiber layer (RNFL) thickness was measured in each patient via OCT. All patients were started on oral medications on the first day of the ELD. Non-obese patients were administered acetazolamide, and obese patients were administered topiramate (TPM) (Table I).

The OCT and ophthalmological examination were repeated on the fifth day. If the papilledema had not decreased, ELD was continued. Thereafter, ophthalmological examination and OCT were repeated on days 7 and 10 of ELD. The ELD kit was removed at the end of the 10th day to avoid the increased risk of contamination (20). Before ELD removal, the last ICP pressure (obtained 24 h after clamping the ELD) was noted for each patient. If this value was >280 mm H_2O and/or there was no improvement in papilledema, an LPS system was implanted.

All patients who benefited from the oral medications and ELD were followed up every 6 weeks. During the follow-up, the CSF pressure was measured via LP and neurological and ophthalmological examinations were performed. OCT was repeated during two visits. Routine follow-up was scheduled for 3 months, 6 months, and 1 year accordingly.

The results were analyzed using IBM SPSS (version 20.0, USA). Descriptive statistics are reported as mean ± standard deviation. The mean OCT-RNFL thickness was analyzed using paired t-test. All statistical tests were two-tailed, and a p-value of <0.05 was considered statistically significant.

Table I: Summary of Demographic and Clinical Data of Patient Cohort

Patient	Age (yrs.)	Sex	BMI	MRI	CSF Pressure (mmH_2O)	Complaint	Treatment	CSF Pressure (Post ELD) (mmH_2O)	RNFL (at presentation) (R-L)	RNFL (Post ELD) (R-L)	LP Shunt	Follow-up period (mo)	Outcome
1	5.8	F	N	PES, OSD	350	No	ACT+ELD (10 days)	340	310/365	249/278	Yes (2 weeks after ELD)	25.1	Uneventful
2	6.8	F	OW	N	320	No	ACT+ELD (7 days)	190	112/138	109/129	No	5.2	Uneventful
3	10	F	OB	PES, OSD	430	No	TPMX + ELD (7 days)	180	113/113	110/108	No	5.8	Uneventful
4	17.7	F	UW	N	380	No	ACT+ELD (7 days)	140	130/131	124/114	No	8.2	Uneventful
5	10.9	F	OB	PES, OSD	550	H/A, vomiting	ACT+ELD (10 days)	195	231/294	140/165	No	16.5	Uneventful
6	17.5	F	OB	PES, OSD	510	H/A, eye pain	TPMX + ELD (10 days)	210	140/143	146/135	Yes (4 weeks after ELD)	4	Uneventful
7	14.7	M	OW	PES, OSD+ON kinking	450	Precocious Puberty	TPMX + ELD (7 days)	260	234/253	157/153	No	16.9	Uneventful
8	12	M	OB	PES, OSD	650	H/A, 6^{th} palsy	ACT+ELD (10 days)	420	485/484	223/215	Yes (just after ELD)	20	Uneventful
9	5.6	M	OW	PES, OSD	450	H/A, nausea, vomiting	ACT+ELD (8 days)	400	195/175	139/143	Yes (just after ELD)	16.3	Uneventful
10	6.4	M	N	PES, OSD	360	6^{th} palsy	ACT+ELD (10 days)	300	121/115	117/112	No	2	Uneventful
11	12.8	F	OW	PES, OSD	470	H/A	ACT+ELD (10 days)	260	139/128	130/114	No	2	Uneventful
Mean	10.9	--	--	--	447	--	--	263.1 ($p<0.01$)	200.9/212.6	149.4/151.4 ($p<0.05$)			

ACT: *Acetazolamide;* ***CSF:*** *Cerebrospinal fluid;* ***ELD:*** *external lumbar drainage;* ***H/A:*** *headache;* ***L:*** *left;* ***LP:*** *lumboperitoneal;* ***mo:*** *months;* ***N:*** *normal;* ***OB:*** *Obese;* ***OSD:*** *Optic nerve sheath dilatation,* ***OW:*** *Over weight;* ***UW:*** *Underweight;* ***PES:*** *Partial empty sella;* ***RNFL:*** *Retinal nerve fiber layer thickness;* ***TPMX:*** *Topiramate;* ***yrs:*** *Years*

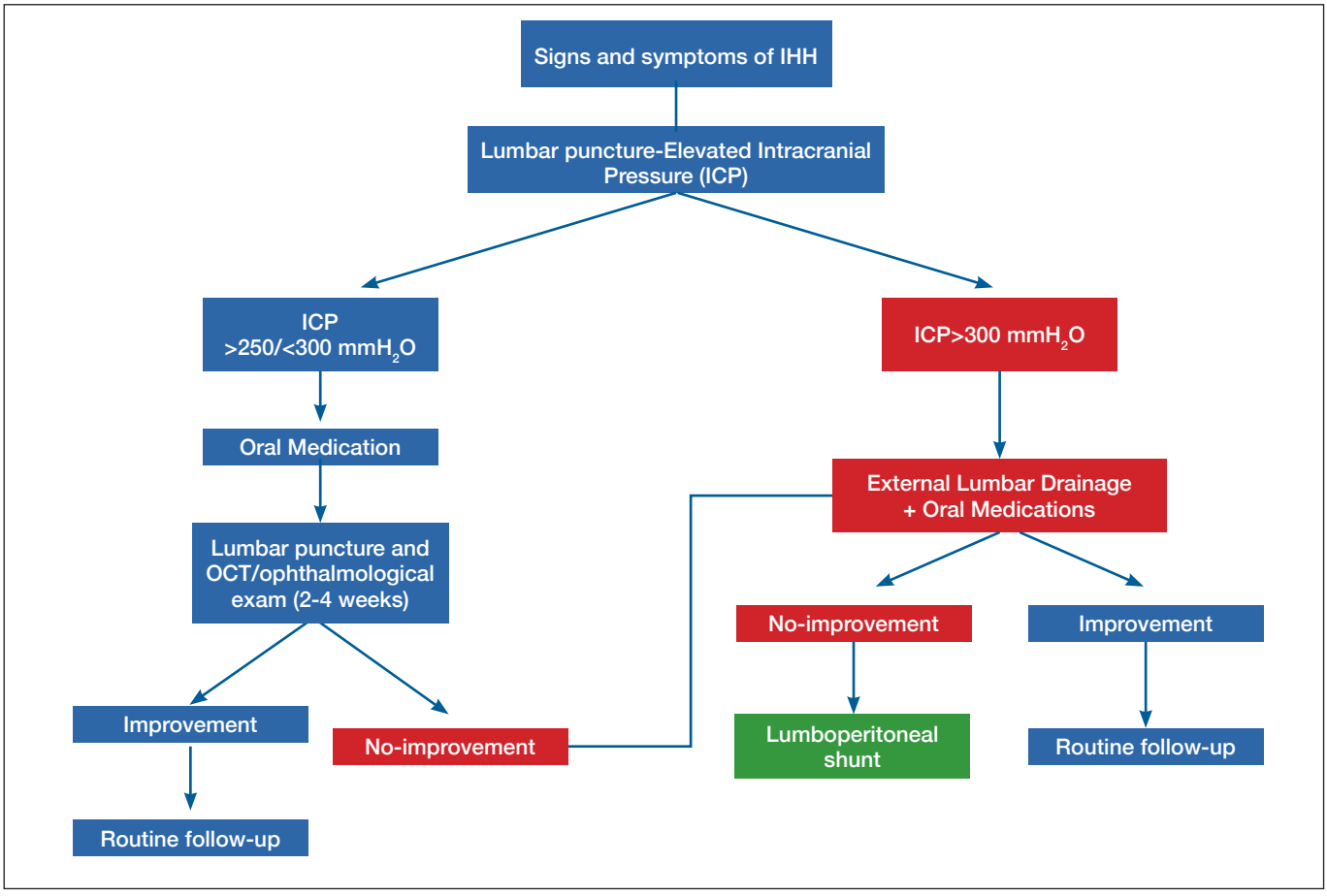

Figure 1: Our pediatric idiopathic intracranial hypertension patient management algorithm.

RESULTS

The study included 11 patients (7 females and 4 males). The mean age at the time of diagnosis was 10.9 ± 4.4 years (range, 5.6–17.7 years). The mean follow-up period was 11.1 ± 8.1 months (range, 2–25.1 months). Five children presented with headaches, and four of them had additional presentations such as lateral gaze palsy and double vision, nausea, vomiting, or pain in the eye. Among the remaining 6 children who did not have headache, one had isolated right lateral gaze palsy and one had precocious puberty. None of the patients had concomitant venous sinus thrombosis. However, one child had a history of venous sinus thrombosis 7 months ago that had resolved. This child and four other children had no complaints, and only bilateral papilledema had been detected in them during the yearly ophthalmological examinations. Bilateral papilledema had been detected in all the study participants during an ophthalmological examination at admission. Body mass index were interpreted according to the age–sex-matched percentiles of Turkish children (5). One patient was underweight (female), two patients had normal weight (1 female and 1 male), four patients were overweight (2 female and 2 male), and four patients were obese (3 female and 1 male).

In eight patients, the MRIs demonstrated increased CSF content within the optic nerve sheath and a partially empty sella. In the remaining three patients, the MRIs were completely normal.

Eight patients were administered acetazolamide, and three patients were administered TPM. These medications were concurrently started with ELD insertion and followed-up by the same pediatric neurologist. The medications were continued after ELD withdrawal in accordance with our pediatric IIH treatment algorithm. The demographic and clinical data of our cohort are summarized in Table I.

The mean CSF opening pressure at the time of diagnosis was 447 ± 97 mm H_2O. The mean CSF opening pressure was 477.5 ± 112.5 mm H_2O in males and 430 ± 85 mm H_2O in females. The mean post-ELD (just before ELD removal) CSF pressure was 263.1 ± 92.4 H_2O. The mean post-ELD CSF pressure was 345 ± 77.2 mm H_2O in males and 216.4 ± 65.2 mm H_2O in females. The CSF pressures had significantly decreased after ELD insertion ($p<0.01$). There was no significant difference in the pre- and post-ELD mean CSF opening pressures between the two sexes. A few patients underwent a post-ELD MRI with contrast, which showed an increase in the diameter of the transverse sinuses (patients 5 and 10).

The mean OCT-RNF thickness at the time of diagnosis was 200.9 ± 113.7 µm in the right eye and 212.6 ± 123.3 µm in the

left eye. The mean post-ELD OCT-RNFL thickness was 149.4 ± 45 µm in the right eye and 151.4 ± 51.3 µm in the left eye. The mean duration of ELD was 8.7 ± 1.4 days (range, 7–10 days). In all children, the RNFL thickness had significantly decreased in both eyes after ELD ($p<0.05$).

Four patients (36.3%) required LPS surgery during the follow-up period. In two patients, although the RNFL thickness had decreased, an LPS was inserted just after ELD removal because the ICP was significantly high (Patients 8 and 9). In Patient 1, although the ICP did not decrease after ELD, LPS implantation was postponed because the RNFL thickness had significantly decreased in both eyes. However, the patient experienced a relapse with an increase in the RNFL thickness 2 weeks after ELD removal. Thus, an LPS was implanted. LPS implantation was also postponed in Patient 6 despite the absence of a significant decrease in RNFL thickness,

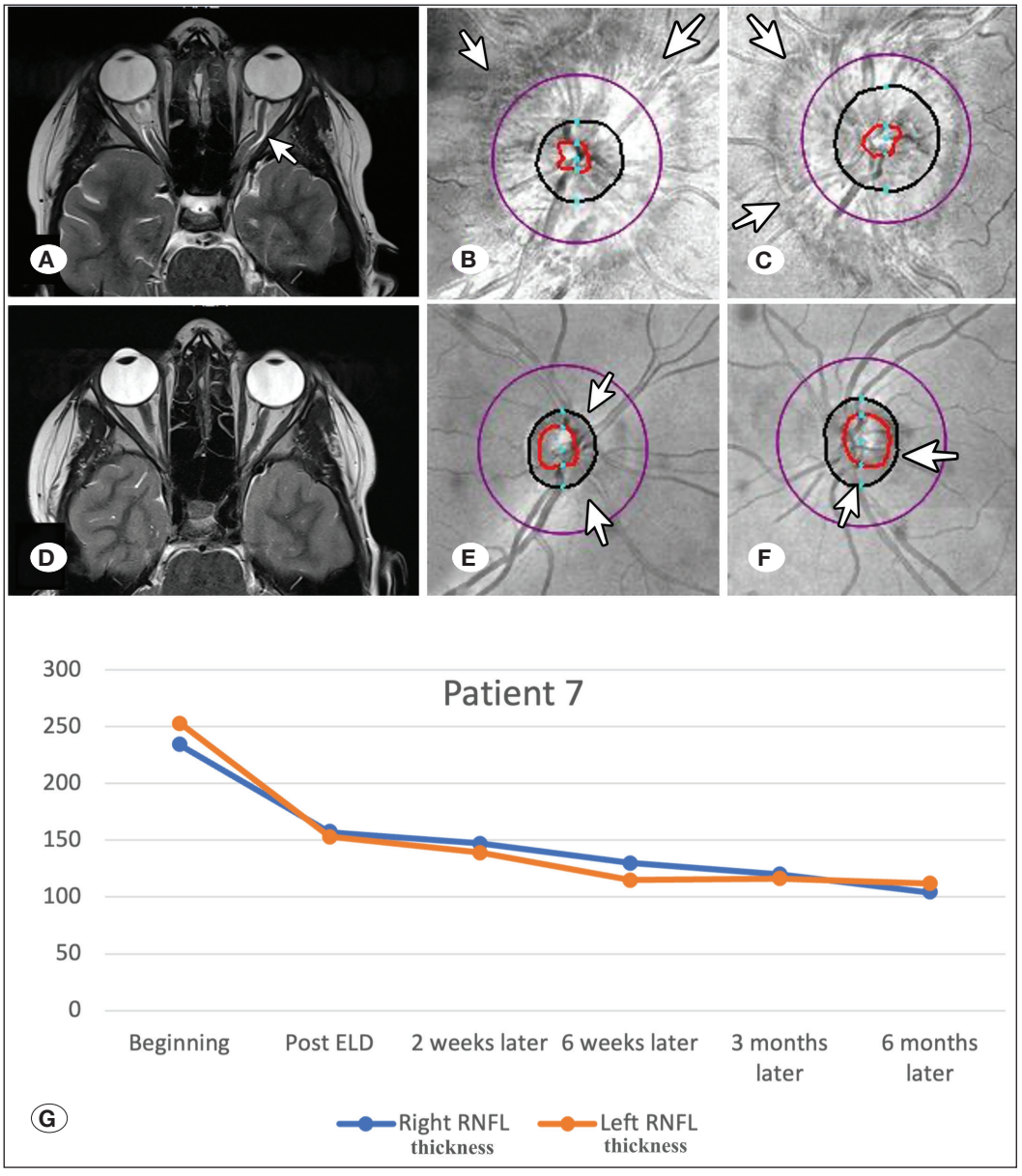

Figure 2: Images of representative Patient 7. **A)** T2-weighted axial MR image obtained before IIH treatment shows optic nerve sheath swelling with optic nerve kinking (arrow). OCT of the **(B)** right and **(C)** left eyes before IIH treatment show obvious swelling around the papillae (arrows). **D)** MRI obtained 6 months after IIH treatment (7 days of ELD + TPM, followed by TPM only) shows complete resolution of the optic nerve sheath swelling and optic nerve kinking. **E, F)** OCT obtained 6 months after the start of IIH treatment shows complete resolution of the swelling around the papilla. **G)** Graph showing the changes in OCT-RNFL thickness values within 6 months of treatment. There is a dramatic decrease in RNFL thickness at the end of the ELD treatment. The decrease in RNFL thickness continued during the follow-up period with oral treatment until physiological values were achieved. **MR:** Magnetic resonance, **IIH:** Idiopathic intracranial hypertension, **OCT:** Optical coherence tomography, **MRI:** Magnetic resonance imaging, **ELD:** External lumbar drainage, **TPM:** Topiramate, **RNFL:** Retinal nerve fiber layer thickness.

because there was a significant decrease in the ICP. However, IIH relapse was observed 4 weeks after ELD removal with an increase in ICP. Thus, she underwent LPS surgery. No relapse of IIH or complications such as infection and intracranial hypotension were reported during the follow-up period in any patient who had undergone LPS surgery. The remaining seven patients who did not undergo LPS surgery remained free of symptoms with a normal CSF pressure, improved ophthalmological findings, and no recurrence. Figure 2 shows the pre- and post-ELD cranial MR and OCT images of Patient 7 who did not undergo ELD. The graph indicates changes in the RNFL thickness with time. Graphs showing changes in RNFL thickness with time in other six patients (Patients 2, 3, 4, 5, 10, and 11) who did undergo ELD are depicted in Figure 3.

DISCUSSION

Although the exact pathophysiology of IIH is unknown, there are some theories that explain the possible mechanisms underlying the disease process (10,18,23-25). The most pronounced one is the collapse of the transverse sinuses, which leads to venous hypertension that decreases the CSF reabsorption and raises the ICP (10). This results in more pressure on the venous sinuses and completes the vicious cycle. However, the first event that triggers these cascade of events remains unknown. Some authors, while supporting this hypothesis, further proposed that development of venous hypertension before the closure of cranial sutures may cause hydrocephalus with dilated ventricles. However, development of venous hypertension after the closure of cranial sutures may cause IIH (18,19). There are several studies on the development of hydrocephalus in babies with achondroplasia and mucopolysaccharidosis in whom jugular foramen stenosis was determined as the cause for intracranial venous hypertension. This further supports the venous hypertension hypothesis (18,23,24).

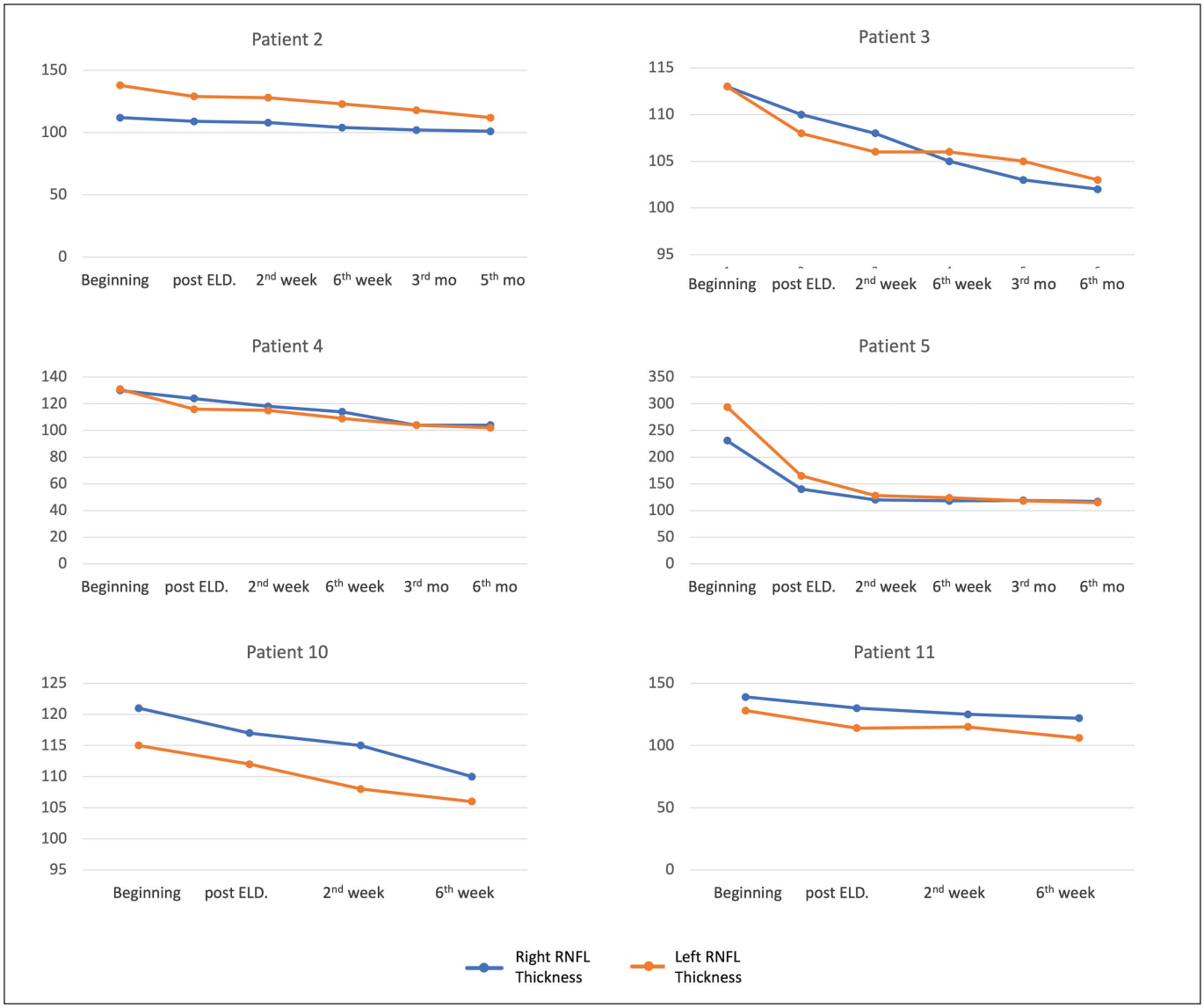

Figure 3: Graphs showing the changes in RNFL thickness over time in Patients 2, 3, 4, 5, 10, and 11.

The venous hypertension theory may also explain the higher incidence of IIH in obese patients. Obesity increases the intraabdominal pressure, which in turn increases the intrathoracic and right atrial pressure as well as the venous pressure within the superior vena cava, internal jugular vein, and, subsequently, intracranial venous sinuses that will impede CSF reabsorption (25).

Besides the more pronounced clinical presentations of IIH, such as headache and vomiting, the main concerns of most clinicians are the clinical or subclinical visual alterations due to optic nerve damage that is a result of chronically increased ICP (3,4). Overt papilledema can be easily diagnosed by an ophthalmologist. However, identification of subtle papilledema requires experience. Therefore, ophthalmological examination results for papilledema may exhibit interobserver variability. OCT can be used to measure RNFL thickness, and it yields objective and reproducible values. Furthermore, it diminishes interobserver variability, making it a practical tool for the diagnosis and follow-up of ophthalmological abnormalities, including papilledema (7,22).

All the patients in our study underwent an ophthalmological examination by the same ophthalmologist and an OCT at the time of admission, on the fifth day of ELD, at the end of ELD (7^{th}–10^{th} days), and on subsequent follow-ups. Similar to the findings of previous studies, we found that the OCT-RNFL values generally correlated with the ICP values during the follow-up (7,22).

Alleviation of symptoms and protection of vision are the two main treatment goals in IIH (4). The commonly used treatment options for IIH are oral medications, serial LP, and lifestyle modifications such as a specific weight-loss diet in overweight and obese patients. If these options fail, an LPS can be placed (3). Less commonly, transverse sinus stenting and ONSF may be attempted before LPS placement. However, they both are associated with considerable complication rates (3,7,11,13,15). The main rationale behind administering oral medications and serial LP is to decrease the intracranial pressure, allow the transverse sinuses to re-expand, and break the vicious cycle of ICP increase (7).

In nearly 85%–90% of the patients, oral medications are effective. However, the remaining patients generally require surgical intervention. The interval between oral acetazolamide use and resolution of ICP ranges between 40 and 90 days in adults (26). Schoeman reported the treatment results of combined acetazolamide and furosemide use, followed by the first LP in pediatric patients with IIH. They reported a decrease in the ICP values after 1 week of treatment, and normal values in all the patients within 6 weeks of treatment. Furthermore, remission of papilledema was observed in all the patients within 8 weeks of treatment (21). Although delayed remission of papilledema may be acceptable, normalization of ICP within 6 weeks after the start of oral medication may be perilous in terms of visual protection in pediatric patients with fulminant IIH.

Serial LPs are uncomfortable and generally not recommended because of complications such as infection, bleeding, and the inclusion of dermoid cysts. Furthermore, while some authors question its therapeutic benefit, others believe that serial LPs are not useful in IIH (2,4,7,12). The therapeutic use of serial LPs is based on the theory of increased ICP and compressed intracranial venous sinuses. However, considering the CSF production rate, a daily withdrawal of a few milliliters of CSF will not interrupt the vicious cycle because it will be reproduced within minutes (29).

Because oral medications require more time to act and serial LPs are ineffective, ELD was considered to continuously drain more CSF under sterile conditions and monitor the ICP. Continuous ICP monitoring helps adjust the CSF drainage rate. None of the patients in our study developed hemorrhagic, infectious, or neurological complications, and all patients demonstrated significant improvement in the ICP and OCT-RNFL thickness values. Including the patients who developed relapses, none of the participants experienced worsening visual functions. After retrospectively evaluating the results of four patients who underwent LPS surgery, we propose that discordant changes in ICP and RNFL thickness values may be an indication for LPS surgery.

Studies on ELD use in pediatric IIH are limited. Furthermore, in these studies, ELD was only used in patients in whom oral medications failed, which was associated with worsening papilledema and/or visual functions (7,10,14). Compared with previous studies that used oral medications alone, we used a combination of oral medications and ELD to enhance resolution of papilledema and ICP reduction (21,26). Our findings suggests that early intervention with ELD, rather than waiting for medication failure, may better preserve visual function in pediatric patients. Moreover, the use of OCT allowed us to objectively monitor the resolution of papilledema, which may have been missed with fundus examination alone

The results of our study demonstrate that the combination of ELD and oral medication was effective in achieving a rapid reduction in the ICP and RNFL thickness. This is particularly significant because prolonged elevated ICP can cause irreversible optic nerve damage. In our cohort, we observed a marked decrease in both ICP and RNFL thickness after ELD, which persisted over the short-term follow-up. This finding aligns with those of previous studies, which also demonstrated the effectiveness of ELD in lowering ICP and protecting against optic nerve damage in patients with IIH (7).

The difference in the follow-up duration between patients who required an LPS and those who did not is notable. Patients without LPS tended to have a shorter follow-up period, because their condition stabilized with the combined ELD and medication approach. This may indicate a faster remission. However, the short follow-up period limits our ability to assess the long-term outcomes such as recurrence of papilledema or elevated ICP. Patients 10 and 11, with notably shorter follow-up periods of 2 months, did not experience a recurrence. However, long-term observation is required to verify the sustained remission. The short follow-up period and considerably small sample size are limitations of the study.

CONCLUSION

Proactive ELD use is an effective method to achieve a rapid decrease in ICP and RNFL thickness with no major complications. Thus, we propose combining ELD with oral medications as a first-line treatment option in pediatric patients with IIH in whom ICP values are more than 300 mmH_2O.

Declarations

Funding: This research did not receive any specific grant from funding agencies in the public, commercial, or not-for-profit sectors.

Availability of data and materials: The datasets generated and/or analyzed during the current study are available from the corresponding author by reasonable request.

Disclosure: The authors declare no competing interests.

AUTHORSHIP CONTRIBUTION

Study conception and design: BT, MMO

Data collection: BT, UI, MAT

Analysis and interpretation of results: BT

Draft manuscript preparation: BT

Critical revision of the article: MMO

All authors (BT, MAT, UI, MMO) reviewed the results and approved the final version of the manuscript.

REFERENCES

1. Bassan H, Berkner L, Stolovitch C, Kesler A: Asymptomatic idiopathic intracranial hypertension in children. Acta Neurol Scand 118:251-255, 2008. https://doi.org/10.1111/j.1600-0404.2008.01007.x
2. Bradshaw P: Benign intracranial hypertension. J Neurol Neurosurg Psychiatry 19:28-41, 1956. https://doi.org/10.1136/jnnp.19.1.28
3. Brazis PW: Clinical review: The surgical treatment of idiopathic pseudotumour cerebri (idiopathic intracranial hypertension). Cephalalgia 28:1361-1373, 2008. https://doi.org/10.1111/j.1468-2982.2008.01778.x
4. Brazis PW: Pseudotumor cerebri. Curr Neurol Neurosci Rep 4:111-116, 2004. https://doi.org/10.1007/s11910-004-0024-6
5. Bundak R, Furman A, Gunoz H, Darendeliler F, Bas F, Neyzi O: Body mass index references for Turkish children. Acta Paediatr 95:194-198, 2006. https://doi.org/10.1080/08035250500334738
6. Corbett JJ, Savino PJ, Thompson HS, Kansu T, Schatz NJ, Orr LS, Hopson D: Visual loss in pseudotumor cerebri. Follow-up of 57 patients from five to 41 years and a profile of 14 patients with permanent severe visual loss. Arch Neurol 39:461-474, 1982. https://doi.org/10.1016/0002-9394(82)90332-4
7. Dotan G, Hadar Cohen N, Qureshi HM, Shapira Rootman M, Nevo Y, Kershenovich A: External lumbar drainage in progressive pediatric idiopathic intracranial hypertension. J Neurosurg Pediatr 28:490-496, 2021. https://doi.org/10.3171/2021.2.PEDS2143
8. Friedman DI, Liu GT, Digre KB: Revised diagnostic criteria for the pseudotumor cerebri syndrome in adults and children. Neurology 81:1159-1165, 2013. https://doi.org/10.1212/WNL.0b013e3182a55f17
9. Gaier ED, Heidary G: Pediatric idiopathic intracranial hypertension. Semin Neurol 39:704-710, 2019. https://doi.org/10.1055/s-0039-1698743
10. Gates P, McNeill P: A possible role for temporary lumbar drainage in the management of idiopathic intracranial hypertension. Neuroophthalmology 40:277-280, 2016. https://doi.org/10.1080/01658107.2016.1220954
11. Goodwin CR, Elder BD, Ward A, Orkoulas-Razis D, Kosztowski TA, Hoffberger J, Moghekar A, Radvany M, Rigamonti D: Risk factors for failed transverse sinus stenting in pseudotumor cerebri patients. Clin Neurol Neurosurg 127:75-78, 2014. https://doi.org/10.1016/j.clineuro.2014.09.015
12. Greer M: Benign intracranial hypertension. Vi. Obesity. Neurology 15:382-388, 1965. https://doi.org/10.1212/WNL.15.4.382
13. Inger HE, McGregor ML, Jordan CO, Reem RE, Aylward SC, Scoville NM, Bai S, Rogers DL: Surgical intervention in pediatric intracranial hypertension: Incidence, risk factors, and visual outcomes. J AAPOS 23:96.e1-96.e7, 2019. https://doi.org/10.1016/j.jaapos.2018.11.006
14. Jiramongkolchai K, Buckley EG, Bhatti MT, Muh CR, Wiggins RE, Jiramongkolchai P, El-Dairi MA: Temporary lumbar drain as treatment for pediatric fulminant idiopathic intracranial hypertension. J Neuroophthalmol 37:126-132, 2017. https://doi.org/10.1097/WNO.0000000000000457
15. Mallery RM, Friedman DI, Liu GT: Headache and the pseudotumor cerebri syndrome. Curr Pain Headache Rep 18:446, 2014. https://doi.org/10.1007/s11916-014-0446-z
16. Rabinowicz IM, Ben-Sira I, Zauberman H: Preservation of visual function in papilloedema observed for 3 to 6 years in cases of benign intracranial hypertension. Br J Ophthalmol 52:236-241, 1968. https://doi.org/10.1136/bjo.52.3.236
17. Reid JE, Reem RE, Aylward SC, Rogers DL: Sixth nerve palsy in paediatric intracranial hypertension. Neuroophthalmol 40:23-27, 2016. https://doi.org/10.3109/01658107.2015.1117498
18. Rekate HL: Pathogenesis of hydrocephalus in achondroplastic dwarfs: A review and presentation of a case followed for 22 years. Childs Nerv Syst 35:1295-1301, 2019. https://doi.org/10.1007/s00381-019-04227-8
19. Rosman NP, Shands KN: Hydrocephalus caused by increased intracranial venous pressure: A clinicopathological study. Ann Neurol 3:445-450, 1978. https://doi.org/10.1002/ana.410030516
20. Schade RP, Schinkel J, Visser LG, Van Dijk JM, Voormolen JH, Kuijper EJ: Bacterial meningitis caused by the use of ventricular or lumbar cerebrospinal fluid catheters. J Neurosurg 102:229-234, 2005. https://doi.org/10.3171/jns.2005.102.2.0229
21. Schoeman JF: Childhood pseudotumor cerebri: Clinical and intracranial pressure response to acetazolamide and furosemide treatment in a case series. J Child Neurol 9:130-134, 1994. https://doi.org/10.1177/088307389400900205
22. Skau M, Yri H, Sander B, Gerds TA, Milea D, Jensen R: Diagnostic value of optical coherence tomography for intracranial pressure in idiopathic intracranial hypertension. Graefes Arch Clin Exp Ophthalmol 251:567-574, 2013. https://doi.org/10.1007/s00417-012-2039-z

23. Solanki GA, Alden TD, Burton BK, Giugliani R, Horovitz DD, Jones SA, Lampe C, Martin KW, Ryan ME, Schaefer MK, Siddiqui A, White KK, Harmatz P: A multinational, multidisciplinary consensus for the diagnosis and management of spinal cord compression among patients with mucopolysaccharidosis VI. Mol Genet Metab 107:15-24, 2012. https://doi.org/10.1016/j.ymgme.2012.07.018
24. Steinbok P, Hall J, Flodmark O: Hydrocephalus in achondroplasia: The possible role of intracranial venous hypertension. J Neurosurg 71:42-48, 1989. https://doi.org/10.3171/jns.1989.71.1.0042
25. Sugerman HJ, Felton WL, 3rd, Sismanis A, Kellum JM, DeMaria EJ, Sugerman EL: Gastric surgery for pseudotumor cerebri associated with severe obesity. Ann Surg 229:634-640; discussion 640-642, 1999. https://doi.org/10.1097/00000658-199905000-00005
26. Tomsak RL, Arysol SN, Bernd FR: Treatment of pseudotumor cerebri with diamox (Acetazolamide). J Clin Neuro-ophthalmol 8:93-98, 1988
27. Troost BT, Sufit RL, Grand MG: Sudden monocular visual loss in pseudotumor cerebri. Arch Neurol 36:440-442, 1979. https://doi.org/10.1001/archneur.1979.00500430070012
28. Wall M, George D: Visual loss in pseudotumor cerebri. Incidence and defects related to visual field strategy. Arch Neurol 44:170-175, 1987. https://doi.org/10.1001/archneur.1987.00520140040015
29. Yasuda T, Tomita T, McLone DG, Donovan M: Measurement of cerebrospinal fluid output through external ventricular drainage in one hundred infants and children: Correlation with cerebrospinal fluid production. Pediatr Neurosurg 36:22-28, 2002. https://doi.org/10.1159/000048344

Turk Neurosurg 35(4):627-635, 2025
DOI: 10.5137/1019-5149.JTN.46875-24.2

Original Investigation

Neuro-Oncology

Received: 07.05.2024
Accepted: 29.10.2024
Published Online: 25.06.2025

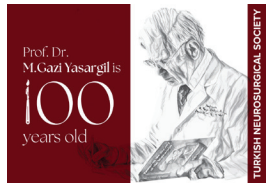

An Ensemble Learning Approach for AI-based Classification of Paraganglioma/ Pheochromocytoma, Low Grade Glioma, and Glioblastoma Tumors

Saliha ACAR[1], Giyasettin OZCAN[2], Eyyup GULBANDILAR[3]

[1]Anadolu University, Computer Research and Application Center, Eskisehir, Türkiye
[2]Bursa Uludag University, Faculty of Engineering, Department of Computer Engineering, Bursa, Türkiye
[3]Eskisehir Osmangazi University, Faculty of Engineering and Architecture, Department of Computer Engineering, Eskisehir, Türkiye

Corresponding author: Saliha ACAR ✉ salihaacar@anadolu.edu.tr

ABSTRACT

AIM: To propose a weighted vote-based ensemble classification method to classify paraganglioma/pheochromocytoma, low-grade glioma, and glioblastoma tumors—conditions that present with similar symptoms—against other central nervous system tumors using clinical and molecular data.

MATERIAL and METHODS: This study utilized clinical and molecular data from The Cancer Genome Atlas database of the United States National Cancer Institute. Initially, categorical variables were transformed into numerical values, and class distribution imbalance was addressed through oversampling. The dataset was split, with 80% used for training across 10 different classical classification algorithms and the remaining 20% reserved for testing. A weighted vote-based ensemble classification algorithm was developed using six classifiers, artificial neural networks, logistic regression, extra trees, random forest, gradient boosting, and extreme gradient boosting, selected for their high classification accuracy. Additionally, feature importance analysis identified the most critical risk factors within the dataset.

RESULTS: The proposed algorithm achieved an accuracy of 90.4% and an area under the receiver operating characteristic curve of 0.968, indicating strong classification performance.

CONCLUSION: The findings from this study suggest that the proposed method could be a valuable tool for supporting treatment planning in central nervous system tumor cases.

KEYWORDS: Central nervous system, Brain tumors, Machine learning, Ensemble classification

INTRODUCTION

Cancer is currently the second leading cause of death globally, following cardiovascular diseases (17). According to the World Cancer Report published by the World Health Organization in 2020, brain and central nervous system cancers were the 17th most common cancer type in 2018, with approximately 297,000 new cases recorded worldwide (Figure 1). The Turkey Cancer Statistics Report by the Ministry of Health indicates that brain and nervous system cancers account for about 2% of all cancer cases across age groups and genders (10). These cancers also rank as the 10th leading cause of cancer-related deaths worldwide (Figure 2) (17).

Gliomas are a type of central nervous system tumor categorized by the World Health Organization into four grades based on histopathological features. Grade 1 gliomas are benign, grow slowly, and have limited spread, while grade 4 gliomas are aggressive and possess metastatic characteristics (15). Gliomas represent nearly 80% of all primary malignant brain tumors, with glioblastoma, a grade 4 tumor, comprising more than 60% of all brain tumors in adults (18).

Saliha ACAR : 0009-0005-9973-4980 Giyasettin OZCAN : 0000-0002-1166-5919 Eyyup GULBANDILAR : 0000-0001-5559-5281

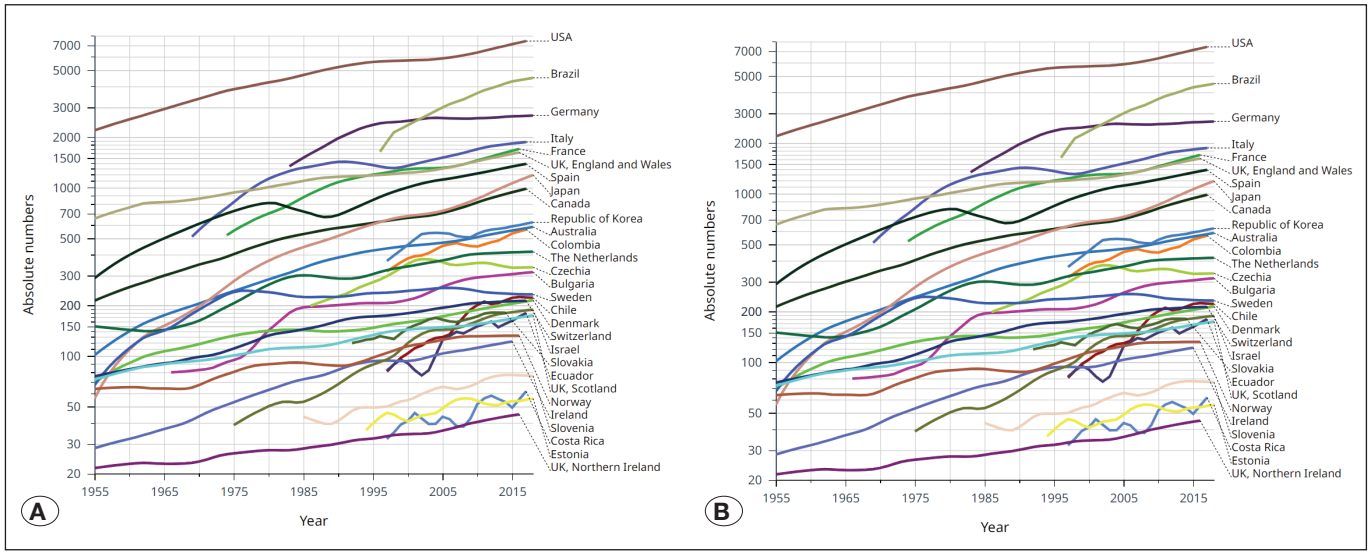

Figure 1: Incidence of brain and other central nervous system cancers **A)** among women **B)** among men (Source: GLOBOCAN)

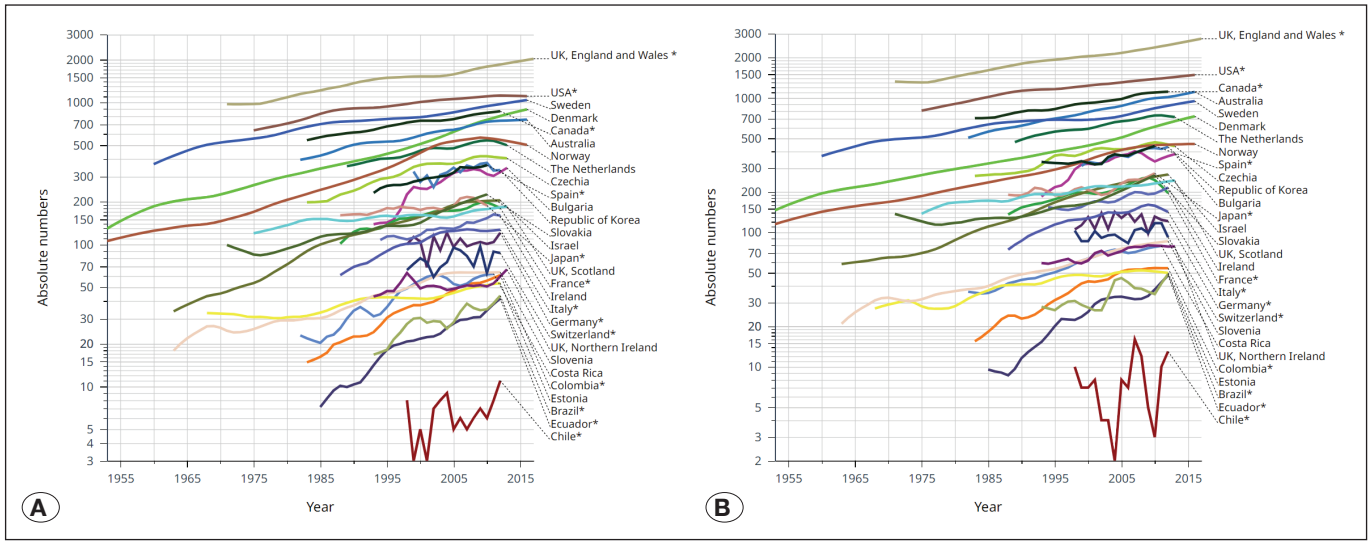

Figure 2: Mortality numbers of brain and other central nervous system cancers **A)** among women **B)** among men (Source: GLOBOCAN).

Paragangliomas are rare neuroendocrine tumors of the nervous system, originating from the adrenal gland or ganglia in various parts of the body. These tumors show significant genetic diversity, with up to 40% of cases linked to germline mutations (16). The molecular pathomechanism of paraganglial tumors remains largely unknown. Pathways, such as activation of the Hypoxia Inducible Factor 1a (HIF1a) related to neoangiogenesis and Ras oncogene activation, are implicated. In head and neck paragangliomas, pseudohypoxia resulting in succinate accumulation due to mitochondrial dysfunction may be a primary mechanism (12). Since the World Health Organization's 4th edition of central nervous system cancer classifications, paragangliomas are no longer classified as benign or malignant, as any lesion may carry metastatic potential, with no definitive features predicting this behavior. Moreover, some tumors are lethal without metastasis due to local invasion involving critical structures (14).

Both gliomas and paragangliomas present with similar symptoms, such as headache, sweating, and tachycardia (10,19). Recently, molecular changes have become increasingly significant in classifying central nervous system tumors; however, clinical features such as age and gender also contribute to tumor grading. Despite this, publicly available datasets often lack sufficient information linking molecular and clinical features that could enhance the value of patient care. Selecting optimal molecular and clinical markers not only reduces healthcare costs and treatment expenses but also helps address growing health inequalities in access to testing. Moreover, this approach improves tumor grading accuracy, allowing for the identification of relevant molecular features for future analysis (18).

A range of treatment options exists for brain and central nervous system tumors. Beyond surgical intervention, treatments

include general radiation therapy, local radiosurgery, and chemotherapy, applied either alone or in combination. Immunotherapy has also emerged as a promising option. However, recent molecular and genetic studies have revealed that glioblastoma (GBM), the most aggressive brain tumor, includes subtypes with unique molecular diagnostic markers that significantly affect patient survival (19). It is now also recognized that paragangliomas, like high-grade tumors, can recur and metastasize (14). Given the similarity in symptoms and affected areas, along with their associated risks, it is essential to distinguish these tumors accurately. The World Health Organization has recently acknowledged that paragangliomas can exhibit aggressive and metastatic behavior, prompting their removal from the category of low-grade central nervous system tumors. Paragangliomas are primarily treated surgically and generally have a higher patient survival rate than gliomas. Thus, determining the tumor type and stage is crucial for effective treatment planning. In this context, further studies on the classification of diverse central nervous system tumors are essential to enhance understanding and improve treatment outcomes.

This study presents a classification method supporting the hypothesis that distinct molecular and clinical data can effectively distinguish paragangliomas from low- and high-grade gliomas. Clinical and mutational datasets from the paraganglioma/pheochromocytoma, low-grade glioma, and glioblastoma projects (TCGA-PGPC, TCGA-LGG, and TCGA-GBM) in The Cancer Genome Atlas (TCGA) database, provided by the US National Cancer Institute, were utilized. To achieve optimal results, the performance of classical machine-learning methods was tested individually, followed by experiments using various combinations of supervised classification models with a weighted voting approach. According to our research, this study is the first classification study that leverages molecular and clinical data to differentiate between paragangliomas and gliomas.

MATERIAL and METHODS

Dataset

This study utilized clinical and molecular data from PGPC, LGG, and GBM, central nervous system tumors with similar symptoms, available in TCGA database by the United States National Cancer Institute (22). The dataset consisted of a total of 1,197 samples across three classes: 0 (PGPC), 1 (LGG), and 2 (GBM). These included 358 samples in the PGPC class, 487 in the LGG class, and 352 in the GBM class.

Each sample was defined by 25 attributes (Table I). Three were clinical attributes, gender, age at diagnosis, and race, while the remaining 22 were molecular attributes related to the tumors. Clinical attributes were transformed into numerical values, and molecular attributes were assigned based on the mutational status of specific genes known to undergo significant mutations in association with these tumors. Each gene was assigned a value of 1 if a mutation was present and 0 if absent.

During preprocessing, records with values such as “not_reported” and “--” in clinical attributes were removed, as they were not expected to contribute to the classification. However, to avoid loss of valuable data in the smaller PGPC class, samples where “Race” was marked as “not_reported” were retained. All samples in the PGPC class, which initially contained fewer records (179) compared to the other classes, were duplicated to reach a total of 358 samples, balancing the dataset.

Proposed Method

Central nervous system tumors account for approximately 1.6% of all human tumors and are among the most complex cancers. Despite their anatomical similarities, these tumors exhibit distinct morphology, etiology, site of origin, molecular biology, and clinical progression (11). Numerous significant prediction and classification studies have been published regarding the grading of nervous system tumors. In this study, we propose a weighted vote-based ensemble classification algorithm for tumor prediction, utilizing clinical and molecular data from PGPC, LGG, and GBM from TCGA database.

Ensemble learning algorithms are among the most effective machine-learning methods in predictive analytics. Ensemble classifiers combine multiple machine-learning algorithms, known as base learners, to create high-accuracy models by integrating several individual classifiers (1).

The proposed weighted vote-based ensemble classification algorithm consists of three stages. In the first stage, the TCGA clinical and molecular dataset is preprocessed. Records with missing data in more than one attribute are eliminated. To address the unbalanced distribution caused by the PGPC class, which contains fewer records (179) than the other classes, all samples belonging to the PGPC class were duplicated, resulting in a total of 358 samples. The data transformations are as follows:

- Age at diagnosis, initially represented as integer values, was converted to floating-point numbers by dividing the total number of days lived by 365.
- Categorical values of the race variable were transformed into integer values ranging from 0 to 3 (White → 0, Black or African American → 1, Asian → 2, American Indian or Alaska Native → 3).
- “Male” values in the gender variable were replaced with 0, while “Female” values were replaced with 1.
- The “Grade” variable, which represents the class label, was assigned the following integer values: 0 for PGPC, 1 for LGG, and 2 for GBM.

These clinical data were then merged with gene mutation status information from the mutation database. Genes with mutations, excluding silent mutations, RNA mutations, and non-coding region mutations, were assigned a value of 1, while those without such mutations were assigned a value of 0. At this stage, driver genes known to be most frequently mutated in the relevant central nervous system tumor types, along with other genes believed to have a differential effect, were selected as attributes.

Table I: Clinical and Molecular Attributes and Value Ranges of TCGA Central Nervous System Tumors

#	Attribute Name	Type	Value Range (or Values)
1	Grade	Class	0 (PCPG) – 1 (LGG) – 2 (GBM)
2	Gender	Clinical	0 (Male) – 1 (Female)
3	Age_at_diagnosis	Clinical	14,42 – 89,29
4	Race	Clinical	0 (White) – 1 (Black or African American) – 2 (Asian) – 3 (American Indian or Alaska Native)
5	IDH1	Molecular	0 (No Mutation) – 1 (Mutation Exists)
6	TP53	Molecular	0 (No Mutation) – 1 (Mutation Exists)
7	ATRX	Molecular	0 (No Mutation) – 1 (Mutation Exists)
8	PTEN	Molecular	0 (No Mutation) – 1 (Mutation Exists)
9	EGFR	Molecular	0 (No Mutation) – 1 (Mutation Exists)
10	CIC	Molecular	0 (No Mutation) – 1 (Mutation Exists)
11	MUC16	Molecular	0 (No Mutation) – 1 (Mutation Exists)
12	PIK3CA	Molecular	0 (No Mutation) – 1 (Mutation Exists)
13	NF1	Molecular	0 (No Mutation) – 1 (Mutation Exists)
14	PIK3R1	Molecular	0 (No Mutation) – 1 (Mutation Exists)
15	FUBP1	Molecular	0 (No Mutation) – 1 (Mutation Exists)
16	RB1	Molecular	0 (No Mutation) – 1 (Mutation Exists)
17	NOTCH1	Molecular	0 (No Mutation) – 1 (Mutation Exists)
18	BCOR	Molecular	0 (No Mutation) – 1 (Mutation Exists)
19	CSMD3	Molecular	0 (No Mutation) – 1 (Mutation Exists)
20	SMARCA4	Molecular	0 (No Mutation) – 1 (Mutation Exists)
21	GRIN2A	Molecular	0 (No Mutation) – 1 (Mutation Exists)
22	IDH2	Molecular	0 (No Mutation) – 1 (Mutation Exists)
23	FAT4	Molecular	0 (No Mutation) – 1 (Mutation Exists)
24	PDGFRA	Molecular	0 (No Mutation) – 1 (Mutation Exists)
25	HRAS	Molecular	0 (No Mutation) – 1 (Mutation Exists)
26	TTN	Molecular	0 (No Mutation) – 1 (Mutation Exists)

In the second stage, classification was performed using ten different classifiers: neural network (NN), logistic regression (LR), extra trees (ET), random forest (RF), naive Bayes (NB), k-nearest neighbors (KNN), support vector machine (SVM), adaptive boosting (AB), gradient boosting (GB), and extreme gradient boosting (XGB). In the third stage, reclassification was conducted using the weighted vote-based ensemble classification algorithm, which included the six classifiers with the highest accuracy rates.

In the final stage, the accuracy and confusion matrix of the prediction results from the weighted vote-based ensemble classification algorithm were generated, and the results were compared to the performance of the individual classifiers. A flow diagram of the proposed algorithm is presented in Figure 3.

Performance Evaluation Metrics

The performance evaluation of a classification model after the training phase is based on its ability to correctly classify examples in the test set. The number of correctly and incorrectly classified instances can be summarized in a matrix known as the confusion matrix, as shown in Table II (3).

The definitions of the values in this table are as follows:

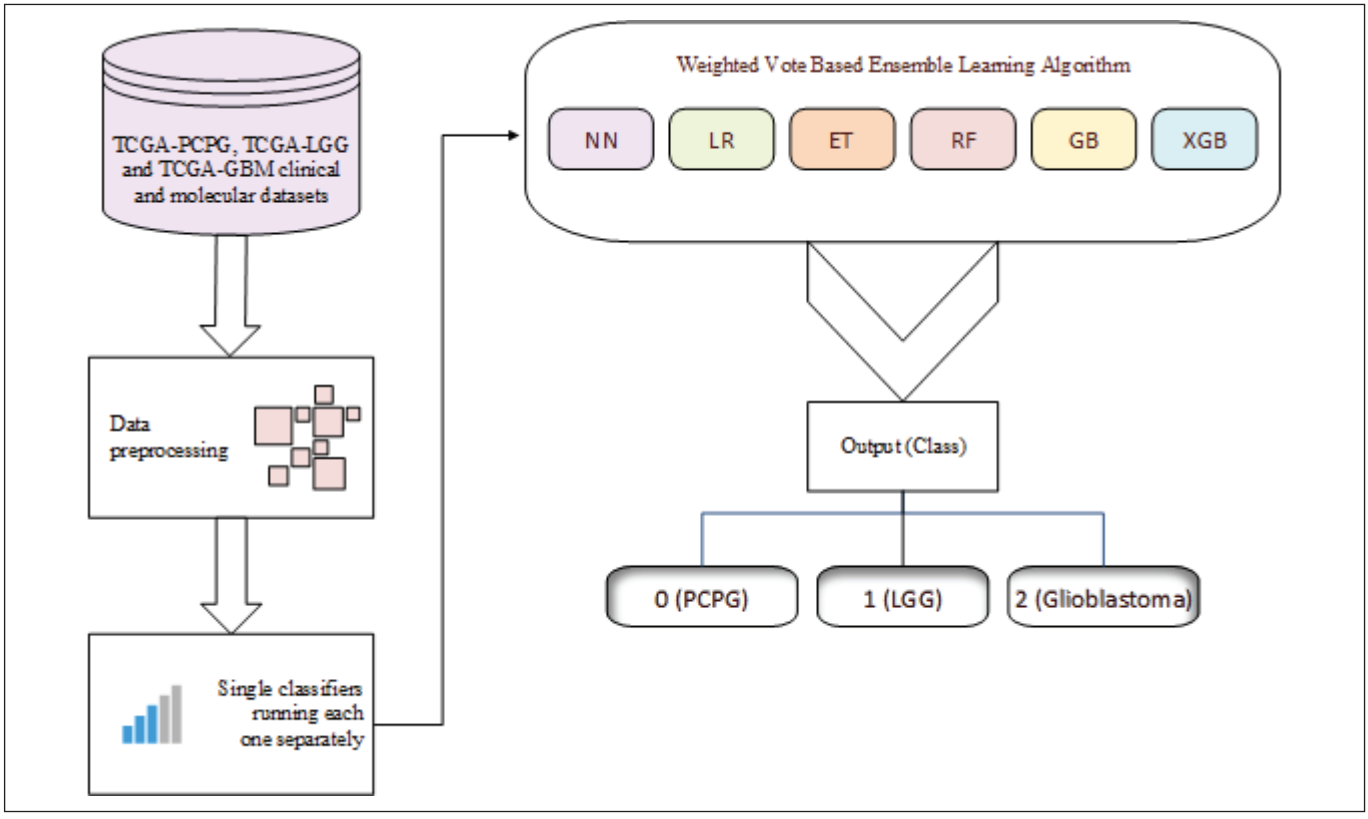

Figure 3: Flow diagram of the proposed classification algorithm.

Table II: Confusion Matrix for Binary Classification

	Predicted: 1	**Predicted: 0**
Actual: 1	TP	FN
Actual: 0	FP	TN

True Positive (TP): The number of samples that are positive (1) and classified as positive.

False Negative (FN): The number of samples that are positive (1) but classified as negative.

False Positive (FP): The number of samples that are negative (0) but classified as positive.

True Negative (TN): The number of samples that are negative (0) and classified as negative.

While the confusion matrix provides general information about the model's performance, various other performance metrics can be derived from it. Accuracy, precision, recall, and F-measure are some of these metrics. Among them, accuracy is one of the simplest and most widely used performance measures, defined as the ratio of correctly classified samples to the total number of samples in the test set. The performance measures for these four metrics are calculated using Equations (1), (2), (3), and (4).

$$\text{Accurarcy (ACC)} = \frac{TP + TN}{TP + TN + FP + FN} \quad (1)$$

$$\text{Recall} = \frac{TP}{TP + FP} \quad (2)$$

$$\text{Precision} = \frac{TP}{TP + FN} \quad (3)$$

$$\text{F - measure} = \frac{2 * Precision * Recall}{Precision + Recall} \quad (4)$$

The F-measure is a hybrid metric designed for evaluating unbalanced classes. The ROC (receiver operating characteristic) curve illustrates the relationship between the false positive rate and the true positive rate at various thresholds. To quantify the effectiveness of this curve, the area under the ROC curve (AUC) or ROC AUC score is calculated. The AUC serves as a measure of separability: the larger the area under the curve, the better the classification algorithm performs in distinguishing between classes (4).

To evaluate the performance of the proposed method alongside classical classification techniques, the performance metrics of accuracy, precision, recall, F-measure, and AUC are employed.

RESULTS

The method proposed in this study, along with the classification techniques used for comparison, was implemented in a Jupyter Notebook environment using the Python programming language on a computer equipped with a 13th Generation Intel Core i9 13900HX processor (2200 MHz), 32 GB of RAM, and a 64-bit Windows 11 Home operating system. The scikit-learn library, known for its extensive user base and comprehensive machine-learning functions, was utilized in the applications.

Figure 4 presents a bar graph illustrating the discriminative importance of the features in the dataset. This graph was generated using the "feature_importances_" function of the RF classifier. As shown in the figure, the mutation status of the IDH1 gene contributes the most to classification success, followed by age at diagnosis and the mutation statuses of the TP53, PTEN, and CIC genes. In the dataset, which comprises a total of 25 attributes, it was observed that reducing the number of attributes through selection negatively impacted classification success. Consequently, all attributes in the dataset were included in the study.

No normalization or standardization was performed on the data. The dataset was divided into training (80%) and testing (20%) subsets. After classifying the data with 10 different single classifiers, the correct classification performances were assessed. The six classifiers with the highest accuracy rates (NN, LR, ET, RF, GB, and XGB) were selected to form an ensemble-based classification structure. The performance comparisons of the proposed weighted vote-based ensemble classification algorithm and the individual classifiers are presented in Table III, while Table IV displays the confusion matrix of the proposed classification algorithm.

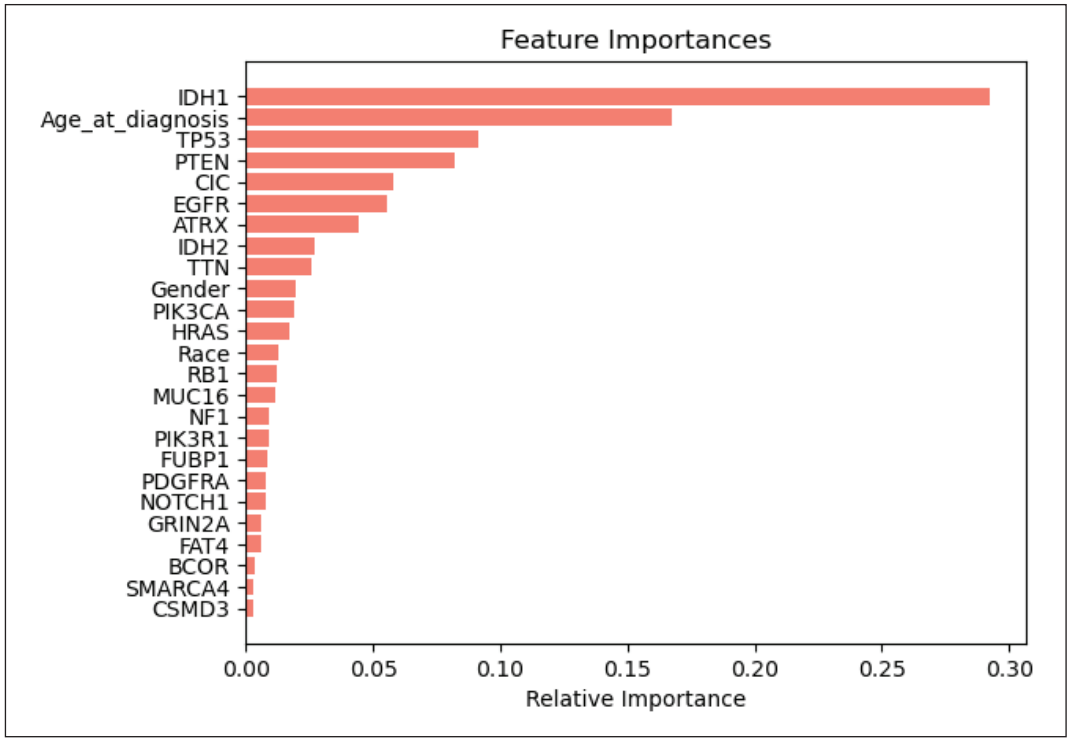

Figure 4: Bar graph showing the importance of the attributes in the dataset.

Table III: Performance Comparison of Individual Classification Algorithms and the Proposed Ensemble-Based Algorithm

	Accuracy	Precision	Recall	F-measure	AUC
Proposed Algorithm	**0.904**	**0.909**	**0.905**	**0.905**	**0.968**
NN	0.888	0.894	0.890	0.890	0.954
LR	0.888	0.894	0.890	0.890	0.956
ET	0.883	0.881	0.884	0.881	0.956
RF	0.875	0.880	0.877	0.875	0.966
GB	0.875	0.878	0.876	0.875	0.957
XGB	0.883	0.883	0.884	0.882	0.966

Table IV: Confusion Matrix of the Proposed Algorithm

	Predicted: 0 (PCPG)	Predicted: 1 (LGG)	Predicted: 2 (GBM)
Actual: 0 (PCPG)	**77**	0	0
Actual: 1 (LGG)	3	**87**	7
Actual: 2 (GBM)	9	4	**53**

Table III demonstrates that the proposed classification algorithm outperforms the individual classifiers in terms of both accuracy and other performance metrics. An examination of the confusion matrix in Table 4 reveals that the algorithm can distinguish the 0-PGPC class with 100% accuracy. However, the accuracy rate for the 2-GBM class decreases to approximately 80%. This trend is consistent across the individual classifiers, indicating that GBM exhibit more complex and heterogeneous characteristics compared to LGG and PGPC. Additionally, the confusion matrix suggests that GBM share more clinical and molecular characteristics with PGPC than with LGG. Nonetheless, the overall performance of the proposed method remains satisfactory, as indicated by the accuracy and F-measure metrics, which are crucial for medical diagnostics.

DISCUSSION

Malignant brain and nervous system tumors are prevalent worldwide and pose significant treatment challenges. Detecting and preventing these tumors at an early stage remains difficult. To aid in early diagnosis, expert systems, artificial intelligence, and machine-learning techniques are increasingly employed to assist healthcare professionals.

Recent advancements in bioinformatics and information technologies have unveiled various molecular and prognostic factors related to central nervous system cancers, enabling researchers to develop diverse classification models. Numerous techniques have been applied in the literature to classify both primary and metastatic brain tumors among various nervous system tumors. For instance, Tasci et al. proposed a hierarchical vote-based ensemble classification model using data from low- and high-grade gliomas sourced from the TCGA and Chinese Glioma Genome Atlas (CGGA) databases. Their results demonstrated accuracy rates of 87.6% and 79.7% on the TCGA and CGGA datasets, respectively (18). Joo et al. classified three tumor types—GBM, central nervous system lymphoma, and brain metastasis—using MRI images with methods such as LASSO, SVM, AdaBoost, and ensemble learning, achieving a classification accuracy of 76.3% with the ensemble learning algorithm (9). Chang et al. utilized convolutional neural networks (CNNs) to predict genetic changes in low- and high-grade gliomas from MRI images, showing that neural networks can yield successful results without necessitating feature selection in image processing. They further enhanced their results by extracting critical features using principal component analysis in the final layer (6). Sarhan's study focused on predicting tumor malignancy from MRI images, achieving an impressive overall classification success of 99.3% by training a dataset that included discriminative features extracted via the Discrete Wavelet Transform algorithm on a CNN (15). Mehrotra et al. also employed MRI images in a transfer learning approach to predict tumor malignancy, achieving 99% accuracy (13). Djirackor et al. presented a model for intraoperative classification of brain tumors, leveraging low-coverage nanopore array and DNA methylation profiles generated through machine-learning algorithms, which resulted in an accuracy of 89% (7). Bathla et al. found that machine-learning and deep-learning algorithms performed comparably in classifying metastatic brain tumors, GBM, and central nervous system lymphoma using MRI data (5). Vidyadharan et al. introduced an ensemble-based machine-learning algorithm utilizing brain images obtained through diffusion tensor imaging to classify low- and high-grade gliomas, achieving 92% sensitivity and 90% specificity (21). In the work of Al-Azwii and Nazarov, a binary classification algorithm demonstrated 96.6% accuracy by training brain image data with an ensemble deep-learning model (2). Similarly, Hossain et al. presented a transfer learning algorithm utilizing various deep-learning architectures on brain MRI images, achieving the highest accuracy rate of 96.94% (8).

A review of the literature reveals that brain tumors are predominantly classified using image data, with success rates that are generally comparable. However, this study takes a different approach by analyzing both molecular and clinical data in a hybrid manner, presenting a multi-class prediction model that includes not only brain tumors but also paragangliomas, which are another type of central nervous system tumor. The inclusion of paragangliomas is significant due to their ability to cause symptoms similar to gliomas and the recent understanding that they can be aggressive and metastatic.

In this study, we introduce a weighted vote-based ensemble classification algorithm that achieves an accuracy of 90.4% for classifying central nervous system tumors, including paragangliomas, LGG, and GBM. These tumors can be diagnosed and treated by specialists in brain and neurosurgery. The classification algorithm presented here aims to assist experts in making informed decisions in the field. The findings suggest that when machine-learning models are trained with the appropriate features, they can effectively facilitate complex, time-consuming, and risky tumor diagnosis procedures.

Despite the promising results, this study has several limitations. First, the data were sourced from a single center's database. Incorporating data from multiple centers would likely yield more accurate and representative results. Second, as the dataset exclusively consists of patients of American origin, the effectiveness of the proposed method may differ among patients of various ethnic backgrounds. Greater ethnic diversity in the data could enhance the generalizability of the findings.

In recent years, the concept has emerged that metabolic reprogramming in cancer cells is an active rather than a passive process. Oncogenes and inactive tumor suppressors directly influence the metabolism of these cells. Altered metabolism in brain and other central nervous system tumors can be utilized for both diagnosis and treatment. Blocking tumor metabolism

as a therapeutic strategy has shown significant promise in preclinical models. However, these studies present substantial challenges due to factors such as blood-brain barrier penetration, the presence of tumor stem cells, tumor heterogeneity, and variations in the microenvironment, all of which may contribute to treatment resistance and tumor recurrence. One potential approach is to block multiple metabolic pathways or to combine metabolic targets with conventional therapies for more effective treatment of these tumors (20).

CONCLUSION

In conclusion, our findings contribute to the development of similar predictive models. This study can be expanded in the future by incorporating various biomedical and molecular data and utilizing a combination of different classification techniques, which could enhance classification success. Furthermore, it can be generalized by including various brain and central nervous system tumors within the system.

Declarations

Funding: This research did not receive any specific grant from funding agencies in the public, commercial, or not-for-profit sectors.

Availability of data and materials: The datasets generated and/or analyzed during the current study are available from the corresponding author by reasonable request.

Disclosure: The authors declare no competing interests.

Ethical statement: Ethical approval is not applicable for this article (https://trdizin.gov.tr/wp-content/uploads/2022/04/TRDizin_etik_ilkeleri_akis_semasi.pdf).

AUTHORSHIP CONTRIBUTION

Study conception and design: SA

Data collection: SA

Analysis and interpretation of results: SA

Draft manuscript preparation: SA

Critical revision of the article: GO

Other (study supervision, fundings, materials, etc...): EG

All authors (SA, GO, EG) reviewed the results and approved the final version of the manuscript.

REFERENCES

1. Akyol K, Karaci A: Diyabet hastaliginin erken asamada tahmin edilmesi icin makine ogrenme algoritmalarinin performanslarinin karsilastirilmasi. Duzce Universitesi Bilim ve Teknoloji Dergisi 9:123-134, 2021. https://doi.org/10.29130/dubited.1014508
2. Al-Azwii ZHN, Nazarov AN: Brain tumor classification based on improved stacked ensemble deep learning methods. Asian Pac J Cancer Prev 24:2141-2148, 2023. https://doi.org/10.31557/APJCP.2023.24.6.2141
3. Almadhoun HR, Abu Naser SS: Detection of brain tumor using deep learning. Int J Acad Eng Rese 6:29-47, 2022
4. Bakir Gungor B, Adanur Dedeturk B, Tasdemir K: Cilt kanseri goruntu siniflandirmasi icin goruntu onislemenin evrisimsel sinir aglari performansi uzerindeki etkileri. Erciyes Universitesi Fen Bilimleri Enstitusu Dergisi 38:190-200, 2022
5. Bathla G, Dhruba DD, Soni N, Liu Y, Larson NB, Kassmeyer BA, Mohan S, Roberts-Wolfe D, Rathore S, Le NH, Zhang H, Sonka M, Priya S: AI-based classification of three common malignant tumors in neuro-oncology: A multi-institutional comparison of machine learning and deep learning methods. J Neuroradiol 51:258-264, 2024. https://doi.org/10.1016/j.neurad.2023.08.007
6. Chang P, Grinband J, Weinberg BD, Bardis M, Khy M, Cadena G, Su MY, Cha S, Filippi CG, Bota D, Baldi P, Poisson LM, Jain R, Chow D: Deep-learning convolutional neural networks accurately classify genetic mutations in gliomas. Am J Neuroradiol 39:1201-1207, 2018. https://doi.org/10.3174/ajnr.A5667
7. Djirackor L, Halldorsson S, Niehusmann P, Leske H, Capper D, Kuschel LP, Pahnke J, Due-Tonnessen BJ, Langmoen IA, Sandberg CJ, Euskirchen P, Vik-Mo EO: Intraoperative DNA methylation classification of brain tumors impacts neurosurgical strategy. Neurooncol Adv 3:vdab149, 2021. https://doi.org/10.1093/noajnl/vdab149
8. Hossain S, Chakrabarty A, Gadekallu TR, Alazab M, Piran MJ: Vision transformers, ensemble model, and transfer learning leveraging explainable AI for brain tumor detection and classification. IEEE J Biomed Health Infor 28:1261-1272, 2023. https://doi.org/10.1109/JBHI.2023.3266614
9. Joo B, Ahn SS, An C, Han K, Choi D, Kim H, Park JE, Kim HS, Lee SK: Fully automated radiomics-based machine learning models for multiclass classification of single brain tumors: Glioblastoma, lymphoma, and metastasis. J Neuroradiol 50:388-395, 2023. https://doi.org/10.1016/j.neurad.2022.11.001
10. Karaca S: Computer-assisted detection of pseudo brain tumors using LSTM deep neural networks on magnetic resonance spectroscopy signals (Unpublished dissertation), Bilecik: Bilecik Şeyh Edebali University, 2020:1-76
11. Kulcu N: Investigation of gene expression changes and pathways that play a role in the progression of glial brain tumors (Unpublished dissertation), Kocaeli: Kocaeli University, 2021:1-131
12. Kusoglu Atalay S: Differential Diagnosis of 'carotid body' paraganglioma and lesions mimicking 'carotid body' paraganglioma (Unpublished dissertation), Ankara: Ankara Yildirim Beyazit University, 2021:1-96
13. Mehrotra R, Ansari MA, Agrawal R, Anand RS: A transfer learning approach for AI-based classification of brain tumors. Machine Learning with Applications 2:100003, 2020. https://doi.org/10.1016/j.mlwa.2020.100003
14. Mete O, Asa SL, Gill AJ, Kimura N, Krijger RR, Tischler A: Overview of the 2022 WHO classification of paragangliomas and pheochromocytomas. Endocrine Pathol 33:90-114, 2022. https://doi.org/10.1007/s12022-022-09704-6
15. Sarhan AM: Brain tumor classification in magnetic resonance images using deep learning and wavelet transform. J Biomed Sci Eng 13:102-112, 2020. https://doi.org/10.4236/jbise.2020.136010

16. Schweizer L, Thierfelder F, Thomas C, Soschinski P, Suwala A, Stichel D, Wefers AK, Wessels L, Misch M, Kim HY, Jödicke R, Teichmann D, Kaul D, Kahn J, Bockmayr M, Hasselblatt M, Younsi A, Unterberg A, Knie B, Walter J, Safatli DA, May SA, Jödicke A, Ntoulias G, Moskopp D, Vajkoczy P, Hepnerr FL, Capper D, Hartmann W, Hartmann C, Deimling AV, Reuss DE: Molecular characterization of CNS paragangliomas identifies cauda equina paragangliomas as a distinct tumor entity. Acta Neuropathologica 140:893-906, 2020. https://doi.org/10.1007/s00401-020-02218-7
17. Siegel RL, Miller KD, Wagle NS, Jemal A: Cancer statistics, 2023. Ca Cancer J Clin 73:17-48, 2023. https://doi.org/10.3322/caac.21763
18. Tasci E, Zhuge Y, Kaur H, Camphausen K, Krauze AV: Hierarchical voting-based feature selection and ensemble learning model scheme for glioma grading with clinical and molecular characteristics. Int J Mol Sci 23:14155, 2022. https://doi.org/10.3390/ijms232214155
19. Tolunay T, Kara F, Keskinkilic B: Turkiye kanser kontrol programi. Ankara: TC Saglik Bakanligi, 2021:511
20. Venneti S, Thompson CB: Metabolic reprogramming in brain tumors. Ann Rev Pathol Mech Dis 12:515-545, 2017. https://doi.org/10.1146/annurev-pathol-012615-044329
21. Vidyadharan S, Rao BVVSNP, Yogeeswari P, Kesavadas C, Rajagopalan V: Accurate low and high grade glioma classification using free water eliminated diffusion tensor metrics and ensemble machine learning. Sci Rep 14:19844, 2024. https://doi.org/10.1038/s41598-024-70627-9
22. Weinstein JN, Collisson EA, Mills GB, Mills Shaw KR, Ozenberger BA, Ellrott K, Shmulevich I, Sander C, Stuart JM: The cancer genome atlas pan-cancer analysis Project. Nat Genet 45:1113-1120, 2013. https://doi.org/10.1038/ng.2764

Turk Neurosurg 35(4):636-643, 2025
DOI: 10.5137/1019-5149.JTN.47938-24.3

Original Investigation

Neuro-Oncology

Received: 25.10.2024
Accepted: 09.04.2025
Published Online: 25.06.2025

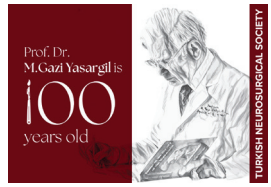

Prediction and Analysis of Risk Factors for Lower Extremity Deep Vein Thrombosis After Craniotomy in Patients with Primary Brain Tumors: A Machine Learning Approach

Lingzhi WU[1]*, Yunfeng ZHAO[1]*, Guangli YAO[2], Xiaojing LI[3], Xiaomin ZHAO[4]

[1]Shanghai Punan Hospital, Department of Respiratory Medicine, Shanghai, China
[2]Shanghai Punan Hospital, Department of B-ultrasound Room of Physical Examination, Shanghai, China
[3]Shanghai Punan Hospital, Department of Nurse, Shanghai, China
[4]Shanghai Punan Hospital GICU, Shanghai, China

*These authors contributed equally to this manuscript

Corresponding author: Xiaomin ZHAO ✉ tjkyc@vip.163.com

ABSTRACT

AIM: To explore the risk factors associated with the occurrence of lower extremity deep vein thrombosis (DVT) after craniotomy in patients with primary brain tumors, and to develop a predictive model using machine learning.

MATERIAL and METHODS: A prospective cohort study was conducted on 140 patients with primary brain tumors who underwent neurosurgical treatment at our hospital between March 2021 and September 2022. A logistic regression analysis was performed to identify independent risk factors associated with postoperative DVT. Additionally, multiple machine learning models were developed and evaluated to determine their predictive performance.

RESULTS: The incidence of lower extremity DVT after craniotomy was 27.9%. Logistic regression identified age [OR=1.07, 95% CI (1.03–1.11)], GCS score [OR=0.88, 95% CI (0.78–0.98)], D-dimer level [OR=1.08, 95% CI (1.02–1.15)], and mechanical ventilation (≥48 hours) [OR=3.83, 95% CI (1.21–12.15)] as independent risk factors ($P<0.05$). The Gradient Boosting Machine (GBM) had the highest prediction accuracy among the assessed machine learning models, achieving an area under the curve (AUC) of 0.850, with a sensitivity of 56.44% and a specificity of 90.09%.

CONCLUSION: Age, D-dimer, and mechanical ventilation (≥48 hours) are independent risk factors for the development of lower extremity DVT after craniotomy in patients with primary brain tumors. The GCS score serves as a potential protective risk factor. The GBM model, with its high AUC and specificity, offers a promising tool for early identification of high-risk patients, potentially informing clinical decision-making and targeted interventions.

KEYWORDS: Brain tumor, Lower extremity, Machine learning, Venous thrombosis

ABBREVIATIONS: DVT: Deep vein thrombosis, **BMI:** Body mass index, **AUC:** Area under the curve, **PE:** Pulmonary embolism, **LR:** logistic regression, **RF:** Random forest, **SVM:** Support vector machine; **GBM:** Gradient boosting machine, **NN:** Neural network, **LDA:** Linear discriminant analysis; **ROC:** Receiver operating characteristic, **GCS:** Glasgow coma scale, **VTE:** venous thromboembolism

Lingzhi WU : 0009-0007-2990-3237
Yunfeng ZHAO : 0009-0000-9059-636X
Guangli YAO : 0009-0000-7064-1311
Xiaojing LI : 0009-0003-9144-2700
Xiaomin ZHAO : 0009-0009-4438-6164

INTRODUCTION

Research has indicated that individuals with primary brain tumors are susceptible to developing deep vein thrombosis (DVT) in their lower limbs. This is mostly attributable to factors such as surgical interventions, lengthy surgical durations, prolonged postoperative bed rest, limb hemiplegia, and hypercoagulable states (6,9,15). DVT is a prevalent and severe vascular condition primarily affecting the deep veins of the lower limbs. The formation of a blood clot, known as a thrombus, in these veins impedes venous blood flow, leading to localized circulation obstruction. Common symptoms encompass swelling, pain, skin discoloration, and varicose veins in the affected limb. If not treated promptly, DVT may result in emboli dislodging and migrating to the pulmonary artery, causing pulmonary embolism (PE), a severe and potentially fatal complication. This is a major contributor to the development of PE. PE is the most severe complication of DVT, manifesting as abrupt chest pain, dyspnea, palpitations, and hypoxemia. In extreme cases, PE can be fatal, with a mortality rate ranging from 9% to 50%, presenting a substantial threat to the patient's life (3,4,10). Research indicates that approximately 50% of PEs are caused by thrombi detaching from the venous wall and passing through the heart to the pulmonary artery (10). Therefore, prompt intervention and preventive measures are essential to reduce the risk of lower extremity DVT in patients with primary brain tumors after craniotomy.

The objective of this study was to identify the risk factors associated with the development of lower extremity deep vein thrombosis (DVT) following craniotomy in patients with primary brain tumors and to develop a predictive model using machine learning techniques. This work seeks to improve the precision of detecting high-risk patients by integrating multiple machine learning models. Early detection and intervention for these patients can diminish the occurrence of DVT, enhance clinical outcomes, and promote improved patient safety and quality of life. The findings of this study provide healthcare professionals with valuable references to guide clinical decision-making and improve postoperative care.

MATERIAL and METHODS

Ethics approval and consent to participate:

All procedures performed in studies were in accordance with the 1964 Helsinki Declaration and its later amendments or comparable ethical standards. Ethical approval for this study was approved by the Ethical Committee of Shanghai Punan Hospital (Approval No. SHSY-IEC-5.0/22K26). All patients gave their written informed consent.

Study Design and Participants

This prospective cohort study included 140 patients with primary brain tumors who underwent craniotomy at the Neurosurgery Department of our hospital between March 2021 and September 2022. Patients were enrolled based on the following inclusion criteria: i. age ≥ 18 years; ii. no thrombi detected by Doppler ultrasound examination of the lower extremities upon admission to the Neurosurgery Department; iii. scheduled for craniotomy for brain tumor resection. Exclusion criteria: i. refusal to participate in the trial; ii. abnormal coagulation function; iii. prior treatment with anticoagulants or thrombus removal before admission; iv. presence of psychiatric disorders.

Collected clinical data included demographic information on gender, age, Body Mass Index (BMI), hypertension, diabetes, Glasgow Coma Scale (GCS), types of brain tumor, duration of stay in the Neurosurgery Department, D-dimer levels on the third day after craniotomy, Caprini score, APACHE II score, mechanical ventilation, deep vein catheterization, muscle strength assessment, presence of infection, and use of vasopressors.

DVT Screening and Diagnosis

All patients received bilateral lower extremity Doppler ultrasound examinations twice a week during hospitalization using the P40 Pro Doppler ultrasound system (SonoScape Medical Corp, P. R. China). DVT was diagnosed based on the following criteria: i. incomplete venous compression under probe pressure; ii. a noticeably enlarged diameter of the thrombosed vein segment, exhibiting varying echo levels from the intraluminal blood clot; iii. color Doppler ultrasound showed color flow imaging during embolization, indicating vein thinning or a lack of blood flow; iv. the pulsed Doppler indicates the absence of a blood flow signal in the thrombus segment, with no respiratory variation observed in the distal thrombus blood flow; v. abnormal Valsalva maneuver.

All Doppler ultrasound diagnoses were performed using P40 Pro (SonoScape Medical Corp, CN) (Figure 1). To ensure diagnostic reliability, all ultrasound examinations were performed by two board-certified radiologists blinded to clinical data.

Statistical Analysis

Data entry was conducted independently by two research nurses and subsequently verified by a third researcher. Continuous variables were expressed as mean ± standard deviation (SD) and assessed using t-tests, whereas categorical variables were denoted as percentages and analyzed with Fisher's exact test or chi-square tests. Univariate logistic regression identified possible risk variables ($p<0.05$), followed by multivariate logistic regression to determine independent predictors, reported as adjusted odds ratios (ORs) with 95% confidence intervals (CIs). Missing data (<5%) were handled by multiple imputation. A significance level of $p<0.05$ was applied, and statistical analyses were performed using Stata 15.0 SE (Texas, USA).

Machine Learning Model Development

Six machine learning algorithms were employed in Orange 3.27.1 (Ljubljana, Slovenia) to construct predictive models for postoperative DVT: logistic regression (LR), random forest (RF), support vector machine (SVM), gradient boosting machine (GBM), neural network (NN), and linear discriminant analysis (LDA). Feature selection was based on clinical relevance and statistical significance, including 10 variables: age, GCS score, APACHE II score, Caprini score, duration of neurosurgical stay (days), D-dimer levels, muscle strength, hypertension,

mechanical ventilation (≥48 hours), and infection. The model's performance was evaluated using 10-fold cross-validation, focusing on metrics such as area under the curve (AUC), classification accuracy, precision (positive predictive value), recall (true positive rate), sensitivity, and specificity.

RESULTS

Comparison of Clinical Data Between Two Groups

This study included a cohort of 140 patients diagnosed with primary brain tumors. Among them, 39 experienced lower extremity DVT, while 101 patients did not develop DVT. The thrombosis group had a markedly higher mean age of 59.51 years in contrast to the non-thrombosis group, which had a mean age of 49.78 years. No significant correlations were found between gender or BMI and the risk of DVT (p=0.5822, p=0.7466, respectively). The thrombosis group exhibited substantially higher values for the APACHE II score (p=0.001), Caprini score (p=0.0367), length of stay in the neurosurgery department (p=0.0066), and D-dimer levels (p=0.0354) compared to the non-thrombosis group. The Glasgow Coma Scale (GCS) score (p=0.0023) was significantly higher in the non-thrombosis group than in the thrombosis group. The thrombosis group had greater proportions of muscle strength ≤3 (p=0.0965), hypertension (p=0.0769), mechanical ventilation (≥48 hours) (p=0.0011), and infection (p=0.0465) compared to the non-thrombosis group. No significant difference in tumor types was noted between the thrombosis and non-thrombosis groups (p=0.697), with gliomas being the predominant tumor type (Table I).

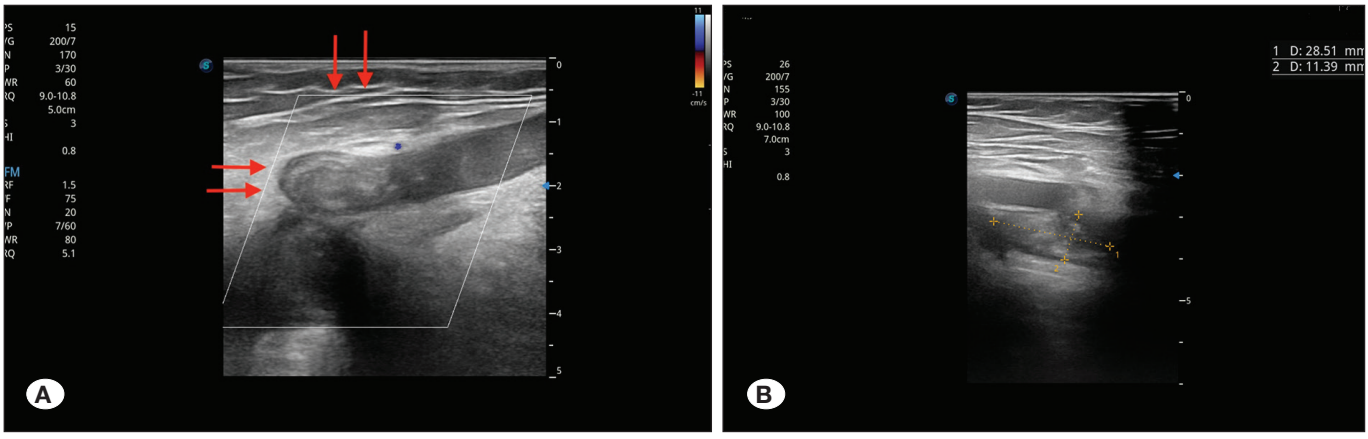

Figure 1: Ultrasound of venous embolism in a 67-year-old female patient. **A)** Color flow Doppler imaging profile image. **B)** Ultrasound transverse profile image.

Table I: Comparison of Clinical Data Between Two Groups

Item	Thrombosis Group (n=39)	Non-thrombosis Group (n=101)	t-value	p-value
Age [years, Mean (SD)]	59.51 (9.74)	49.78 (16.56)	-3.4427	**<0.001**
Gender [n(%)]			-0.5502	0.5822
Male	19 (48.72)	44 (43.56)		
Female	20 (51.28)	57 (56.44)		
GCS score [Mean (SD)]	8.82 (3.89)	11.19 (4.11)	3.1011	**0.0023**
APACHE II score [Mean (SD)]	14.10 (4.75)	10.08 (5.67)	-3.9292	**0.001**
APACHE—II A	3.31 (1.56)	2.25 (1.92)	-3.0830	**0.0025**
APACHE—II B	1.67 (1.27)	1.67 (1.32)	0.0273	0.9783
APACHE—II C	6.18 (3.90)	3.81 (4.10)	-3.1011	**0.0023**
APACHE—II D	2.95 (2.63)	2.39 (2.32)	-1.2411	0.2167
Caprini score [Mean (SD)]	9.82 (2.41)	8.94 (2.13)	-2.1098	**0.0367**
Neurosurgery stay [Mean (SD)]	18.18 (13.30)	11.04 (13.88)	-2.7589	**0.0066**
D-dimer [ug/mL, Mean (SD)]	7.46 (7.97)	4.79 (6.09)	-2.1252	**0.0354**

Table I: Cont.

Item	Thrombosis Group (n=39)	Non-thrombosis Group (n=101)	t-value	p-value
Muscle strength (Medical Research Council Scale) [cases (%)]			1.6622	0.0965
≥4	28 (71.79)	85 (84.16)		
≤3	11 (28.20)	16 (15.84)		
Hypertension [n(%)]			-1.7690	0.0769
Yes	16 (41.03)	26 (25.74)		
No	23 (58.97)	75 (74.26)		
Hyperglycemia [n(%)]			-1.0532	0.2922
Yes	2 (5.13)	11 (10.89)		
No	37 (94.87)	90 (89.11)		
Surgery [n(%)]			0.3079	0.7582
Yes	34 (87.18)	86 (85.15)		
No	5 (12.82)	15 (14.85)		
Central venous catheter [n(%)]			-1.0880	0.2766
Yes	39 (100)	98 (97.03)		
No	0	3 (2.97)		
Hemostatic drugs [n(%)]			1.5158	0.1296
Used	37 (94.87)	100 (99.01)		
Not used	2 (5.13)	1 (0.99)		
Vasopressors [n(%)]			0.8955	0.3705
Used	5 (12.82)	8 (7.92)		
Not used	34 (87.18)	93 (92.08)		
Sedatives/analgesics [n(%)]			1.1345	0.2566
Used	36 (92.31)	86 (85.15)		
Not used	3 (7.69)	15 (14.85)		
Mechanical ventilation (≥48 hours) [n(%)]			3.2758	**0.0011**
Yes	14 (35.90)	12 (11.88)		
No	25 (64.10)	89 (88.12)		
Infection [n(%)]			-1.9910	**0.0465**
Yes	14 (35.90)	20 (19.80)		
No	25 (64.10)	81 (80.2)		

GCS: *Glasgow Coma Scale,* ***APACHE:*** *Acute Physiologic Assessment and Chronic Health Evaluation.*

Univariate Logistic Regression Model

The univariate regression analysis identified several potential risk factors: patient age, APACHE II score, Caprini score, length of stay in the neurosurgery department, D-dimer levels, hypertension, mechanical ventilation (≥48 hours), and infection The GCS score and muscle strength of ≥4 were identified as potential protective factors (Table II).

Table II: Univariate Logistic Regression Model

Item	OR	p-value	95% CI
Age	1.05	**0.002**	(1.02, 1.09)
GCS score	0.87	**0.003**	(0.79, 0.95)
APACHE II score	1.14	**<0.001**	(1.06, 1.23)
Caprini score	1.21	**0.041**	(1.08, 1.45)
Neurosurgery stay	1.03	**0.011**	(1.01, 1.06)
D-dimer	1.06	**0.040**	(1.00, 1.11)
Muscle strength (Medical Research Council Scale)			
≤3	Ref		
≥4	0.24	**0.001**	(0.10, 0.53)
Hypertension			
No	Ref		
Yes	2.01	0.080	(0.92, 4.37)
Mechanical ventilation (≥48 hours)			
No	Ref		
Yes	4.15	**0.002**	(1.70, 10.11)
Infection			
No	Ref		
Yes	2.27	**0.049**	(1.00, 5.13)

GCS: *Glasgow coma scale,* ***APACHE:*** *Acute physiologic assessment and chronic health evaluation.*

Table III: Multivariate Logistic Regression Model

Item	OR	p-value	95% CI
Age	1.07	**0.001**	(1.03, 1.11)
GCS score	0.88	**0.021**	(0.78, 0.98)
D-dimer	1.08	**0.009**	(1.02, 1.15)
Mechanical ventilation (≥48 hours)			
No	Ref		
Yes	3.83	**0.023**	(1.21, 12.15)

GCS: *Glasgow Coma Scale.*

Multivariate Logistic Regression Model

In the multivariate regression model, we observed that the probability of post craniotomy lower extremity DVT increased by 7% for each additional year of patient age. For each one-point reduction in the Glasgow Coma Scale (GCS) score, the risk of lower extremity DVT after craniotomy decreased by 12%. Furthermore, we discovered that the incidence of lower extremity DVT after craniotomy rose by 8% with each unit increase in patient D-dimer (ug/mL) levels. Besides, patients who underwent mechanical ventilation for over 48 hours exhibited a 2.83-fold increased risk of lower extremity DVT post-craniotomy in comparison to those ventilated for less 48 hours (Table III).

The 10-Fold Cross-Validation Performance of the Machine Learning Models

Table IV displays the results of 10-fold cross validation of machine learning models including LR, RF and SVM. It

Table IV: The 10-Fold Cross-Validation Performance of the Machine Learning Models

Model	True Positive	False Positive	True Negative	False Negative	Sensitivity	Specificity	AUC	CA
GBM	22	10	91	17	56.44%	90.09%	0.850	0.807
RF	18	9	92	21	46.15%	91.09%	0.809	0.786
NN	19	11	90	20	48.72%	89.11%	0.781	0.779
LR	17	10	91	22	43.59%	90.09%	0.779	0.771
SVM	13	7	94	26	33.33%	93.07%	0.698	0.764
LDA	19	10	91	20	48.72%	90.09%	0.694	0.786

GBM: *Gradient boosting machine,* ***RF:*** *Random forest,* ***NN:*** *Neural network,* ***LR:*** *Logistic regression,* ***SVM:*** *Support vector machine,* ***LDA:*** *Linear discriminant analysis.*

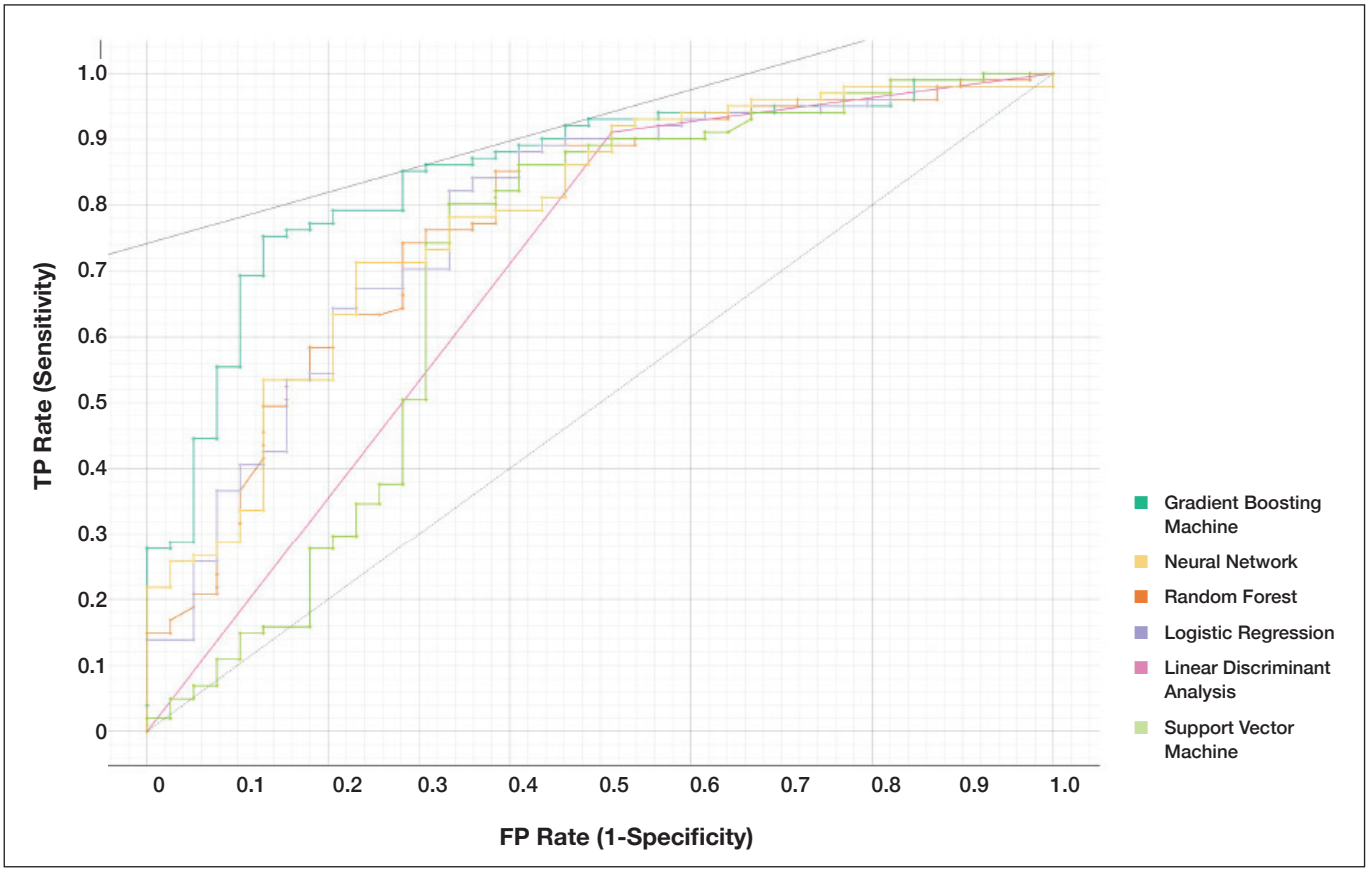

Figure 2: Area under the receiver-operating characteristic curves of machine learning algorithms.

illustrates that all models achieved a specificity of 85%; however, their sensitivity was generally low, with only the Gradient Boosting Machine (GBM) exceeding 50%. The GBM model had the highest AUC (0.850), making it the optimal model in our analysis (Figure 2).

DISCUSSION

This study revealed a 27.9% incidence of lower extremity DVT in patients with primary brain tumors after craniotomy, comparable to the 31.1% incidence reported by Guo et al. (4). Among the 140 patients, those who developed lower extremity DVT were significantly older than those who did not ($p<0.001$). Multivariate analysis indicated that the age (OR=1.07, 95% CI=1.03–1.11) was an independent risk factor for lower extremity DVT in patients with primary brain tumors who had craniotomy. This finding is in line with prior research (3,12). Older patients have heightened vulnerability to DVT due to decreased vascular elasticity, augmented endothelial roughness, weakened muscle pump function, and concomitant diseases such as hypertension, diabetes, and

hyperlipidemia. These factors lead to endothelial damage and elevated levels of various coagulation factors (4,8,11,18).

The study demonstrated a substantial decrease in GCS scores in the DVT group as compared to the non-DVT group ($p<0.002$). Additionally, the multivariate logistic regression model indicated that higher GCS scores (OR=0.88, 95% CI=0.78–0.98) serve as protective factors against lower extremity DVT. This may be attributed to the fact that patients with lower GCS scores are more likely to experience consciousness disorders, limb movement disorders, and prolonged bed rest, leading to slower blood circulation and subsequent DVT development (2). According to literature, D-dimer is a soluble degradation product of cross-linked fibrin generated by the fibrinolytic system, with elevated levels occurring as a result of thrombus fibrinolysis during thrombosis (1). Continuous monitoring of D-dimer levels can signify the patient's hypercoagulable status and act as a sensitive predictor for venous thromboembolism (VTE). Timely recognition of increased D-dimer levels can facilitate the promptly diagnosing DVT in the lower extremities (13,16). Logistic regression analysis in this study identified elevated D-dimer levels (odds ratio=1.040, 95% CI=1.008–1.074) as an independent risk factor for lower extremity DVT. This implies that, in the context of clinical treatment, it is crucial to meticulously monitor D-dimer levels and thoroughly evaluate the results in patients having craniotomy for primary brain tumors. Besides, this study identified mechanical ventilation (≥48 hours) as an independent risk factor for lower extremity DVT after craniotomy. Furthermore, the risk of developing DVT rises with the duration of mechanical ventilation. Prolonged utilization of mechanical ventilation results in extended periods of bed rest and limited physical activity. This leads to a decrease in blood flow rate in the veins of the lower extremities. Moreover, it raises the risk of developing DVT due to potential endothelial damage and a hypercoagulable state. In addition, prolonged mechanical ventilation may result in additional issues such as infection and inflammatory reactions, which further raise the likelihood of DVT occurring (17,19).

In Jin et al.'s study on cancer-related DVT prediction models, logistic regression emerged as the optimal model, but its AUC was relatively low at 0.773 (5). Qiao et al.'s research on major sellar region tumors, linear discriminant analysis (LDA) was reported as the best-performing model (AUC = 0.869) (14). This model is limited in scope, as it only predicts DVT occurrence following surgery in the sellar region and cannot be generalized to brain tumors in other areas (14).

In contrast, our machine learning model offers broader applicability by predicting DVT after craniotomy across various brain tumor types while maintaining high accuracy. However, akin to the models in both Jin et al.'s and Qiao et al.'s studies, our model similarly shows relatively low sensitivity. This issue likely arises from imbalanced datasets, wherein the quantity of non-DVT cases substantially exceeds DVT cases, leading the model to favor the majority class (non-DVT) to enhance overall accuracy. Machine learning models often encounter difficulties with class imbalances, adversely affecting their capacity to reliably predict minority outcomes such as DVT.

The risk prediction model for lower extremity deep vein thrombosis established in this work holds great significance. Neurosurgical intensive care unit (ICU) physicians occasionally refrain from early anticoagulant administration due to the potential risks of new or worsening bleeding in numerous patients. A study on trauma patients revealed that the utilization of anticoagulants resulted in a 13-fold increase in the probability of clot enlargement (7). Currently, there are no conclusive international guidelines for the administration of anticoagulants in neurosurgical ICU patients. This study aims to identify the risk variables associated with DVT in individuals receiving neurosurgery. The objective is to aid physicians in assessing the probability of lower extremity DVT in ICU patients and promptly identifying individuals at elevated risk for proactive anticoagulant therapy.

Nevertheless, this study is subject to specific limitations. First, the sample utilized to examine lower extremities DVT following craniotomy in patients with primary brain tumors was sourced from a single institution (a tertiary hospital in Shanghai), potentially constraining the generalizability of the results. Second, the selection of model features and data quality were constrained by the hospital's records and measurement standards. Although the model emphasizes predictive performance, it may overlook causal relationships and the dynamic nature of DVT risk over time. Third, the potential influence of the surgical team, including variations in surgical techniques, intraoperative management, and postoperative care, was not considered, thus introducing unmeasured confounding. The lack of multi-center validation further restricts the model's applicability to broader populations. Future studies should focus on validating the model with multi-center datasets, integrating new critical factors, amalgamating traditional statistical techniques to improve interpretability, and investigating time-series analyses to identify temporal variations in risk. Acknowledging these limitations will improve the transparency and efficacy of the research.

CONCLUSION

Using logistic regression analysis, our study identified advanced age, GCS score, D-dimer levels, and prolonged mechanical ventilation (≥48 hours) as independent risk factors for lower extremity DVT after craniotomy in patients with primary brain tumors. Furthermore, a machine learning-based model was developed to predict DVT risk. The integration of machine learning enhances predictive accuracy and serves as a valuable tool for early identification of high-risk patients, potentially guiding clinical decision-making and tailored therapies. However, given the study's limitations, including the single-center design, future research should prioritize validating the model with multi-center datasets and exploring other clinical variables to further improve its performance and generalizability.

Declarations

Funding: This work was supported by the construction funding of clinical characteristic discipline of Shanghai Pudong health system (PWYts2021-04), and the key discipline construction project of Shanghai Pudong health system (PWZxk2022-24).

Availability of data and materials: The datasets generated and/or analyzed during the current study are available from the corresponding author by reasonable request.

Disclosure: The authors declare no competing interests.

AUTHORSHIP CONTRIBUTION

Study conception and design: LW, YZ, XL, XZ

Data collection: LW, YZ, XL

Analysis and interpretation of results: LW, YZ, GY, XL, XZ

Draft manuscript preparation: LW, YZ, GY, XL, XZ

Critical revision of the article:

Other (study supervision, fundings, materials, etc...): GY

All authors (LW, YZ, GY, XL, XZ) reviewed the results and approved the final version of the manuscript.

REFERENCES

1. Bockenstedt P: D-dimer in venous thromboembolism. New Engl J Med 349:1203-1204, 2003. https://doi.org/10.1056/NEJMp030084
2. Cole KL, Nguyen S, Gelhard S, Hardy J, Cortez J, Nunez JM, Menacho ST, Grandhi R: Factors associated with venous thromboembolism development in patients with traumatic brain injury. Neurocrit Care 40:568-576, 2024. https://doi.org/10.1007/s12028-023-01780-8
3. Connolly ID, Cole T, Veeravagu A, Popat R, Ratliff J, Li G: Craniotomy for resection of meningioma: An age-stratified analysis of the MarketScan longitudinal database. World Neurosurg 84:1864-1870, 2015. https://doi.org/ 10.1016/j.wneu.2015.08.018
4. Guo F, Shashikiran T, Chen X, Yang L, Liu X, Song L: Clinical features and risk factor analysis for lower extremity deep venous thrombosis in Chinese neurosurgical patients. J Neurosci Rural Pract 6:471-476, 2015. https:// 10.4103/0976-3147.169801
5. Jin S, Qin D, Liang B-S, Zhang LC, Wei XX, Wang YJ, Zhuang B, Zhang T, Yang ZP, Cao YW: Machine learning predicts cancer-associated deep vein thrombosis using clinically available variables. Int J Med Inform 161:104733, 2022. https://doi.org/ 10.1016/j.ijmedinf.2022.104733
6. Kyrle PA, Eichinger S: Deep vein thrombosis. The Lancet 365:1163-1174, 2005. https://doi.org/ 10.1016/S0140-6736(05)71880-8
7. Levy AS, Salottolo K, Bar-Or R, Offner P, Mains C, Sullivan M, Bar-Or D: Pharmacologic thromboprophylaxis is a risk factor for hemorrhage progression in a subset of patients with traumatic brain injury. J Trauma 68:886-894, 2010. https://doi.org/ 10.1097/TA.0b013e3181d27dd5
8. Li Q, Yu Z, Chen X, Wang J, Jiang G: Risk factors for deep venous thrombosis of lower limbs in postoperative neurosurgical patients. Pakistan J Med Sci 32:1107-1112, 2016. https://doi.org/ 10.12669/pjms.325.10481
9. Liu H, Chen X, Wang Z, Liu Y, Liu M: High systemic inflammation response index level is associated with an increased risk of lower extremity deep venous thrombosis: A large retrospective study. Ann Med 55:2249018, 2023. https://doi.org/10.1080/07853890.2023.2249018
10. Meignan M, Rosso J, Gauthier H, Brunengo F, Claudel S, Sagnard L, d'Azemar P, Simonneau G, Charbonnier B: Systematic lung scans reveal a high frequency of silent pulmonary embolism in patients with proximal deep venous thrombosis. Arch Int Med 160:159-164, 2000. https://doi.org/10.1001/archinte.160.2.159
11. Minet C, Potton L, Bonadona A, Hamidfar-Roy R, Somohano CA, Lugosi M, Cartier JC, Ferretti G, Schwebel C, Timsit JF: Venous thromboembolism in the ICU: Main characteristics, diagnosis and thromboprophylaxis. Critical Care 19:1-9, 2015. https://doi.org/ 10.1186/s13054-015-1003-9
12. Prabhakaran K, Gogna S, Lombardo G, Latifi R: Venous thromboembolism in geriatric trauma patients—risk factors and associated outcomes. J Surg Res 254:327-333, 2020. https://doi.org/ 10.1016/j.jss.2020.05.008
13. Pulivarthi S, Gurram MK: Effectiveness of d-dimer as a screening test for venous thromboembolism: An update. North Am J Med Sci 6:491-499, 2014. https://doi.org/10.4103/1947-2714.143278
14. Qiao N, Zhang Q, Chen L, He W, Ma Z, Ye Z, He M, Zhang Z, Zhou X, Shen M: Machine learning prediction of venous thromboembolism after surgeries of major sellar region tumors. Thromb Res 226:1-8, 2023. https://doi.org/ 10.1016/j.thromres.2023.04.007
15. Rethinasamy R, Alias A, Kandasamy R, Raffiq A, Looi MC, Hillda T: Deep vein thrombosis and the neurosurgical patient. Malaysian J Med Sci 26:139-145, 2019. https://doi.org/10.21315/mjms2019.26.5.13
16. Righini M, Perrier A, De Moerloose P, Bounameaux H: D-Dimer for venous thromboembolism diagnosis: 20 years later. J Thromb Haemost 6: 1059-1071, 2008. https://doi.org/10.1111/j.1538-7836.2008.02981.x
17. Tran A, Fernando SM, Rochwerg B, Cook DJ, Crowther MA, Fowler RA, Alhazzani W, Siegal DM, Castellucci LA, Zarychanski R: Prognostic factors associated with development of venous thromboembolism in critically ill patients—a systematic review and meta-analysis. Crit Care Med 50:e370-e381, 2022. https://doi.org/ 10.1097/CCM.0000000000005382
18. Viarasilpa T, Panyavachiraporn N, Marashi SM, Van Harn M, Kowalski RG, Mayer SA: Prediction of symptomatic venous thromboembolism in critically ill patients: The ICU-venous thromboembolism score. Crit Care Med 48:e470-e479, 2020. https://doi.org/ 10.1097/CCM.0000000000004306
19. Wang L, Ma X, Chen Y, Gao S, Pan W, Chen J, Su L, He H, Long Y, Yin C: Factors influencing DVT formation in sepsis. Thromb J 22:11, 2024. https://doi.org/ 10.1186/s12959-024-00582-y

Turk Neurosurg 35(4):644-651, 2025
DOI: 10.5137/1019-5149.JTN.47482-24.2

Original Investigation

Neurotrauma

Received: 24.08.2024
Accepted: 25.10.2024
Published Online: 25.06.2025

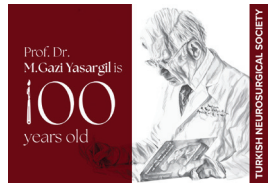

Thromboelastography in Patients with Chronic Subdural Hematoma: A Prospective Pilot Study

Xiaolin DU, Cheng WANG, Rukai JIAO, Xiaopeng DENG, Junquan CHEN, Chengming ZHOU, Kun ZHOU

The Jinyang Hospital Affiliated to Guizhou Medical University, Department of Neurosurgery, 550084, Guiyang, Guizhou Province, China

Corresponding author: Kun ZHOU ✉ zhoukdoct@163.com

ABSTRACT

AIM: To evaluate association between chronic subdural hematoma (CSDH) and thromboelastography (TEG).

MATERIAL and METHODS: A prospective pilot study was conducted on 52 patients with CSDH. The primary outcomes were CSDH severity, recurrence rate, and outcome. The secondary outcome was the association between TEG parameters and the risk factors of CSDH.

RESULTS: The association between the preoperative TEG parameters and the primary outcomes was compared. Results revealed no statistically significant association between the primary outcomes and admission modified Rankin scale score and follow-up GOS score. The R values significantly differed between patients with recurrence and those without (p=0.045). Further subgroup analysis of TEG parameters revealed that patients with R values ≥ 5 had a significantly high incidence of recurrence (1.231, 95% confidence interval [CI]: 0.973–1.557], p=0.025). However, further logistic regression analysis did not reveal significant results (1.198, 95% CI: 0.855–1.680, p=0.293). Moreover, the association between the preoperative TEG parameters and the secondary outcomes was compared. Results revealed a statistically significant association between the secondary outcomes and hematoma thickness and LY30 values (p=0.039), midline shift and Angle (p=0.043), and multiplicity of the hematoma cavity and MA (p=0.022). Further, the secondary outcomes were also significantly associated with postoperative TEG parameters such as multiplicity of the hematoma cavity and LY 30 value (p=0.011) and residual hematoma at follow-up (MA, p=0.001).

CONCLUSION: Due to the small sample size, the efficacy of TEG parameters in predicting CSDH recurrence is unclear. However, TEG parameters are associated with the imaging characteristics of CSDH, and they can also be used to predict the absorption of hematoma. Nevertheless, large-scale prospective cohort studies should be performed to further validate the findings of this study.

KEYWORDS: Chronic subdural hematoma, Thromboelastography, Blood coagulation, Risk factors, Recurrence

ABBREVIATIONS: CSDH: Chronic subdural hematoma, **CI:** Confidence interval, **DM:** Diabetes mellitus, **GOS:** Glasgow Outcome Scale, **IQR:** Interquartile range, **INR:** International normalized ratio, **mRS:** Modified Rankin scale, **OR:** Odds ratio, **PT:** Prothrombin time, **RCT:** Randomized controlled trials, **TEG:** Thromboelastography

INTRODUCTION

Chronic subdural hematoma (CSDH) is a common type of neurosurgical disease in elderly patients, and the incidence of CSDH is increasing annually (11). Thromboelastography (TEG) is a technique that can reflect the dynamic change in blood coagulation. Compared with the conventional methods for coagulation function detection, it can assess the coagulation function of patients more comprehensively and effectively. At present, it is widely used in various clinical aspects such as cardiopulmonary bypass surgery, liver transplantation surgery, traumatic hemorrhagic shock, cardiac

Xiaolin DU : 0000-0001-9587-8323
Cheng WANG : 0009-0001-8942-1818
Rukai JIAO : 0009-0000-8672-9481
Xiaopeng DENG : 0009-0005-8115-6836
Junquan CHEN : 0009-0005-7179-2070
Chengming ZHOU : 0009-0000-8132-3204
Kun ZHOU : 0009-0004-9983-2786

surgery, prediction of risk factors related to the expansion of hypertensive cerebral hemorrhage hematoma, and individualized platelet therapy guidance, which can monitor the coagulation function of patients and guide treatment (12,15,27). However, the possible association between TEG parameters and CSDH is still unclear. The association between TEG parameters and the primary and secondary outcomes of CSDH was compared. The primary outcome was CSDH severity (based on the admission modified Rankin scale [mRS] score), recurrence rate, and prognosis (according to the mRS score and Glasgow Outcome Scale [GOS] score). The secondary outcome was the association between TEG parameters and the risk of CSDH. Relevant papers on the factors associated with CSDH recurrence, which include hematoma multiplicity, hematoma thickness, and degree of midline shift, were examined (16). Thus far, no relevant studies have reported an association between TEG parameters and CSDH.

MATERIAL and METHODS

Patients

The current study was approved by the ethical committee of our institution (approval number: 2021-XM013), and informed consent was obtained from all patients. In total, 60 patients with CSDH underwent surgery from February 2021 to June 2022, and blood samples were collected for TEG before and 3–5 days after emergency surgery. Some patients were excluded due to the following reasons: accidental death during follow-up (n=1), lack of preoperative TEG (n=2), inconsistent detection methods used in TEG (n=2), and unwillingness to return to the hospital for head CT scan after recovering well that resulted in incomplete data (n=3). Finally, 52 patients, including 39 men (75%), 13 women (25%), 1 with preoperative aspirin, 1 treated with preoperative aspirin and clopidogrel, and 1 receiving preoperative warfarin anticoagulation, were examined.

Variables and criteria

The case report form and imaging findings of 52 patients were analyzed. Further, the following parameters were examined: clinical variables – demographic characteristics (sex and age), previous medical history, neurological assessment at admission and discharge (mRS score), and GOS score at the 3-month follow-up (Table I); imaging data – multiplicity of the hematoma cavity, hematoma thickness, and midline shift (Table I); and laboratory data – all TEG parameters, primarily R value, K value, Angle, MA, confidence interval (CI), and LY 30 value (Table I). Head CT scans were performed within 24 h after surgery. Meanwhile, the number of complications in perioperative patients was recorded (Table II).

The inclusion criteria were patients with CSDH confirmed on head CT scan or magnetic resonance imaging, with clear surgical indications. The exclusion criteria were as follows: patients with an acute subdural hematoma and those who underwent craniotomy.

Surgical procedures and general management

The procedure was as follows: All patients underwent emergency surgery within 24 h of admission. The cranium at the thickest part of the CSDH, usually at the parietal tuber of the skull, was perforated. After a dural incision, a silicon drainage tube (Medtronic) was inserted into the subdural hematoma cavity for drainage (no negative pressure drainage), and irrigation was then performed. Air was replaced with saline after skin suture to prevent recurrence (23).

Routine brain CT scan was performed at 1, 3, 9, and 90 days after the surgery. Recurrence was defined as a patient with CSDH who developed another hematoma in the ipsilateral subdural space within 3 months after the initial surgery and developed symptoms requiring re-surgery.

TEG parameters

The TEG device and reagent were produced by Guizhou Jinjiu Biotech Co., Ltd. The TEG parameters were determined in accordance with the reagent instructions. The normal ranges for each parameter were as follows: R value, 5–10 min; K value, 1–3 min; Angle, 53°–72°; MA value, 50–70 min; CI, –3 to 3; and LY30 value, 0%–8%.

Statistical Analysis

Data were assessed independently by double-person and double-computer enrollment and analyzed using the Statistical Package for the Social Sciences software version 23.0. The means ± standard deviation for quantitative data with a normal distribution and two independent sample *t*-tests were used to compare data between groups. Quantitative data with a non-normal distribution were expressed as medians (interquartile ranges, IQR), and the Mann–Whitney *U* test was used for between-group comparisons. Qualitative data (categorical variables) were expressed as frequency and percentage and were compared using the X^2 test or the Fisher's exact test. Linear regression analysis, logistic regression analysis, and subgroup analysis was performed to evaluate the associations between TEG parameters and CSDH. The differences in these tests were statistically significant with $p<0.05$.

RESULTS

This prospective study included 52 patients. In total, 3 (5.8%) patients were classified under the recurrence group (mean age: 77.0 ± 8.0 years; two men/ratio: 66.4%) and 49 under the non-recurrence group (mean age: 67.2 ± 13.6 years; 37 men/ratio: 75.5%). Table I shows the basic clinical data between the two groups.

Each preoperative TEG parameter was a quantitative variable, normal test against the normal distribution. The Mann–Whitney *U* test was used to compare the association between CSDH recurrence and non-recurrence as well as sex, age, hypertension, diabetes mellitus (DM), smoking and trauma history, R value, K value, Angle, MA, CI, and LY 30 value (Table I). Results showed that R values, history of DM, and mRS score at discharge were significantly associated with recurrence (Table I). Further subgroup analyses showed that an R value ≥ 5 and mRS score ≥ 2 at hospital discharge were associated with recurrence, with p values of 0.025 and 0.005, respectively (Table III). However, linear and logistic regression

Table I: Basic Information of the Patients in Two Groups

Variables	No Recurrence	Recurrence	Total	p-value
No. (%)	49 (94.2)	3 (5.8)	52 (100)	
Sex, n (%)				1.000
Male	37 (75.5)	2 (66.7)	39 (75)	
Female	12 (24.5)	1 (33.3)	13 (25)	
Age in yrs, mean ± SD*	67.2 ± 13.6	77.0 ± 8.0	67.8 ± 13.4	0.225
Age group, yrs, n (%)				0.246
≥75	15 (30.6)	2 (66.7)	17 (32.7)	
<75	34 (69.4)	1 (33.3)	35 (67.3)	
Medical history, n (%)				
Hypertension	14 (28.6)	2 (66.7)	16 (30.8)	0.221
Diabetes	1 (2.0)	2 (66.7)	3 (57.7)	0.007[a]
Antithrombotic use, n (%)				1.000
No	46 (93.9)	3 (100)	52 (100)	
Antiplatelet	2 (4.1)	0 (0)	2 (3.8)	
Warfarin	1 (2.0)	0 (0)	1 (1.9)	
Smoking, n (%)	15 (30.6)	0 (0)	15 (28.8)	0.548
Trauma, n (%)	33 (67.3)	3 (100)	36 (69.2)	0.544
Radiological findings, n (%)				
Preop hematoma width ≥ 20 mm	27 (55.1)	0 (0)	27 (51.9)	0.104
Preop hematoma width, median (IQR)	22.0 (11.0)	16	20.4 (10.8)	0.201
Preop midline shift ≥ 10 mm	16 (32.7)	1 (33.3)	16 (30.8)	1.000
Preop midline shift, median (IQR)	7.0 (6.0)	5.0	7.0 (6.0)	0.453
Multiplicity of hematoma cavity	29 (59.2)	3 (100)	32 (61.5)	0.276
Trabecular type, n (%)	23 (46.9)	1 (33.3)	24 (46.2)	1.000
Side of op, n (%)				0.129
Unilat	39 (79.6)	1 (33.3)	40 (76.9)	
Bilat	10 (20.4)	2 (66.7)	12 (23.1)	
Urokinase Instillation	23 (46.9)	1 (33.3)	24 (46.2)	1.000
Drain insertion, n (%)	49 (100)	3 (100)	52 (100)	
Surgical details (continued)				
No. of hours until drain removal, median (IQR)	40.0 (25.5)	40.0 (25.0)	40.0 (25.5)	0.502
Postop pneumocephalus	17 (34.7)	3 (100)	20 (38.5)	0.052
Preop mRS score, mean ± SD*	2.80 ± 1.21	4.00 ± 0.00	2.87 ± 1.21	0.077
mRS score at discharge, mean ± SD*	0.71 ± 0.94	2.00 ± 0.11	0.79 ± 0.96	**0.013**[a]
GOS score, mean ± SD*	4.90 ± 0.31	4.67 ± 0.58	4.88 ± 0.32	0.228
Preop TEG parameters, mean ± SD*				
R	4.5 ± 2.3	6.0 ± 0.8	4.6 ± 2.3	**0.045**[a]
K	2.2 ± 1.4	2.7 ± 0.9	2.2 ± 1.4	0.199
Angle	62.3 ± 11.8	55.5 ± 6.3	61.9 ± 11.7	0.152
MA	57.3 ± 11.7	57.9 ± 7.1	57.3 ± 11.4	0.969
CI	0.4 ± 3.1	-1.5 ± 1.2	0.3 ± 3.1	0.063
LY30	1.6 ± 7.0	0.03 ± 0.06	1.5 ± 6.8	0.596

** Values are expressed as means ± standard deviations.* ***IQR:*** *interquartile range;* [a] *Significant.*

analyses revealed no significant association between R values and mRS score at discharge, with p values of 0.293 and 0.914, respectively (Tables IV and V). Meanwhile, univariate and multivariate logistic regression analyses revealed that patients with DM who developed CSDH significantly differed from those without DM (p=0.007). Moreover, further univariate logistic analysis (0.010, 95% CI: 0.0004–0.234, p=0.004) and multivariate logistic analysis (0.023, 95% CI: 0.001–0.770, p=0.035) indicated significant differences.

Table II: Complications Observed in the Perioperative Period

Complications	No. of Pts
Acute SDH	1
Acute EDH	2
ICH	0
Seizures	0
Subdural empyema	0
Bacterial infection	0
Viral encephalitis	1
Postop pneumocephalus	20

***SDH:** Subdural hematoma; **EDH:** Epidural hematoma; **pts:** Patients; **ICH:** Intracerebral hemorrhage.*

Further, 52 patients who had a follow-up GOS score and good prognosis were included in the analysis, and there was no significant association between the TEG parameters and prognosis (Table VI). This might be attributed to the combined use of postoperative urokinase treatment and oral atorvastatin (2,11).

Table III: Subgroup Analysis of Recurrence of CSDH

Variables	OR	95% CI	p-value
Age group, yrs			
≥75	1.101	0.917-1.322	0.246
≥70	1.047	0.912-1.201	0.603
R group			
≥5	1.231	0.973-1.557	**0.025** [a]
≥4.5	1.143	0.982-1.329	0.092
Preop hematoma width ≥20 mm	0.880	0.761-1.017	0.104
Preop midline shift ≥10 mm	1.002	0.867-1.157	0.704
mRS score at discharge≥2	0.143	0.072-0.284	**0.005** [a]

***OR:** Odds ratio; **CI:** Confidence interval; [a] Significant.*

Table IV: Univariable and Multivariable Logistic Regression Analysis of the Association between CSDH Recurrence and Various Variables

Variables	Univariate Analysis		Multivariate Analysis	
	OR (95% CI)	p-value	OR (95% CI)	p-value
Age≥75	1.079 (0.955-1.218)	0.223	0.071 (0.0004-11.516)	0.309
Sex (Male)	0.649 (0.054-7.802)	0.733	1.056 (0.019-58.923)	0.979
Diabetes (Yes)	0.010 (0.0004-0.234)	**0.004** [a]	0.023 (0.001-0.770)	**0.035** [a]
R	1.198 (0.855-1.680)	0.293	1.469 (0.769-2.803)	0.244
Preop mRS score	3.077 (0.715-13.230)	0.131	4.808 (0.044-529.884)	0.513
GOS score	0.227 (0.019-2.977)	0.259	0.249 (0.005-11.482)	0.477

***OR:** Odds ratio; **CI:** Confidence interval; [a]Significant.*

Table V: Univariable and Multivariable Linear Regression Analyses of the Association between TEG Parameter R Value and Various Variables

Variables	Univariate Analysis		Multivariate Analysis	
	B (95% CI)	p-value	B (95% CI)	p-value
Age	-0.037 (-0.085-0.011)	0.124	-0.037 (-0.086-0.013)	0.140
Drainage time	0.023 (0.002-0.043)	**0.030** [a]	0.021 (0.001-0.042)	**0.043** [a]
mRS score at discharge	-0.037 (-0.723-0.649)	0.914	0.202 (-0.562-0.965)	0.598
GOS score	0.843 (-1.178-2.864)	0.838	0.508 (-1.725-2.742)	0.649

*B, coefficient from linear regression model; **CI:** Confidence interval; [a] Significant.*

Results revealed a significant association between the secondary outcomes and TEG parameters such as sex (R value, p=0.004); K value, p=0.001), Angle (p=0.009), MA (p=0.016), CI (p=0.0004), hematoma thickness and LY30 value (p=0.039), midline shift and Angle (p=0.043), and multiplicity of the hematoma cavity and MA (p=0.022) (Table VI).

The postoperative TEG parameters were measurement data, and the normality test indicated that the R value, K value, and MA did not have a normal distribution, and Angle and CI had a normal distribution. Differences between the two groups were assessed using the Mann–Whitney U test or t-test. The postoperative TEG parameters were not significantly associated with primary outcomes such as preoperative mRs score, recurrence, and prognosis (Table VI). There was a significant comparison between the secondary outcomes and postoperative TEG parameters such as sex (K value, p=0.001; Angle, p=0.026), multiplicity of the hematoma cavity and LY 30 value (p=0.011), and residual hematoma at follow-up (MA, p=0.001).

In addition, the association between R value, K value, Angle, MA, CI, and LY 30 values before and after surgery was compared. Results showed that the K values and CI significantly differed before and after surgery, with *P* values of 0.028 and 0.049, respectively (Table VII).

Table VI: Relationship between TEG Parameters and the Primary and Secondary Outcome Variables

TEGs Variables	median (IQR)or mean ± SD*	Preop mRS score	Recurrence	mRS score at discharge	GOS score	Sex	Hematoma width	Midline shift	Multiplicity of hematoma	Residual hematoma
Preop R	4.3 (2.3)	0.985	**0.045** [a]	0.798	0.367	**0.004** [a]	0.206	0.738	0.792	0.394
Preop K	1.8 (1.1)	0.208	0.199	0.405	0.639	**0.001** [a]	0.851	0.113	0.511	0.985
Preop Angle	63.9 (14.9)	0.535	0.152	0.508	0.148	**0.009** [a]	0.280	**0.043** [a]	0.836	0.697
Preop MA	58.3 (12.3)	0.255	0.969	0.844	0.875	**0.016** [a]	0.657	0.056	**0.022** [a]	0.420
Preop CI	0.3 (2.9)	0.257	0.063	0.915	0.650	**0.0004** [a]	0.407	0.088	0.202	0.542
Preop LY30	0.0 (0.4)	0.591	0.596	0.444	0.304	0.575	**0.039** [a]	0.990	0.728	0.765
Postop R	4.0 (1.9)	0.373	0.979	0.638	0.198	0.462	0.632	0.783	0.836	0.804
Postop K	1.4 (0.9)	0.468	0.422	0.893	0.244	**0.001** [a]	0.894	0.360	0.467	0.353
Postop Angle	67.5 ± 8.8	0.833	0.703	0.901	0.387	**0.026** [a]	0.448	0.755	0.786	0.105
Postop MA	60.5 (10.7)	0.671	0.317	0.961	0.207	0.110	0.105	0.364	0.386	**0.001** [a]
Postop CI	1.2 ± 2.6	0.898	0.398	0.790	0.615	0.172	0.483	0.820	0.745	0.057
Postop LY30	0.5 ± 0.8	0.837	0.459	0.647	0.789	0.591	0.928	0.231	**0.011** [a]	0.965

**Values are expressed as means ± standard deviations or median (IQR); Mann–Whitney analysis or T-test; [a] Significant.*
***R:** Reaction time, **K:** Clot formation time, **MA:** Maximum amplitude, **CI:** Coagulation index , **LY30:** Lysis at 30 minutes.*
***Additional Notes:** K is also termed Fibrin Polymerization Time in some contexts, emphasizing fibrinogen conversion kinetics*

Table VII: Clinical and Biochemical Data of the Patients in Two Groups Comparison of R, K, Angle, Ma, Ci And LY30 before and after Operation

Variables	Preop TEG parameters, mean ± SD*	Postop TEG parameters, mean ± SD*	Total	p-value
R	4.6 ± 2.3	3.8 ± 2.0	4.2 ± 2.2	0.124
K	2.2 ± 1.4	1.9 ± 1.75	2.1 ± 1.5	**0.028** [a]
Angle	61.9 ± 11.7	66.9 ± 10.4	64.1 ± 11.3	**0.038** [a]
MA	57.3 ± 11.4	57.6 ± 13.6	57.5 ± 12.3	0.339
CI	0.3 ± 3.1	1.4 ± 2.4	0.8 ± 2.8	**0.049** [a]
LY30	1.5 ± 6.8	2.9 ± 15.8	2.2 ± 11.6	0.332

**Values are expressed as means ± standard deviations; [a] Significant.*
***R:** Reaction time, **K:** Clot formation time, **MA:** Maximum amplitude, **CI:** Coagulation index , **LY30:** Lysis at 30 minutes.*

DISCUSSION

The bleeding source, pathogenesis, and factors responsible for CSDH recurrence are not well understood. The formation of mixed hematomas may be related to fibrinolytic factors, as reported in the literature (28). Excessively clogged hematomas are believed to be responsible for relapse and progressive enlargement of CSDH. Previous studies have revealed that coagulation factor XIII (FXII) deficiency may play a pathophysiological role in spontaneous CSDH (22). Excessive fibrinolysis and hyperfibrinolysis were observed in CSDH, and a high expression of fibrinogen degradation products (FDPs) was detected in hematomas, with a decrease in the production of coagulation factors II, V, VII, VII, VIII, IX, X, XI, and XII. As reported in the literature (9), the conventional coagulation test parameters APTT, PT, and INR were associated with CSDH severity. This indicates that coagulation dysfunction can be related to CSDH. TEG is a real-time whole-coagulation test that provides dynamic information about total hemostasis. To evaluate the association between TEG parameters and subdural hematoma, no similar studies have been published. We assessed the impact of preoperative demographic and clinical characteristics, imaging findings, postoperative clinical data, imaging data, and recurrence rate at follow-up and outcomes with respect to TEG parameters and CSDH-related factors. Studies have shown that TEG is a rapid, real-time complete coagulation test that may help to predict the severity of CSDH and assess whether the hematoma is well absorbed.

The incidence rate of CSDH recurrence varies with surgical treatment, ranging from 2.3% to 38.7% (16). The risk of coagulation dysfunction recurrence was doubled (14). Of the 52 patients in this group (excluding those with incomplete data), three presented with recurrence, with a recurrence rate of 5.8%. The low recurrence rate in this group may be attributed to the use of urokinase and atorvastatin (2,11). Results showed that patients with a previous history of diabetes may be more likely to relapse. This is probably because hyperglycemia can increase the anaerobic glycolysis of nerve cells in the ischemic area of compressed brain tissues, and then produce high levels of lactic acid, causing a strong oxidative stress response. By contrast, due to the continuous increase in blood glucose levels, patients can maintain higher blood glucose levels, can increase blood viscosity and oxygen levels during brain metabolism, can cause the accumulation of lactate content in the body, enhance the production of vascular endothelial cells due to acidic conditions, promote capillary permeability, and increase the risk of blood leakage in the outer membrane. By contrast, based on previous studies (6,24), lactate levels can increase the production of MMP-3 and MMP-9, which, in turn, disrupts the blood–brain barrier. MMPs may be involved in the angiogenesis of CSDH, causing recurrence (8). Hyperglycemia is a risk factor of CSDH recurrence, which is consistent with previous studies (3,17,25).

The coagulation reaction time (R) refers to the time from the start of the coagulation system to the start of fibrin clot formation. This reflects the comprehensive effect of coagulation factors and the reserve of coagulation factors. A prolonged R value indicates the lack of coagulation factors, hypocoagulability state, and high bleeding risk. On the contrary, it shows the enhanced activity of coagulation factors, hypercoagulability state, and high thrombotic risk. There was a statistically significant difference in terms of R values between the recurrence and nonrecurrence groups. A subgroup analysis revealed that patients with a R value ≥ 5 had a significantly increased recurrence rate. However, further logistics regression analysis did not show statistically significant results. The final results did not significantly differ, which might be caused by the small sample size. Therefore, large-scale case studies should be performed to further validate the efficacy of R values in predicting CSDH recurrence. The author believes that the consumption of coagulation factors and the formation of hematoma can lead to the development of CSDH. Patients without recurrence have a low R value, and the consumption of coagulation factors leads to the hypercoagulability state of the blood. A subgroup analysis showed that an R value ≥ 5 was a risk factor for recurrence, possibly due to the abnormal consumption process of coagulation factors. This mechanism results in the abnormal consumption mechanism of potential coagulation factors, which ultimately affects CSDH recurrence. Nevertheless, further studies must be confirmed to validate our results. In addition, the long retention time of the drainage tube after CSDH will lead to an increased risk of infection, and there was a statistically significant difference between the R value and drainage time. The preoperative R value could predict the retention time of the drainage tube (Table V).

Previous reports in the literature have revealed that stroke is related to coagulation function in both sexes (19). Notably, the TEG parameters are related to sex, which indicates that sex is also a factor affecting the coagulation mechanism of CSDH. Previous studies have found that the preoperative CSDH severity and prognosis were significantly related to the thickness of hematoma, the degree of midline shift, and the multiplicity of hematoma (7,16,26). If the hematoma is thicker and there is a greater midline shift, the condition is more serious. The preoperative LY 30 value was associated with hematoma thickness, the degree of midline shift and Angle value, and hematoma multiplicity and MA value. This indicated that the TEG parameter might indirectly reflect the severity of CSDH. CSDH and postoperative residual hematoma are a risk factor of recurrence (26), and whether the hematoma can be fully absorbed during follow-up is still challenging to predict. Meanwhile, the postoperative MA value can predict whether the complete absorption of hematomas can be achieved within 3 months after surgery. MA is the maximum strength or hardness of reactive blood clots, mainly reflecting the number and function of platelets. This may indicate that blood clots formed by repeated chronic bleeding in CSDH are more rigid and, therefore, more difficult to absorb. Therefore, more studies with a larger sample size should be performed.

Previous studies have revealed that the parameters related to blood routine and traditional coagulation tests are associated with CSDH (1,4,18). Among them, the neutrophil-to-lymphocyte ratio (NLR), peripheral blood eosinophil levels, and serum FDP upon admission were associated with CSDH relapse. Meanwhile, APTT, PT, and INR were associated with the severity of CSDH (9). In addition, differences in fibrinogen

and D-dimer concentrations were observed in different types of CSDH hematoma fluid. These differences were related to CSDH hematoma density (18). Perioperative may affect the coagulation function has been confirmed (13,21), and whether before and after surgery will affect coagulation function in CSDH patients is unclear. Therefore, the association between the pre- and postoperative R, K, Angle, MA, CI, and LY 30 values was compared. Based on this finding, the K and CI values significantly differed before and after surgery. Hence, the CSDH perioperative coagulation status will change.

Previous research has confirmed that plasminogen activator inhibitor type I (PAI-1) deficiency may cause CSDH recurrence (20). Moreover, PAI-1 deficiency can be treated with oral aminohexanic acid to reduce the recurrence rate. Antifibrinolytic drugs can stop bleeding by inhibiting plasminogen activation and plasmin activity. In clinical cases and retrospective studies (5,10), tranexamic acid, as an antifibrinolytic agent, was an effective treatment for CSDH as it promotes hematoma absorption and reducing relapse. However, it was not effective in the treatment of CSDH in other studies. The author hypothesized that this may be related to the influence of cases. In particular, if there is a greater number of patients with hyperfibrinolysis, the treatment seems effective. However, if the number of patients with hyperfibrinolysis is low, the results may appear invalid. Therefore, patients with coagulation-related abnormalities should be further screened. According to the presence of hyperfibrinolysis, individualized medications may be provided to patients with hyperfibrinolysis to reduce hematoma, reduce recurrence. Meanwhile, patients without hyperfibrinolysis should avoid taking tranexamic acid because antifibrinolytic drugs will increase the incidence of thrombosis. Preoperative CT scan imaging density is correlated with LY 30 values, which can reflect the fibrinolytic state. A high LY 30 value increases hyperfibrinolysis. Therefore, further studies with a larger sample size must be conducted to evaluate the association between TEG and subdural hematoma, which can then provide theoretical support for the use of tranexamic acid in CSDH treatment.

Limitations

The current study had several limitations. First, this was a single-center prospective study, with a small sample size and uneven sample distribution. Hence, some bias might have existed, and the ability to demonstrate statistical significance could have been limited. Second, it is challenging to completely unify the follow-up time. The average follow-up time of this group was 3 months. Third, some patients were lost to follow-up, resulting in incomplete clinical data collection. Therefore, a prospective, multicenter clinical trial with a large sample size should be performed to further explore the association between TEG parameters and CSDH.

CONCLUSION

TEG is a rapid, real-time complete coagulation test, and TEG parameters are associated with the risk of CSDH. Due to the small sample size, whether TEG can predict CSDH recurrence was unclear. However, the preoperative LY 30 value, Angle, and MA values are related to hematoma thickness, midline shift degree, and multiplicity of the hematoma cavity, respectively, which may be an indirect indicator of CSDH severity. MA can be a risk factor for poor hematoma absorption in responsive patients. Moreover, the presence of DM is still a risk factor of CSDH recurrence. Therefore, large-scale case studies should be performed to further validate these findings.

ACKNOWLEDGMENTS

We would like to thank Ms.Xiaoli Du for her help with data entry for this study and Bullet Edits Limited for the linguistic editing and proofreading of the manuscript.

Declarations

Funding: This work was supported by the High Level Innovative Talent Support Program for young people of Guiyang Health Committee (Grant No:2021-24).

Availability of data and materials: The datasets generated and/or analyzed during the current study are available from the corresponding author by reasonable request.

Disclosure: The authors declare no competing interests.

AUTHORSHIP CONTRIBUTION

Study conception and design: XD, KZ

Data collection: CW, RJ, XDe, JC, CZ

Analysis and interpretation of results: XD, KZ

Draft manuscript preparation: XD, CW, RJ, XDe, JC, CZ

Critical revision of the article: XD, CW, RJ, XDe, JC, CZ, KZ

Other (study supervision, fundings, materials, etc...): XD, CW, RJ, XDe, KZ

All authors (XD, CW, RJ, XDe, JC, CZ, KZ) reviewed the results and approved the final version of the manuscript.

REFERENCES

1. Chen S, Shao L, Ma L: Peripheral blood eosinophil and classification of residual hematoma help predict the recurrence of chronic subdural hematoma after initial surgery. Front Surg 9:970468, 2022. https://doi.org/10.3389/fsurg.2022.970468.
2. Cheung EYH, Chan DYC, Lee MWY, Hung CY, Pang KY: Urokinase is safe and effective in reducing recurrence in chronic subdural hematoma after burr-hole drainage. World Neurosurg 164:e1209-e1213, 2022. https://doi.org/10.1016/j.wneu.2022.05.143.
3. Chon KH, Lee JM, Koh EJ, Choi HY: Independent predictors for recurrence of chronic subdural hematoma. Acta Neurochir (Wien) 154:1541-1548, 2012. https://doi.org/10.1007/s00701-012-1399-9.
4. de Oliveira AJM, Solla DJF, de Oliveira KF, Amaral BS, Andrade AF, Kolias AG, Paiva WS: Postoperative neutrophil-to-lymphocyte ratio variation is associated with chronic subdural hematoma recurrence. Neurol Sci 43:427-434, 2022. https://doi.org/10.1007/s10072-021-05241-y.
5. de Paula M, Ribeiro BDC, Melo MM, de Freitas PVV, Pahl FH, de Oliveira MF, Rotta JM: Effect of postoperative tranexamic acid on recurrence rate and complications in chronic subdural hematomas patients: Preliminary results of a randomized controlled clinical trial. Neurosurg Rev 46:90, 2023. https://doi.org/10.1007/s10143-023-01991-9.

6. Hafez S, Abdelsaid M, El-Shafey S, Johnson MH, Fagan SC, Ergul A: Matrix metalloprotease 3 exacerbates hemorrhagic transformation and worsens functional outcomes in hyperglycemic stroke. Stroke 47:843-851, 2016. https://doi.org/10.1161/STROKEAHA.115.011258.
7. Han MH, Ryu JI, Kim CH, Kim JM, Cheong JH, Yi HJ: Predictive factors for recurrence and clinical outcomes in patients with chronic subdural hematoma. J Neurosurg 127:1117-1125, 2017. https://doi.org/10.3171/2016.8.JNS16867.
8. Hua C, Zhao G, Feng Y, Yuan H, Song H, Bie L: Role of matrix metalloproteinase-2, matrix metalloproteinase-9, and vascular endothelial growth factor in the development of chronic subdural hematoma. J Neurotrauma 33:65-70, 2016. https://doi.org/10.1089/neu.2014.3724.
9. Idowu OE, Oyeleke SO, Vitowanu JM: Impact of inflammatory cell ratio, biomarkers, activated partial thromboplastin time and prothrombin time on chronic subdural haematoma severity and outcome. Eur J Trauma Emerg Surg 48:1085-1092, 2022. https://doi.org/10.1007/s00068-021-01665-5.
10. Immenga S, Lodewijkx R, Roos Y, Middeldorp S, Majoie C, Willems HC, Vandertop WP, Verbaan D: Tranexamic acid to prevent operation in chronic subdural haematoma (TORCH): Study protocol for a randomised placebo-controlled clinical trial. Trials 23:56, 2022. https://doi.org/10.1186/s13063-021-05907-0.
11. Jiang R, Zhao S, Wang R, Feng H, Zhang J, Li X, Mao Y, Yuan X, Fei Z, Zhao Y, Yu X, Poon WS, Zhu X, Liu N, Kang D, Sun T, Jiao B, Liu X, Yu R, Zhang J, Gao G, Hao J, Su N, Yin G, Zhu X, Lu Y, Wei J, Hu J, Hu R, Li J, Wang D, Wei H, Tian Y, Lei P, Dong JF, Zhang J: Safety and efficacy of atorvastatin for chronic subdural hematoma in chinese patients: A randomized clinicaltrial. JAMA Neurol 75:1338-1346, 2018. https://doi.org/10.1001/jamaneurol.2018.2030.
12. Kawano-Castillo J, Ward E, Elliott A, Wetzel J, Hassler A, McDonald M, Parker SA, Archeval-Lao J, Tremont C, Cai C, Pivalizza E, Rahbar MH, Grotta JC: Thrombelastography detects possible coagulation disturbance in patients with intracerebral hemorrhage with hematoma enlargement. Stroke 45:683-688, 2014. https://doi.org/10.1161/STROKEAHA.113.003826.
13. Leal-Noval SR, Fernandez-Pacheco J, Casado-Mendez M, Cancela P, Narros JL, Arellano-Orden V, Dusseck R, Diaz-Martin A, Munoz-Gomez M: A prospective study on the correlation between thromboelastometry and standard laboratory tests - influence of type of surgery and perioperative sampling times. Scand J Clin Lab Invest 80:179-184, 2020. https://doi.org/10.1080/00365513.2019.1704051.
14. Lee JY, Ebel H, Ernestus RI, Klug N: Various surgical treatments of chronic subdural hematoma and outcome in 172 patients: Is membranectomy necessary? Surg Neurol 61:523-527; discussion 527-528, 2004. https://doi.org/10.1016/j.surneu.2003.10.026.
15. Liu Z, Chai E, Chen H, Huo H, Tian F: Comparison of thrombelastography (TEG) in patients with acute cerebral hemorrhage and cerebral infarction. Med Sci Monit 24:6466-6471, 2018. https://doi.org/10.12659/MSM.910121.
16. Motiei-Langroudi R, Stippler M, Shi S, Adeeb N, Gupta R, Griessenauer CJ, Papavassiliou E, Kasper EM, Arle J, Alterman RL, Ogilvy CS, Thomas AJ: Factors predicting reoperation of chronic subdural hematoma following primary surgical evacuation. J Neurosurg 129:1143-1150, 2018. https://doi.org/10.3171/2017.6.JNS17130.
17. Pang CH, Lee SE, Kim CH, Kim JE, Kang HS, Park CK, Paek SH, Kim CH, Jahng TA, Kim JW, Kim YH, Kim DG, Chung CK, Jung HW, Yoo H: Acute intracranial bleeding and recurrence after bur hole craniostomy for chronic subdural hematoma. J Neurosurg 123:65-74, 2015. https://doi.org/10.3171/2014.12.JNS141189.
18. Park SH, Kang DH, Park J, Hwang JH, Hwang SK, Sung JK, Hamm IS: Fibrinogen and D-dimer analysis of chronic subdural hematomas and computed tomography findings: A prospective study. Clin Neurol Neurosurg 113:272-276, 2011. https://doi.org/10.1016/j.clineuro.2010.11.014.
19. Roy-O'Reilly M, McCullough LD: Sex differences in stroke: The contribution of coagulation. Exp Neurol 259:16-27, 2014. https://doi.org/10.1016/j.expneurol.2014.02.011.
20. Rughani AI, Holmes CE, Penar PL: A novel association between a chronic subdural hematoma and a fibrinolytic pathway defect: Case report. Neurosurgery 64:E1192; discussion E1192, 2009. https://doi.org/10.1227/01.NEU.0000345650.60160.07.
21. Schietroma M, Carlei F, Mownah A, Franchi L, Mazzotta C, Sozio A, Amicucci G: Changes in the blood coagulation, fibrinolysis, and cytokine profile during laparoscopic and open cholecystectomy. Surg Endosc 18:1090-1096, 2004. https://doi.org/10.1007/s00464-003-8819-0.
22. Shim YS, Park CO, Hyun DK, Park HC, Yoon SH: What are the causative factors for a slow, progressive enlargement of a chronic subdural hematoma? Yonsei Med J 48:210-217, 2007. https://doi.org/10.3349/ymj.2007.48.2.210.
23. Shimamura N, Ogasawara Y, Naraoka M, Ohnkuma H: Irrigation with thrombin solution reduces recurrence of chronic subdural hematoma in high-risk patients: Preliminary report. J Neurotrauma 26:1929-1933, 2009. https://doi.org/10.1089/neu.2009.0879.
24. Snarska KK, Bachorzewska-Gajewska H, Kapica-Topczewska K, Drozdowski W, Chorazy M, Kulakowska A, Malyszko J: Hyperglycemia and diabetes have different impacts on outcome of ischemic and hemorrhagic stroke. Arch Med Sci 13:100-108, 2017
25. Song DH, Kim YS, Chun HJ, Yi HJ, Bak KH, Ko Y, Oh SJ: The predicting factors for recurrence of chronic subdural hematoma treated with burr hole and drainage. Korean J Neurotrauma 10:41-48, 2014. https://doi.org/10.5114/aoms.2016.61009.
26. Stanisic M, Pripp AH: A reliable grading system for prediction of chronic subdural hematoma recurrence requiring reoperation after initial burr-hole surgery. Neurosurgery 81:752-760, 2017. https://doi.org/10.1093/neuros/nyx090.
27. Subramanian M, Kaplan LJ, Cannon JW: Thromboelastography-guided resuscitation of the trauma patient. JAMA Surg 154:1152-1153, 2019. https://doi.org/10.1001/jamasurg.2019.3136.
28. Yadav YR, Parihar V, Namdev H, Bajaj J: Chronic subdural hematoma. Asian J Neurosurg 11:330-342, 2016. https://doi.org/10.4103/1793-5482.145102.

Turk Neurosurg 35(4):652-660, 2025
DOI: 10.5137/1019-5149.JTN.49120-25.2

Original Investigation

Neuroanatomy

Received: 11.05.2025
Accepted: 06.06.2025
Published Online: 25.06.2025

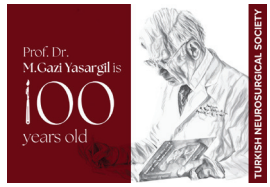

Anatomical Segmentation and Connectivity of the Uncinate Fasciculus

Sevki Serhat BAYDIN[1], Ozan BARUT[1,2], Baris KUCUKYURUK[3], Ozan HASIMOGLU[2,4], Necmettin TANRIOVER[2,3]

[1]Ondokuz Mayis University, Faculty of Medicine, Department of Neurosurgery, Samsun, Türkiye
[2]Cerrahpasa Medical Faculty, Istanbul University – Cerrahpasa, Microsurgical Neuroanatomy Laboratory, Department of Neurosurgery, Istanbul, Türkiye
[3]Cerrahpasa Medical Faculty, Istanbul University - Cerrahpasa, Department of Neurosurgery, Istanbul, Türkiye
[4]Basaksehir Cam and Sakura City Hospital, Department of Neurosurgery, Istanbul, Türkiye

Corresponding author: Sevki Serhat BAYDIN ✉ drsserhatb@gmail.com

ABSTRACT

AIM: To provide a detailed anatomical segmentation of the uncinate fasciculus (UF) and to identify its cortical and subcortical connections using complementary white matter dissection and diffusion-weighted imaging tractography techniques.

MATERIAL and METHODS: Human cadaveric cerebral hemsipheres were used to perform fiber dissections of the UF using the Klingler technique. The tract was anatomically segmented based on its spatial relationships with surrounding structures. In parallel, high-resolution diffusion MRI data from healthy subjects were analyzed using deterministic tractography methods to reconstruct the UF and validate the anatomical segmentation.

RESULTS: Dissection studies revealed three distinct segments of the UF—temporal, insular, and frontal—based on their anatomical trajectories. Tractography findings supported this segmentation and demonstrated specific patterns of connectivity: the temporal segment connected the anterior temporal lobe to the amygdala and insula; the insular segment traversed the limen insulae; and the frontal segment projected to Brodmann areas 10, 11, 47, as well as the anterior cingulate cortex. These findings were consistent across all subjects.

CONCLUSION: This study presents a novel three-segment model of the UF, integrating findings from both dissections and tractography. The identified connectivity patterns enhance our understanding of frontal-temporal network organization and provide valuable insights for neurosurgical approaches and neuropsychiatric research.

KEYWORDS: Uncinate Fasciculus, Uncinate pole, Cingulate pole, Fiber dissection, White matter, Tractography

ABBREVIATIONS: AC: Anterior commissure, **AF:** Arcuate fasciculus, **ALS:** Anterior limiting sulci, **APS:** Anterior perforated substance, **DWI:** Diffusion-weighted imaging, **EC:** External capsule, **IFOF:** Inferior fronto-occipital fasciculus, **ILF:** Inferior longitudinal fasciculus, **ILS:** Inferior limiting sulci, **NAc:** Nucleus accumbens, **SI:** Substantia innominata, **SLF:** Superior longitudinal fasciculus, **SLS:** Superior limiting sulci, **UF:** uncinate fasciculus

Sevki Serhat BAYDIN : 0000-0001-9041-7229
Ozan BARUT : 0000-0001-6572-9589
Baris KUCUKYURUK : 0000-0002-0077-110X
Ozan HASIMOGLU : 0000-0003-1394-5188
Necmettin TANRIOVER : 0000-0001-7628-9443

INTRODUCTION

The uncinate fasciculus (UF), initially described by Johann Christian Reil in 1809 as a "broad band bridging the frontal and temporal lobes," has undergone significant conceptual refinements over time (32). Later, Karl Burdach further characterized it as "curved fibers extending laterally and basally from the frontal region of the external capsule" (32). As a major association pathway linking medial temporal regions to the dorsolateral prefrontal cortex, the UF plays a pivotal role in higher-order cognitive functions, including episodic memory — particularly the encoding of temporal and spatial contexts — as well as in lexical retrieval of semantic knowledge. Beyond its contributions to memory, the UF is fundamental to social and emotional regulation by connecting limbic and paralimbic structures, thus influencing decision-making processes and behavioral control mechanisms (5,8,13,25,33).

Anatomically, the UF constitutes a direct, monosynaptic, long association tract that bridges the frontoorbital cortex with the anterior temporal lobe (10). Despite considerable research efforts, a definitive consensus on the precise cortical terminations of the UF remains elusive (2,14,22). Its central location within the brain's architecture renders it critical for cognitive-emotional integration and implicates it in various neuropsychiatric and developmental disorders (14,32). The fascicle is also frequently interrupted during surgeries in and around the region of insula and the transylvian approaches to the mesial temporal lobe (1,37). The UF is also affected by traumatic brain injuries, owing to its connections with both frontal and temporal regions (17,20).

Given its complex anatomical organization, diverse cortical projections, and prominent clinical relevance, achieving a more refined understanding of the internal architecture of the UF is imperative. Although previous studies have attempted to delineate its segmentation, ambiguities regarding its precise internal structure persist. Accordingly, the present study seeks to advance the anatomical comprehension of the UF by thoroughly analyzing its fiber composition and cortical terminations using complementary methodologies: white matter dissection and diffusion-weighted imaging (DWI) tractography.

MATERIAL and METHODS

Twelve human hemispheres were fixed in a 10% formalin solution for a minimum of two months, following the fixation technique originally described by Klingler (18). Following fixation, the arachnoid mater, pia mater, and vascular structures were removed under a Zeiss surgical microscope (Carl Zeiss AG, Oberkochen, Germany). The specimens were then frozen at -16°C for a minimum of three weeks. Prior to dissection, they were thawed in running tap water for one hour and subsequently stored in a 70% ethanol solution between procedures. Microsurgical dissections were conducted under magnifications ranging from x4 to x40 using a Zeiss surgical microscope and a Rhoton microsurgical instrument set. The fiber dissection proceeded systematically from lateral to medial and from inferior to superior orientations. At each step, the spatial relationships between the UF fibers and surrounding neuroanatomical structures were carefully examined. High-resolution photographs were captured at each stage using a Canon EOS 550D DSLR camera equipped with a fixed 100 mm macro lens, mounted on a professional Manfrotto tripod.

Diffusion tractography was performed utilizing DSI Studio software (http://dsi-studio.labsolver.org) with DWI data derived from the Human Connectome Project, encompassing a cohort of 1065 healthy individuals. A deterministic tractography algorithm was applied, with anisotropy and angular thresholds randomly varied within standardized parameters. A multishell diffusion acquisition strategy was employed with b-values set at 990, 1985, and 2980 s/mm^2. DWI was sampled isotropically at 2.0 mm resolution, with a diffusion sampling length ratio of 1.7. A deterministic tractography algorithm was used for fiber tracking. Only fibers ranging from 10 mm to 200 mm in length were included; shorter or excessively long tracts were excluded. A total of 16 iterations of tract refinement were conducted to eliminate spurious trajectories, ensuring anatomical accuracy in fiber reconstruction.

RESULTS

Lateral to Medial Dissection of the Uncinate Fasciculus: Insular Segmentation and Revealing Insular Relationships

Following periinsular decortication in the left hemisphere, two prominent superficial long association fibers in the periinsular area were revealed. These were the superior longitudinal fasciculus (SLF), which travels above the Sylvian fissure and the insula to provide frontoparietal connections, and the arcuate fasciculus (AF), which surrounds the Sylvian fissure and insula to establish frontotemporal connections (Figure 1A).

Following removal of the opercular association fibers, the anterior, superior, and inferior limiting sulci (ALS, SLS, and ILS) of the insula were clearly identified (Figure 1A, B). The claustrum, located at the apex of the insula, along with the external capsule (EC), was exposed. The EC comprises a dorsal portion formed by claustrocortical fibers and a ventral portion formed by fibers of the UF and the inferior fronto-occipital fasciculus (IFOF). The IFOF courses between the frontal and occipital cortical regions, while the UF provides long-range frontotemporal connectivity (Figures 1A, B; 3A, B) (34).

Based on the boundaries formed by the ALS and ILS, we segmented the UF into frontal, insular, and temporal parts (Table I). The insular segment of the UF is located lateral to the anterior perforated substance (APS) and the substantia innominata (SI), at the level of the limen insula (11,29). This segment forms the lateral boundary of the SI. The anterior boundary of the SI is formed by the internal capsule. Its posterior boundary is formed by the anterior commissure, coursing from anteromedial to posterolateral (Figures 1E, F; 3B, C).

After removal of the ventral AF, located dorsal to the ILS, the IFOF, which coursed toward the sagittal stratum, was visualized along with the fibers of the temporal segment of the UF projecting toward the temporal lobe (Figure 1C, D). The posterior boundary of the insular segment of the UF was defined by the AC and ILS, specifically where the AC and IFOF converge

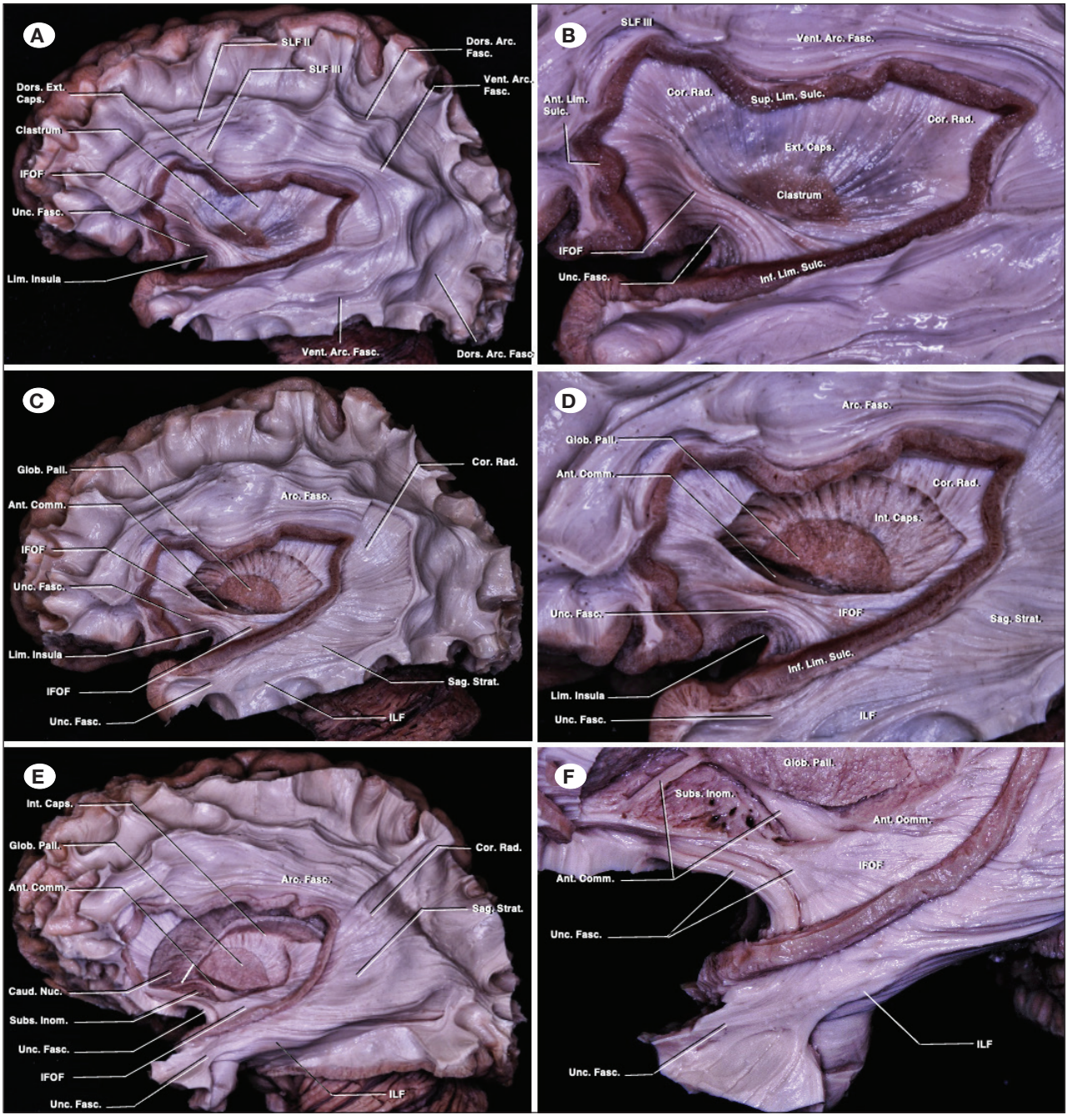

Figure 1: Gradual lateral to medial fiber dissection on the left cerebral hemisphere. **A)** Initial white matter dissection of the periinsular and insular region. SLF II runs between the middle frontal gyrus and the angular gyrus, whereas SLF III courses along the frontoparietal operculum between the pars orbitalis and the supramarginal gyrus. The ventral AF originates from the middle temporal gyrus, passes through the supramarginal gyrus, and projects to the inferior frontal gyrus. In contrast, the dorsal AF begins in the middle and inferior temporal gyri, traverses the angular gyrus, and also projects to the inferior frontal gyrus. **B)** Removal of the opercular cortex reveals the EC, formed dorsally by claustrocortical fibers and ventrally by the IFOF and UF. The claustrum is exposed at the apex of the insula. The dorsal EC, located around the SLS, merges with internal capsule fibers and contributes to the corona radiata by passing deep to the SLF and AF. The main trunks of the UF and IFOF were revealed at the level of the limen insula and the insular apex. **C, D)** With further dissection, the ventral AF has been removed, revealing the IFOF and UF passing beneath the ALS and ILS. The AC, GP, and internal capsule are also identified. Continued dissection exposes the sagittal stratum, showing the IFOF coursing posteriorly and the UF curving anteroinferiorly toward the temporal lobe. **E, F)** The anterior limb of the internal capsule is resected to better visualize the UF trajectory. The posterior limb of the AC and adjacent GP are exposed. The convergence of the AC, UF, and IFOF at the level of the ILS is observed. Deeper structures, including the caudate nucleus, SI, and internal capsule are revealed.

Table I: Anatomical Segmentation and Structural Relationships of the Uncinate Fasciculus (UF)

Segment	Subdivision	Anatomical Boundaries	Neighboring Structures	Cortical Connections / Pathways
Frontal Segment	Anterolateral UF	Lateral to olfactory sulcus	Lateral & posterior orbital gyri, pars orbitalis	Orbitofrontal cortex, anterior insula
	Dorsomedial UF	Medial to olfactory sulcus, beneath medial orbital gyrus	Gyrus rectus, nucleus accumbens, anterior-ventral cingulum	Gyrus rectus, medial orbitofrontal cortex, cingulate pole
Insular Segment	Anterolateral UF	Between ALS and ILS; lateral to substantia innominata	Anterior perforated substance, external capsule, insular apex	Frontal-insular transition zone; contributes to frontotemporal connectivity
	Dorsomedial UF	Medial portion of insular segment, lateral to anterior commissure	Substantia innominata, deep insular white matter	Projects medially toward mesial temporal structures
Temporal Segment	Anterolateral UF	Lateral to collateral sulcus	Temporal pole, inferior longitudinal fasciculus	Temporal pole, inferior temporal gyrus
	Dorsomedial UF	Medial to collateral sulcus	Parahippocampal gyrus, amygdala, cingulum	Amygdala, parahippocampal gyrus; merges with cingulum at the uncinate pole
Uncinate Pole	Convergence zone	Inferolateral to the amygdala	Amygdala, anterior temporal lobe, dorsomedial UF, cingulum bundle	Intersection of cingulum and dorsomedial UF; potential hub for temporolimbic connectivity

ALS: *Anterior limiting sulci,* ***ILS:*** *Inferior limiting sulci.*

into the sagittal stratum. The ALS constituted the boundary between the frontal and insular segments of the UF (Figure 1D), corresponding to the most anterolateral portion of the AC (Figure 1F).

In the lateral dissection, after looping around, the temporal segment of the UF followed an anterolateral course as it traveled with the inferior longitudinal fasciculus (ILF) toward the temporal pole (Figures 1F, 3A). Deep to the SI and IFOF fibers, the dorsomedial UF fibers disappeared toward the mesial temporal area (Figure 1F).

The insular segment of the UF was further divided based on the direction of the fibers. The more lateral group was defined as the anterolateral UF, while the more medial group was defined as the dorsomedial UF (Figure 1D, E, F) (Table I).

Inferior to Superior Dissection of the Uncinate Fasciculus: Frontal and Temporal Segmentation and Revealing the Cingulate and Uncinate Pole

Following decortication of the frontoorbital area, inferior frontal gyrus, and limen insula from the basal surface, the frontal cortical structures were exposed. In the frontoorbital region, composed of the the anterior, lateral, medial, and posterior orbital gyri, was separated from the gyrus rectus via the olfactory sulcus (Figure 2A).

Fibers of the insular segment of the UF extend toward the frontal segment from the deep portion of the ALS, which constitutes the anterior boundary of the limen insula and is ventrally related to the APS. The frontal segment of the UF extends laterally from the olfactory sulcus and distributes in the orbitofrontal cortex anterior to the medial and lateral olfactory striaes. It was observed to have two distinct layers, displaying long anterolateral and short dorsomedial courses (Figures 2A, 2B; 3D). Based on this frontal distribution, the UF was segmented into the anterolateral UF and dorsomedial UF (2).

The anterolateral UF separates from the dorsomedial fibers and projects to the lateral, anterior, and posterior orbital gyri, as well as to the pars orbitalis. The dorsomedial UF turns medially at the frontal base, courses beneath the olfactory sulcus within the medial orbital gyrus, and reaches the gyrus rectus. At the posterior part of the prefrontal cortex, near the septal area, the region referred to by Yasargil as the “cingulate pole” is located (36). Here, the dorsomedial segment of the UF intersects with the ventral extension of the cingulum bundle (Figures 2B; 3E, F, G). Before merging with the cingulum, dorsomedial UF fibers course over the medial and inferior surfaces of the NAc, sending fibers to it (2).

On the inferior surface of the hemisphere, the parahippocampal gyrus, collateral sulcus, and inferior temporal gyrus were dissected (Figure 2). The temporal segment of the UF, turning toward the temporal pole from the depth of the ILS, diverges into the dorsomedial UF medially and anterolateral UF laterally relative to the collateral sulcus. The anterolateral UF fibers that travel lateral to the collateral sulcus terminate in the temporal pole alongside the ILF, which connects the visual areas of the occipital lobe to the inferior temporal gyrus (Figures 1F; 2A, B) (34). Medial to the collateral sulcus, the dorsomedial UF was observed extending toward the parahippocampal gyrus and the amygdala (Figure 2C, D).

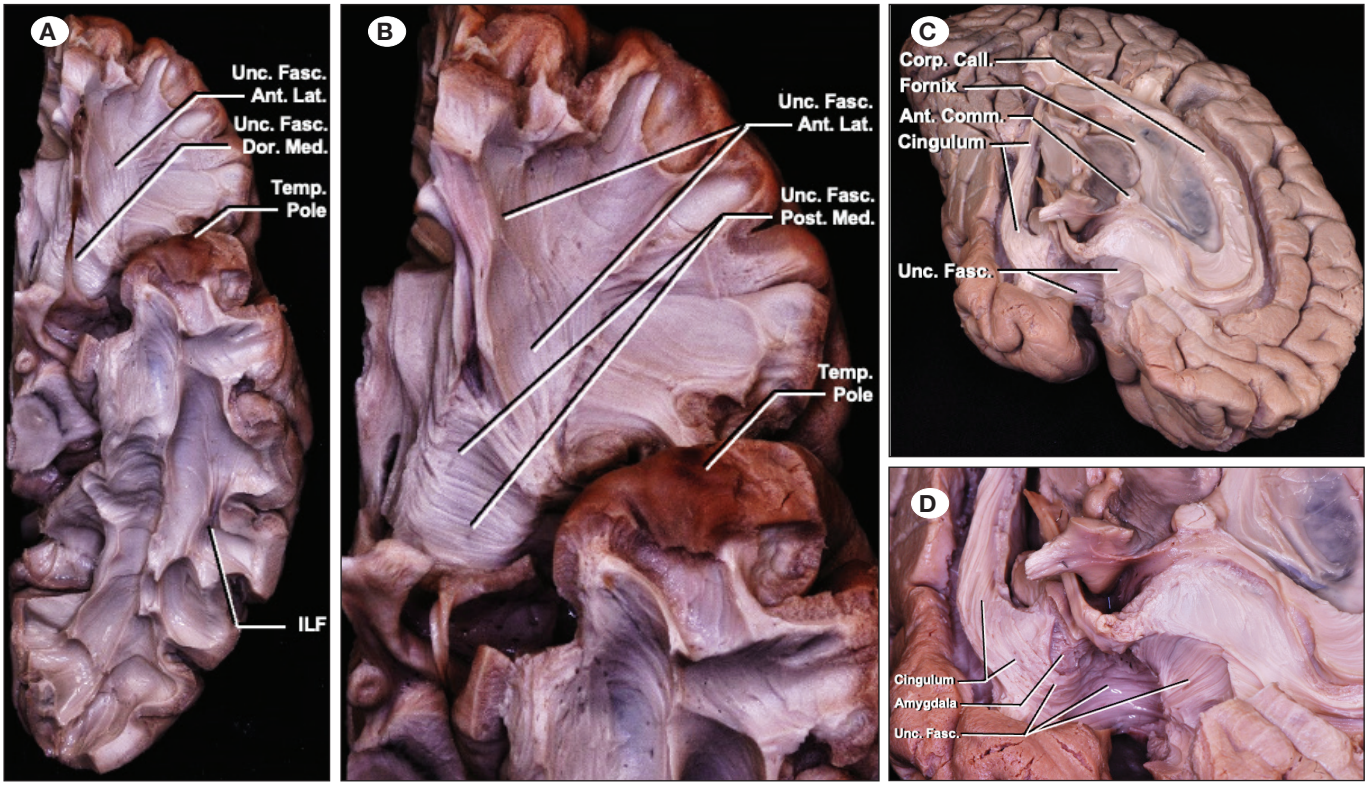

Figure 2: Inferior to superior dissection of the UF on the left cerebral hemisphere, illustrating frontal and temporal segmentations and their anatomical targets. **A)** After decortication of the ventral surface, the orbitofrontal cortex and temporal pole are exposed. The anterolateral UF is visualized projecting toward the anterior, lateral, and posterior orbital gyri. The dorsomedial UF courses medially beneath the olfactory sulcus, toward the gyrus rectus and septal area. **B)** Continued dissection at a deeper level shows both UF components projecting from the ALS. The anterolateral UF is directed laterally to the orbital gyri, while the dorsomedial UF extends medially to the gyrus rectus and septal cortex. The temporal segment of the UF is visualized turning around the limen insula toward the temporal pole. **C)** The AC, corpus callosum, and fornix are revealed medially. The dorsomedial UF fibers intersect with the anterior cingulum bundle near the so-called "cingulate pole" at the subcallosal area. The convergence of these limbic structures is noted anterior to the septal area. **D)** The terminal portions of the dorsomedial UF fibers are shown approaching the amygdala and parahippocampal gyrus. The uncinate pole is illustrated as the junction point of the dorsomedial UF and the cingulum, deep to the uncus and adjacent to the mesial temporal lobe structures.

Within the depth of the parahippocampal gyrus, extending from the isthmus of the cingulate gyrus to the anterior temporal pole, lie the fibers of the cingulum bundle, which connect the medial frontal and parietal areas to the medial temporal lobe (Figure 2C, D) (2,31). The cingulum and dorsomedial UF fibers converge inferolaterally to the amygdala, forming the uncinate pole (Figures 2D; 3E, F, G).

DISCUSSION

The UF is a long association fiber tract that exhibits a characteristic hook-like trajectory around the limen insula. It forms cortico-cortical connections between the subcallosal area, gyrus rectus, pars orbitalis, and frontoorbital cortex with the superior, middle, and inferior temporal gyri, as well as the anterior portions of the uncus (2,10,15,22,27,28,32). Dejerine was the first to describe not only the classical hook-shaped fibers of the UF but also fibers that appear flattened or even reversed in orientation (9). We define the UF as a ventral limbic pathway that connects the rostral, inferior, ventral, and medial temporal regions with the medial and orbital frontal cortices. Furthermore, our findings support recent discussions suggesting that the UF is not solely composed of hook-shaped fibers, but also includes segments that reverse direction within the orbitofrontal and parahippocampal cortices. The primary focus is to provide a detailed anatomical segmentation of the UF by evaluating the frontal and temporal cortical termination sites in relation to their functional associations.

Building upon the classification proposed by Ebeling and Cramon, we refined the anatomical boundaries of the compact UF trunk based on its relationship to the ILS (10). Accordingly, we defined three main segments: frontal, insular, and temporal. Each segment was further subdivided into dorsomedial and anterolateral components, based on their orientation and cortical termination patterns beyond the limiting sulci (Table I).

Cortical fibers associated with the claustrum, known as the EC fibers, are divided into dorsal and ventral components. The dorsal EC consists of claustrocortical fibers, while the ventral EC is composed of the UF and IFOF (12). The dorsal EC

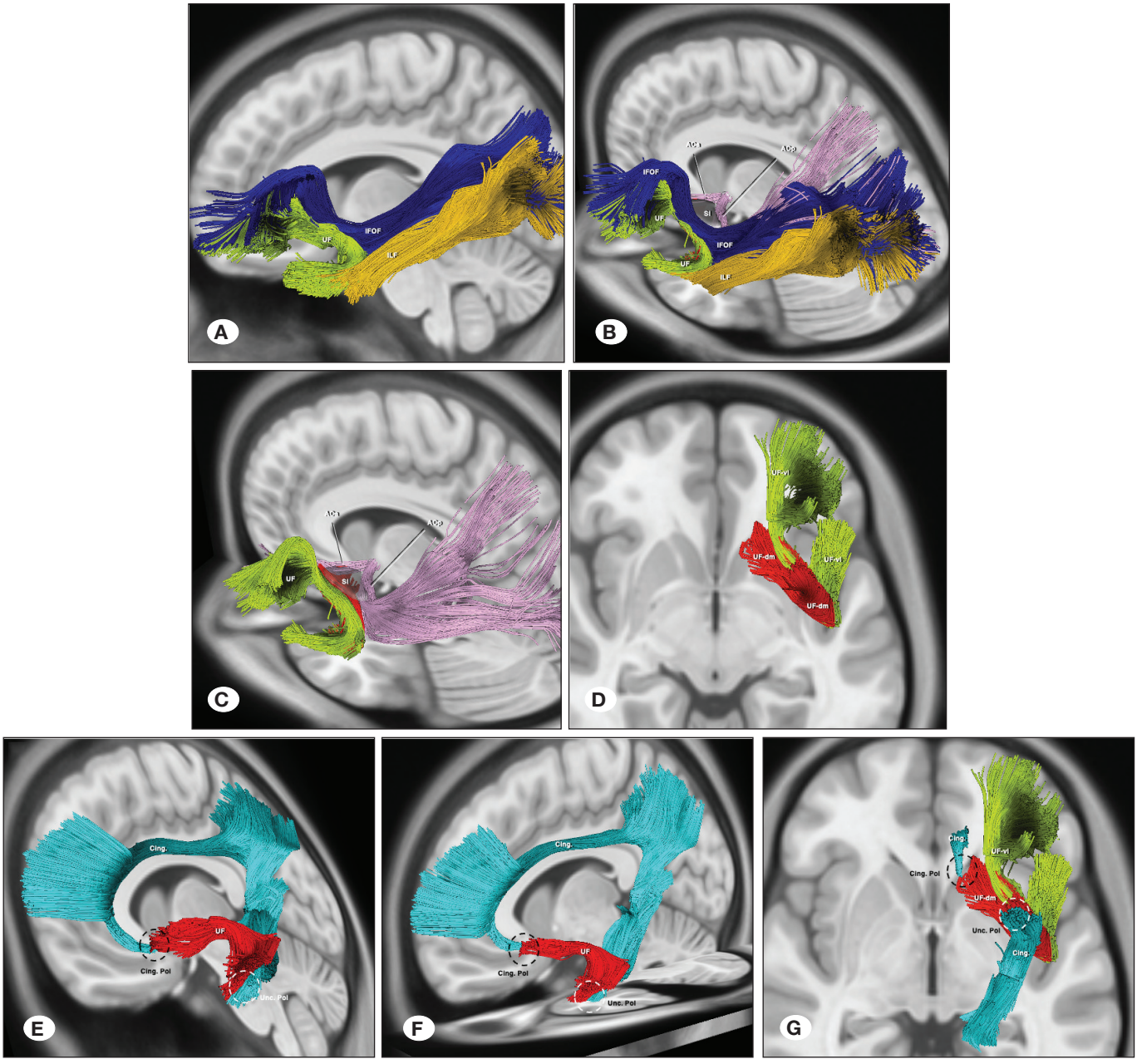

Figure 3: DWI tractography images derived from healthy subjects to assess the integrity of the fiber dissection results and display relevant UF connections on the left cerebral hemisphere. All tracts were generated using deterministic tractography with analysis performed in DSI Studio. The anisotropy threshold was randomly selected, and the angular threshold was randomly varied between 15° and 90°. Step size was randomly set between 0.5 and 1.5 voxels. **A)** Left medial view showing the ILF, IFOF, and UF **B)** Slightly deeper dissection reveals the anterior and posterior limbs of the AC (ACa and ACp, respectively), situated between the SI and ventral striatum. The dorsomedial UF courses medially and superiorly, **C)** IFOF was removed. The ventrolateral UF and dorsomedial UF are clearly distinguished by their orientation around the limen insula and SI. **D)** The ventrolateral and the dorsomedial UF viewed from below. The dorsomedial UF fibers approach the medial temporal lobe, while the anterolateral UF courses laterally toward the temporal pole, running parallel to the ILF. **C, D)** The dorsomedial UF courses medially and inferiorly, in contrast to the more lateral and superior anterolateral UF fibers that extend toward the temporal pole. **E, F, G:** The anatomical convergence of the dorsomedial UF fibers with the anterior cingulum is shown at both poles: the cingulate pole at the frontal base and the uncinate pole at the temporal base. These two anatomical hubs represent critical junctions in the limbic circuitry. **G)** Basal view illustrating the relationship between the UF and cingulum.

includes long association fibers that connect the claustrum with cortical regions ranging from the supplementary motor area anteriorly to the posterior parts of the parietal lobe (12). These fibers merge with the internal capsule in the region of the SLS, contributing to the corona radiata (Figure 1). The ventral EC is formed dorsally by the IFOF and ventrally by the UF (12). The IFOF comprises fronto-occipital association fibers that connect the middle and inferior frontal gyri (particularly the pars orbitalis and pars triangularis) with the posterior parietal and occipital lobes (12,14). In our study, we demonstrated the compact arrangement of these tracts at the insular apex, with the IFOF occupying the superior position and extending fronto-occipitally, and the UF located inferiorly with a fronto-temporal course (Figure 1). As the UF fibers course toward the temporal pole and mesial temporal region, they diverge from the IFOF at the level of the ILS, turning anteroinferiorly. Notably, this region also corresponds to the area where AC fibers and IFOF fibers interdigitate to form the sagittal stratum. The insular segment of the UF occupies the insular apex as a compact fiber bundle, situated between the APS and the extreme capsule (10,32).

Previous studies have described that the inferior and medial fibers of the UF course rostrally between the APS and the putamen, while its lateral fibers intermingle with fibers from the genu of the corpus callosum, projecting into the frontoorbital and lateral frontal lobes (32). Based on our lateral to medial dissections, the first fibers encountered were the anterolateral UF bundle of the insular segment, which extended from the temporal pole to the lateral, anterior, and posterior orbital gyri, as well as the pars orbitalis (2). Deeper dissection revealed another group of fibers located adjacent to the SI and APS, forming the dorsomedial UF bundle. These fibers originated in the mesial temporal region and coursed toward the gyrus rectus, septal area, and NAc (2). Adopting the segmentation proposed by Ebeling and Cramon into temporal, insular, and frontal components, we further classified the insular segment of the UF into anterolateral and dorsomedial subcomponents (Table I) (10).

Recent studies have demonstrated that the frontal cortical terminations of the UF extend beyond the traditionally accepted orbitofrontal cortex and pars orbitalis, encompassing a broader area of the frontal lobe (22). In a previous study, we reported that the UF projects to the frontoorbital area, septal area, NAc, and the superolateral frontal lobe (2). Hau et al. further described UF projections to widespread regions of the lateral prefrontal cortices, including the superior, middle, and inferior frontal gyri (15). Leng et al. documented terminations in the middle frontal gyrus, pars orbitalis, and pars triangularis (21), while Liakos et al. observed projections to the posterior orbital lobule, pars orbitalis, gyrus rectus, and subgenual area (22). In our current study, we show that UF fibers diverge into distinct trajectories within the frontal lobe, originating from the ALS to reach various cortical targets (2). As the distance from the APS increases, the anterolateral UF of the insular segment, located in its lateral compartment, follow a relatively straight horizontal course toward the anterior, lateral, and posterior orbital gyri, as well as the pars orbitalis (Figure 1). In contrast, the dorsomedial fibers located in the medial compartment of the insular segment change their orientation along the ALS, curving anteriorly and medially as they extend. These dorsomedial fibers have a shorter trajectory than the anterolateral fibers and project to the gyrus rectus, septal area, and NAc (Figure 2).

Early studies have described the terminations of the UF predominantly in the temporal pole, as well as in the superior and middle temporal gyri, fusiform gyrus, and entorhinal cortex (9,10). Additionally, several investigations have reported UF projections to the cingulate gyrus and amygdala (6,7,19,33). However, Hau et al. did not identify these projections in their dissections and suggested that such discrepancies might be attributable to the presence of adjacent pathways, such as amygdalo-temporal or amygdalo-prefrontal tracts, that may have been misattributed to the UF (16). We demonstrated that the insular segment of the UF, as defined in our study, curves from the level of the ILS and proceeds toward the temporal pole, amygdala, and medial temporal areas. Martino et al. reported that the anterior boundary of the optic radiation, located beneath the ILS, coincides with the transition point between the UF and IFOF (24). We confirmed that from the level of the ILS—the point marking the transition between the IFOF and UF—the insular segment of the UF curves into two distinct trajectories, which we define as the temporal segment of the UF. Among these, the anterolateral UF fibers project toward the temporal pole, while the dorsomedial UF fibers course medially toward the medial temporal region (Figures 1, 2).

The limbic system, comprising white matter pathways that mediate cortical and corticocortical connections involved in memory, emotion, and behavior regulation, is anatomically represented by the cingulate cortex, orbitofrontal cortex, hippocampus, amygdala, NAc, thalamic nuclei, and mammillary bodies (4). The cingulum and the UF constitute the dorsal and ventral limbs of the limbic axis, respectively (32). As a dorsal limbic pathway, the cingulum bundle connects the frontal, parietal, and cingulate cortices with the ventral temporal cortex. It is implicated in memory processing, decision-making, and emotional regulation, with the left cingulum particularly associated with intellectual performance and cognitive functioning (23,26,31). On the other hand, the UF serves as the most lateral component of the ventral limbic stream, connecting the rostral, inferotemporal, and ventral temporal cortices with medial and orbital frontal areas (2,26,32). UF has been associated with multimodal sensory integration, behavior inhibition modulated by the reward–pleasure system, and visual memory (14). Together, the cingulum and UF form an alternative limbic circuit resembling the Papez circuit, encircling nearly the entire medial hemisphere (2). This circuit is completed at two key junctions, previously described as the *"cingulate pole"* by Yasargil and the *"uncinate pole"* by Baydin et al. (2,35). In our study, we observed that the cingulum merges with the anteromedial fibers of the UF on the dorsomedial surface of the uncus in close association with the amygdala, thereby forming the uncinate pole. Furthermore, we identified the cingulate pole, defined by Yasargil as the convergence zone between the subcallosal and paracingulate cortices and the posterior prefrontal cortex, where the cingulum and dorsomedial UF fibers intersect deep to the gyrus rectus and septal area, medial to the NAc (Figures 2, 3).

Additionally, our results support the existence of amygdalo-accumbens connections mediated by dorsomedial UF fibers, consistent with previous reports describing the amygdalo-accumbens pathway (Figures 2, 3) (3,30).

CONCLUSION

In this study, we provided a detailed anatomical segmentation of the UF through combined white matter dissection and tractography. We demonstrated that the UF can be systematically divided into frontal, insular, and temporal segments, each with distinct dorsomedial and anterolateral subcomponents based on their cortical trajectories and anatomical relationships. Our findings not only refine the classical descriptions of the UF but also emphasize its critical role within the limbic system, highlighting its contributions to the integration of emotional, cognitive, and behavioral processes. By elucidating the internal organization and cortical terminations of the UF, this study offers a valuable framework for understanding its involvement in both normal brain function and a variety of neurological and psychiatric disorders.

ACKNOWLEDGEMENTS

Part of the cadaver dissections in this study was performed at the University of Florida under the guidance of Professor Albert L. Rhoton Jr. We thank him and the Albert L. Rhoton Neuro-Microanatomy Laboratory for their contributions.

Ethical approval is not applicable for this article (https://trdizin.gov.tr/wp-content/uploads/2022/04/TRDizin_etik_ilkeleri_akis_semasi.pdf).

The authors sincerely thank those who donated their bodies to science so that anatomical research could be performed. Results from such research can potentially increase mankind's overall knowledge that can then improve patient care. Therefore, these donors and their families deserve our highest gratitude.

Declarations

Funding: The authors declare no competing financial interests and no sources of funding and support, including any for equipment and medications.

Availability of data and materials: The datasets generated and/or analyzed during the current study are available from the corresponding author by reasonable request.

Disclosure: The authors declare no competing interests.

AUTHORSHIP CONTRIBUTION

Study conception and design: SSB, OB, NT
Data collection: SSB, OB, BK
Analysis and interpretation of results: OB, OH
Draft manuscript preparation: SSB, OB, BK, OH
Critical revision of the article: SSB, NT
Other (study supervision, fundings, materials, etc...): NT
All authors (SSB, OB, BK, OH, NT) reviewed the results and approved the final version of the manuscript.

REFERENCES

1. Baran O, Balak N, Baydin S, Aydin I, Kayhan A, Evran S, Kemerdere R, Tanriover N: Assessing the connectional anatomy of superior and lateral surgical approaches for medial temporal lobe epilepsy. J Clin Neurosci 81:378-389, 2020. https://doi.org/10.1016/j.jocn.2020.10.016
2. Baydin S, Gungor A, Tanriover N, Baran O, Middlebrooks EH, Rhoton Jr AL: Fiber tracts of the medial and inferior surfaces of the cerebrum. World Neurosurgery 98:34-49, 2017. https://doi.org/10.1016/j.wneu.2016.05.016
3. Baydin S, Yagmurlu K, Tanriover N, Gungor A, Rhoton Jr AL: Microsurgical and fiber tract anatomy of the nucleus accumbens. Oper Neurosurg 12:269-288, 2016. https://doi.org/10.1227/NEU.0000000000001133
4. Catani M, Dell'Acqua F, De Schotten MT: A revised limbic system model for memory, emotion and behaviour. Neurosci Biobehav Rev 37:1724-1737, 2013. https://doi.org/ 10.1016/j.neubiorev.2013.07.001.
5. Catani M, Mesulam M: The arcuate fasciculus and the disconnection theme in language and aphasia: History and current state. Cortex 44:953-961, 2008. https://doi.org/10.1016/j.cortex.2008.04.002.
6. Croxson PL, Johansen-Berg H, Behrens TE, Robson MD, Pinsk MA, Gross CG, Richter W, Richter MC, Kastner S, Rushworth MF: Quantitative investigation of connections of the prefrontal cortex in the human and macaque using probabilistic diffusion tractography. J Neurosci 25:8854-8866, 2005. https://doi.org/10.1523/JNEUROSCI.1311-05.2005.
7. de Schotten MT, Dell'Acqua F, Valabregue R, Catani M: Monkey to human comparative anatomy of the frontal lobe association tracts. Cortex 48:82-96, 2012. https://doi.org/10.1016/j.cortex.2011.10.001
8. de Zubicaray GI, Rose SE, McMahon KL: The structure and connectivity of semantic memory in the healthy older adult brain. Neuroimage 54:1488-1494, 2011. https://doi.org/10.1016/j.neuroimage.2010.08.058
9. Dejerine J: Anatomy of the Nervous Centers, volume 1 (in French). Paris, France: Rueff & Cie, 1895
10. Ebeling U, Cramon DV: Topography of the uncinate fascicle and adjacent temporal fiber tracts. Acta Neurochir 115:143-148, 1992. https://doi.org/10.1007/BF01406373
11. Erkan B, Hergunsel B, Barut O, Saygi T, Kocak B, Gungor A, Yagmurlu K, Tanriover N: Ventral amygdalofugal pathway as an integrated surgically important network: Microsurgical anatomy and segmentation based on fiber dissection. J Neurosurg 1:1-15, 2024. https://doi.org/10.3171/2024.1.JNS231541
12. Fernández-Miranda JC, Rhoton AL, Kakizawa Y, Choi C, Álvarez-Linera J: The claustrum and its projection system in the human brain: A microsurgical and tractographic anatomical study. J Neurosurg 108:764-774, 2008. https://doi.org/10.3171/JNS/2008/108/4/0764
13. Grabenhorst F, Rolls ET: Value, pleasure and choice in the ventral prefrontal cortex. Trends Cogn Sci 15:56-67, 2011. https://doi.org/10.1016/j.tics.2010.12.004

14. Gungor A, Baydin S, Middlebrooks EH, Tanriover N, Isler C, Rhoton AL: The white matter tracts of the cerebrum in ventricular surgery and hydrocephalus. J Neurosurg 126:945-971, 2017. https://doi.org/10.3171/2016.1.JNS152082
15. Hau J, Sarubbo S, Houde JC, Corsini F, Girard G, Deledalle C, Crivello F, Zago L, Mellet E, Jobard G: Revisiting the human uncinate fasciculus, its subcomponents and asymmetries with stem-based tractography and microdissection validation. Brain Struct Funct 222:1645-1662, 2017. https://doi.org/10.1007/s00429-016-1298-6
16. Hau J, Sarubbo S, Perchey G, Crivello F, Zago L, Mellet E, Jobard G, Joliot M, Mazoyer BM, Tzourio-Mazoyer N: Cortical terminations of the inferior fronto-occipital and uncinate fasciculi: Anatomical stem-based virtual dissection. Frontiers in Neuroanatomy 10:58, 2016. https://doi.org/10.3389/fnana.2016.00058
17. Johnson CP, Juranek J, Kramer LA, Prasad MR, Swank PR, Ewing-Cobbs L: Predicting behavioral deficits in pediatric traumatic brain injury through uncinate fasciculus integrity. J Int Neuropsychol Soc 17:663-673, 2011. https://doi.org/10.1017/S1355617711000464.
18. Klingler J: Erleichterung der makrokopischen Präparation des Gehirns durch den Gefrierprozess. Orell Füssli, 1935.
19. Klingler J, Gloor P: The connections of the amygdala and of the anterior temporal cortex in the human brain. J Comp Neurol 115:333-369, 1960. https://doi.org/10.1002/cne.901150305
20. Kucukyuruk B, Richardson RM, Wen HT, Fernandez-Miranda JC, Rhoton Jr AL: Microsurgical anatomy of the temporal lobe and its implications on temporal lobe epilepsy surgery. Epilepsy Res Treat 2012:769825, 2012. https://doi.org/10.1155/2012/769825
21. Leng B, Han S, Bao Y, Zhang H, Wang Y, Wu Y, Wang Y: The uncinate fasciculus as observed using diffusion spectrum imaging in the human brain. Neuroradiol 58:595-606, 2016. https://doi.org/10.1007/s00234-016-1650-9
22. Liakos F, Komaitis S, Drosos E, Neromyliotis E, Skandalakis GP, Gerogiannis AI, Kalyvas AV, Troupis T, Stranjalis G, Koutsarnakis C: The topography of the frontal terminations of the Uncinate fasciculus revisited through focused Fiber dissections: shedding light on a current controversy and introducing the insular apex as a key anatomoclinical area. World Neurosurgery 152:e625-e634, 2021. https://doi.org/10.1016/j.wneu.2021.06.012
23. Lövblad KO, Schaller K: Surgical anatomy and functional connectivity of the limbic system. Neurosurgical Focus 27:E3, 2009. https://doi.org/10.3171/2009.5.FOCUS09103
24. Martino J, da Silva-Freitas R, Caballero H, de Lucas EM, García-Porrero JA, Vázquez-Barquero A: Fiber dissection and diffusion tensor imaging tractography study of the temporoparietal fiber intersection area. Oper Neurosurg 72:ons 87-ons 98, 2013. https://doi.org/10.1227/NEU.0b013e318274294b.
25. Parker GJ, Luzzi S, Alexander DC, Wheeler-Kingshott CA, Ciccarelli O, Ralph MAL: Lateralization of ventral and dorsal auditory-language pathways in the human brain. Neuroimage 24:656-666, 2005. https://doi.org/10.1016/j.neuroimage.2004.08.047.
26. Pascalau R, Stănilă RP, Sfrângeu S, Szabo B: Anatomy of the limbic white matter tracts as revealed by fiber dissection and tractography. World Neurosurgery 113:e672-e689, 2018. https://doi.org/10.1016/j.wneu.2018.02.121.
27. Peltier J, Verclytte S, Delmaire C, PruVo JP, Godefroy O, Le Gars D: Microsurgical anatomy of the temporal stem: Clinical relevance and correlations with diffusion tensor imaging fiber tracking. J Neurosurg 112:1033-1038, 2010. https://doi.org/10.3171/2009.6.JNS08132.
28. Peuskens D, van Loon J, Van Calenbergh F, Van den Bergh R, Goffin J, Plets C: Anatomy of the anterior temporal lobe and the frontotemporal region demonstrated by fiber dissection. Neurosurgery 55:1174-1184, 2004. https://doi.org/10.1227/01.neu.0000140843.62311.24.
29. Rhoton Jr AL: The cerebrum. Neurosurgery 51:S1-51, 2002. https://doi.org/10.1097/00006123-200210001-00002.
30. Rigoard P, Buffenoir K, Jaafari N, Giot JP, Houeto JL, Mertens P, Velut S, Bataille B: The accumbofrontal fasciculus in the human brain: A microsurgical anatomical study. Neurosurgery 68:1102-1111, 2011. https://doi.org/10.1227/NEU.0b013e3182098e48.
31. Saygi T, Avyasov R, Barut O, Daglar Z, Baran O, Hasimoglu O, Altinkaya A, Tanriover N: Microsurgical anatomy of the isthmic cingulum: a new white matter crossroad and neurosurgical implications in the posteromedial interhemispheric approaches and the glioma invasion patterns. Neurosurg Rev 46:82, 2023. https://doi.org/10.1007/s10143-023-01982-w.
32. Schmahmann J, Pandya D: Fiber pathways of the brain. New York: Oxford University Press, 2006
33. Von Der Heide RJ, Skipper LM, Klobusicky E, Olson IR: Dissecting the uncinate fasciculus: Disorders, controversies and a hypothesis. Brain 136:1692-1707, 2013. https://doi.org/10.1093/brain/awt094.
34. Yagmurlu K, Vlasak AL, Rhoton Jr AL: Three-dimensional topographic fiber tract anatomy of the cerebrum. Oper Neurosurg 11:274-305, 2015. https://doi.org/10.1227/NEU.0000000000000704.
35. Yasargil MG: Microneurosurgery of CNS Tumors. Stuttgart: George Thieme Verlag, 1996
36. Yasargil MG: Microneurosurgery, Volume IV A: CNS Tumors: Surgical Anatomy, Neuropathology, Neuroradiology, Neurophysiology, Clinical Considerations, Operability, Treatment Options. Thieme, 2013.
37. Yeni SN, Tanriover N, Uyanik O, Ulu MO, Ozkara C, Karaagac N, Ozyurt E, Uzan M: Visual field defects in selective amygdalohippocampectomy for hippocampal sclerosis: The fate of Meyer's loop during the transsylvian approach to the temporal horn. Neurosurgery 63:507-515, 2008. https://doi.org/10.1227/01.NEU.0000324895.19708.68.

Turk Neurosurg 35(4):661-666, 2025
DOI: 10.5137/1019-5149.JTN.46851-24.3

Original Investigation
General Neurosurgery and Miscellaneous-Others

Received: 02.05.2024
Accepted: 20.10.2024
Published Online: 25.06.2025

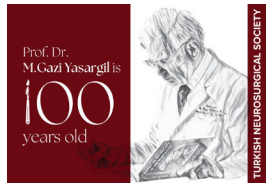

Radioanatomical Assessment of the Sphenoid Ridge in Chiari Type I Malformation

Baran Can ALPERGIN[1], Umit EROGLU[2], Fatih YAKAR[3], Umit KARADAGOGLU[2], Omer Mert OZPISKIN[2], Elif GOKALP[2], Muhammet Enes GURSES[4], Mert CETIN[5], Orhan BEGER[6]

[1]Ankara Etlik City Hospital, Department of Neurosurgery, Ankara, Türkiye
[2]Ankara University, Faculty of Medicine, Department of Neurosurgery, Ankara, Türkiye
[3]Pamukkale University, Faculty of Medicine, Department of Neurosurgery, Denizli, Türkiye
[4]University of Miami, Miller School of Medicine, Department of Neurological Surgery, Miami, Florida, USA
[5]Gaziantep University, Faculty of Medicine, Term V Student, Gaziantep, Türkiye
[6]Gaziantep University, Faculty of Medicine, Department of Anatomy, Gaziantep, Türkiye

Corresponding author: Umit EROGLU ✉ umitkovikeroglu@hotmail.com

ABSTRACT

AIM: To compare the sphenoid ridge (SR) morphology in patients with Chiari type I malformation (CIM) with healthy subjects.

MATERIAL and METHODS: Three dimensional (3D) computed tomography scans of 49 (25 men / 24 women) CIM patients aged 45.84±18.04 years, and 52 (26 men / 26 women) healthy subjects aged 43.46±11.62 years were included in the investigation. The angulation and dimension of SR were measured for both groups.

RESULTS: Compared with the controls, CIM patients had greater lesser wing (LW) length ($p<0.001$) and LW width in the midline ($p<0.001$), but shorter LW width in the midpoint ($p=0.001$), LW width in the lateral point ($p<0.001$), and LW angle ($p<0.001$). In CIM, two configurations regarding LW angle types were observed: Type B in 75 LWs (76.5%) and Type C in 23 LWs (23.5%). In controls, two configurations regarding LW angle types were observed: Type A in 35 LWs (33.7%) and Type B in 69 LWs (66.3%). The distribution of the types according to study groups demonstrated that CIM affected significantly LW angle types ($p<0.001$).

CONCLUSION: LW angle and length may represent middle fossa depth and anterior fossa width, respectively; thus, CIM subjects possess shallow middle fossa and wider anterior fossa.

KEYWORDS: Chiari type I malformation, Sphenoid bone, Sphenoid ridge, Lesser wing, Computed tomography

INTRODUCTION

The sphenoid ridge (SR), the bony frontier between the anterior fossa and middle fossae, is described as the curved posterior sharp margin of the sphenoid bone's lesser wing (LW) (6,12,14,24). This edge is bounded medially by the anterior clinoid process, and laterally by the pterion, which displays the Sylvian point's approximate position (6,12). Pathologies directly related to SR are rare, but some surgeons report fibrous dysplasia and meningiomas arising from this edge (6). In addition, certain pathologies such as middle cerebral artery aneurysms may require a surgical procedure, including extensively removal of SR (14). Anatomical information about SR morphology (including its angulation, dimension and shape) may be beneficial for neurosurgeons in avoiding injury to adjacent structures (e.g., orbital branch of the middle meningeal artery, trochlear nerve, superior ophthalmic vein, and oculomotor nerve), when applying surgical procedures such as pterional orbitozygomatic approach or SR keyhole approach (6,8,12,14,24). Moreover, SR may serve as a reference point during these approaches, as this edge forms

Baran Can ALPERGIN : 0000-0002-3575-0480 Umit KARADAGOGLU : 0009-0008-6565-102X Muhammet Enes GURSES : 0000-0001-7141-0654
Umit EROGLU : 0000-0001-8623-071X Omer Mert OZPİSKİN : 0000-0002-8261-1766 Mert CETIN : 0000-0002-7165-7646
Fatih YAKAR : 0000-0001-7414-3766 Elif GOKALP : 0000-0001-7022-4286 Orhan BEGER : 0000-0002-4932-8758

a border between the frontal and temporal lobes of the brain (14). Therefore, neuroradiologists and neurosurgeons should wise well up to SR morphology to successfully carry out an operation.

Current studies displayed that the whole skull base's osseous components are substantially affected by Chiari type I malformation (CIM), likely resulting from a mesodermal failure (15,22). Nwotchouang et al. observed that such subjects had about 38% bigger sphenoid sinus volume by the side of healthy controls (15). In our opinion, this condition may result major alterations in anatomical properties of structures associated with the sphenoid bone (e.g., LW, sella turcica, and optic canal). For example, CIMs possess smaller sella volume and area, greater angle of the optic canal in axial plane, shorter and wide-angled anterior clinoid process, longer optic strut, longer anterior fossa, and more pneumatized posterior clinoid process by comparison healthy controls (2,4,15-18,22). Differences of skull base morphologies of CIM patients from normal subjects may affect the selection of surgical procedure, intraoperative orientation, and positioning of the patient's head (2,15-18). However, our current knowledge (including morphometric evaluations, precise SR-related anatomical descriptions, and different surgical approach assessments) is mainly obtained from normal subjects (1,8,10,11,14,23,24). Thus, we think that novel studies focused on SR morphology in subjects with different malformations such as CIM are required for determining whether anatomical properties of SR are altered in CIM or not, by comparison healthy individuals. The main goal of our work is to evaluate the angulation and dimension of SR in CIM for improving the present literature data regarding morphometric properties of their cranial base.

MATERIAL and METHODS

Ethics Statement

The Clinical Research Ethics Committee approved ethically our retrospective examination (confirmation no: 2024/97, date: 20.02.2024).

Study Population

Study population was divided into two groups, CIMs and controls. Patient folders were evaluated to create these groups. Patient files included the following data: complaints, cure methods, radiologic views (CT: computed tomography, and MRI: magnetic resonance imaging), diagnosis procedures, demographic information (gender, age, etc.), and hospital admission/discharge dates.

Inclusion and Exclusion Criteria

Patients were diagnosed as CIM if they had tonsillar herniation over 5 mm downward from the foramen magnum, but no a history of meningomyelocele. In these patients, the circulation of the cerebrospinal fluid was impaired at the level of the foramen magnum. They had balance problems (gait disturbance), and also intense neck pain and vigorous headache, aggravated by Valsalva (sneezing, coughing, straining, etc.). Thus, CIM patients underwent operation, after radiological and clinical diagnosis.

In CIM, inclusion criteria were as follows: a) patients with high-quality preoperative MRI and CT slices, and b) patients diagnosed with CIM after radiological and clinical examinations between 2010-2023. Exclusion criteria were as follows: a) patients with other types of Chiari malformation, b) patients with any disorders regarding the cranial base (e.g., tumor), and c) CIM patients with a history of operation related the anterior and middle fossae.

In controls, inclusion criteria were as follows: a) subjects with high-quality MRI and CT slices, and b) normal subjects. Exclusion criteria were as follows: a) subjects with any malformation or genetic disorder, b) subjects with any disease such as tumors, and c) subjects with a history of medical or surgical treatment related to the skull base.

CT Protocol

The raw data were obtained using a 64-row multidetector scanner (Aquillion 64, Toshiba Medical Systems, Tokyo, Japan). Coronal, sagittal and axial slices were acquired by processing this data. A software (RadiAnt DICOM, Medixant, Poznan, Poland) was used to obtain information about SR.

Measured Parameters

Measurements were performed using 3D CT images (Figure 1).

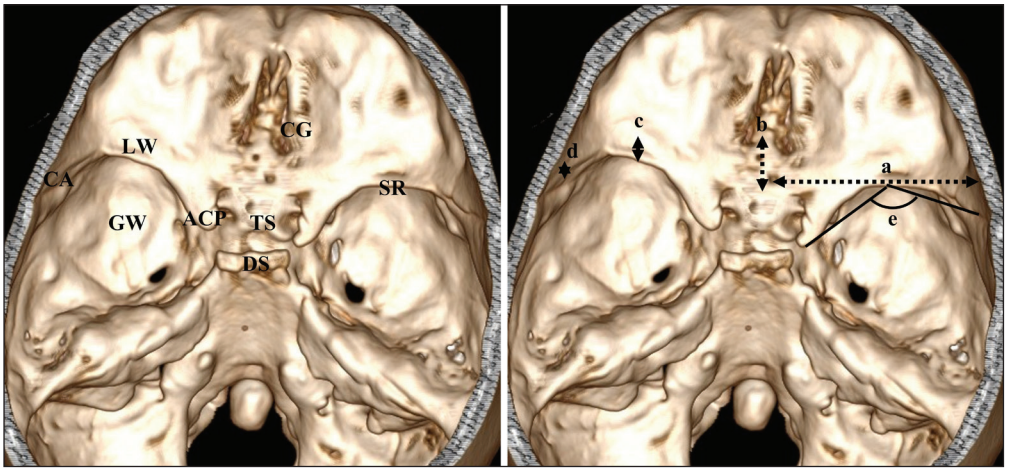

Figure 1: Skull base and measured parameters. **a:** LWL; **b:** LWW-ML; **c:** LWW-MP; **d:** LWW-L; and **e:** LWA; **SR:** sphenoid ridge; **DS:** dorsum sellae; **TS:** tuberculum sellae; **ACP:** anterior clinoid process; **GW:** greater wing; **CA:** crista alaris; **LW:** lesser wing; and **CG:** crista galli.

Considering the previous studies (8, 24), five parameters were measured to obtain data about SR. The explanations of the parameters were as follows: a) LWL: the length of the lesser wing, b) LWW-ML: the width of the lesser wing in the midline, c) LWW-MP: the width of the lesser wing in the midpoint, d) LWW-L: the width of the lesser wing in the lateral tip, and e) LWA: the angle of the lesser wing. Considering the work of Kahilogullari et al. (8), LWA was classified as three types: Type A (LWA > 130°), Type B (130° > LWA > 110°), and Type C (LWA < 110°).

Statistical Analysis

Pearson correlation coefficient test was applied to see correlations between LWL, LWA, LWW-ML, LWW-MP and LWW-L. The student's t-tests were utilized to make gender (the independent test), group (the independent test), and side (the paired test) comparisons. Chi-square test was utilized to assess relations of LWA types with the study groups. Shapiro-Wilk test was used to assess normality control of the dataset. SPSS (IBM, Armonk, NY) was used to perform statistical evaluations. The "p<0.05" was considered significant.

RESULTS

CIM group consisted of 49 (25 men / 24 women) patients aged 45.84±18.04 years. Control group consisted of 52 (26 men / 26 women) healthy subjects aged 43.46±11.62 years. Our findings are as follows:

- Compared to the controls, CIM subjects had greater LWL (p<0.001) and LWW-ML (p<0.001), but shorter LWW-MP (p=0.001), LWW-L (p<0.001) and LWA (p<0.001) (Table I).
- In the CIM group, all parameters were similar for sexes and sides (p>0.05). In controls, all parameters except LWA were similar for sexes and sides (p>0.05). Men had greater LWA in comparison with women (p=0.008) (Table II).
- In comparison with control males, CIM males had greater LWL (p<0.001), but shorter LWW-MP (p=0.033), LWW-L (p<0.001) and LWA (p<0.001). By comparison control females, CIM females had greater LWL (p<0.001) and LWW-ML (p=0.001), but shorter LWW-MP (p=0.017), LWW-L (p<0.001) and LWA (p<0.001) (Table III).

Table I: Comparison of CIM and Controls

Parameters	CIM	Controls	p-value
LWL (mm)	52.45 ± 5.25	41.23 ± 8.30	**<0.001**
LWW-ML (mm)	9.92 ± 1.85	8.75 ± 1.25	**<0.001**
LWW-MP (mm)	3.08 ± 1.28	3.52 ± 0.45	**0.001**
LWW-L (mm)	1.88 ± 0.51	2.76 ± 0.69	**<0.001**
LWA (°)	116.42 ± 5.16	126.19 ± 7.73	**<0.001**

Table II: Sex and Side Comparisons for CIM and Controls

Group	Parameters	Male	Female	p-value	Right	Left	p-value
CIM	LWL (mm)	52.41 ± 5.37	52.50 ± 5.19	0.933	52.03 ± 6.39	52.87 ± 3.83	0.437
	LWW-ML (mm)	9.52 ± 1.53	10.33 ± 2.08	0.124	-	-	-
	LWW-MP (mm)	3.09 ± 1.19	3.07 ± 1.38	0.965	3.12 ± 1.36	3.04 ± 1.20	0.767
	LWW-L (mm)	1.81 ± 0.50	1.96 ± 0.52	0.166	1.86 ± 0.42	1.91 ± 0.59	0.645
	LWA (°)	117.32 ± 4.97	115.48 ± 5.24	0.077	116.49 ± 5.63	116.35 ± 4.70	0.892
Controls	LWL (mm)	41.48 ± 8.42	40.98 ± 8.24	0.764	41.49 ± 7.59	40.97 ± 9.01	0.748
	LWW-ML (mm)	8.80 ± 1.31	8.70 ± 1.21	0.773	-	-	-
	LWW-MP (mm)	3.47 ± 0.47	3.56 ± 0.44	0.291	3.62 ± 0.40	3.42 ± 0.48	0.114
	LWW-L (mm)	2.77 ± 0.69	2.76 ± 0.70	0.946	2.46 ± 0.67	3.06 ± 0.58	0.052
	LWA (°)	128.17 ± 8.30	124.21 ± 6.61	0.008	126.75 ± 7.95	125.63 ± 7.53	0.464

Table III: Sex Comparison for Both Groups

Parameters	CIM Male	Control Male	p-value	CIM Female	Control Female	p-value
LWL (mm)	52.41 ± 5.37	41.48 ± 8.42	<0.001	52.50 ± 5.19	40.98 ± 8.24	**<0.001**
LWW-ML (mm)	9.52 ± 1.53	8.80 ± 1.31	0.077	10.33 ± 2.08	8.70 ± 1.21	**0.001**
LWW-MP (mm)	3.09 ± 1.19	3.47 ± 0.47	0.033	3.07 ± 1.38	3.56 ± 0.44	**0.017**
LWW-L (mm)	1.81 ± 0.50	2.77 ± 0.69	<0.001	1.96 ± 0.52	2.76 ± 0.70	**<0.001**
LWA (°)	117.32 ± 4.97	128.17 ± 8.30	<0.001	115.48 ± 5.24	124.21 ± 6.61	**<0.001**

Table IV: Correlations Between the Parameters for CIM and Controls

Group	Parameters	LWW-ML	LWW-MP	LWW-L	LWA
CIM	LWL	-0.038	0.184	0.043	0.056
		0.794	0.070	0.674	0.582
	LWW-ML		-0.165	-0.079	-0.168
			0.258	0.590	0.248
	LWW-MP			0.168	-0.103
				0.098	0.314
	LWW-L				-0.139
					0.172
Control	LWL	**0.700****	**0.688****	**0.588****	0.107
		<0.001	**<0.001**	**<0.001**	0.281
	LWW-ML		**0.481****	0.159	0.037
			<0.001	0.259	0.794
	LWW-MP			**0.217***	0.058
				0.027	0.559
	LWW-L				0.034
					0.733

:** *p<0.05,* *:** *p<0.01, Bold values indicate statistically significant correlations.*

Table V: Distribution of LWA Types according to Study Groups

Groups	Type A	Type B	Type C	Total	p-value
CIM	0	75 (76.5%)	23 (23.5%)	98	
Controls	35 (33.7%)	69 (66.3%)	0	104	**<0.001**
Total	35	144	23	202	

- In the CIM group, positive or negative correlations were not found between the parameters. In controls, positive correlations were found between LWL and LWW-ML (p<0.001, *r*=0.700), between LWL and LWW-MP (p<0.001, *r*=0.688), between LWL and LWW-L (p<0.001, *r*=0.588), between LWW-ML and LWW-MP (p<0.001, *r*=0.481), and between LWW-MP and LWW-L (p=0.027, *r*=0.217) (Table IV).
- In the CIM group, two configurations regarding LWA types were observed: Type B in 75 LWs (76.5%) and Type C in 23 LWs (23.5%). Type A was not observed in CIM. In controls, two configurations regarding LWA types were observed: Type A in 35 LWs (33.7%) and Type B in 69 LWs (66.3%). Type C was not found in controls. The distribution of LWA types according to study groups was presented in Table V, which displayed that this classification was affected by CIM (p<0.001).

DISCUSSION

CIM is described as tonsillar herniation over 5 mm downward from the foramen magnum on MRI (9). It has an incidence of 0.24-3.6% (9). This malformation is considered mainly due to deviations in occipital somite development, arising from the paraxial mesoderm (3). In CIM, osseous components of the posterior fossa are primarily affected and this leads to about 25% reduction in fossa volume (3,21). The most obvious sign of volumetric shrinkage is the overcrowding of the hindbrain, which results in various symptoms (3,9,21). The current investigations show that the whole skull base's osseous components are substantially affected by CIM, likely resulting from a mesodermal failure (15,22). For instance, in comparison with normal subjects, such patients possess longer anterior fossa (22). Similar to CIM, the whole skull base's osseous components are substantially affected by Chiari type II malformation (CIIM) (19). For instance, in comparison with normal subjects, CIIMs had taller pituitary gland with no pathology, longer tuberculum sellae, shorter dorsum sellae, and shallow sella (19). Patel et al. stated that this condition may cause a misinterpretation like the enlargement of the pituitary gland, as the shallow sella may cause the normal gland to appear taller than normal on MRI (19). In these regards, we believe that novel examinations are required for determining whether CIM and CIIM affect morphological properties of anatomical structures like SR present in the anterior fossa and/or middle fossa.

Variations and anomalies of SR and LW have surgical implications (7,8,24). Although rare, the following variations or anomalies have been reported: fusion with the greater wing, absent LW ossification, absent LW, and LW pneumatization (7,24). Lin et al. found that the Sylvian fissure was negatively correlated with SR, and thus a shallow ridge could result in a deep fissure (11). Moreover, abnormalities of the ridge may be related to certain diseases such as Apert syndrome and neurofibromatosis type-1 (7,24). In Apert syndrome, subjects possess perpendicularly angulated SRs (24). When approaching to superior orbital fissure through the pterional technique, LW's removal may require (13). In patients with cerebral aneurysms arising from components of the circle of Willis and especially the middle cerebral artery, neurosurgeons may completely remove SR (i.e., the entire area between the anterior clinoid process and crista alaris) to more easily open the Sylvian fissure and visualize those vessels (14). In addition, LW may be used as a guide to move from lateral to medial when approaching to the cavernous sinus (5). Detailed anatomical definitions, expanded morphometric datasets, novel classifications, and radioanatomic examinations of surgical approaches may be beneficial for neurosurgeons to reduce morbidity - mortality rates (8,10,11,23,24). However, the available literature related to the ridge is primarily based on normal pediatric or adult individuals (1,8,10,24). For this reason, our results may be useful for clinicians to understand anatomical features of the anterior and middle cranial bases in CIM patients.

Substantial differences were found between the measurements of study groups. By comparison controls, CIM patients had greater LWL ($p<0.001$) and LWW-ML ($p<0.001$), but shorter LWW-MP ($p=0.001$) and LWW-L ($p<0.001$). In 180 healthy children aged 1-18 years, Alpergin et al. measured LWW-L, LWW-MP, LWW-ML and LWL as 1.91 ± 0.64 mm, 2.84 ± 0.81 mm, 7.78 ± 1.74 mm, and 28.48 ± 8.15 mm, respectively. They determined that these parameters increased with growth (1). Our measurements in controls were distinctly greater than their pediatric measurements. Tubbs et al. studied on 35 adult dry skulls and 15 adult fixed-cadavers, and measured LWW-L (2 mm), LWW-MP (20 mm), LWW-ML (15 mm) and LWL (right: 40 mm, left: 42 mm) (24). Kizilkanat et al. studied on 42 adult dry skulls, and measured LWW-L (2.6 ± 0.6 mm), LWW-ML (20 ± 2.9 mm) and LWL (left: 44.8 ± 4.2 mm, right: 46.6 ± 4 mm) (10). Our mean values of LWW-L and LWL in controls were compatible with the adult literature data, but our mean values of LWW-ML and LWW-MP in controls were distinctly smaller than the adult literature data (10,24). In both groups, no significant differences were observed between the measurements of the right and left sides, similar to the study of Alpergin et al. (1). In CIM, all parameters were similar for sexes. In controls, LWW-L, LWW-MP, LWW-ML and LWL were similar for sexes, but LWA was greater in men than women. Alpergin et al. observed that LWW-MP were greater in men than women (1). These measurements may aid in estimating the relationship between SR and adjacent structures. For instance, a small ridge can correlate with the proximal Sylvian fissure's lateral deviation (20).

CIM patients (116.42 ± 5.16°) had smaller LWA, compared to controls (126.19 ± 7.73°). Kahilogullari et al. conducted on 40 adult dry skulls, and measured LWA as 118° on the right, and 119° on the left. They also conducted on CT images of 40 patients, and measured LWA as 114.9° on the right, and 116.5° on the left (8). Our mean value of LWA in controls was distinctly greater than their measurements. In CIM, two configurations regarding LWA types were observed: Type B in 75 LWs (76.5%) and Type C in 23 LWs (23.5%). In controls, two configurations regarding LWA types were observed: Type A in 35 LWs (33.7%) and Type B in 69 LWs (66.3%). The distribution of LWA types according to study groups displayed that LWA types was affected by this malformation. CIM patients had distinctly smaller LWA in comparison with controls. Kahilogullari et al. identified three types in dry skulls (Type A: 27%, Type B: 43%, and Type C: 28%) and in CT images (Type A: 26%, Type B: 42%, and Type C: 31%). Interestingly, we did not observe Type C in controls, and Type A in CIM. They determined that SR angle was positively correlated with the middle fossa depth (8). In this regard, we think that CIM patients have shallow middle fossa compared to controls.

CONCLUSION

LWA and LWL may represent middle fossa depth and anterior fossa width, respectively; thus, subjects with CIM possess a shallow middle fossa and a wider anterior fossa.

Declarations

Funding: This research did not receive any specific grant from funding agencies in the public, commercial, or not-for-profit sectors.

Availability of data and materials: Available with the author on request.

Disclosure: The authors declare no competing interests.

AUTHORSHIP CONTRIBUTION

Study conception and design: BCA, UE, FY, MEG
Data collection: UK, OMO, EG
Analysis and interpretation of results: BCA, OB
Draft manuscript preparation: BCA, MC, OB
Critical revision of the article: BCA, UE, FY, MEG
All authors (BCA, UE, FY, UK, OMO, EG, MEG, MC, OB) reviewed the results and approved the final version of the manuscript.

REFERENCES

1. Alpergin BC, Eroglu U, Ozpiskin OM, Demiryurek S, Gedikli F, Al Khudari MQMG, Beger O: Anatomical features of the sphenoid ridge in the pediatric population. Childs Nerv Syst 40:2287-2294, 2024. https://doi.org/10.1007/s00381-024-06391-y
2. Alpergin BC, Eroglu U, Zaimoglu M, Kilinc MC, Ozpiskin OM, Erdin E, Beger O: Topographic anatomy and pneumatization of the posterior clinoid process in Chiari type I malformation. World Neurosurg 185:e767-e773, 2024. https://doi.org/10.1016/j.wneu.2024.02.130
3. Aydin S, Hanimoglu H, Tanriverdi T, Yentur E, Kaynar MY: Chiari type I malformations in adults: A morphometric analysis of the posterior cranial fossa. Surg Neurol 64:237-241, 2005. https://doi.org/10.1016/j.surneu.2005.02.021

4. Bas G, Ozkara E, Ozbek Z, Naderi S, Arslantas A: Sella volume and posterior fossa morphometric measurements in Chiari type 1. Turk Neurosurg 33:290-295, 2023. https://doi.org/10.5137/1019-5149.JTN.40088-22.4
5. Coscarella E, Baskaya MK, Morcos JJ: An alternative extradural exposure to the anterior clinoid process: The superior orbital fissure as a surgical corridor. Neurosurgery 53:162-166, 2003. https://doi.org/10.1227/01.neu.0000068866.22176.07
6. Guinto G, Abello J, Félix I, González J, Oviedo A: Lesions confined to the sphenoid ridge: Differential diagnosis and surgical treatment. Skull Base Surg 7:115-121, 1997. https://doi.org/10.1055/s-2008-1058602
7. Jacquemin C, Mullaney P, Bosley TM: Abnormal development of the lesser wing of the sphenoid with microphthalmos and microcephaly. Neuroradiology 43:178-182, 2001. https://doi.org/10.1007/s002340000455
8. Kahilogullari G, Uz A, Eroglu U, Apaydin N, Yesilirmak Z, Baskaya MK, Egemen N: Does the sphenoid angle effect the operation strategy? Anatomical and radiological investigation. Turk Neurosurg 22:618-623, 2012. https://doi.org/10.5137/1019-5149.JTN.5790-12.0
9. Kahn EN, Muraszko KM, Maher CO: Prevalence of Chiari I malformation and syringomyelia. Neurosurg Clin N Am 26:501-507, 2015. https://doi.org/10.1016/j.nec.2015.06.006
10. Kizilkanat ED, Boyan N, Tekdemir I, Soames R, Oguz O: Surgical importance of the morphometry of the anterior and middle cranial fossae. Neurosurg Q 17:60-63, 2007. https://doi.org/10.1097/WNQ.0b013e318033a5b7
11. Lin J, Nauta HJ, Olivero W: Anatomical relationships between Sylvian fissure and the sphenoid ridge. Neurol Res 23:645-646, 2001. https://doi.org/10.1179/016164101101198947
12. MacCarty CS: Meningiomas of the sphenoidal ridge. J Neurosurg 36:114-120, 1972. https://doi.org/10.3171/jns.1972.36.1.0114
13. Morard M, Tcherekayev V, de Tribolet N: The superior orbital fissure: A microanatomical study. Neurosurgery 35:1087-1093, 1994. https://doi.org/10.1227/00006123-199412000-00011
14. Nathal E, Gomez-Amador JL: Anatomic and surgical basis of the sphenoid ridge keyhole approach for cerebral aneurysms. Neurosurgery 56:178-185, 2005. https://doi.org/10.1227/01.neu.0000145967.66852.96
15. Nwotchouang BST, Eppelheimer MS, Bishop P, Biswas D, Andronowski JM, Bapuraj JR, Frim D, Labuda R, Amini R, Loth F: Three-dimensional CT morphometric image analysis of the clivus and sphenoid sinus in Chiari malformation type I. Ann Biomed Eng 47:2284-2295, 2019. https://doi.org/10.1007/s10439-019-02301-5
16. Ozalp H, Ozgural O, Alpergin BC, Inceoglu A, Ozalp S, Armagan E, Ucar H, Beger O: Analysis of the cranial aperture of the optic canal in Chiari type I malformation. Turk Neurosurg 34:1081-1092, 2024. https://doi.org/10.5137/1019-5149.JTN.45482-23.2
17. Ozalp H, Ozgural O, Alpergin BC, Inceoglu A, Ozalp S, Armagan E, Ucar H, Beger O: Analysis of the prechiasmatic sulcus in Chiari malformation type I. World Neurosurg 175:e1149-e1157, 2023. https://doi.org/10.1016/j.wneu.2023.04.083
18. Ozalp H, Ozgural O, Alpergin BC, Inceoglu A, Ozalp S, Armagan E, Ucar H, Beger O: Assessment of the anterior clinoid process and optic strut in Chiari malformation type I: A computed tomography study. J Neurol Surg B Skull Base 85:302-312, 2023. https://doi.org/10.1055/s-0043-57248, 2023
19. Patel D, Saindane A, Oyesiku N, Hu R: Variant sella morphology and pituitary gland height in adult patients with Chiari II malformation: Potential pitfall in MRI evaluation. Clin Imaging 64:24-28, 2020. https://doi.org/10.1016/j.clinimag.2020.02.014
20. Sato S, Kashimura H, Akamatsu Y, Fujiwara S, Kubo Y, Ogasawara K: Small sphenoid ridge as a factor associated with laterally deviated proximal Sylvian fissure in patients undergoing pterional craniotomy. World Neurosurg 167:e705-e709, 2022. https://doi.org/10.1016/j.wneu.2022.08.069
21. Schady W, Metcalfe RA, Butler P: The incidence of craniocervical bony anomalies in the adult Chiari malformation. J Neurol Sci 82:193-203, 1987. https://doi.org/10.1016/0022-510x(87)90018-9
22. Sgouros S, Kountouri M, Natarajan K: Skull base growth in children with Chiari malformation Type I. J Neurosurg 107:188-192, 2007. https://doi.org/10.3171/PED-07/09/188
23. Spiriev T, Poulsgaard L, Fugleholm K: One piece orbitozygomatic approach based on the sphenoid ridge keyhole: Anatomical study. J Neurol Surg B Skull Base 77:199-206, 2016. https://doi.org/10.1055/s-0035-1564590
24. Tubbs RS, Salter EG, Oakes WJ: Quantitation of and measurements utilizing the sphenoid ridge. Clin Anat 20:131-134, 2007. https://doi.org/10.1002/ca.20255

Turk Neurosurg 35(4):667-671, 2025
DOI: 10.5137/1019-5149.JTN.47423-24.1

Case Report

Received: 24.08.2024
Accepted: 07.10.2024
Published Online: 25.06.2025

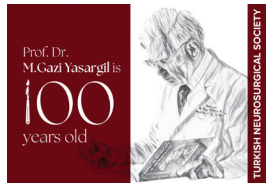

Bilateral Thalamic Edema Caused by Tentorial Galenic Dural Arteriovenous Fistula and Sinus Thrombosis: Successful Endovascular Therapy

Xiaolong LIANG[1], Li WANG[1], Yumin YANG[1], Aiguo LI[1], Yangyun HAN[1], Jian YANG[1], Xiaodong LONG[1], Chaohua WANG[2], Jie LIU[3]

[1]Sichuan Clinical Research Center for Neurological Diseases, Deyang Hospital affiliated to Chengdu University of Chinese Medicine, Department of Neurosurgery, Deyang, China
[2]Sichuan University, West China School of Medicine and West China Hospital, Department of Neurosurgery, Chengdu, China
[3]The Second Affiliated Hospital of Guilin Medical College, Department of Neurosurgery, Guangxi, China

Corresponding author: Aiguo LI ✉ liaiguo74@163. com

ABSTRACT

Bilateral thalamic edema is commonly caused by vascular, toxic/metabolic, neoplastic, and infectious factors. However, dural arteriovenous fistulas (DAVFs) are a relatively rare and often overlooked cause, with an incidence rate of about 8%. Tentorial dural arteriovenous fistulas (TDAVFs) represent a rare subtype. Cerebral angiography often shows TDAVFs with reflux into cortical or subarachnoid veins and retrograde deep drainage through the vein of Galen, which is associated with a high risk of hemorrhage—97% of cases involve hemorrhage and exhibit aggressive neurological behavior. Venous sinus thrombosis, high-flow arteriovenous malformations, or a combination of both can result in venous hypertension, leading to bilateral thalamic dysfunction. The arterial supply to TDAVFs is complex, involving meningeal arteries from the vertebral and internal carotid arteries, which are difficult to cannulate, increasing the risk of complications due to retrograde embolic flow compared to external carotid artery (ECA) feeders. Transvenous navigation to deep lesions around the tentorium is also challenging. Additionally, TDAVFs often drain into subarachnoid or cortical veins rather than their associated sinus (Borden Type III), making transvenous embolization impossible. The middle meningeal artery, which supplies more than two-thirds of the cranial dura, is the primary dural feeder. In this article, we presented a unique case of symptomatic bilateral thalamic edema caused by both a tentorial galenic DAVF and straight sinus thrombosis of the cerebral deep venous system, and we detailed our treatment approach and experience.

KEYWORDS: Tentorial dural arteriovenous fistula, TDAVF, Thalamic edema, Sinus thrombosis, Endovascular treatment

INTRODUCTION

Intrantracranial dural arteriovenous fistulas (DAVFs) account for approximately 10% to 15% of all intracranial arteriovenous malformations. They commonly occur in areas such as the cavernous sinus, transverse sinus, sigmoid sinus, and sagittal sinus. These fistulas typically form on the walls of the venous sinuses and are often multiple (1,9). Tentorial dural arteriovenous fistulas (TDAVFs) are a rare subtype of DAVFs, with an incidence rate of about 12% (12). They are generally considered to have the most life-threatening vascular structures, with an aggressive prognosis and natural history. Bilateral thalamic edema can have many causes, but DAVFs are a relatively uncommon and under-recognized cause, with an incidence rate of about 8% (6). Here, we presented a patient with bilateral thalamic edema caused by a TDAVF, successfully treated with transarterial embolization. The patient's deep venous drainage remained intact, and their cognitive function significantly improved over a few weeks.

Xiaolong LIANG : 0000-0002-4145-9315
Li WANG : 0009-0001-9771-4952
Yumin YANG : 0000-0001-5136-3133
Aiguo LI : 0009-0009-4346-2022
Yangyun HAN : 0000-0001-7788-990X
Jian YANG : 0000-0001-6318-8854
Xiaodong LONG : 0009-0008-8877-855X
Chaohua WANG : 0009-0007-8658-8720
Jie LIU : 0009-0000-4293-1266

CASE REPORT

A 67-year-old healthy man was brought to the emergency department by his son, presenting with mental status changes after one month of progressively increasing somnolence and confusion. He had no focal neurological deficits and could follow simple instructions, but was unable to follow more complex commands. A subsequent magnetic resonance imaging (MRI) scan showed bilateral thalamic and left parietal lobe hyperintensity with minimal mass effect. The scan revealed a "butterfly" appearance, suggesting a lesion crossing the midline through the inter-thalamic adhesion (Figure 1). Magnetic resonance perfusion (MRP) showed that the lesion in the left occipital lobe was lower and longer than the contralateral side. Regional cerebral blood flow (rCBF) and regional cerebral blood volume (rCBV) were decreased, and mean transit time (MTT) was prolonged in both thalami. A preoperative sagittal magnetic resonance venography (MRV) scan demonstrated chronic thrombosis of the straight sinus and a tentorial galenic DAVF (Figure 2). Further angiography confirmed a TDAVF, with supply from branches of the right occipital artery and retrograde venous drainage into the vein of Galen, internal cerebral veins, and the right parietal cortical veins. No filling of the straight sinus was observed, consistent with thrombosis (Figure 3). Given that the middle meningeal artery is the primary dural artery, supplying more than two-thirds of the cranial dura(12), the fistula was embolized using Onyx (eV3) via a transarterial approach (Figure 4). Deep venous drainage remained intact, and the patient's cognitive abilities significantly improved within a few weeks (Figure 1-D).

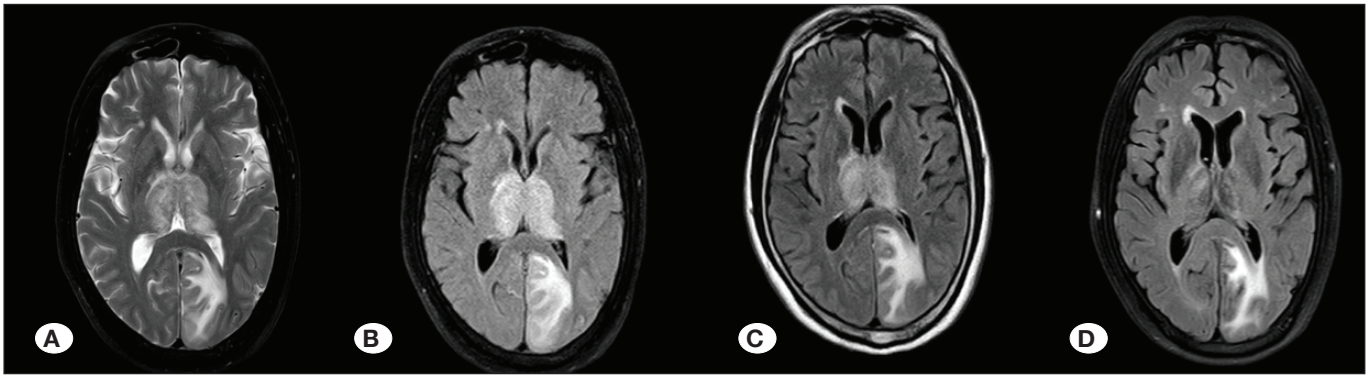

Figure 1: MRI **A)** T2-weighted axial and **B)** FLAIR demonstrating bilateral thalamic and left parietal lobe hyperintensity with minimal mass effect. Note the "butterfly" appearance suggesting a lesion crossing the midline through the interthalamic adhesion. **C)** FLAIR demonstrating bilateral thalamic and left parietal lobe hyperintensity reducing after postoperative one day. **D)** Images obtained 3 weeks after endovascular embolization of DAVF. FLAIR MRI showing resolution of bi-thalamic hyperintensities.

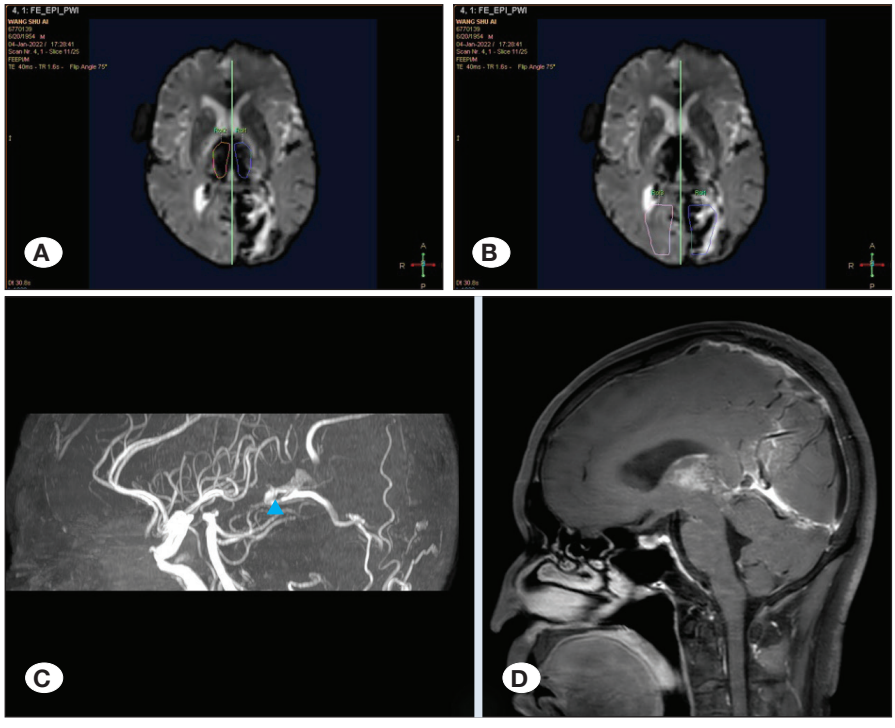

Figure 2: MRP (magnetic resonance perfusion weighted imaging) **A)** The rCBF, rCBV and MTT in the lesion area of left occipital lobe were lower and longer than contralateral. **B)** The rCBF, rCBV decreased and MTT prolonged in bilateral thalamus. **C, D)** Preoperative MRVs demonstrating occlusion of the straight sinus and Tentorial Galenic dural Arteriovenous Fistula (blue arrowhead).

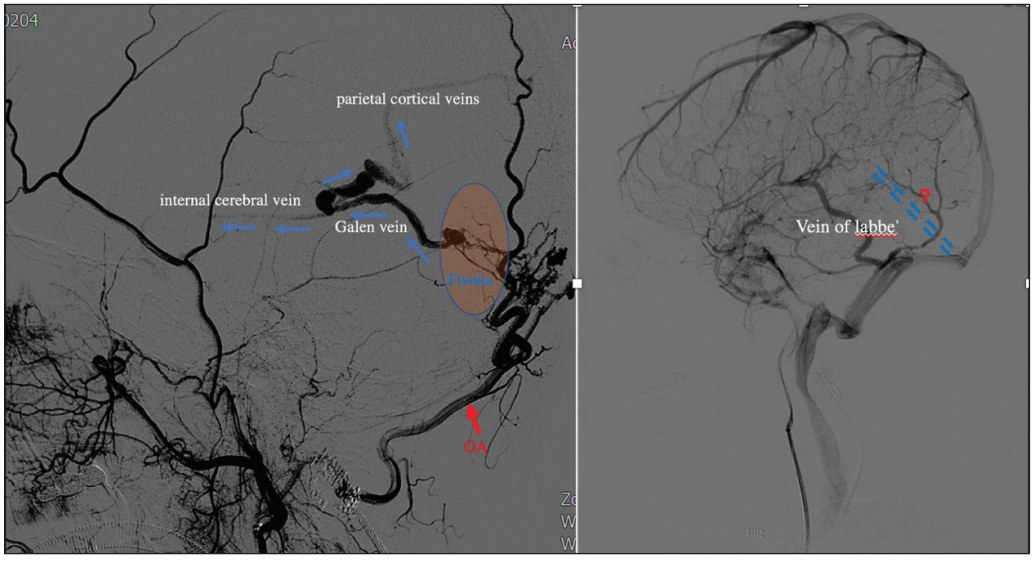

Figure 3: Right external carotid artery angiography shows a tentorial galenic DAVF (Borden type III,Cognard type III) with supply from the branches of the right occipital artery (OA red arrow), with retrograde venous drainage into the vein of Galen and internal cerebral veins as well as into the right parietal cortical veins. No filling of distal the straight sinus (dashed lines) was noted, consistent with thrombosis.

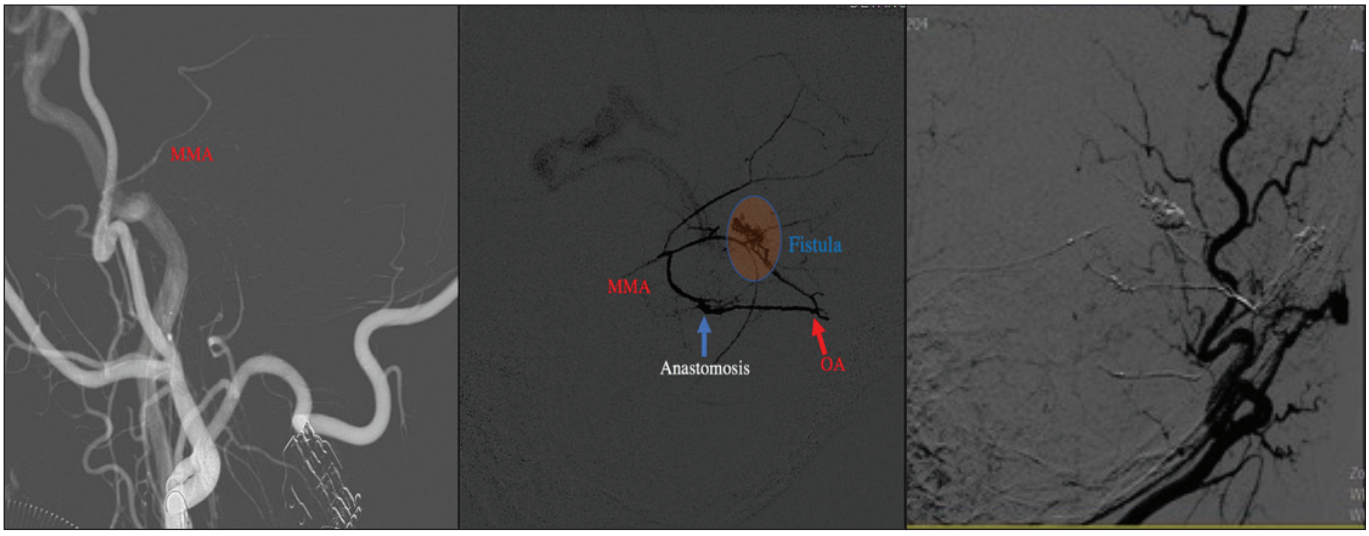

Figure 4: During the operation, Right middle meningeal angiography shows the middle meningeal artery and he branches of the right occipital artery exists collateral anastomoses (blue arrow). Selective angiogram of right external carotid artery demonstrates complete obliteration of the fistula.

DISCUSSION

Diseases affecting the thalamus are broad in their etiologies, including infectious, inflammatory, neoplastic, toxic/metabolic, and vascular causes, such as arterial cerebral infarction, venous thrombosis, arteriovenous malformations, and atypical posterior reversible encephalopathy syndrome (PRES). Typically, DAVFs are not commonly listed in the classic radiological differential diagnosis for thalamic lesions (5,17). DAVFs are relatively rare, with an incidence rate of about 8%, and are an often under-recognized cause of thalamic edema. The natural history, clinical presentation, and prognosis of TDAVFs are closely related to their venous drainage patterns (7,15). Clinically, Borden types IIa+b and IIITDAVFs are more frequently encountered, indicating retrograde leptomeningeal venous drainage, with or without sinus drainage (16,19). In our case, the patient had a DAVF involving the cortical veins of the right parietal cortex, the vein of Galen, and the straight sinus. Due to prolonged venous hypertension, patients with TDAVFs often present with progressive neurological deficits and/or intracranial hemorrhage (16,19). Therefore, there is a strong indication for treatment to prevent catastrophic complications (1). Neuroimaging is crucial for diagnosing TDAVFs. Plain computed tomography (CT) scans can rapidly identify subarachnoid or intraventricular hemorrhage, and three-dimensional CT reconstruction can reveal varicose draining veins. MRI can visualize the tentorial subarachnoid space, bulging at the tentorial edge, and distorted vascular flow voids, often indicating venous congestion and tumor-like changes. On T2-weighted images, the thalamus, midbrain, cerebellum, and high cervical spinal cord may show high-signal changes due to secondary edema from venous hypertension (4). However, these imaging

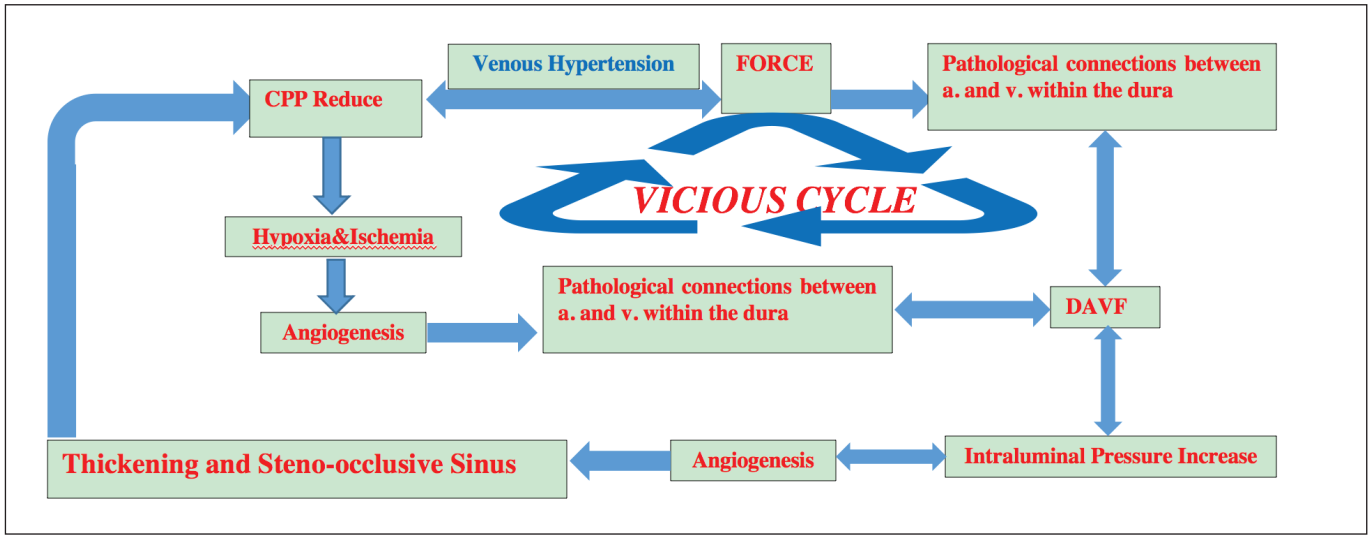

Figure 5: The "Vicious Circle" mechanism of dural arteriovenous fistula.

findings lack specificity and can be confused with intracranial demyelinating lesions, tumors, or inflammation. Angiography remains the gold standard for diagnosis. The feeding arteries and draining veins of TDAVFs are complex and often originate from six different sources: the artery of Bernasconi-Cassinari (11), the middle meningeal artery, the posterior meningeal artery, the artery of Davidoff-Schechter (2), scalp arteries, and miscellaneous branches of the external carotid artery (12). The venous drainage of the thalamus typically occurs via the cerebral deep venous system, with the anterior septal vein and thalamostriate vein draining into the internal cerebral vein, which joins the basal vein of Rosenthal to form the vein of Galen. The vein of Galen and inferior sagittal sinus unite to form the straight sinus, which drains into the torcular Herophili (14). This complex angioarchitecture often leads to progressive cognitive dysfunction, aphasia, ataxia, and focal neurological deficits (6,8,10,16). Given the complexity of TDAVFs, selective angiography should be performed on both internal and external carotid arteries, as well as the vertebral arteries, to identify all potential feeding routes and allow for more treatment options. In our case, conventional angiography did not initially show the feeding arteries of the middle meningeal artery. Based on the theory of anastomoses between meningeal arteries at the skull base, we performed selective angiography on the right middle meningeal artery, which revealed collateral anastomoses between the middle meningeal artery and branches of the right occipital artery. This case highlighted a successful endovascular approach for TDAVF, using the middle meningeal artery, which passes through the foramen spinosum. The fistula was super-selectively catheterized and successfully embolized via a transarterial approach. Anticoagulation is typically the primary treatment for sinus thrombosis (18). In this case, however, anticoagulation alone was not considered due to the "vicious cycle" mechanism of DAVF (Figure 5). Abnormal blood flow through the fistula drains via the pial veins, predominantly flowing retrograde into the straight sagittal sinus through the dilated parietal cortical veins at the tentorial incisura, with some flow directed into the internal cerebral vein. High-flow arterial blood enters the thin-walled cortical veins, causing passive dilation and high tension due to turbulent flow. This, along with turbulence at the junction of draining veins and venous sinuses, predisposes the area to thrombosis formation. Thrombosis further increases pressure in the proximal draining veins, leading to morphological adaptations such as tortuosity, venous bulbs, or venous lakes to compensate for the high pressure. Additionally, the high-pressure state triggers an inflammatory response that stimulates angiogenic and epidermal growth factors, resulting in further thickening and arterialization of the veins. This vicious cycle significantly increases the risk of rupture and hemorrhage in TDAVFs compared to other DAVFs, where abnormal blood flow enters the venous sinus directly. Because of the inherent risk of DAVF rupture and the limited likelihood of symptom improvement without intervention, we opted for endovascular treatment rather than anticoagulation alone. Furthermore, intracranial DAVFs combined with cerebral vein thrombosis were not typically associated with a worse prognosis (3).

CONCLUSION

Encouragingly, we have illustrated the potential formation mechanism of the DAVF, and the TDAVF was successfully embolized through the optimal channel of the middle meningeal artery ("All roads lead to Fistula"). Based on the anastomotic theory between the meningeal arteries at the skull base, this case demonstrates an excellent endovascular approach for TDAVF. The middle meningeal artery, emerging from the foramen spinosum, was super-selectively catheterized via angiography, allowing precise identification of the fistula shunt and successful embolization of the TDAVF via a transarterial approach. This method ingeniously overcame the challenges posed by the deep anatomical location of the TDAVF, as well as the difficulties of microsurgical exposure and resection. Moreover, it minimized the risk of severe complications, such as embolic material retrogradely flowing into branches of the internal carotid artery and vertebral artery.

ACKNOWLEDGEMENTS

Consent to participate: Informed consent was obtained from all individual participants included in the study.

Consent to publication: This patient gave his informed consent for the publication and medical records for the figures and video recordings.

Declarations

Funding: This work was supported by the Science and Technology Project of Deyang City, Sichuan Province (Key research and development guidance in the field of Social Development) 2023SZZ026.

Availability of data and materials: The datasets generated and/or analyzed during the current study are available from the corresponding author by reasonable request.

Disclosure: The authors declare no competing interests.

AUTHORSHIP CONTRIBUTION

Study conception and design: XL, AL, YH, CW

Data collection: XL, LW, AL, YH, JY, CW

Analysis and interpretation of results: XL, YY, AL, YH, CW

Draft manuscript preparation: XL, YH, LW, AL

Critical revision of the article: XL, LW, AL, DL, JY

Other (study supervision, fundings, materials, etc...): XL, LW, YH, JL

All authors (XL, LW, YY, AL, YH, JY, XL, CW, JL) reviewed the results and approved the final version of the manuscript.

REFERENCES

1. Alkhaibary A, Alnefaie N, Alharbi A, Alammar H, Arishy AM, Alshaya W, Khairy S: Intracranial dural arteriovenous fistula: A comprehensive review of the history, management, and future prospective. Acta Neurol Belg 123:359-366, 2023. https://doi.org/10.1007/s13760-022-02133-6.
2. Bhatia KD, Kortman H, Wälchli T, Radovanovic I, Pereira VM, Krings T: Artery of davidoff and schechter supply in dural arteriovenous fistulas. AJNR Am J Neuroradiol 41:300-304, 2020. https://doi.org/10.3174/ajnr.A6380.
3. Cohen C, Lenck S, Talbi A, Ifergan H, Premat K, Boulouis G, Janot K, Boch AL, Magni C, Herbreteau D, Sourour N, Shotar E, Barrot V, Clarencon F: Intracranial dural arteriovenous fistulas: association with cerebral venous thrombosis, baseline aggressiveness, and clinical outcomes. A retrospective multicenter study on 263 consecutive patients and literature review. Neurosurg Focus 56:E9, 2024. https://doi.org/10.3171/2024.1.FOCUS23748.
4. Cox M, Rodriguez P, Mohan S, Sedora-Roman NI, Pukenas B, Choudhri O, Kurtz RM: Tentorial dural arteriovenous fistulas as a cause of thalamic edema: 2 cases of an important differential diagnosis to consider. Neurohospitalist 11:33-39, 2021. https://doi.org/10.1177/1941874420944333.
5. de Freitas Ribeiro BN, Marchiori E: Evaluation of neuroimaging findings in thalamic lesions: What can we think?. Radiol Bras 54:341-347, 2021. https://doi.org/10.1590/0100-3984.2020.0129.
6. Ferrazzoli V, Picchi E, Pitocchi F, Vattermoli L, Pucci N, Di Giuliano F, Wlderk A, Bagnato MR, Da Ros V, Garaci F, Floris R: Bithalamic infarction in a tentorial dural artero-venous fistula and thalamic dementia: A case report and systematic review. Neurol Sci 44:2291-2304, 2023. https://doi.org/10.1007/s10072-023-06716-w.
7. Hiramatsu M, Haruma J, Sugiu K, Tanaka S: Angioarchitecture and associated dural arteriovenous fistulas of the superior petrosal sinus and petrosal vein. No Shinkei Geka 52:596-604, 2024. https://doi.org/10.11477/mf.1436204953.
8. Holekamp TF, Mollman ME, Murphy RK, Kolar GR, Kramer NM, Derdeyn CP, Moran CJ, Perrin RJ, Rich KM, Lanzino G, Zipfel GJ: Dural arteriovenous fistula-induced thalamic dementia: Report of 4 cases, 2016. J Neurosurg 124:1752-1765. https://doi.org/10.3171/2015.5.JNS15473.
9. Howard BM, Barrow DL: Carotid cavernous fistula. Neurosurg Clin N Am 35:319-329, 2024. https://doi.org/10.1016/j.nec.2024.02.004.
10. Khan A, Elkady A, Rahametallah M, Bakheet MF: Dural arteriovenous fistula presenting as a rapidly progressive thalamic dementia: A case report. Cureus 14:e29392, 2022. https://doi.org/10.7759/cureus.29392.
11. Kutia SA, Yarovaya OY, Kuznetsova EV, Obukhova DD, Kuznetsov VI: Clinical anatomy of the Bernasconi-Cassinari artery. Zhurnal Nevrologii i Psikhiatrii imeni S.S. Korsakova 124:12-17, 2024. https://doi.org/10.17116/jnevro202412403212.
12. Lawton MT, Sanchez-Mejia RO, Pham D, Tan J, Halbach VV: Tentorial dural arteriovenous fistulae: Operative strategies and microsurgical results for six types. Neurosurgery 62:110-125, 2008. https://doi.org/10.1227/01.neu.0000317381.68561.b0.
13. Martins C, Yasuda A, Campero A, Ulm AJ, Tanriover N, Rhoton A Jr: Microsurgical anatomy of the dural arteries. Neurosurgery 56:211-251, 2005. https://doi.org/10.1227/01.neu.0000144823.94402.3d.
14. Ono M, Rhoton AL Jr, Peace D, Rodriguez RJ: Microsurgical anatomy of the deep venous system of the brain. Neurosurgery 15:621-657, 1984. https://doi.org/10.1227/00006123-198411000-00002.
15. Prenc M, Žižek H, Radić P, Škoro M, Novak AM, Čulo B, Kalousek V: Step-by-step venous navigation in treatment of tentorial dural arteriovenous fistula supplied by artery of Bernasconi and Cassinari. Interv Neuroradiol, 2024 (Online ahead of print). https://doi.org/10.1177/15910199241258656.
16. Rezende MTS, Trivelato FP, de Castro-Afonso LH, Nakiri GS, Silva CCM, Abud TG, Colli BO, Ulhôa AC, Abud DG: Endovascular treatment of tentorial dural arteriovenous fistulas using the transarterial approach as a first-line strategy. Oper Neurosurg 20:484-492, 2021. https://doi.org/10.1093/ons/opaa477.
17. Van Cauter S, Severino M, Ammendola R, Van Berkel B, Vavro H, van den Hauwe L, Rumboldt Z: Bilateral lesions of the basal ganglia and thalami (central grey matter)-pictorial review. Neuroradiology 62:1565-1605, 2020. https://doi.org/10.1007/s00234-020-02511-y.
18. Weimar C, Beyer-Westendorf J, Bohmann FO, Hahn G, Halimeh S, Holzhauer S, Kalka C, Knoflach M, Koennecke HC, Masuhr F, Mono ML, Nowak-Göttl U, Scherret E, Schlamann M, Linnemann B: New recommendations on cerebral venous and dural sinus thrombosis from the German consensus-based (S2k) guideline. Neurol Res Pract 6:23, 2024. https://doi.org/10.1186/s42466-024-00320-9.
19. Zhang G, Zhang W, Chang H, Shen Y, Ma C, Mao L, Li Z, Lu H: Endovascular treatment strategy and clinical outcome of tentorial dural arteriovenous fistula. Front Neurol 14:1315813, 2024. https://doi.org/10.3389/fneur.2023.1315813.

Turk Neurosurg 35(4):672-676, 2025
DOI: 10.5137/1019-5149.JTN.46720-24.2

Case Report

Received: 15.04.2024
Accepted: 25.10.2024
Published Online: 25.06.2025

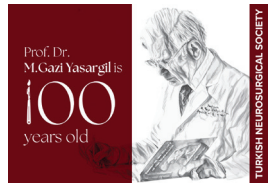

Traumatic Spinal Epidural Hematoma Associated with Cervical Nerve Root Avulsion without Vertebral Fractures: Case Report

Rafael APONTE-CABALLERO[1,2], Valentina OSEJO-ARCOS[1,2], Luis Carlos AVELLANEDA C[3], Humberto MADRINAN-NAVIA[1,2], Mario FERNANDO RODRÍGUEZ S[1,3], William Mauricio RIVEROS-CASTILLO[1,2], Javier Mauricio SAAVEDRA G[1,3], Camilo E PEÑA[1,3]

[1]Center for Research and Training in Neurosurgery (CIEN), Bogotá, Colombia
[2]Universidad del Rosario, School of Medicine, Bogotá, Colombia
[3]Orinoquia Hospital, Neurosurgery Department, Yopal, Colombia

This study has been presented at the EANS 2021 between 3 and 10 October, 2021 in Hamburg, Germany

Corresponding author: Rafael APONTE-CABALLERO ✉ rafael.aponte@urosario.edu.co

ABSTRACT

Traumatic spinal epidural hematoma (TSEH) is a rare condition that may cause acute spinal cord compression and lead to irreversible neurological impairment. TSEH not only compresses the cord, but it can also worsen cervical nerve root avulsion. To our knowledge, only five cases of combined TSEH and cervical nerve root avulsion have been reported in the literature. We present the case of a 42-year-old woman who suffered a motorcycle accident. On admission, she presented with mild traumatic brain injury and cervical spine and right shoulder trauma. A physical examination revealed numbness and flaccid paresis in her right arm, compromising the C5 to T1 dermatomes and myotomes. MRI images showed evidence of a right anterolateral spinal epidural hematoma (SEH) that extended from the C2 to C7 vertebral levels. MRI and electromyography findings of the presence of a pseudomeningocele from the C4-C5 to C7-T1 levels indicating brachial plexus neurotmesis supported the presence of a cervical nerve root avulsion associated with TSEH. Cervical plexus syndrome requires a comprehensive diagnostic workup. SEH should be considered a cause of nerve root avulsion and brachial plexus syndrome. We believe that the extension of SEH into the intervertebral foramina could be a radiological sign related to nerve root avulsion.

KEYWORDS: Spinal cord, Epidural, Brachial plexus neuropathies

INTRODUCTION

Spinal epidural hematoma (SEH) is a rare condition that causes acute spinal cord compression and may lead to irreversible neurological impairment (9,13). This condition requires early diagnosis and high-priority surgery because early evacuation is associated with better functional outcomes in certain cases (9,13). Although multiple causative factors have been described, 40–50% of cases are of unknown origin. The remaining cases can be attributed to trauma, surgically induced lesions, malignancy, and other causes (1,9,13). Spontaneous SEH is defined as a hematoma that appears after a minor trauma that is not sufficiently severe to cause vertebral fractures (VFs) or a hematoma without an identifiable cause (1,9,13). A traumatic spinal epidural hematoma (TSEH) is uncommon, occurring in only 0.5–1.7% of all spinal injuries,

Rafael APONTE-CABALLERO : 0000-0002-2740-8837
Valentina OSEJO-ARCOS : 0000-0002-2037-0506
Luis Carlos AVELLANEDA C : 0000-0002-2833-2985
Humberto MADRINAN-NAVIA : 0000-0001-7862-4057
Mario Fernando RODRIGUEZ S : 0000-0002-2093-9299
William Mauricio RIVEROS-CASTILLO : 0000-0003-3978-2153
Javier Mauricio SAAVEDRA G : 0000-0001-9935-3903
Camilo E PEÑA : 0000-0001-8006-2348

but it is often associated with VFs (2,3,8). TSEH presents more frequently in men, with the usual location being the posterior aspect of the spinal canal (9,13).

The presence of nerve root avulsion (NRA) and TSEH on the cervical spine (C-spine) is rare, with only five cases reported in the literature (3–5,10,15). This combination can occur when a sufficiently disruptive force exerted on the spine exceeds the nerve root's elastic limit and causes its separation from the spinal cord (12). Herein, we describe the case of a 42-year-old woman with a brachial plexus NRA related to a high-impact cervical injury and subsequent TSEH.

CASE REPORT

History and Physical Examination

A 42-year-old woman presented to the emergency department after a motorcycle accident in which she suffered mild trauma to her right shoulder, cervical spine, and head. Her medical history was unremarkable.

Her vital signs and mental status were normal. A physical examination revealed numbness and flaccid paresis of the right arm involving the C5 to T1 myotomes. She also had areflexia of the biceps, brachioradialis, and triceps muscles.

Imaging and Management

X-rays and CT scans of the cervical and thoracic spine showed a fracture of the right first rib but no C-spine lesion. A C-spine MRI conducted due to the neurological deficit revealed a right SEH that extended from the C2-C7 vertebral levels and compromised the C4-C5, C5-C6, and C6-C7 right foramina. The SEH was associated with a right anterior subdural spinal hematoma that deviated posteriorly and contralaterally (Figure 1). An MRI of the brachial plexus also demonstrated edema and altered signal intensity in the scalene muscles (SMs), which hindered the optimal visualization of the plexus trunks on the right side (Figure 2).

The neurological status of the patient remained stable during the ER visit. Conservative medical treatment with rehabilitation was initiated, and an outpatient-clinic follow-up was scheduled.

A follow-up performed one month after the traumatic lesion revealed no change in the patient's right superior limb monoplegia. However, a C-spine MRI taken during that visit showed absorption of the SHE, and a brachial plexus MRI revealed a pseudo-meningocele arising from the C4-C5 to C7-T1 levels (Figure 3).

Electromyography and nerve conduction velocity tests revealed H-reflexes and F-waves, indicating brachial plexus neurotmesis, denervating lesions, and limited voluntary activity from the primary inferior trunk. Conservative treatment with physical therapy was prescribed.

DISCUSSION

Our literature review uncovered only five reported cases of cervical TSEH associated with brachial plexus nerve root avulsion (Table I) (3–5,10,15). All five cases were preceded by high-energy trauma that caused nonvertebral fractures. Our findings are consistent with these previous reports, as our patient presented with only a rib fracture. Moreover, the

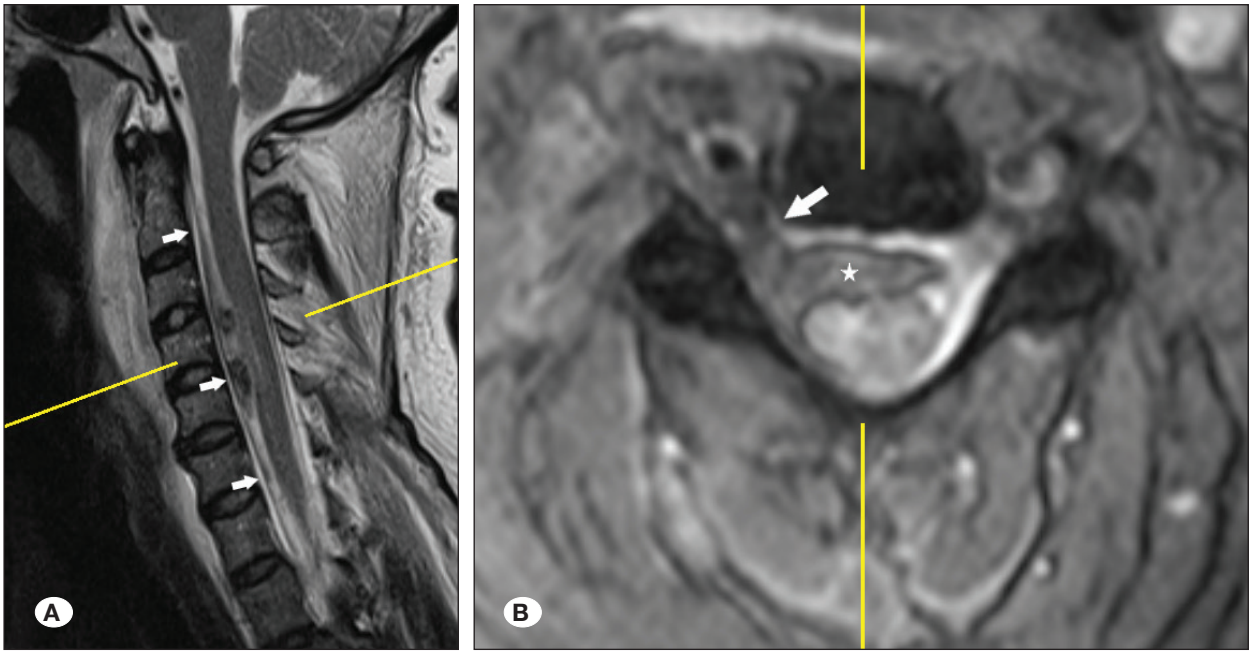

Figure 1: Cervical spine MRI. **A)** T2 sagittal sequence showing an anterior spinal hematoma (white arrows) that extends from C2-C7 with subdural characteristics due to preservation of peridural fat. **B)** T2 axial sequence, showing right anterolateral subdural hematoma (white star), causing posterior spinal cord compression limited by a denticulate ligament. The epidural component extends from the C4 to C5 right foramen (white arrow).

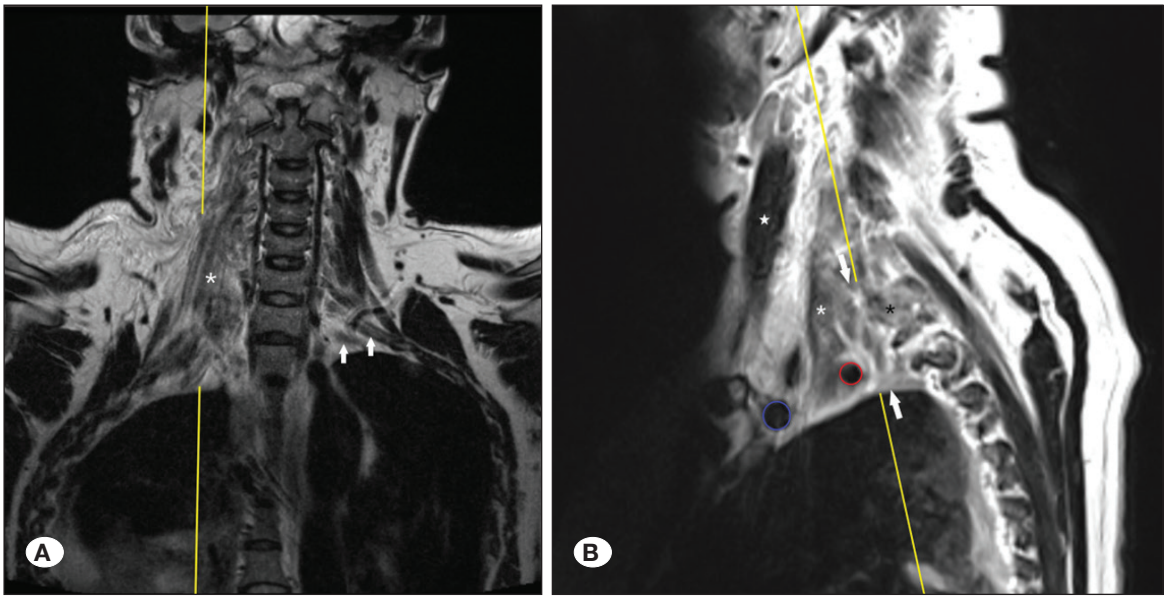

Figure 2: MRI of the brachial plexus. **A)** T2W coronal sequence showing edema of the right scalene muscles (SM) (white asterisk) that obscures the trunks of the right plexus, which can be seen contralaterally (white arrows). **B)** T2W sagittal sequence showing the trunks of the right plexus (white arrows) and the anterior and middle SM (white and black asterisks). The edema of the SM can be compared with the normal sternocleidomastoid muscle (white star).

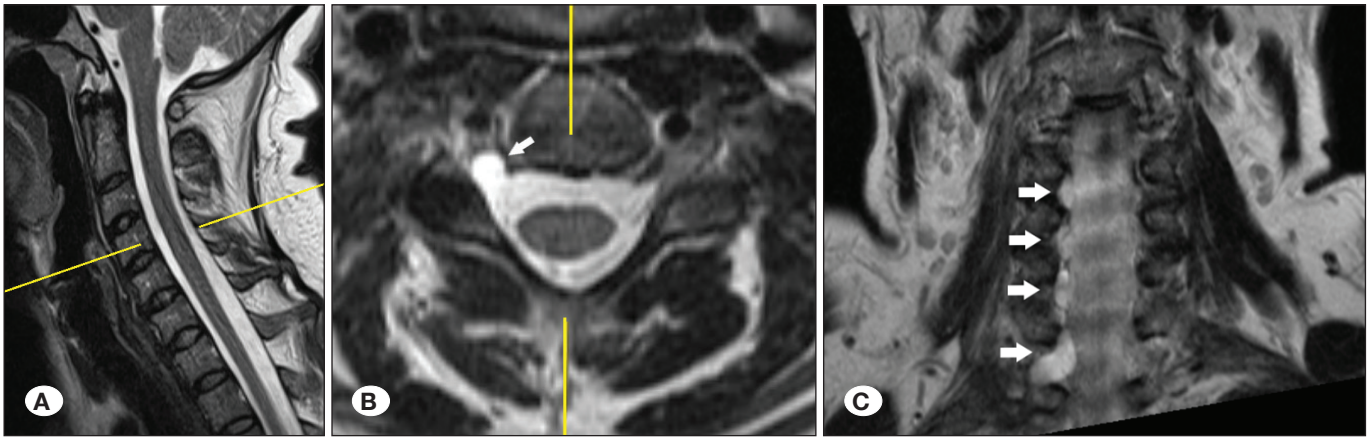

Figure 3: T2W cervical spine MRIs at 30-day follow-up. **A)** Sagittal view. **B)** Axial view of C4-C5 vertebral levels showing complete hematoma reabsorption. Presence of C4-C5 right pseudomeningocele (white arrow). **C)** Coronal view, showing C4-C5 to C7-T1 right pseudomeningoceles (white arrows).

Table I: Comparative Table of Published Cases Involving a Combination of Cervical Spine Epidural Hematoma and Nerve Root Avulsion in the Brachial Plexus

Case	Non-Cervical Fracture	C-spine Fracture	Electrophysiologic Study	Sphincter Injury	Spinal Level	Surgical Treatment	Outcome of motor deficit at follow-up
Giugale et al. (4)	Yes	Yes	Yes	No	C2-T4	Yes[a]	Not mentioned
Haider et al. (5)	Yes	No	No	No	C5-T11	No	No improvement
Newman et al. (10)	Yes	No	No	No	C5-T10	No	No improvement
Garg et al. (3)	Yes	No	Yes	No	C3-T2	Yes[a]	No Improvement
Zubair et al. (15)	Yes	Yes	No	No	C6-T1	No	Partial Improvement
Current Case	Yes	No	Yes	No	C4-C7	No	No Improvement

a: Significant cervical spinal cord compression.

high-energy trauma associated with motorcycle accidents increases the risk of brachial plexus lesions (11). These lesions affected the entirety of the brachial plexus in 64.4% of the cases and the superior trunk in 25% of the cases. They are most frequently encountered as neurapraxia and axonotmesis, which account for 41.6% and 50% of SEH cases, respectively. The least frequent injury type is neurotmesis, which occurs in the remaining 8.4% of cases (8). When SEH is associated with nerve root avulsion, the most frequent symptoms are cervicalgia, thoracic pain, hemiparesis, radicular pain, and Brown–Sequard syndrome (6,7,14).

Of the six reported cases, including this one, only two involved VF. Garg et al. and Giugale et al. described fractures at the C1, C7, and T1 vertebrae (3,4). When the nerve roots are stretched beyond their elastic limits, this raises the possibility of traumatic avulsion of the cervical nerve roots, resulting in separation from the spinal cord (12). Therefore, by definition, VF is not a prerequisite for trauma-causing NRA.

As in our case, Giugale et al. and Garg et al. used MRI to diagnose brachial plexus injuries. They also carried out electromyography to assess the type of nerve lesion and to improve diagnostic accuracy (3,4). In these studies, the most frequent MRI finding associated with brachial plexus avulsion was a pseudomeningocele in the intervertebral foramina. The MRI receiver operating characteristics (ROC) used to diagnose pseudomeningocele increase when MRI is performed 30 days after the primary lesion (7). However, pseudomeningocele is not present in all cases of traumatic NRA (13). Moreover, the use of diffusion tensor imaging (DTI) of the spinal cord to visualize inflammatory and degenerative disorders, such as Brown-Séquard syndrome, is increasing (2). However, the improvement in diagnostic accuracy using DTI in patients with traumatic monoparesis requires further assessment.

In the present case, the SEH extended to the intervertebral foramina. In our opinion, this wide extension of bleeding could be an early sign of NRA, and it may contribute to an increase in the exerted tractive force of high-impact trauma, thereby worsening the avulsion. Further studies are needed to assess the sensitivity and specificity of this sign, as well as the validity of this hypothesis. The diagnostic workup of the case is summarized in a timeline that could be used in future cases of C-spine trauma associated with monoparesis (Figure 3). The present case had diagnostic intricacies because, in cervical trauma, the areas that are first evaluated are usually the C-spine and spinal cord, not the peripheral nerves. One month after the initial complaint, electromyography was performed, and a C-spine MRI was repeated. Both tests confirmed peripheral nerve avulsion.

In previous reports, all patients were admitted to the emergency department and presented with flaccid monoplegia in their affected superior limb. Only two cases had motor deficits in a different limb. The case reported by Newman et al. involved a 3-year-old child with a contralateral upper limb strength of 3/5, whereas the case by Garg et al. involved a 33-year-old man with paraparesis. However, both patients had full recovery from their non-nerve avulsion motor deficits (3,10). Decompressive surgery was performed in only two cases to alleviate spinal cord compression in life-threatening segments (4,15). Conservative treatment is recommended in most instances unless the patient presents signs of compressive myelopathy. In these situations, decompressive surgery becomes mandatory even though this intervention will not impact the prognosis of NRA (5,10,15).

CONCLUSION

SEH is deemed a surgical emergency due to its potential to cause irreversible neurological impairment and life-threatening lesions. Nevertheless, when SEH is associated with mild symptoms, medical treatment is a reasonable alternative. TSEH should be ruled out as a possible contributing factor to brachial plexus neurotmesis. Further studies are needed to create a more thorough diagnostic algorithm for cervical NRA that presents as brachial plexus neurotmesis.

ACKNOWLEDGEMENTS

We thank Monica Madore for editing a draft of this manuscript.

Declarations

Funding: This research did not receive any specific grant from funding agencies in the public, commercial, or not-for-profit sectors.

Availability of data and materials: The datasets generated and/or analyzed during the current study are available from the corresponding author by reasonable request.

Disclosure: The authors declare no competing interests.

AUTHORSHIP CONTRIBUTION

Study conception and design: RAC, VOA, CEP

Data collection: RAC, LCAC, HMN

Analysis and interpretation of results: RAC, HMN, MFR

Draft manuscript preparation: RAC, VOA, WMRC, JMSG

Critical revision of the article: MFR, WMRC, JMSG, CEP

Other (study supervision, fundings, materials, etc...): JMSG, WMRC

All authors (RAC, VOA, LCAC, HMN, MFR, WMRC, JMSG, CEP) reviewed the results and approved the final version of the manuscript.

REFERENCES

1. Brichko L, Giddey B, Tee J, Niggemeyer L, Fitzgerald M: Cervical spine traumatic epidural haematomas: Incidence and characteristics. EMA - Emerg Med Australas 30:359–365, 2018. https://doi.org/10.1111/1742-6723.12920
2. Fujiyoshi K, Konomi T, Yamada M, Hikishima K, Tsuji O, Komaki Y, Momoshima S, Toyama Y, Nakamura M, Okano H: Diffusion tensor imaging and tractography of the spinal cord: From experimental studies to clinical application. Exp Neurol 242:74–82, 2013. https://doi.org/10.1016/j.expneurol.2012.07.015

3. Garg K, Satyarthee GD, Singla R, Sharma BS: Extensive long-segment cervicothoracic traumatic spinal epidural hematoma with avulsion of C7, C8, and T1 nerve roots. J Neurosci Rural Pract 5:414-416, 2014. https://doi.org/10.4103/0976-3147.140007
4. Giugale JM, Henrikson KJ, Baronne LM, Lee JY: Traumatic brachial plexus root avulsion and cervical spine epidural hematoma in an 18-year-old man. Spine J 15:365-366, 2015. https://doi.org/10.1016/j.spinee.2014.09.024
5. Haider AS, Watson IT, Sulhan S, Leonard D, Arrey EN, Khan U, Nguyen P, Layton KF: Traumatic cervical nerve root avulsion with pseudomeningocele formation. Cureus 9:e1028, 2017. https://doi.org/10.7759/cureus.1028
6. Laohaprasitiporn P, Wongtrakul S, Vathana T, Limthongthang R, Songcharoen P: Is pseudomeningocele an absolute sign of root avulsion brachial plexus injury? J hand Surg Asian-Pacific Vol 23:360–363, 2018. https://doi.org/10.1142/S2424835518500376
7. Lee HS, Ju C Il, Kim SW: Traumatic cervical epidural hematoma without osseous fracture presenting as hemiparesis. Korean J Neurotrauma 15:209–213, 2019. https://doi.org/10.13004/kjnt.2019.15.e26
8. de Moraes FB, Kwae MY, da Silva RP, Porto CC, Magalhães D de P, Paulino MV: Clinical aspects of patients with traumatic lesions of the brachial plexus following surgical treatment. Rev Bras Ortop 50:556–561, 2015. https://doi.org/10.1016/j.rboe.2015.08.015
9. Muñoz González A, Cuello JP, Rodríguez Cruz PM, Iglesias Mohedano AM, Domínguez Rubio R, Romero Delgado F, García Pastor A, Guzmán de Villoria Lebiedziejswki J, Fernández García P, Romero Martínez J, Ezpeleta Echevarri D, Díaz Otero F, Vázquez Alen P, Villanueva Osorio JA, Gil Núñez A: Spontaneous spinal epidural haematoma: A retrospective study of a series of 13 cases. Neurologia 30:393-400, 2015. https://doi.org/10.1016/j.nrleng.2014.03.005
10. Newman WC, Tempel ZJ, Tyler-Kabara EC: Posttraumatic cervical nerve root avulsion with epidural hematoma. World Neurosurg 84:1177.e9-1177.e11, 2015. https://doi.org/10.1016/j.wneu.2015.06.050
11. Oberlin C: Brachial plexus palsy in the adult: A systematic approach to root lesions. Chir Main 22:273–284, 2003. https://doi.org/10.1016/j.main.2003.09.008
12. Sunderland S: Mechanisms of cervical nerve root avulsion in injuries of the neck and shoulder. J Neurosurg 41:705-714, 1974. https://doi.org/10.3171/jns.1974.41.6.0705
13. Tamburrelli FC, Meluzio MC, Masci G, Perna A, Burrofato A, Proietti L: Etiopathogenesis of traumatic spinal epidural hematoma. Neurospine 15:101-107, 2018. https://doi.org/10.14245/ns.1834938.469
14. Tanaka M, Ikuma H, Nakanishi K, Sugimoto Y, Misawa H, Takigawa T, Ozaki T: Spinal cord herniation into pseudomeningocele after traumatic nerve root avulsion: Case report and review of the literature. Eur Spine J 17:263–266, 2008. https://doi.org/10.1007/s00586-007-0537-1
15. Zubair M, Ravindran T, Chan CYW, Saw LB, Kwan MK: Acute brown-séquard syndrome following brachial plexus avulsion injury a report of two cases. Hong Kong J Emerg Med 18:347–351, 2011. https://doi.org/10.1177/102490791101800515